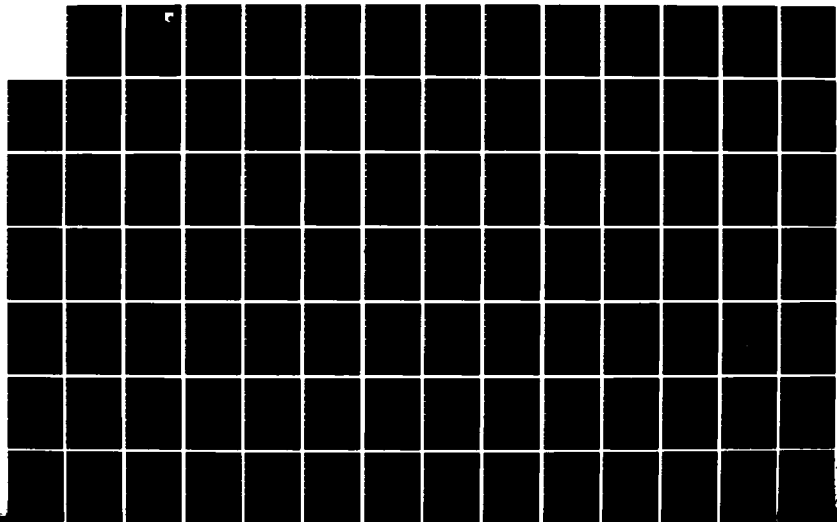AD-A141 210   KINETIC-ELASTIC APPROACH FOR TIME-DEPENDENT RHEOLOGICAL   1/3
               DATA ON SLURRY FU.. (U) OHIO STATE UNIV RESEARCH
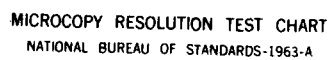   FOUNDATION COLUMBUS   R S BRODKEY ET AL. JAN 84
UNCLASSIFIED   OSURF-762084/712747 AFWAL-TR-83-2085   F/G 20/4   NL

MICROCOPY RESOLUTION TEST CHART

NATIONAL BUREAU OF STANDARDS-1963-A

AFWAL-TR-83-2085

AD-A141 210

KINETIC-ELASTIC APPROACH FOR TIME-DEPENDENT
RHEOLOGICAL DATA ON SLURRY FUELS AND POLYMERS
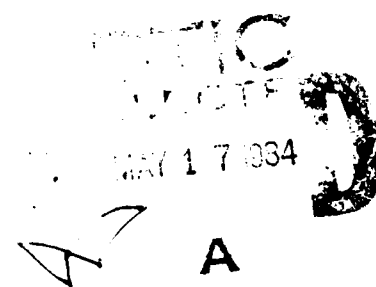
Robert S. Brockey

The Ohio State University Research Foundation
13 4 Kinnear Road
Columbus, Ohio 43212

January 1984

Final Report for Period March 1980 - September 1982

Approved for public release; distribution unlimited.

AERO PROPULSION LABORATORY
AIR FORCE WRIGHT AERONAUTICAL LABORATORIES
AIR FORCE SYSTEMS COMMAND
WRIGHT PATTERSON AIR FORCE BASE, OHIO 45433

DTIC
FILE COPY

84 05 15 226

TERESA A. BOOS
Fuels Branch, Fuels and Lubrication Division
Aero Propulsion Laboratory

ARTHUR V. CHURCHILL
Chief, Fuels Branch
Fuels and Lubrication Division
Aero Propulsion Laboratory

FOR THE COMMANDER

ROBERT D. SHERRILL, Chief
Fuels and Lubrication Division
Aero Propulsion Laboratory

REPORT DOCUMENTATION PAGE	READ INSTRUCTIONS BEFORE COMPLETING FORM	
1. REPORT NUMBER AFWAL-TR-83-2085	**2. GOVT ACCESSION NO.** AD-A141210	**3. RECIPIENT'S CATALOG NUMBER**
4. TITLE (and Subtitle) KINETIC-ELASTIC APPROACH FOR TIME-DEPENDENT RHEOLOGICAL DATA ON SLURRY FUELS AND POLYMERS	**5. TYPE OF REPORT & PERIOD COVERED** Final Report for Period Mar 80 – Sep 82	
	6. PERFORMING ORG. REPORT NUMBER 762084/712747	
7. AUTHOR(s) Robert S. Brodkey (K. Park, S. Weng, A. Ouibrahim, S. F. Lin)	**8. CONTRACT OR GRANT NUMBER(s)** F33615-80-C-2021	
9. PERFORMING ORGANIZATION NAME AND ADDRESS The Ohio State University Research Foundation, 1314 Kinnear Road Columbus, Ohio 43212	**10. PROGRAM ELEMENT, PROJECT, TASK AREA & WORK UNIT NUMBERS** P.E. 62203F 3048-05-91	
11. CONTROLLING OFFICE NAME AND ADDRESS Aero Propulsion Laboratory (AFWAL/POSF) Air Force Wright Aeronautical Laboratories (AFSC) Wright-Patterson Air Force Base, Ohio 45433	**12. REPORT DATE** January 1984	
	13. NUMBER OF PAGES 212	
14. MONITORING AGENCY NAME & ADDRESS(if different from Controlling Office)	**15. SECURITY CLASS. (of this report)** Unclassified	
	15a. DECLASSIFICATION/DOWNGRADING SCHEDULE	

16. DISTRIBUTION STATEMENT (of this Report)

Approved for public release; distribution unlimited.

17. DISTRIBUTION STATEMENT (of the abstract entered in Block 20, if different from Report)

18. SUPPLEMENTARY NOTES

19. KEY WORDS (Continue on reverse side if necessary and identify by block number)

rheology, slurry fuels, JP-10, jet fuel, carbon black slurries, sheer thinning, sheer thickening, thixotropic, dilation, polymer solution, lubricants, non-Newtonian flow

20. ABSTRACT (Continue on reverse side if necessary and identify by block number)

At The Ohio State University, we have been developing our kinetic interpretation of non-Newtonian fluid behavior under support from the Aero Propulsion Laboratory with materials of interest to the Air Force. Specifically, we have considered slurry fuel systems and a reference, high-viscosity lubricant (5P4E). In addition, we continued to obtain data on a polymeric system previously studied by us so as to ascertain the adequacy of our measurements and of our theory.

(continued on reverse side)

DD FORM 1473 EDITION OF 1 NOV 65 IS OBSOLETE

Block 20: Abstract (continued)

The kinetic theory is a phenomenological rate concept used to describe the time rate of change of a material structure. We call this part of the development "the kinetic model for thixotropic change." Corresponding to the thixotropic fluid structure is a thixotropic structural viscosity and a corresponding thixotropic stress. The real stress in the system is different from the thixotropic stress because of the elastic properties of the material. Our "elastic model for viscoelasticity" utilizes a modified version of Oldroyd's development in convected coordinates. A combination of the two models allows the representation of rheological data with what we call "the kinetic-elastic model."

To date we have shown conclusively that much of the older data could not be used because of instrumentation problems. We have obtained new polymer data (polymethylmethacrylate in DEP, PMMA/DEP) with our improved instrumentation and data acquisition system. Using this new data has allowed for the first time a critical test of the kinetic-elastic theory. The comparison between the polymer data and the theory are very good. We wish to study further the variation of parameters and a possible modification of the elastic part of the theory. We have completed our measurements of a number of low viscosity slurry fuels and have completed an extensive data gathering program on the reference lubricant. The slurry fuels are clearly non-Newtonian, and thixotropic, and some have a low critical yield stress that must be exceeded before they will flow. These materials are rheologically complex and turn out to be similar to another colloidial material we studied some years ago. We have also developed the kinetic-elastic theory to account for the yield stress. The comparison of slurry data to the theory is adequate but the logic use could be improved. The reference lubricant was found to be Newtonian at room temperature. As the temperature was reduced towards the pour point (-5 C), the material's viscosity increased rapidly and the material became non-Newtonian and viscoelastic. We have formulated and applied to a test set of this data a method to remove the effect of the upper cone movement during transient testing. Since this material is so much like the polymeric material, we plan to eventually reduce the data and interpret the results in terms of the kinetic-elastic theory as used for the polymeric data.

FOREWORD

The pre ent work has been carried out under contrac: number F33615-80-C-2021 w th Wright-Patterson Air Force Base over the period from March 24, 1°80 to September 30, 1982.

There a e available through University Microfilms, Ph.D. theses by Park (1981) and Lin (1983) that provide more details on some aspects of this study.

A1

CONTENTS

Page

LIST OF FIGURES

i.

LIST OF TABLES

OBJECTIVES

Our charge in the study covered by this final report was threefold :

1) To establish the adequacy of the time dependent polymer data previously obtained; if inadequate, to obtain a new set of data and to evaluate the kinetic-elastic approach for the representation of this data.

2) To obtain rheological data on a variety of potential carbon black – JP-10 slurry fuel formulations in order to help establish their general rheological characteristics as a function of shear level and temperature and to adapt the kinetic-elastic approach for the description of such materials.

3) To obtain, if time permitted, a data set for the high viscosity reference lubricant 5P4E.

Our objectives have been accomplished and this report provides the detailed summary of our efforts.

SIGNIFICANCE

Systems that involve rheological fluids, such as those found in polymer processing and in the fields of fuels and lubricants, often involve rapid-response, unsteady-state conditions. A rheological model must be able to adequately represent data in the time domain. The model should also be able to account for changes in concentration and temperature. As important is that the constants and parameters of the model have basic meaning that can be interpreted in terms of the fluid's composition and can be related to the performance of the fluid in its application. Ideally, one would like to know enough about the fluid's rheology so that modifications of the fluid can be made in response to a change in the fluid's performance in a system. Such change would be caused, for example, by more severe conditions or by a change in the physical system itself. The "kinetic-elastic model" developed at Ohio State has the potential of representing complex rheological data. The general approach of our effort is one of a complete characterization of any given non-Newtonian material so that one can apply this information to evaluate the flow of the material.

The work has significance with respect to the flow of various exotic materials such as thick slurry fuels, shale oil products, coal-oil mixtures, and modern lubricants. There is, for example, amazingly little known about the flow properties of slurry materials with yields. There is no adequate means of representing such data when the material has viscoelastic characteristics. It is a simple matter to extend our approach to allow description of materials of this nature. Such an analysis would apply to slurry fuels and coal-oil mixtures. It has only been in recent years that workers involved in lubrication have come to realize that materials they are dealing with are highly non-Newtonian and viscoelastic in their characteristics. Indeed, modern lubricants contain a high amount of polymeric additives and these are notoriously viscoelastic. It is interesting to speculate that the elastic characteristics involved in sudden deformation could be an explanation as to why some lubricants fail at high stress conditions at low temperatures.

SUMMARY OF RESEARCH ENDEAVORS

In our original proposal we provided a detailed summary of the field, our earlier endeavors, and a detailed development of the theory. We repeat this material here as Appendix D. Included in the review is a literature survey of the limited work done by others on lubricants and on slurry fuels.

The various approaches towards the elucidation of the rheological characteristics of materials generally fall into one of five classifications: empirical, phenomenological (mostly rate processes), linear viscoelastic, nonlinear viscoelastic, and microrheological analyses. The empirical methods correlate data by curve-fitting techniques. The rate theories have as their basis the assumption that the nonlinear characteristics can be associated with some structural change of the material whether it involves particle associations and dissociations, link formations and ruptures, or molecular entanglements and disentanglements. The linear viscoelastic models are based upon linear combinations of Hook's law of elasticity and Newton's law of viscosity. The nonlinear viscoelastic models are based on continuum mechanics and nonlinear combination mechanical models. Finally, microrheological analysis starts with the basic molecular or microscopic variables such as particle sizes, molecular interactions, and chain lengths. A simplified mechanism is proposed, and then it is mathematically represented and solved.

Each approach has made contributions to the field, but with the present state-of-the-art, we cannot completely describe the non-Newtonian behavior even in simple geometries. Steady-state flow behavior has been extensively investigated, and the representations available are adequate. However, little is understood about the unsteady-state flow, such as shear stress and normal stress growth after the onset of a sudden shear rate. The theories in the literature are not always able to predict, for example, stress growth at a given constant shear rate from data obtained on other experiments.

Our efforts over the past two years were both experimental and theoretical. The experimental work involved a complete analysis of our older data on the PMMA/DEP polymeric system so as to determine the adequacy of the data. We made the necessary repairs to the R-16 instrument to improve it so that adequate data for the polymer system could be obtained. This involved instrument repair and installing a new data acquisition system. The R-16 instrument was modified further to allow accurate measurements to be made on low viscosity materials such as the slurry-fuel and typical lubricants. In addition, the limited temperature control system was changed so that measurements could be made at reduced temperatures. Measurements were then made on both the Haake system and the R-16 instrument over a range of temperatures for the slurry-fuel and lubricant materials. Finally, the theory was tested and adapted to fit the data. In the next section, a detailed review is given of the accomplishments outlined above. Here, these efforts are briefly reviewed in less detail to give the reader a feel for our efforts.

We were unable to find any data in the literature that was taken with high enough time resolution to allow evaluation of the parameters of our kinetic-elastic model. Thus, we turned to the evaluation of our own data on PMMA/DEP. The sets of data for data evaluation were very carefully reduced to remove noise. Although the result of our analysis raised some questions as to the adequacy of this data, we felt that the transient sets of data were satisfactory. The measurement of the exact time delay from the moment of activation of the brake-drive switch to the shear stress signal is important in obtaining the true initial slope at zero time in a stress build-up experiment. The response time obtained is better than 0.01 second.

With the simplest form of the kinetic equation of $A \rightleftarrows B$, no combination of constants would provide an adequate fit. In order to improve the model so that it would fit all types of data, two steps were found necessary. As was done earlier and described in the review presented in Appendix D, the first step was to use a more empirical form for the elastic part of the theory. Rather than picturing the problem as a coupled elasto-viscous phenomena, the older view pictured the elastic contribution as an elastic response to a changing viscosity basis as caused by the kinetic change. The second step required was to modify the simple one-step kinetic model of $A \rightleftarrows B$ to $A \rightleftarrows B \rightleftarrows C$. In the initial tests of this idea, quite satisfactory fits to the transient data were obtained.

A detailed reevaluation of all the equilibrium data was made as well as an in-depth evaluation of one constant shear rate experiment at a shear rate of $10.8 \ \text{sec}^{-1}$.

A preliminary estimate of the kinetic constants for the experimental run had to be made so that there would be a good starting point for the optimization of the constants. A study of the effect of the variation of the various constants of the kinetic-elastic approach on the final response curve was probably one of the most interesting results of the analysis. These results provided the guidelines necessary for the optimization by iteration. The optimization of constants was not done by computer optimization procedures because of the large number of constants involved. Rather the results of the previous parametric study were used to adjust the theoretical curve to obtain the best fit to the data. This was accomplished by human iteration using the computer graphics system. The predicted data from the kinetic-elastic theory deviated approximately 3.95% from the transient experimental data for the constant shear rate experiments. The value of the parameters that were varied generally increased over the range from 3.4 to 21.5 sec^{-1}.

For the stress relaxation experiments, various reasonable assumptions for the initial conditions of the shear rate did not affect the elastic equation prediction. The normal assumption of no shear rate during the entire stress relaxation was adequate. However, a combination of thixotropic viscosity and the elastic equation was necessary to account for the elastic contribution to the stress relaxation. An improved prediction of stress decay was obtained by modest changes of the kinetic constants. It was concluded either that the data available were not good or that the elastic equation of the theory for stress relaxation was not exactly correct.

6

The initial shear rate for the constant shear stress experiments should be less than 0.001 sec^{-1} and the value of the second modulus elastic parameter is much smaller than the first. The modified kinetic-elastic theory shows excellent agreement between the experimental and predicted shear strain data for the constant shear stress experiments. The average percent standard deviation from the experimental strain data was approximately 1.80% from the constant shear stress experiments.

The first elastic modulus parameter cannot be considered a constant because it is affected by the level of shear rate. The modulus parameter for stress relaxation is different from that for stress growth. The second parameter has no significant dependency on shear rate for the constant shear stress experiment.

In general, we can conclude that a two-step reaction concept of thixotropy coupled with a changing viscosity basis for the elastic response shows excellent agreement with steady shear rate, constant shear rate, and constant shear stress experiments. The theory predicts well the stress overshoot at high shear rates and unsteady shear rate variation at constant shear stress. The present theory cannot use a constant value of viscosity (η_0) in the elastic equation to describe stress relaxation experiments. However, the value of η_t in the elastic equation with slightly modified values of the kinetic parameters predicts well the shear stress relaxation results.

As a result of further analysis of the kinetic theory, we discovered that there could be a more valid interpretation of the upper Newtonian viscosity than we have made in the past. In general, we had previously taken the upper Newtonian viscosity as the solvent viscosity (in this case 0.09 poise). However, molecular theory of viscous polymer solutions shows that the upper Newtonian viscosity is probably much higher than this (in the range of 500 to 12,000 poise for our solutions). Even with this major change, the data cannot be fitted with the simple one step kinetics; thus, the more complicated two step kinetics are still required.

It may be that the adequate fit obtained from the two-step model is a consequence of the model having more adjustable constants rather than being a better representation of the kinetic change mechanism. There is, for example, an inconsistency in that we use η_0 in the stress growth, but must use η_t in the stress relaxation. We were not sure at this point if the theory or the polymer data was the problem. Thus, we undertook two steps. First, since the polymer data being used was the noisy data obtained several years ago by Song, we obtained a completely new set of polymer data as described in the next section. The new data was quite good and no noise removal (filtering) was needed. The second step was a soul-searching analysis of the kinetic-elastic theory.

Why should the two-step model be necessary when the one-step concept is simpler and has fewer adjustable constants? At this point we made a concession to history and our own work. We had been forcing the first elasticity parameter to be a function of shear rate level only. Historically it has been taken as a spectrum of values at any one shear rate, i.e., a range of values that come into

play at various times. This is in agreement with our earlier work which showed that the parameter determined from oscillatory data is both a function of shear level and frequency of oscillation. We had not used this concept because we thought the parameter could be a constant and that the variation observed could be a result of the variation of η_t. In this, we were incorrect. The modification to our one-step theory is almost trivial; i.e., the modulus parameters are now real parameters and as such are determined so as to give a perfect fit for the one-step model. The test comes from the simplicity of representation of the parameters and from comparison of values obtained from other independent experiments. The results of this new approach are very promising. The values of the constants for the representation of the parameters were determined independently for each shear rate. Therefore, if any of them varied with the shear rate that variation would be clearly observed. Only three of the constants showed a systematic variation: the forward specific rate constant, the initial (or primary) value of the elastic parameter, and the final (or asymptotic) value of the elastic parameter. Further investigation of the effect of variations in the elastic part of the theory must await future work under the renewal of the contract. The details of the polymer data acquisition, analysis, and the new developments are included in the next section. In addition, suggestions for further work are included.

The flow behavior of suspensions encompasses the full range of material characteristics. They can vary in consistency from fluids to almost solids, and they can be Newtonian or non-Newtonian. Dilute suspensions often behave as simple Newtonian liquids. As the concentration of particles increases, suspensions become non-Newtonian. Thixotropy, shear-thinning, rheopexy, and even viscoelasticity can be seen in such systems. At certain concentrations, suspensions may even function as solids. In order to handle suspensions properly during processing or pumping, their flow behavior should be well understood and characterized.

Carbon-black has been widely used as a filler or reinforcing agent in rubbers, paints, and other polymers. Though carbon black can modify the properties of polymers, like smooth low-swell extrusion, it also changes the rheological properties of the system. The change of rheological properties depends on the fundamental properties of the carbon additive: particle size, porosity, and structure. Besides being used as a filler in polymers, to increase the available energy per unit mass as a solid fuel, carbon black, a combustible solid, has been added to a liquid fuel, JP-10, to form a higher energy slurry fuel.

Though the presence of solids increases the available energy, the flow behavior of the slurry is made complicated by the solids. The slurry is no longer a simple Newtonian fluid in spite of having a Newtonian solvent, JP-10. Its rheological properties become difficult to characterize as a result of the combination of solid and liquid properties. In order to add to our knowledge about the slurry fuels, their rheological properties (viscosity, elasticity, and plasticity) were studied and analyzed in detail. These details can be found in the next section and are briefly cited here.

8

Slurry fuels show non-Newtonian fluid behavior under imposed forces. The shear stress-shear rate relationships were studied as a function of time over a wide range of shear rates and temperatures. Since the deviation from Newtonian behavior is due to the presence of solids, the non-Newtonian characteristics are highly dependent on the solid properties: type of solid, particle size, concentration, shape, and distribution. No effort was made to relate the rheological characteristics to the properties of solids in this preliminary study. Instead, slurries with different particle sizes and stabilizers (as supplied) were studied to provide general insights into the rheological nature of such materials. These should be useful to the researcher to help design the proper formulation.

In order to have a better understanding of the flow mechanism of the slurries, both transient and steady state conditions were measured. Transient data was obtained by suddenly imposing a step change of shear rate on the system and measuring the shear stress as a function of time. It was found that slurry fuels possess a time-dependent behavior called thixotropy. Elasticity, another property that can be seen in suspensions due to the interactions of particles, was estimated from the transient data.

Yield stress is still another pronounced property of suspensions. The yield stress must be overcome by any pumping system and will dictate the maximum power required. The yield stresses of the slurry fuels were determined and studied to see how they affect the flow.

The change of the viscosity of fuels with temperature is important, especially at low temperatures. Viscosity is due to the internal friction between molecules in liquids. Since temperature is a measurement of molecular motion, temperature is the most important variable affecting the viscosity of suspensions. As the temperature drops, the solid properties of the system could dominate and be critical for pumping. In practice, the viscosity of fuels should be as little temperature-dependent as possible so as to minimize the required power at low temperatures. The viscosity of the slurries was studied over a wide range of temperatures.

The final objective was to construct a rheological equation of state that could be used with the equations of motion to predict complicated flow behavior of slurries in practical situations. To accomplish this, the kinetic-elastic model was modified to describe the complex behavior of suspensions. The fit of the model to the equilibrium data is excellent. The fit in the time domain is not as precise, but is adequate. Certainly it could be improved with increased knowledge of the mechanism of the initial break-down of the solid structure. It is this study that would be a part of our renewal contract and is given in more detail in the next section.

Besides the collection and analysis of data for the polymer system and the in-depth data on the slurry fuels, additional data was obtained on the reference lubricant 5P4E. This data has been obtained over a wide range of temperatures

and because of its polymer like nature should be interpreted similarly. The
data set as well as the future work necessary to analyze this data is detailed
in the next section.

DETAILS OF RESEARCH RESULTS

I. POLYMERIC MATERIAL

We were unable to find any data in the literature that was taken with high enough time resolution to allow evaluation of the parameters of our Kinetic-Elastic model. Thus, we turned to the evaluation of our own data on PMMA/DEP.

A. Instrument Response

Since the elastic modulus parameter of the Kinetic-Elastic model is related with the initial slope at zero time, it is important to establish the exact time delay from the moment of activation of the break-drive unit of the Weissenberg rheogoniometer to the appearance of the shear stress signal. Thus, the measurement of the mechanical response of the Model R-16 Weissenberg rheogoniometer was undertaken for analyzing the transient data during the initial period of stress growth. The resulting data and analysis allowed us to obtain the time-delay to the true beginning in a stress-buildup experiment. The response time obtained was much faster than that suggested in the instruction manual (about 0.04 seconds). The response times of the viscometer at constant shear rates of 3.408 sec^{-1}, 10.8 sec^{-1} and 21.48 sec^{-1} are 0.009 sec, 0.007 sec, and 0.008 sec respectively.

B. Noise

The sets of data for data evaluation were very carefully reduced so as to remove any extraneous noise introduced from the gearbox system. We feel that the transient sets of data are satisfactory.

C. Theory for One-Step Reaction

Appendix B of the proposal gives a complete tabulation of the equations of the modified Kinetic-Elastic theory used in the initial theory evaluation. The necessary equations from that Appendix are reproduced here as Appendix B. Equations 1, 6, and 7 are the kinetic rate expressions. Equation 11 is the elastic contribution. Equations 12 to 14 are used to evaluate the equilibrium constants. Equations 4, 5, and 8 are used for fitting of the stress growth data.

C.1 Equilibrium Evaluation for One-Step Reaction

The evaluation of the equilibrium kinetic constants (K and p) of the Kinetic-Elastic model has been done at the equilibrium state. These and other constants of the theory are noted in Appendix B of this report and in more detail in Appendix B of the proposal. In this analysis, 4 combinations of m, n, and a were used (m = 1, n = 2 or 3, a = 1 or 3.5). The results show that all combinations of m, n, and a give reasonable prediction of the shear rate and equilibrium shear stress. The values obtained for p and K are listed in Park's thesis (75)*. The maximum range of % deviation of the predicted shear rate and equilibrium stress are 19% and 16%, respectively. The equilibrium constants (p and K) show a weak dependency on concentration. The p values are slightly more sensitive to concentration change than the K values.

---

* Specific thesis cited herein are given in the proposal reference list reproduced here as Appendix A.

The values of p and K for one concentration (48%) and one shear rate
(10.8 sec^{-1}) were adjusted slightly to improve the equilibrium (steady state)
fit. The transient data was then used to fit the entire curve. The initial
slope was used to establish the elastic parameter. Various parameter search
techniques were used to establish the remaining constants. A typical example is
shown in Figure 1.

With the simplest form of the kinetic equation of A $\vec{\leftarrow}$ B as described in the
original proposal, no combination of constants would provide an adequate fit.
If the time to the peak in the response curve were matched, the degree of
overshoot was excessive. If the amplitude of the over-shoot was matched, the
time to the peak was too short. The poor initial fit is a result of the
non-flexible nature of the model, i.e., logically satisfactory but not
satisfactory for an empirical fit.

D. Two-Step Reaction

In order to improve the model so that it would fit all types of data, two
steps were necessary. The first step was to use a more empirical form for the
elastic part of the theory as was done earlier and is described in the review of
our proposal. Rather than picturing the problem as a coupled elasto-viscous
phenomena, we used the older view which pictured the elastic contribution as an
elastic response to a changing viscosity basis as caused by a kinetic change.
The second step required was to modify the simple one-step kinetic model of
A $\vec{\leftarrow}$ B to something more complex like A $\vec{\leftarrow}$ B $\vec{\leftarrow}$ C. This change makes evaluation of
the constants more difficult. All of the variables, constants, and parameters
used in the sequel are given in Table I and have the same parallel meaning as
the corresponding terms have in the one step reaction; e.g., K_A and K_B are
the two equilibrium constants that are now needed to replace K; m_1, m_2,
n_1, n_2 are reaction orders needed to replace m and n, etc.

D.1 Equilibrium Evaluation for Two-Step Reaction

The value of a was selected as 3.5 based on previous work and not
modified or adjusted in any way. The value of η_∞ was taken as 0.09 poise based
on experimental analysis and not modified or adjusted. Six combinations of
m_1, m_2, n_1, and n_2 were selected for testing. These six were selected
based on logical arguments for the orders of the forward and reverse reactions.
The variation of the parameter S was studied for each of the six cases. (The
parameter S is defined in equation (L) and (M) in Table I). The specific
evaluation of the constants was done by first using equation (E) to obtain K_A
and p_A from a log-log plot of the LHS (left-hand-side) against the equilibrium
shear stress τ_{eg}. The constants K_B and p_B were then evaluated in a
similar manner using equation (F) and the values of K_A and p_A evaluated in
the previous step. Values of S below 2 resulted in F being negative, which is
unrealistic. Too high values of S reverted the two step kinetics to the older
single step system. Since the selection of S was not critical to fit the data,
a value of 2.5 was selected for further evaluation of the data. All six cases
for S = 2.5 were quite satisfactory and within the scatter of the experimental
equilibrium data.

From past work on equilibrium data, we have learned that data at low rates
of shear should be weighted less than that at higher rates. This is a result of
F_A being near unity. When the term that involves 1 - F_A is evaluated, we

12

Experimental data set #322

A⇌B, coupled with ？ in elastic response

Shear Stress

Time

Figure ... ... of kinetic-elastic model for one set of constants.

13
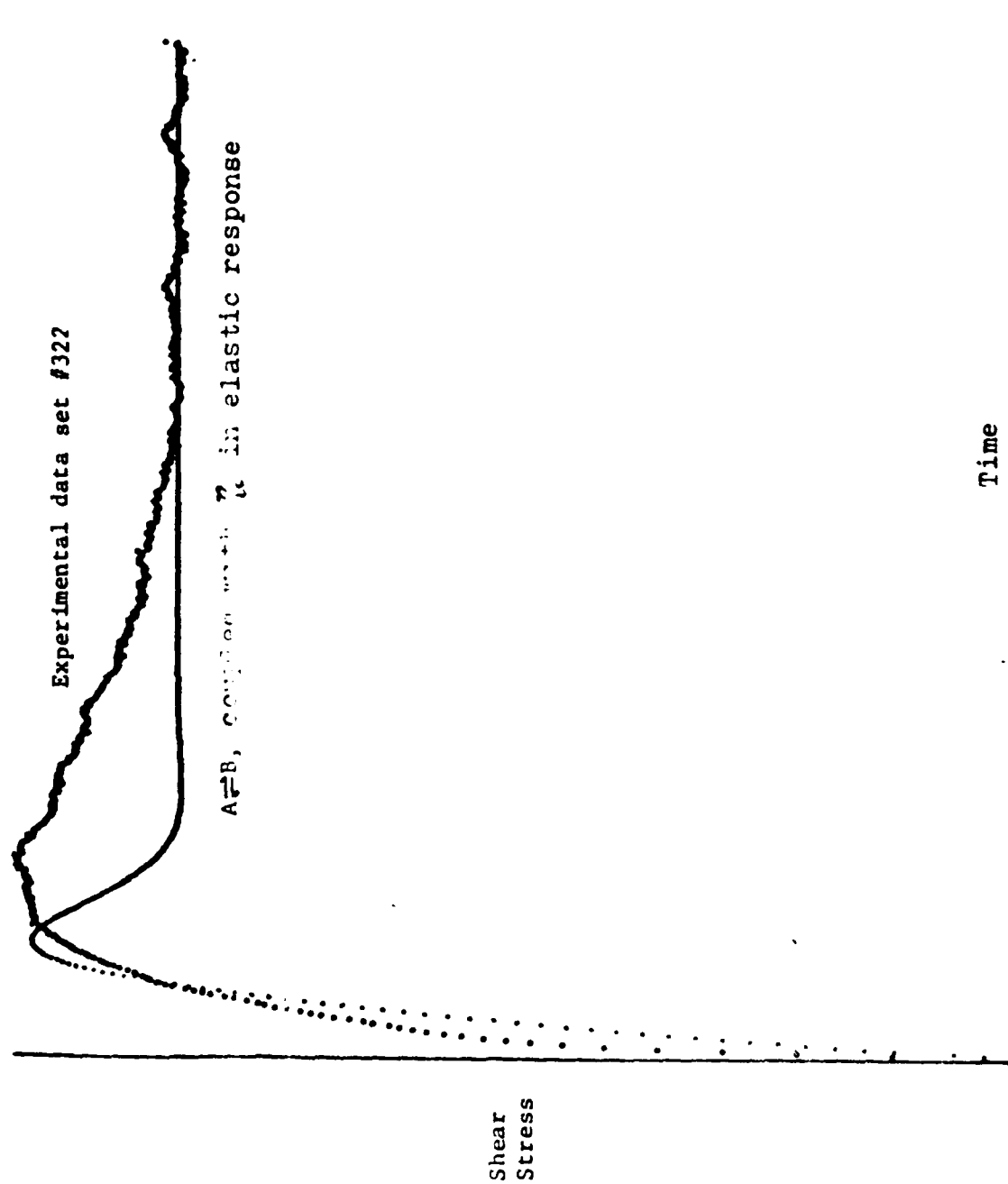
TABLE I

SUMMARY OF EQUATIONS FROM KINETIC-ELASTIC THEORY

(A) $-(dCF_A/dt) = k_1\tau^{p_1}(CF_A)^{m_1} - (k_3 + k_2\tau^{p_2})(CF_B)^{n_1}$

(B) $(dCF_B/dt) = k_1\tau^{p_1}(CF_A)^{m_1} - (k_3 + k_2\tau^{p_2})(CF_B)^{n_1}$

$$- k_4\tau^{p_4}(CF_B)^{m_2} + (k_6 + k_5\tau^{p_5})(CF_C)^{n_2}$$

(C) $\tau + (\eta_o / G_1)\, d\tau/dt) = \eta_t[\dot{\gamma} + (\eta_o/G_2)(d\dot{\gamma}/dt)]$

(D) $F_B = (1/3)(1 - F_A)$ $\qquad F_A = (n_t^{1/a} - n_\infty^{1/a}) / (n_0^{1/a} - n_\infty^{1/a})$

(E) $\dfrac{C^{n_1-m_1}(1 - F_{A,eq})^{n_1}}{C_{A,eq}^{m_1}} = k_A \tau_{eq}^{p_A}$

(F) $\dfrac{C^{n_2-m_1(m_1/n_1)}[1 - F_A - (k_A \tau_{eq}^{p_A} F_A^{m_1} C^{n_1-m_1})^{1/n_1}]^{n_2}}{F_A^{m_1 m_2/n_1} k^{n_2/n_1} \tau_{eq}^{p_A(m_2/n_1)}} = k_B \tau_{eq}^{p_B}$

(G) $\tau = \eta_t \dot{\gamma} (1 - e^{-G_1 t/\eta_o})$

(H) $\tau_n = (\eta_t \dot{\gamma} / \tau_{eq})(1 - e^{-G_1 t/\eta_o})$

(I) $\eta_t = [F_A(\eta_0^{1/a} - \eta_\infty^{1/a}) + \eta_\infty^{1/a}]^a$

(J) $-(dF_A/dt)_{t,\gamma} = k_1 \tau^{p_1} C^{m_1-1} F_A^{m_1}$

(K) $-(dF_A/dt)_{t,\gamma} = k_1 \eta_o^{p_1} C^{m_1-1} \dot{\gamma}$

14

TABLE I (continued)

(L) $$\frac{[1 - (1/S)] (dF_A/dt)}{(c^{n_2-1}/k_B \tau^{p_B})(1 - F_A - F_B)^{n_2} - c^{m_2-1} F_B^{m_2}} = k_4 \tau^{p_4}$$

(M) $$\frac{[1 - (1/S)](dF_A/dt)}{c^{m_2-1}[(1/S)(1 - F_A)]^{m_2}[(\frac{1 - F_A}{1 - F_{A,eq}})^{2-m_2} - 1]} = k_4 \tau^{p_4}$$

(N) $$obj(\%) = \sqrt{\frac{\sum_1^N \left(\frac{\tau_{calc} - \tau_{exp}}{\tau_{exp}}\right)^2}{N - 1}} \times 100$$

SUMMARY OF EQUATIONS FOR STRESS RELAXATION EXPERIMENTS (ADDITIONAL)

(O) $$\tau + (n_t/G_1)(d\tau/dt) = 0$$

SUMMARY OF ADDITIONAL EQUATIONS FOR SHEAR RATE CH NG

(P) $$\dot{\gamma} = \dot{\gamma}_0 (1 - \beta t)$$

(Q) $$\frac{d\tau_n}{dt} = (G_1/\eta_{eq})(n_t \dot{\gamma}/\tau_{eq})[1 - \beta t - (n_{eq}\beta/G_2)] - \tau_n$$

(R) $$\tau_n = \tau/\tau_{eq}$$

15

Figure 2

26 DATA SET OF FMMA/DEP AT 92 DEGREE C.
■ - ACTUAL DATA
- - PREDICTION WITH M1=1 M2=2 N1=2 N2=2 A=3.5 S=2.5

LOG [EQUILIBRIUM SHEAR STRESS]

LOG ((1-F)**N)*CONC** (N)-M)) / (F**M)*S**N))

LHS of equation (E)
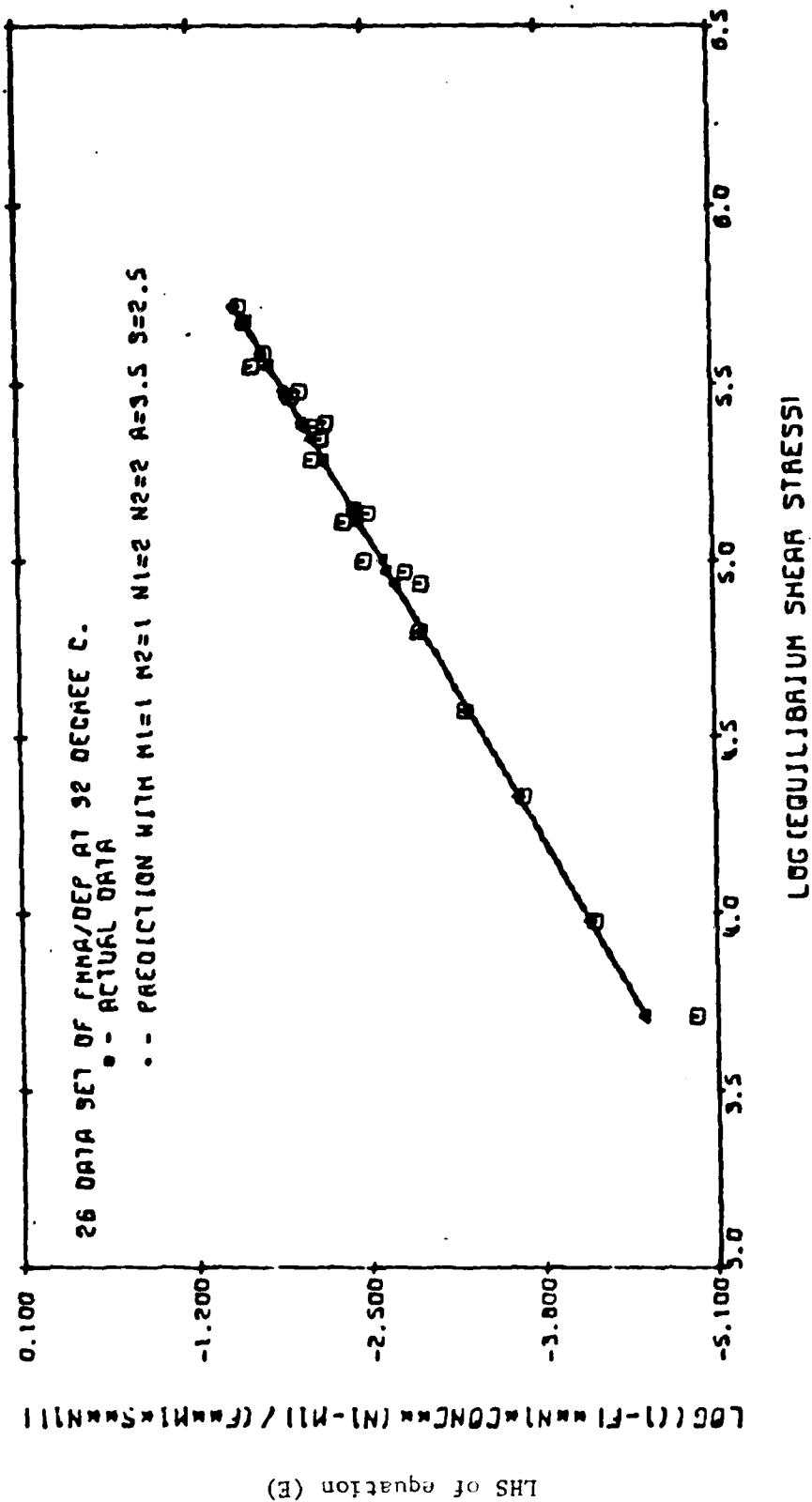
Figure 2. Evaluation of K_A and P_λ.

16

introduce considerable error due to the taking of differences of large numbers. Thus, the equilibrium results were evaluated by using a variable weighting factor to improve fit. To illustrate the adequacy of the data fit, Figure 2 gives the evaluation of K_A and p_A from the plot according to equation (E) and Figure 3 gives the evaluation of K_B and P_B from the plot according to equation (F). These are presented only for case 1, but all other cases were nearly as good. Finally, Figure 4 gives the final backcalculated result of the experimental and predicted basic shear diagram equilibrium results for this same case. Clearly these results are more than adequate to represent the data over a range of concentrations.

D.2 Transient Evaluation of Two-Step Reaction for Stress Growth

As was seen in the previous section, and as was true with the one-step model, no problems were experienced in fitting the equilibrium data. Completely adequate fits were obtained in all cases. However, the fits to the complete transient curves were only somewhat improved over those shown in Figure 1 (see Figure 5). This result strongly suggested that the kinetic aspect of the theory was not the main cause of the equation's failure to provide an adequate fit for the data.

In addition to the kinetic change, a change in the elastic response formulation of the theory was made. Rather than picturing the problem as a coupled elasto-viscous phenonena, an older view of the elastic contribution being an elastic response to a changing viscosity basis as was used by the kinetic change was used. In the initial tests of this idea, quite satisfactory fits to the transient data were obtained (see Figure 6).

Preliminary values for kinetic constants. A preliminary estimate of all the kinetic constants was made so that there would be a good starting point for the optimization of constants.

The procedure for evaluation of k_1 and p_1 is first to calculate F_A from the data using equations (G) and (I) and then to plot this F_A as a function of time. The calculation can be done since G_1 will have been previously estimated from the initial slope of the data and η_0 is known. From the plot, the initial rate can be obtained from the slope at $t = 0$, i.e., an evaluation of the term $- (dF_A/dt)_{t=0}$. Equation (A) at time zero reduces to equation (J), which in turn can be rearranged to equation (K) by using initial conditions. A plot of the LHS of equation (K) versus $\dot{Y}$ will give a slope of p_1, and from the intercept, the concentration, and η_0, k_1 can be calculated. Since p_2 and k_2 are uniquely related to p_1, k_1, K_A, and p_A, k_2 and p_2 are also known (for k_2 evaluation it is assumed that $k_3 = 0$). The constant k_3 appears in the rate equations in (A) and (B) of Table I. It describes the Browning motion build-up of structure as is explained in Appendix B of the proposal. The term, k_3, is small compared to the term to which it must be added. Since data at various shear rates were used in this evaluation, values were not obtained that are a function of shear rate. The value for p_1 was 0.3879 and that for k_1 was 0.2204. These values will serve as the initial estimates for optimization at all shear rates.

Evaluation of the preliminary values for p_4 and k_4 was more difficult because data near equilibrium had to be used. Equation (D), with a fixed value of S of 2.5, was used to obtain d_B/dt from the values of dF/dt previously

17
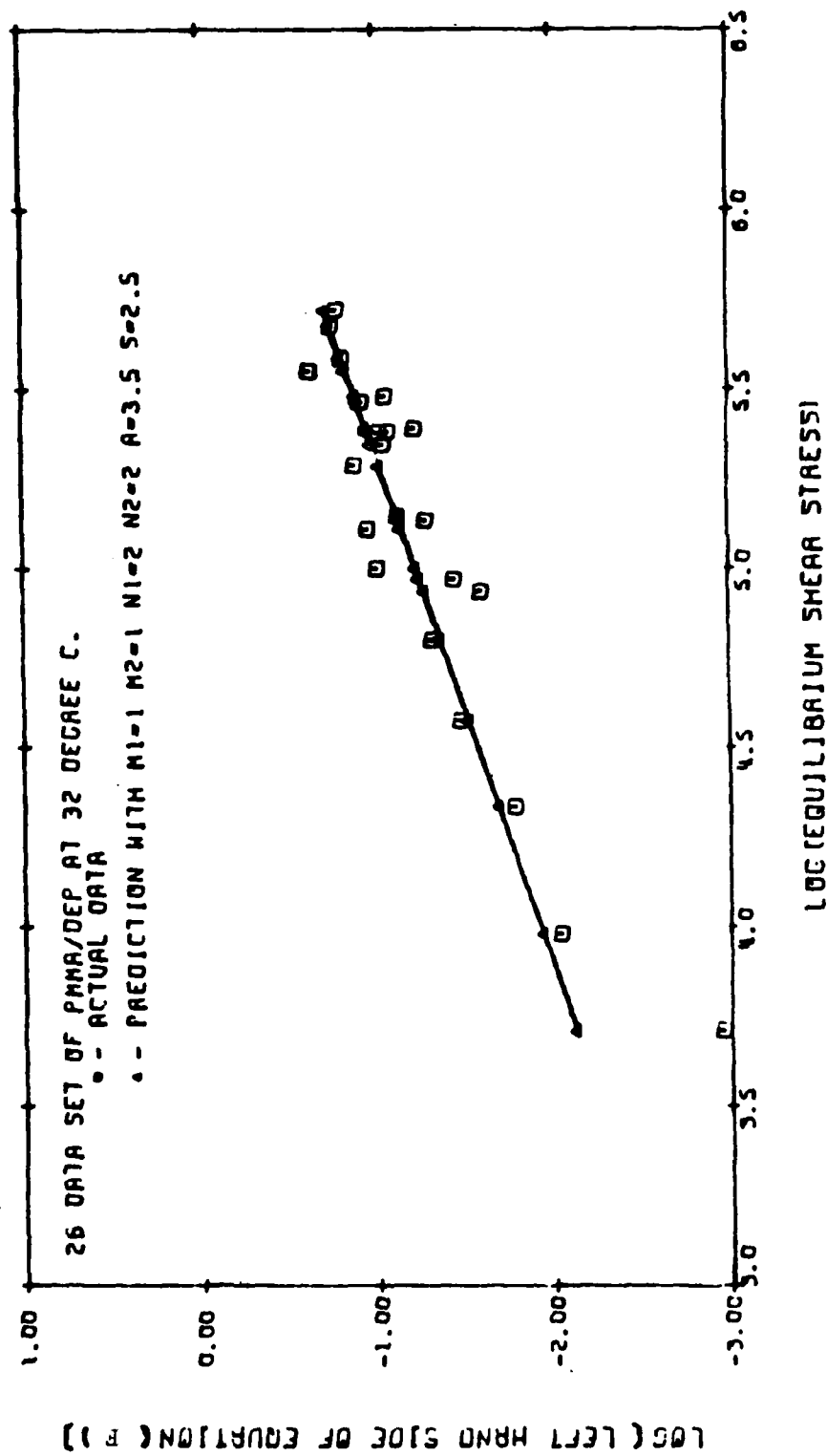
Figure 3. Evaluation of K_D and p_B.

18

BACKCALCULATION OF EQUILIBRIUM SHEAR STRESS
● - EXPERIMENTAL DATA
• -PREDICTION WITH M1=1 M2=1 N1=2 N2=2 A=3.6 S=2.5

40 % PMMA/DEP

35 % PMMA/DEP

30 % PMMA/DEP

10^2

10^1

10^{-0}

10^{-1}

10^7

10^6

10^5

10^4

10^3

LOG(SHEAR RATE)

L FC(EQUILIBRIUM SHEAR STRESS)

Figure 4. Basic shear diagram for PMMA/DEP at 32 degree C.

A⇌B⇌C, coupled with % in elastic response

Experimental data set #322

Shear Stress

Time
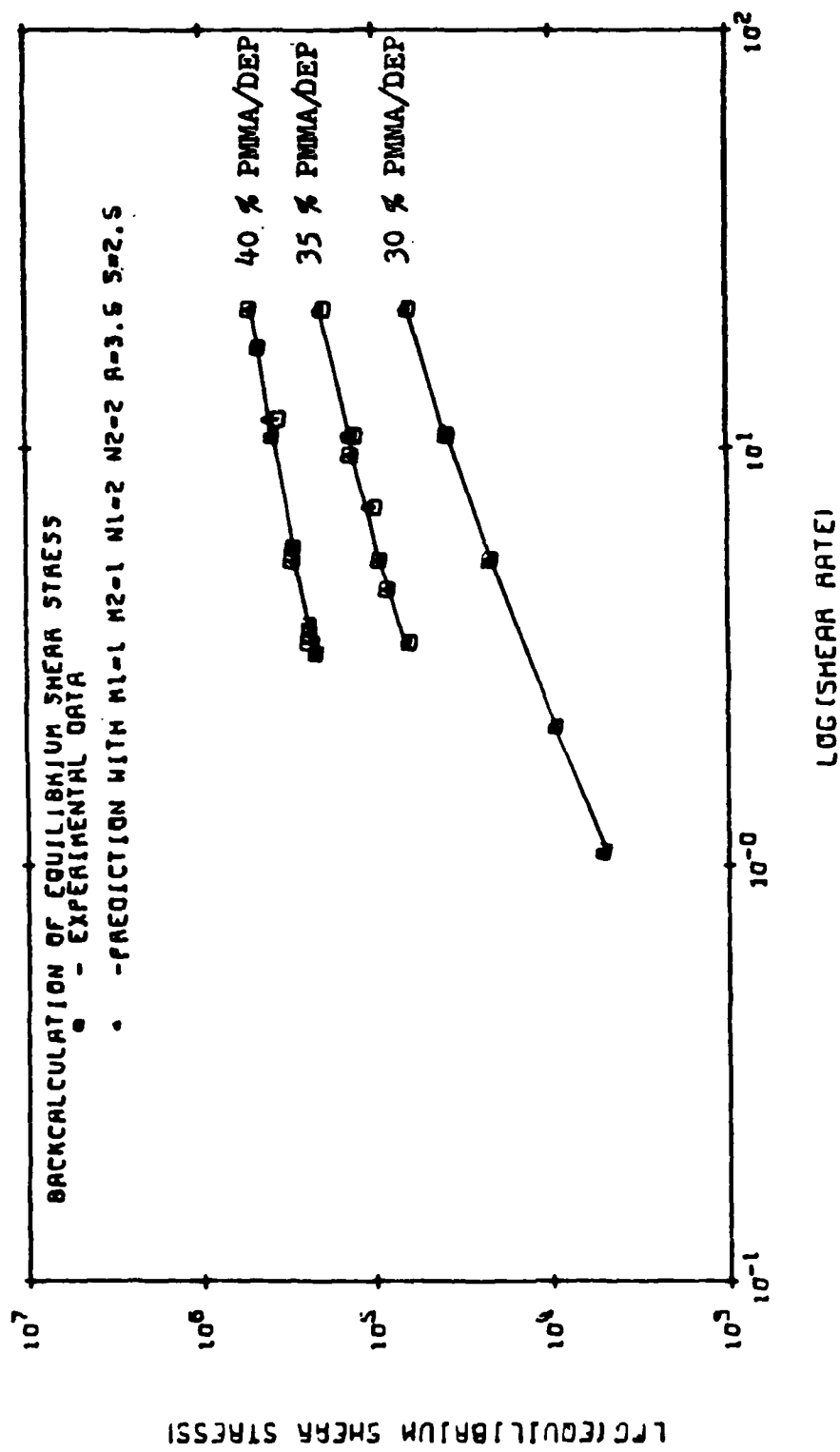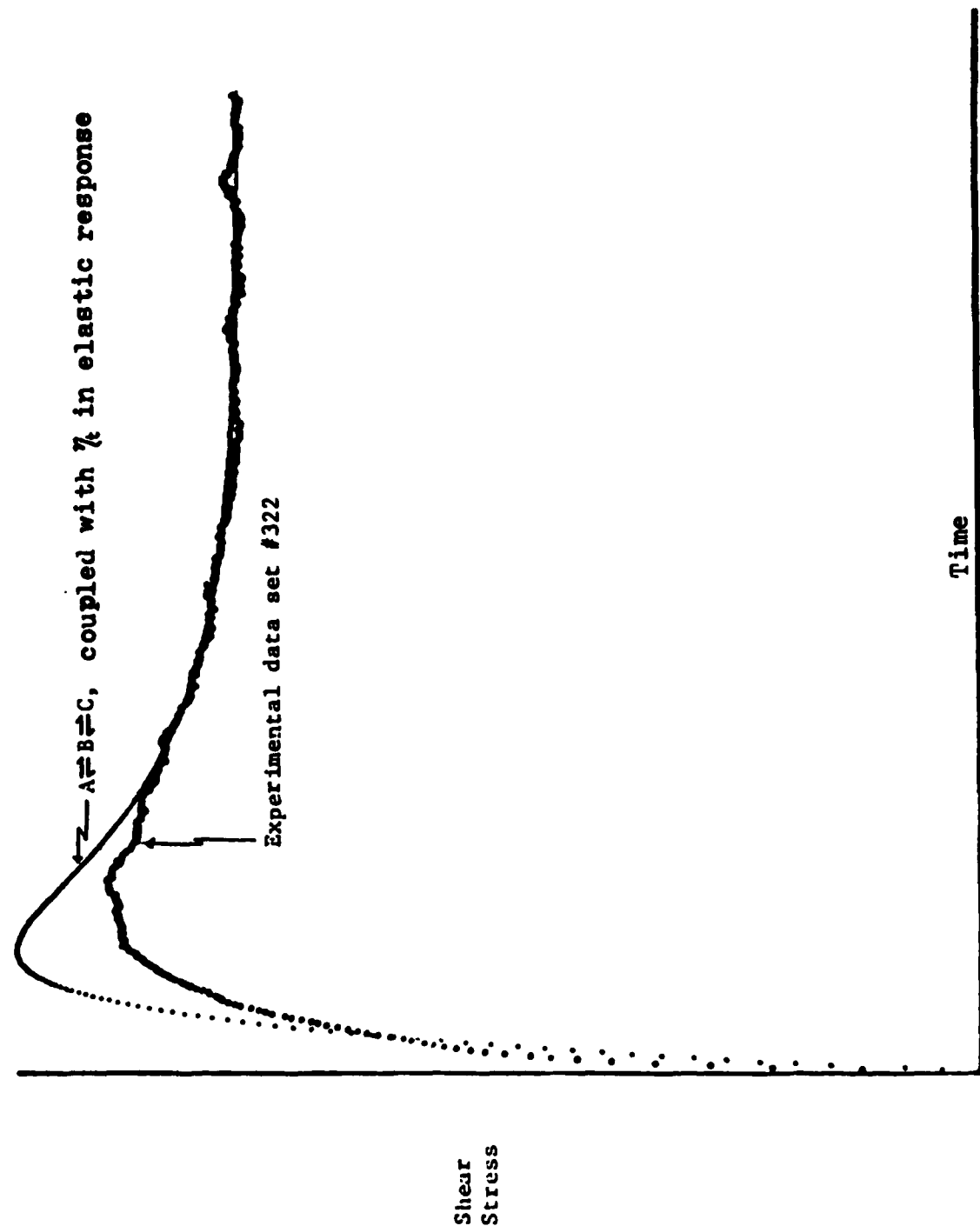
Figure 5. Comparison of experimental data to complex reaction form of kinetic-elastic model for one set of constants.
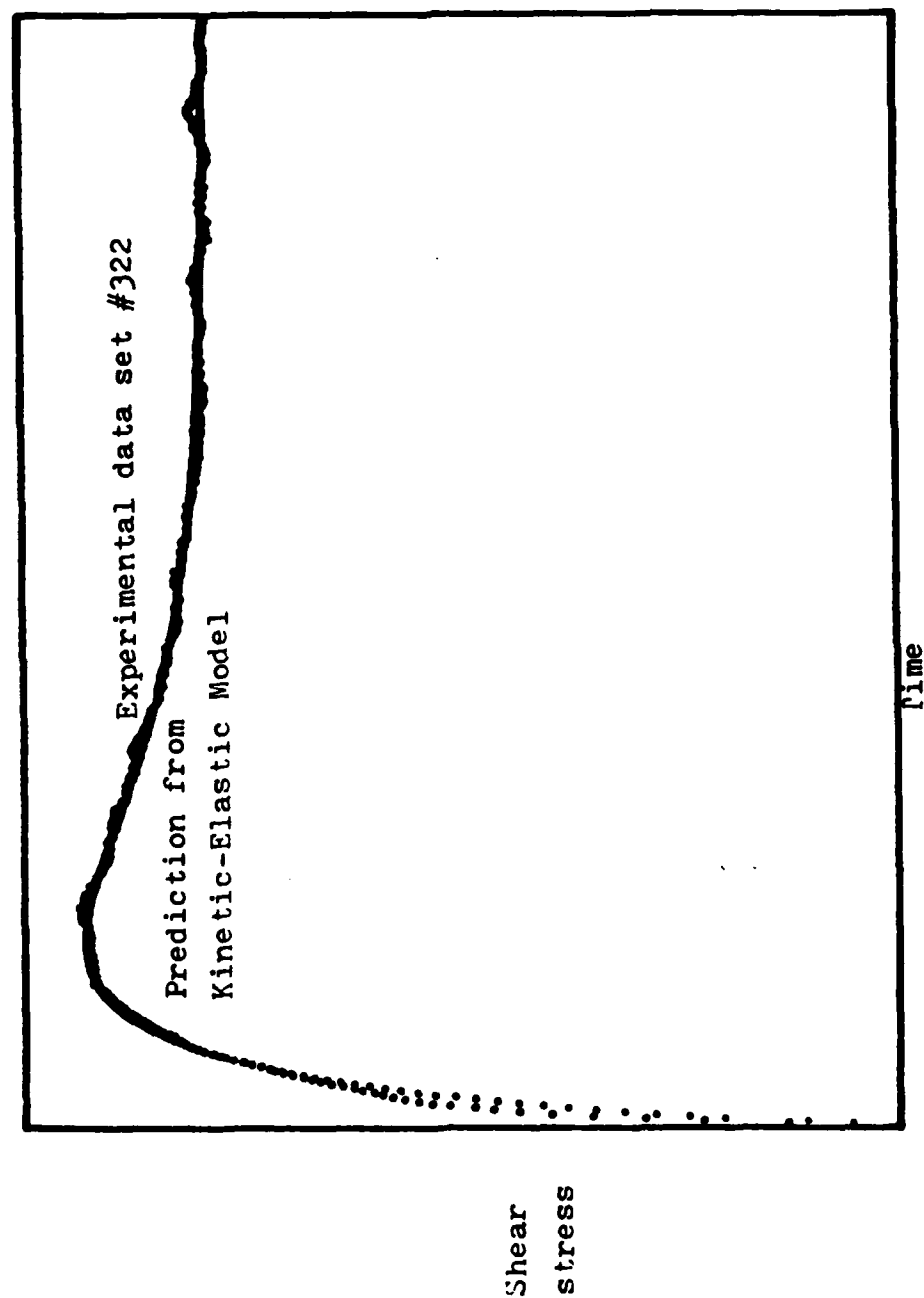
Figure 6. Comparison of experimental data to complex reaction and elastic-response to a changing viscosity of kinetic-elastic model for one set of constants.

21

calculated from equations (G) and (I). After some rearrangement of equations
(A), (B), and (D) as well as the introduction of the relation between k_4,
k_5, and K_B and of that between p_4, p_5, and p_B, equation (L) can be
obtained.

After further multiplication, this can be rearranged into a more convenient form
given by equation (M). A plot of the LHS of equation (M) versus the shear
stress provides for the evaluation of p_4 and k_4, from which p_5 and k_5
can be readily obtained with the assumption of $k_6 = 0$. This is clearly
parallel to taking $k_3 = 0$ in the same equation. All cases were evaluated.

Parametric analysis of equations. A study of the effect of the variation
of the various constants of the kinetic-elastic approach on the final response
curve produced one of the most interesting results of the analysis. A figure is
needed to show each constant. Figure 7 shows the effect of K_A; the data curve
for run #322 is shown for comparison. Figure 8 shows the effect of G_1 that
changes both the initial slope and the peak overshoot value. The figures for the
effect of the other parameters can be found in reference 74. These results
provide the guidelines necessary for the optimization by iteration to be
described next.

Optimization of constants. The optimization of constants was not done by
computer optimization procedures because of the large number of constants
involved. Rather the results of the previous parametric study were used to
adjust the theoretica curve so as to obtain the best fit to the data. This was
accomplished by human iteration using the computer graphics system. The
specific procedure was first to plot the experimental data. The equilibrium
constants were then adjusted to provide the best fit for the specific run. This
involved only a small change in p_A; K_A, K_B, and p_B remained as
previously estimated. Next G_1 was adjusted, if necessary, to give the best
fit for the initial slope. Finally p_1 and p_4 were slightly adjusted to
provide the best final fit for the system. The constants k_1 and k_4 were not
changed from their initial estimates. Recall that the trend in changing them
was exactly the same as changing p_1 and p_4. As a test on the adequacy of
the fit, a mean squared deviation given as equation (N) in Table I was used.
The result is shown in Figure 9. The final values for all constants and all of
the plotted results can be found in reference 74. The standard deviation of all
of the data was less than 4%.

D.3 Transient Evaluation of Two-Step Reaction for Stress Relaxation

The constants from the stress growth experiment were used to predict
stress relaxation. A constant viscosity (η_{eq}), which poorly predicted
results, was used in the elastic equation. Much better results were obtained
when we replaced η_{eq} with a variable viscosity (η_t). The equations used are
given in Table I. We found that using a constant viscosity was better for
stress growth and a variable viscosity was better for stress relaxation. We are
uncomfortable with this, but have no explanation for the results.

The results of the parametric study show that the stress decay increases at
a faster rate with an increase in G_1 (see Figure 10). p_A has an effect on
the initial slope. G_1 controls the initial slope. p_1 has the same effect
as p_A. p_4 has an effect on the curve near the equilibrium state. The

22
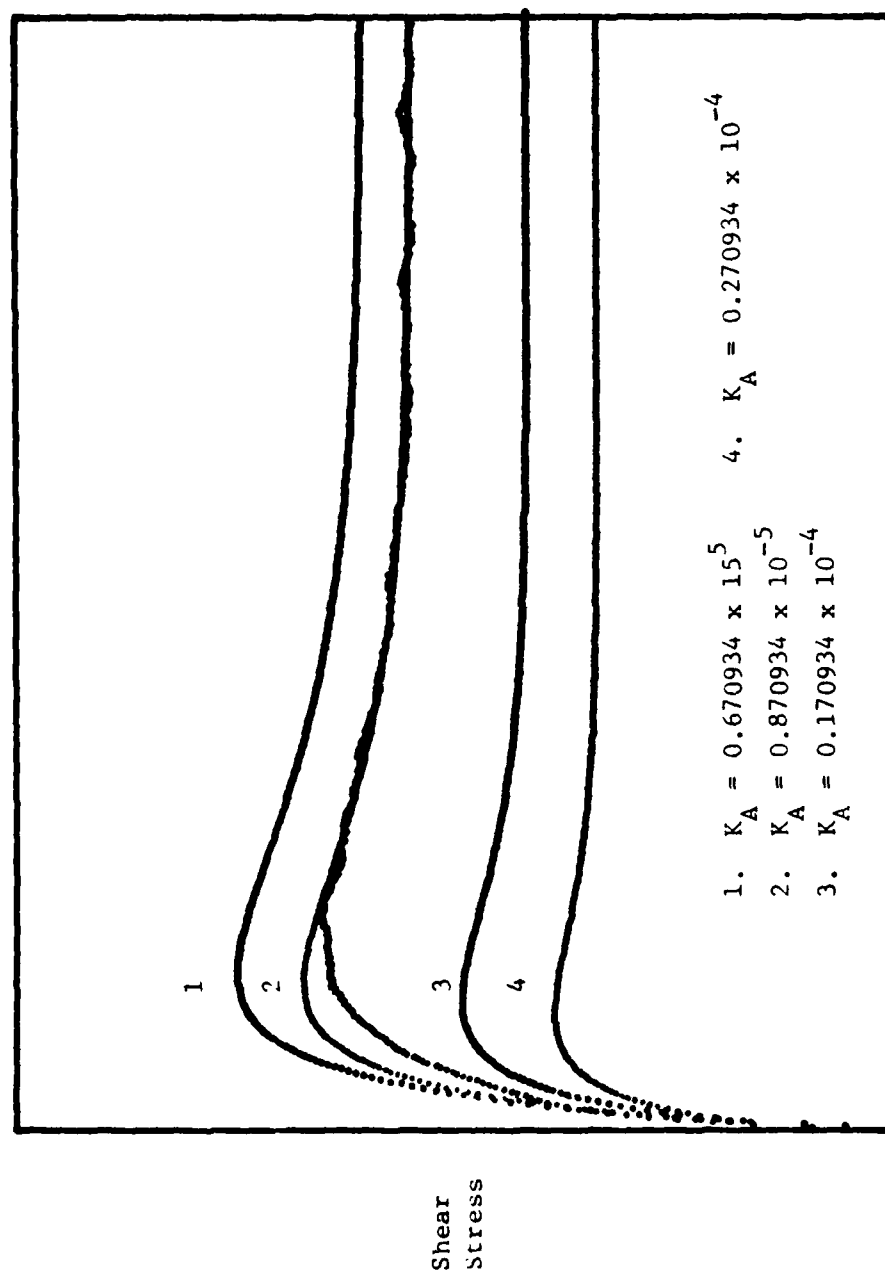
Figure 7. Effect of K_A on the response curve of the shear stress at the constant shear rate for one set of constants.

1. $K_A = 0.670934 \times 15^5$
2. $K_A = 0.870934 \times 10^{-5}$
3. $K_A = 0.170934 \times 10^{-4}$
4. $K_A = 0.270934 \times 10^{-4}$

Shear Stress

time

23
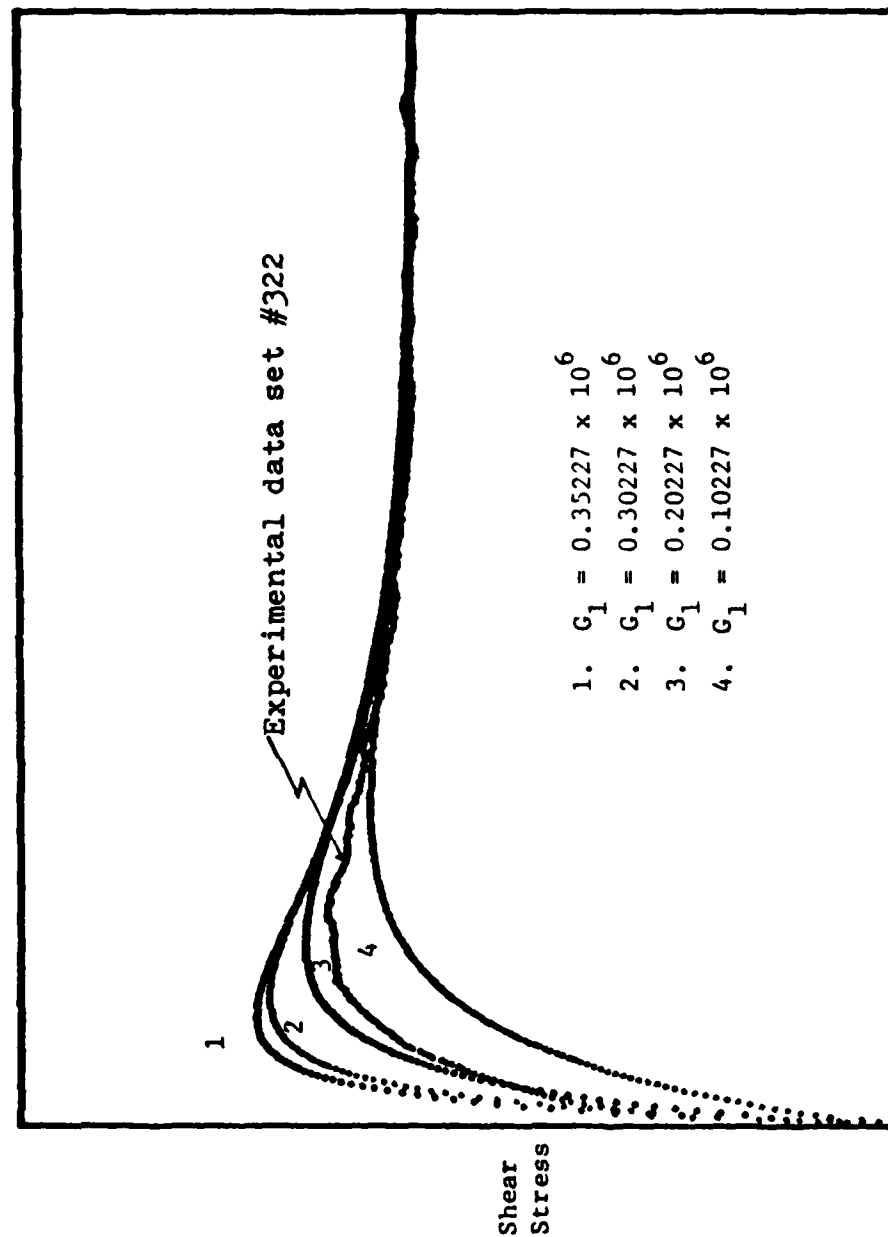
Figure 8. Effect of G_1 on the response curve of the shear stress at the constant shear rate for one set of constants.

24
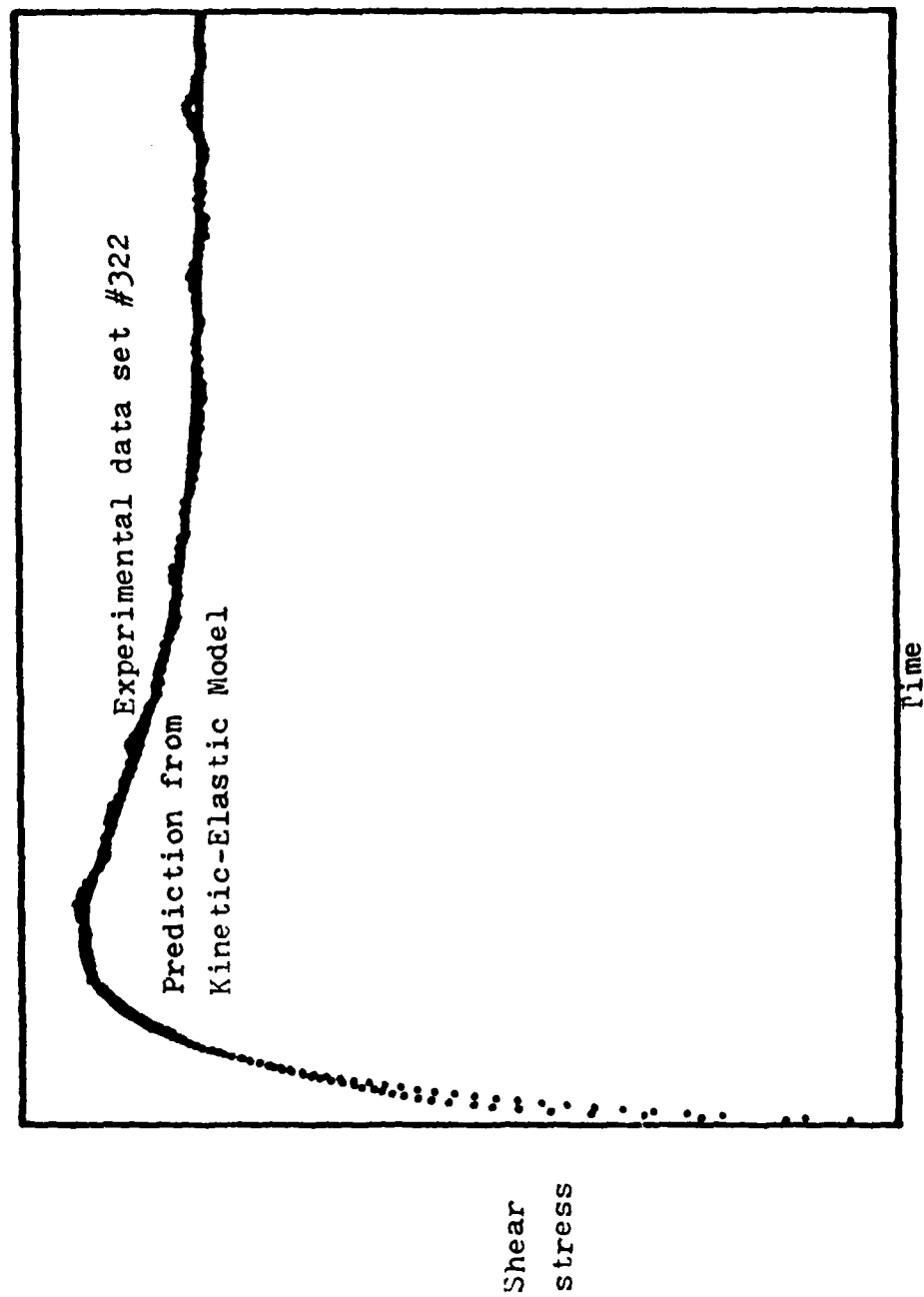
Figure 9. The best fitting result for case 2($M_1 = 1, M_2 = 1, N_1, N_2 = 2$)

25

RUN10 322

PA= 0.829100D+00
KA= 0.870934D-05
PB= 0.709567D+00
KB= 0.169825D-04
EQUIL.VIS= 0.129844D+05
FEQ= 0.780418D+00
P1= 0.387900D+00
K1= 0.220400D+00
K3= 0.000000D+00
P4= -0.225000D+00
K4= 0.230420D+02
K6= 0.000000D+00

1. $G_1 = 0.1 \times 10^5$

2. $G_1 = 0.4 \times 10^5$

Shear Stress

Time
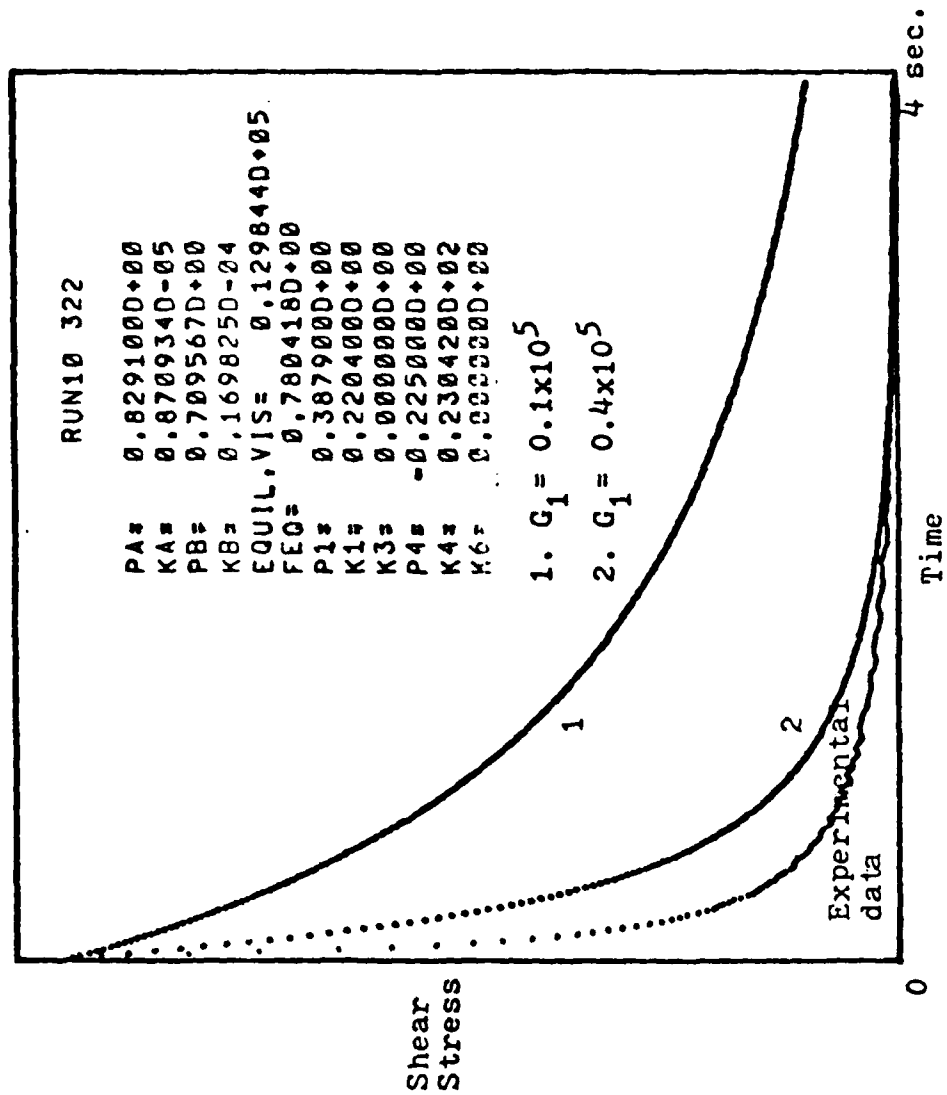
Figure 10. Effect of G_1 in equation (G) for the shear stress relaxation.

higher p_4, the higher the tail part of the curve. However, p_4 has no significant effect within a range of -0.29 to -0.14. κ_4 has the same effect as p_4, but no significant effect within the above range.

Use of the maximum values for the parameters that were observed for stress growth provided a reasonable prediction for the stress decay. Therefore, the equilibrium and kinetic constants, except p_1, were retained and the value of G_1 was used as 0.5×10^5 dyne/cm^2 for all the data sets. Here, p_1 was changed within a range of 0.26 to 0.30 for the best fit.

The standard deviation was used as a fitting criteria; the average value was 0.05. Comparison of one of the predicted results to the experimental data is illustrated in Figure 11.

Effect of Initial Conditions. Previously we assumed that the shear rate dropped instantaneously to zero at the initial time of the stress relaxation experiment. Since this is not exactly true, we realized that the initial shape of the relaxation curve could be affected. Thus, we modified the analysis to allow a nonzero initial shear rate condition. Due to a response delay in the Weissenberg rheogoniometer, the lower plate of the rheogoniometer continues to rotate for a very short time after the brake switch for the lower plate is activated. To approximate this alternate initial condition, the shear rate was expressed as a function of time rather than being set to zero. The resulting set of equations that must be simultaneously integrated is the same with only the first equation for the viscoelastic part of the theory requiring modification.

Since the brake-drive system response time of the rheogoniometer was within 0.01 seconds, the value of β should be between 100 and 150. The term β is defined in equation (9) in Table I. The result of the parametric study of the β -effect showed that a value of β between 25 to 200 had no significant effect during stress relaxation.

The normally assumed initial condition of zero shear rate is clearly satisfactory for the stress relaxation experiment.

D.4 Transient Evaluation for Two-Step Reaction for Shear Change at Constant Stress

The shear strain data during the constant shear stress experiments is not contaminated by noise, since the motor drive system is disengaged. Thus, the raw data obtained by Song was directly analyzed.

Since the constant stress experiments introduce one new elastic parameter (G_2), but no new parameters as far as the kinetic part of the theory is concerned, the equilibrium shear stress was carefully compared to those at constant shear rate (CSR) in order to apply values of the kinetic parameters obtained at CSR for analysis of shear strain data. Since the raw data taken by Song was shear strain instead of shear rate, the elastic equation was numerically integrated again to obtain the shear strain. Another reason for this procedure is that the numerical integration involves less error than numerical differentiation, which tends to amplify small variations. Therefore, comparison of shear rate was made indirectly by strain curves.
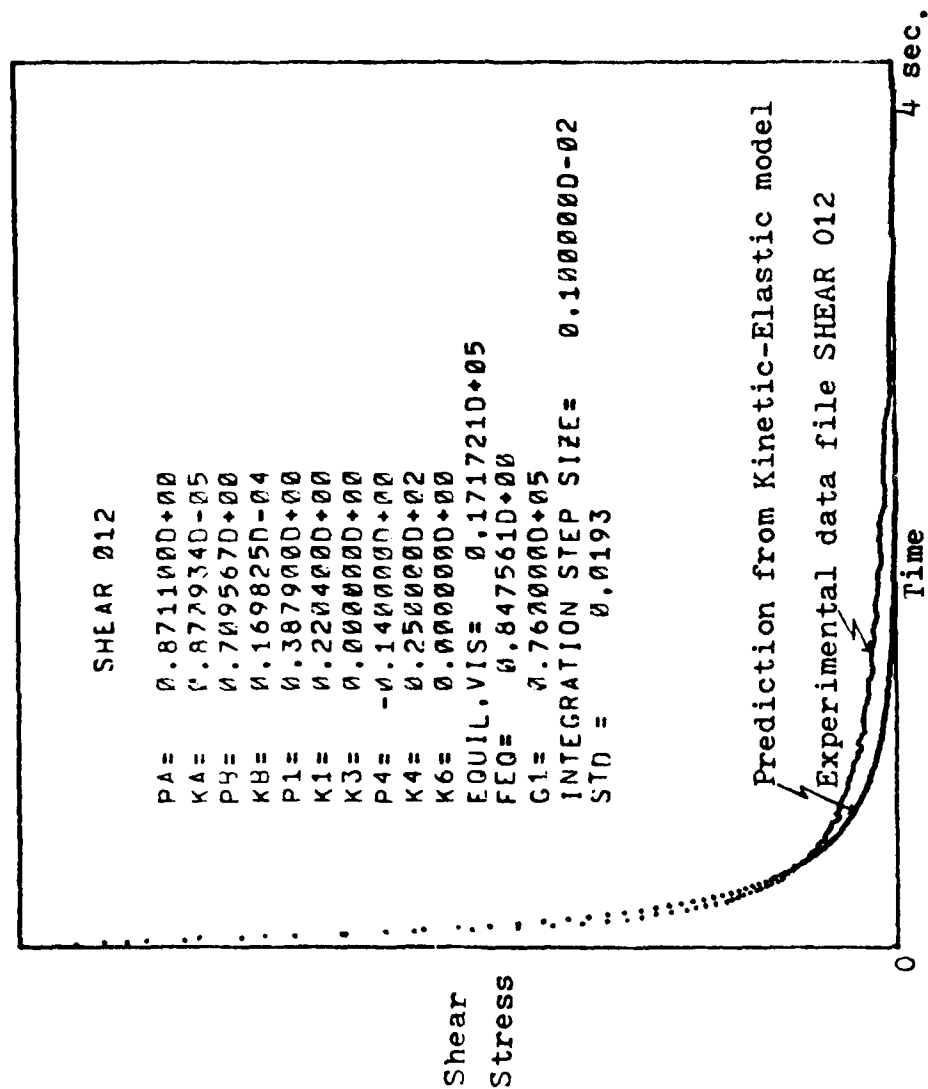
Figure 11. Comparison of the shear stress relaxation data to the predicted results (SHEAR 012).

The values of the parameters obtained from the constant shear rate experiments (having the same equilibrium shear stress as those at the constant shear stress experiments) were directly used for the analysis of transient shear strain and shear rate during the first 5 seconds of the experiment.

The results of a parametric study show that the initial condition of the shear rate ($\dot{\gamma}_n$ at $t = 0$) has a shifting effect on the origin (zero time) and that $\dot{\gamma}/\dot{\gamma}_{n,t=0}$ should be less than 0.01 sec^{-1}. The elastic parameter G_2 has an effect on curvature of shear strain. The larger the value of G_2, the more convex the strain curve. Values of G_2 less than 100 have no significant effect.

The elastic parameter (G_2) is the only parameter that was used to control the strain curve and was found to be approximately 100 dyne/cm for the best fit. This value of G_2 is much smaller than those obtained by other researchers. Even though the decreased value of G_2 gets closer to the experimental shear strain curve, the result shows that the final value of G_2 obtained for each stress level has no dependency on the shear stress.

The prediction of the shear strain with the model was compared to the experimental data and the percent standard deviation (PSTD) for the entire data set was about 1.27%. In order to show the excellent agreement between the experimental and predicted shear strain data, a typical plot is shown in Figure 12.

E.   Comparison of Kinetic-Elastic Two-Step Reaction Results with Earlier Efforts

The theory has been analyzed for stress growth, stress relaxation, constant shear stress experiments and oscillation experiments by earlier researchers. These previous researchers have used the simple one-step reaction concept of A $\rightleftarrows$ B for the kinetic part of the theory. However, in this work, the old theory had to be modified by introducing a two-step reversible reaction (A $\rightleftarrows$ B $\rightleftarrows$ C) concept. Therefore, the values of the constants and parameters from the present work will be different from those obtained by others.

The previous researchers provided values of an elastic modulus parameter, G_1, for their models. Song (10) calculated G_1 from the initial slope, but he had difficulty in obtaining the true initial slope due to the noise and not knowing the exact zero in time. Thus, he obtained his values of G_1 from the approximated slope by the simple window averaging technique. The values of G_1 obtained by Song were within the range of 66,000 to 110,000 dyne/cm^2, which were determined at the shear rates of 1.08 sec^{-1} and 21.48 sec^{-1}, respectively. His results showed that G_1 increased with an increase in shear rate. This trend of G_1 is in agreement with the results of the present work.

Pandalai (12) obtained the values of G_1 by a linear interpolation for his oscillation experiments based on the fact that the elastic parameters (G_1 and G_2) are functions of concentration. In his work, the value of G_1 increased with an increase in shear rate. However, the value of G_1 was dependent on the value of k_2 used to fit the initial slope in his work. Another interesting observation by Pandalai was that a much higher value of G_1 had to be used for the stress relaxation experiments to obtain an adequate fit. Pandalai's results

29
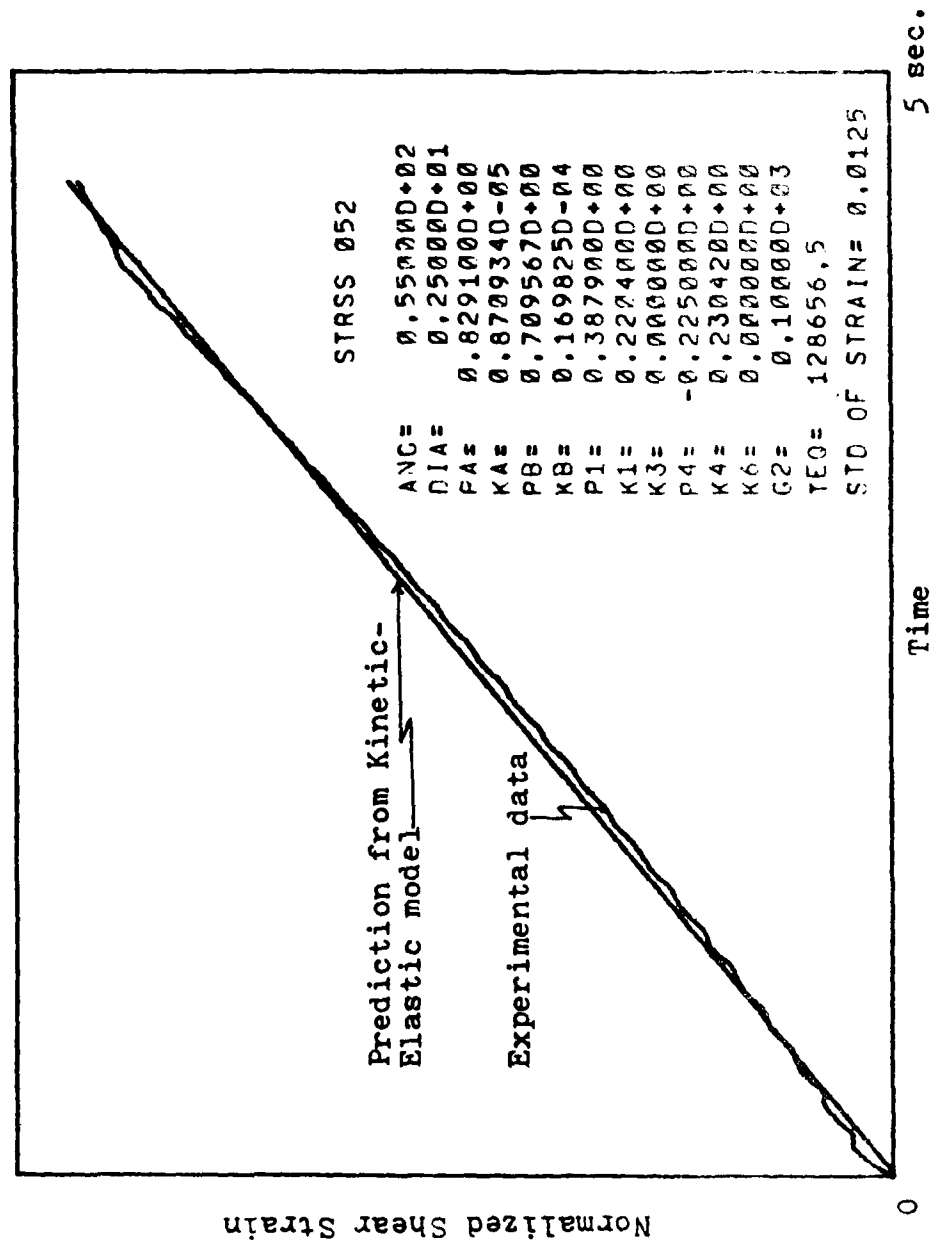
Figure 12. Comparison of the shear strain data and predicted results (STRSS 052).

STRSS 052

ANC=	0.55000D+02
DIA=	0.25000D+01
FA=	0.82910D+00
KA=	0.87093D-05
PB=	0.70956D+00
KB=	0.16982D-04
P1=	0.38790D+00
K1=	0.22240D+00
K3=	0.00000D+00
P4=	-0.22500D+00
K4=	0.23042D+00
K6=	0.00000D+00
G2=	0.10000D+03
TEQ=	128656.5
STD OF STRAIN=	0.0125

Prediction from Kinetic-Elastic model

Experimental data

Normalized Shear Strain

Time

5 sec.

0

30

differ from the present work which shows a much smaller value of C_1 for the stress decay compared with the value for stress overshoot.

Lander (13) extensively studied the elastic modulus parameters (G_1 and G_2) by oscillation methods. The effects of oscillatory frequency, shear rate and temperature were all considered. He calculated G_1 for five different oscillatory frequencies within the range of 0.03 to 3.0 Hz at four different temperatures. In Lander's work, the values of G_1 and G_2 were obtained by extrapolations to zero amplitude of oscillation. He concluded that the values of G_1 increased with oscillatory frequency and decreased with temperature. The viscosity effect on G_1 in his work is similar to the effect of the oscillatory frequency. For the shear rate effects on G_1, the value of G_1 goes to zero as the upper Newtonian region is approached. However, the effect of shear rate on G_1 from Lander's work is contrary to those obtained from the present Kinetic-Elastic model. Also, the value of G_1 obtained by Lander in the near non-Newtonian transition area should be reexamined at higher shear rates. Lander had difficulty establishing the value of G_1 from his oscillatory tests at shear rates over 4 sec^{-1}.

In the present work, the values of G_1 for the constant shear rate experiments are obtained from the initial slope of the filtered data. The value of G_2 is obtained from the constant shear stress experiments and is the only parameter to control the shear strain curve.

Tables II and III summarize the values of the elastic modulus parameters obtained in this work and by other researchers.

A conclusion from this work and that done by others is that the elastic modulus cannot be considered constant, but is a function of shear rate.

F. Conclusions for Kinetic-Elastic Theory – Phase I

In general, we can conclude that a two-step reaction concept of thixotropy coupled with a changing viscosity basis for the elastic response shows excellent agreement with steady, constant shear rate, and constant shear stress experiments. The theory predicts well the stress overshoot at high shear rates and unsteady shear rate variation at constant shear stress. The present theory cannot use a constant value of viscosity (η_o) in the elastic equation to describe stress relaxation experiments. However, the value of η_t in the elastic equation with slightly modified values of the kinetic parameters predicts well the shear stress relaxation results. It is recognized that the Kinetic-Elastic approach has great potential for the representation of rheological data for both transient and equilibrium states but requires further development.

More specific conclusions are

1. The measurement of the exact time delay from the moment of activation of the brake-drive switch of the shear stress signal is important in obtaining the true initial slope at zero time in a stress build-up experiment. The response time obtained is better than 0.01 second.

31

Table II Comparison of G_1 obtained by various investigators using PMMA in DEP.

Investigators	Range of G_1 (dyne/cm^2)	Remarks
Present work by Park	102,270∿272,270	obtained with shear rates of 3.408 to 21.48 sec^{-1}. 35% PMMA in DEP only.
Song	66,000∿110,000	obtained with shear rates of 1.08 to 21.48 sec^{-1}. 30%, 35% and 40% PMMA in DEP.
Pandalai	30,000∿180,000	obtained with oscillatory frequencies of 0.1563 Hz to 1.19 Hz. 38.5% PMMA in DEP.
Lander	13,660∿133,800	obtained at zero shear rate with the oscillatory frequencies of 0.3 Hz to 3.0 Hz. 30%, 35% and 40% PMMA in DEP.

Table III Comparison of G_2 obtained by various investigators using PMMA in DEP.

Investigator	Range of G_2 (dyne/cm^2)	Remarks
Present work by Park	100∿1,000	obtained with shear stress of 85,810 to 136,510 dyne/cm^2. 35% PMMA in DEP only.
Song	40,000∿700,000	obtained with shear stress of 85,810 to 136,510 dyne/cm^2. 30%, 35% and 40% PMMA in DEP.
Pandalai	12,000∿30,000	obtained with oscillatory frequencies of 0.1563 Hz to 1.19 Hz. 38.5% PMMA in DEP.
Lander	36,700∿934,000	obtained at zero shear rate with the oscillatory frequencies of 0.3 Hz to 3.0 Hz. 30%, 35% and 40% PMMA in DEP.

32

2. Separation of noise from the fast response signal is essential for the analysis of the transient data at constant shear rates. A fast Fourier analysis has been effectively used for the noise removal process. The net result obtained was a clean response curve. The contamination noise was approximately 30 Hz and probably is from the 1800 rpm (30 Hz) motor.

3. With the simplest form of the kinetic equation of $A \rightleftarrows B$, no combination of constants provided an adequate fit.

4. In order to improve the model, three alternate forms were introduced: 1) The simple one-step kinetics of $A \rightleftarrows B$, coupled with the lower Newtonian viscosity (η_0) in the elastic response fails to improve the fit significantly, 2) A two-step reaction kinetic concept of $A \rightleftarrows B \rightleftarrows C$, coupled with the normal viscoelastic response was introduced and was only a slight improvement over the simpler one-step model. Thus, it was concluded that the kinetic aspect of the theory could not be the main cause of the failure to provide an adequate fit to the data. 3) The two-step reaction kinetics of $A \rightleftarrows B \rightleftarrows C$, coupled with the time constant of η_0/G_1 for the elastic response, was used to obtain quite satisfactory fits to the transient data.

5. Among 6 combinations of m_1, m_2, n_1 and n_2 tested, $m_1 = 1$, $m_2 = 1$, $n_1 = 1$ and $n_2 = 2$ (both forward rate orders are unity as well as the reverse rate for the first reaction, with the reverse rate for the second reaction being two) produce the best fit.

6. A new parameter S, which is only valid at the equilibrium state, was introduced for the evaluation of the value of F_B of the intermediate. A value of 2.5 for S was selected for further evaluation of the data, since the value of S was not critical to the fit of the data.

7. It was found that a weighting factor to compensate for small values of log (τ_{eq}) improved the fit. The results were more than adequate to represent the data over a range of concentrations.

8. A study of the effect of parameters of the Kinetic-Elastic approach for the stress overshoot experiments is an essential part of the optimization of the various constants. The results of a parameter analysis provided the guidelines necessary for the optimization using an interactive computer graphics system.

9. The present Kinetic-Elastic theory shows excellent agreement with both steady state and transient data for the constant shear rate experiments. For the constant shear rate experiments, the percent standard deviation from the experimental data was approximately 6.13% for the equilibrium state and 1.58% for the transient experimental data. The prediction of stress overshoot at the shear rate of 21.48 sec^{-1} was excellent with a percent standard deviation of only 1.09%.

33

10. For the constant shear rate experiments, k_3 and k_6 have no significant effects within the range of 0 to 10 and 0 to 18, respectively.

11. The same elastic parameters and kinetic constants (except k_1) cannot be used to predict the results of the stress growth for all the constant shear rate experiments. The parameters and constants were a function of shear rate. The values of the parameters and constants were found to generally increase over the range from 3.4 to 21.5 sec^{-1}.

12. For the stress relaxation experiments, various reasonable assumptions for the initial conditions of the shear rate do not affect the elastic equation prediction. The normal assumption of no shear rate during the entire stress relaxation is adequate.

13. A combination of thixotropic viscosity and the elastic equation is necessary to account for the elastic contribution to the stress relaxation. An improved prediction of stress decay was obtained by modest changes of the kinetic constants. It was concluded that either the data available are not good or that the elastic equation of the theory for stress relaxation is not exactly correct.

14. The initial shear rate for the constant shear stress experiments should be less than $0.001 \ sec^{-1}$. The value of G_2 is much smaller than G_1 and is about 100 dyne/cm^2.

15. Cone angle and plate diameter have no significant effect on constant shear stress experiments.

16. The elastic modulus parameter cannot be considered a constant. G_1 is affected by the level of shear rate. G_1 for stress relaxation is not the same as G_1 for stress growth. G_2 has no significant dependency on shear stress for the constant shear stress experiments.

17. The present Kinetic-Elastic theory shows excellent agreement between the experimental and predicted shear strain data for the constant shear stress experiments. For the constant shear stress experiments the average percent standard deviation from the experimental strain data was approximately 1.80%.

Some General Conclusions are

1. A two-step reaction concept of thixotropy coupled with a changing viscosity basis for the elastic response shows excellent agreement with steady, constant shear rate, and constant shear stress experiments. The theory predicts well the stress overshoot at high shear rates and the unsteady shear rate variation at constant shear stress.

34

2. The present theory cannot use a constant value of viscosity (η_o) in the elastic equation to describe stress relaxation experiments. However, the value of η_t in the elastic equation with slightly modified values of the kinetic parameters predicts well the shear stress relaxation results.

G. Re-evaluation of the Basic Kinetic-Elastic Concepts

Although the data can be fitted with the two-step model there are too many adjustable constants. The need for two-step versus one-step kinetics is not satisfying and there are some inconsistencies in the theory. Thus, even though the fit is quite good, we made the decision to initiate a second phase of our data analysis in which we would retain the one-step model and try to determine why it does not fit the data adequately. First, we recognized the upper-Newtonian limit was not the solvent viscosity but rather something much larger. Second, only one term in one equation needed revision to satisfy a known limit. Finally, the viscoelastic constant, G_1 was probably not a constant but a function of shear rate which varies with stress level. We also recognized that the data base upon which all our conclusions were being based was not the best.

G.1 Re-evaluation of the Upper-Newtonian Viscosity Limit

As a result of further analysis of the kinetic theory, we discovered that there could be a more valid means of interpreting the upper Newtonian viscosity than has been used in the past. In general, we have taken the upper Newtonian viscosity as the solvent viscosity (in this case 0.09 poise). However, from molecular theory of viscous polymer solutions the upper Newtonian viscosity is probably much higher than this.

From the analysis by F. Bueche*, the upper Newtonian viscosity could be interpreted as shown in Figure 13. The upper Newtonian viscosity lies at the same molecular weight as the lower Newtonian viscosity, but on a line that is the extrapolation of the viscosity-molecular weight. This line is marked "A" in Figure 13.

For PMMA in DE':

$$M_{c, \text{ solution}} = (1.18/C) \, 10,500 \qquad (1)$$

where C is the concentration in gm/cm^3. At M_c,

$$= K_1 \, M_c^{3.4} = K_2 \, M_c^{1.4} \qquad (2)$$

The values of M_c and η_∞ (upper Newtonian viscosity) for the three solutions studied by Song are tabulated in Table IV. Note how different the values are from the solvent viscosity of 0.09 poise.

---

* Bueche, F., J. Appl. Phys. 26167, 738 (1955).

35
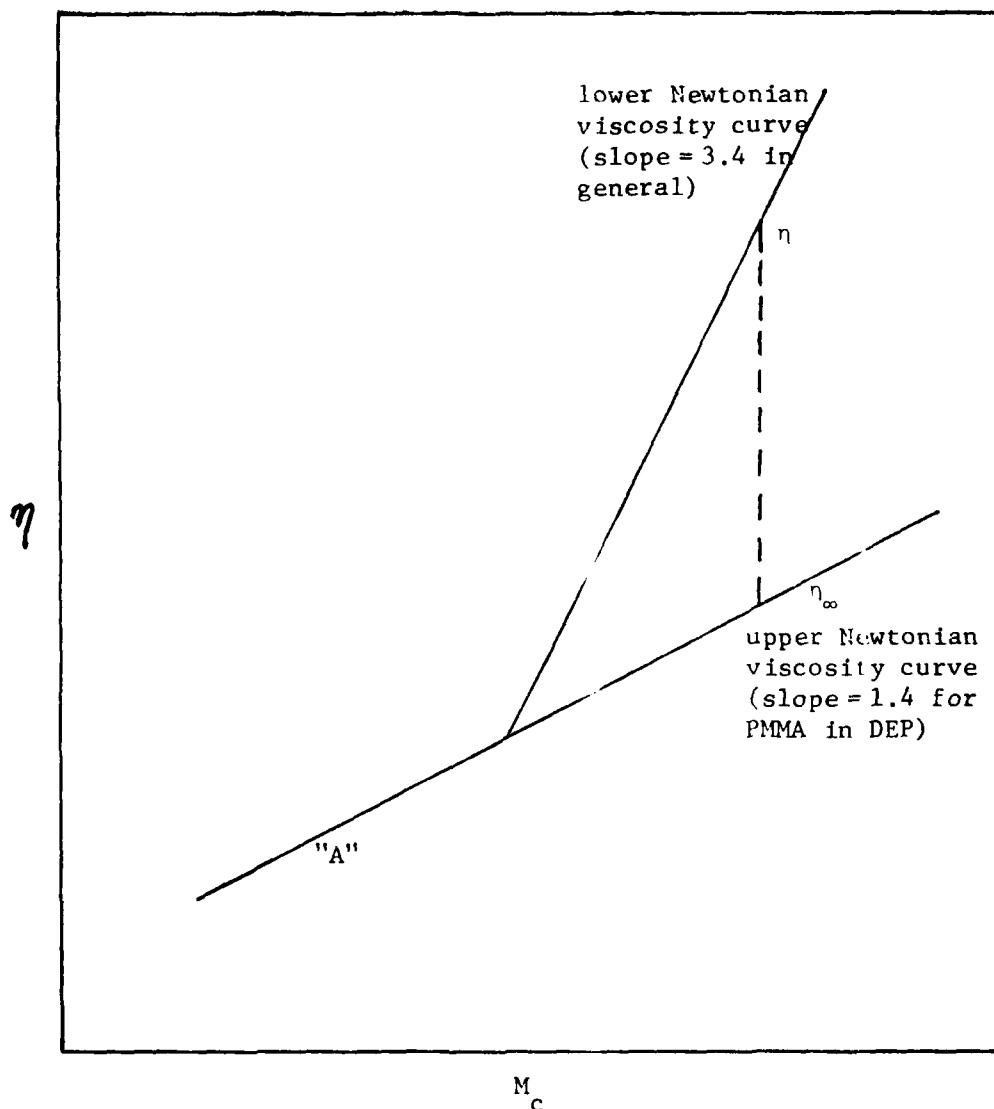
Figure 13. Viscosity versus molecular weight curve.

Table IV Molecular Weight Parameters for PMMA

	C(g/cm^3)	(poise)	M_c	K_1	K_2	η_∞(poise)
1	0.33	5000	3.76×10^4	4.38×10^{-5}	3.11×10^{-14}	533
2	0.387	30132	3.20×10^4	1.92×10^{-4}	1.87×10^{-13}	2335
3	0.443	200000	2.80×10^4	9.73×10^{-4}	1.24×10^{-12}	1.18×10^4

In spite of the vast difference in η_∞ in the old and new evaluation, there was no difference in our ability to fit the data. At this point we simply did not know if the problem was the data (Song's) or the theory; thus, we decided to also obtain a new set of polymer data.

G.2 Re-evaluation of the Theory for the One-Step Reaction

If one solves Eq. (9) of Appendix C of the proposal for η_t, one obtains

$$\eta_t = \tau / [\dot\gamma - (\tau/G_1)] \tag{3}$$

which in the limit of $t = 0$ is indeterminate and must be considered wrong. The viscosity is certainly not 0, 1, or ∞. If Eq. (9) of Appendix C is modified to Eq. (C) of Table I (with $G_2 = \infty$)

$$\tau + (\eta_o/G_1) \, \dot\tau = \eta_t \dot\gamma \tag{4}$$

as used by us earlier and used by Park (74), then,

$$\eta_t = [\tau + (\eta_o/G_1) \, \dot\tau] / \dot\gamma \tag{5}$$

which in the limit of $t = 0$ given $\eta_t = \eta_o$, is logically correct. We know that this equation cannot fit stress relaxation with G_1 constant. It is obvious that using G_1 as a constant was an error and that G_1 is actually a function of τ or F (i.e., time in our experiment).

Two approaches have been used for the systematic evaluation of the constants for this new version of the kinetic-elastic theory. Most of the evaluation is exactly the same as our previous endeavors but there are some differences associated with obtaining some of the constants. A series of programs was developed in order to obtain the best values of the constants. Parallel computations were made in order to ascertain that the programs and techniques were valid. Both the main University computer and a simulator

37

package available on our departmental VAX 11/780 system were used for this. The latter programs are quite short. The first program is used to adjust the p and K values from the equilibrium evaluation. This is exactly as was done previously (see Figure 14). The same program is further used to adjust the initial slope of the curve, $G_1(0)$, which gives the initial values for the elasticity parameter. Again, this is as previously done, except previously G_1 was assumed constant (see Figure 15). The values of p_1 and k_1 are roughly set by past experience. The second program uses initial rate theory for a more accurate evaluation of the constant p_1. With this new value of p_1, the values selected in the first program are checked. If they are inadequate, slight variations are made. With the constants now selected, the first program is used to establish k_1 more accurately so that the thixotropic stress intersects the experimental stress at the maximum point. This is a new fitting technique (see Figure 16). The same program is then used to see if k_3 (taken as zero) can help the shape of a curve near equilibrium. So far it has been zero. Having now established all of the constants, the third program can calculate G_1 as a function of time so as to provide the final fit. Once G_1 has been evaluated for all of the runs, the values can be plotted as a function of shear stress or F (conversion of the thixotrophic structure) to establish the universality of the parameter. It is specifically this procedure, just outlined, that will be described in more detail after the obtaining of new polymer data is described.

H. New Polymer Data

H.1 Problems

As previously reported, the R16 unit had considerable noise that made it difficult (impossible?) to establish the initial slope for stress growth. This slope provides the value of G_1 from the kinetic-elastic theory. Most of the noise was removed through instrument repair and adjustment by Mr. Spooner of Sangamo. Recent tests on polymethylmethacrylate show that the noise has been considerably reduced but is still large enough to introduce more error than desired in obtaining G_1. Running the instrument in reverse and using the piezoelectric crystal in tension eliminated the noise to a satisfactory level.

To obtain improved data for testing of our viscoelastic model for polymer solutions, it was necessary to obtain a complete set of equilibrium and transient data using the Weissenberg Rheogoniometer. Prior to the experiment, a calibration curve of torque versus voltage was found and was linear. The gap size transducer and the analog recorder were also calibrated. None of the calibrations are presented here but can be found in our monthly reports. Problems were encountered with the range switch of the charge amplifier; thus, the units were returned to the manufacturer for reconditioning and calibration.

In spite of all our efforts we still were not satisfied with the output. New data sets were taken using the LSI-11/VAX 11-780 data acquisition system (see Figure 17) and as noted by the arrow the noise problem still existed but was not extreme. Thus, the noise was still coming from somewhere in the gear system.

38

SHEAR RATE, ETA0, ETAINF, P, AND K ARE
11.03000 79500.00000   0.10000   1.49130 0. 262 E-08
P1, K1, K3 AND G1 ARE
0.10000E-03   0.21920E+00   0.00000E+00   0.95480E+05
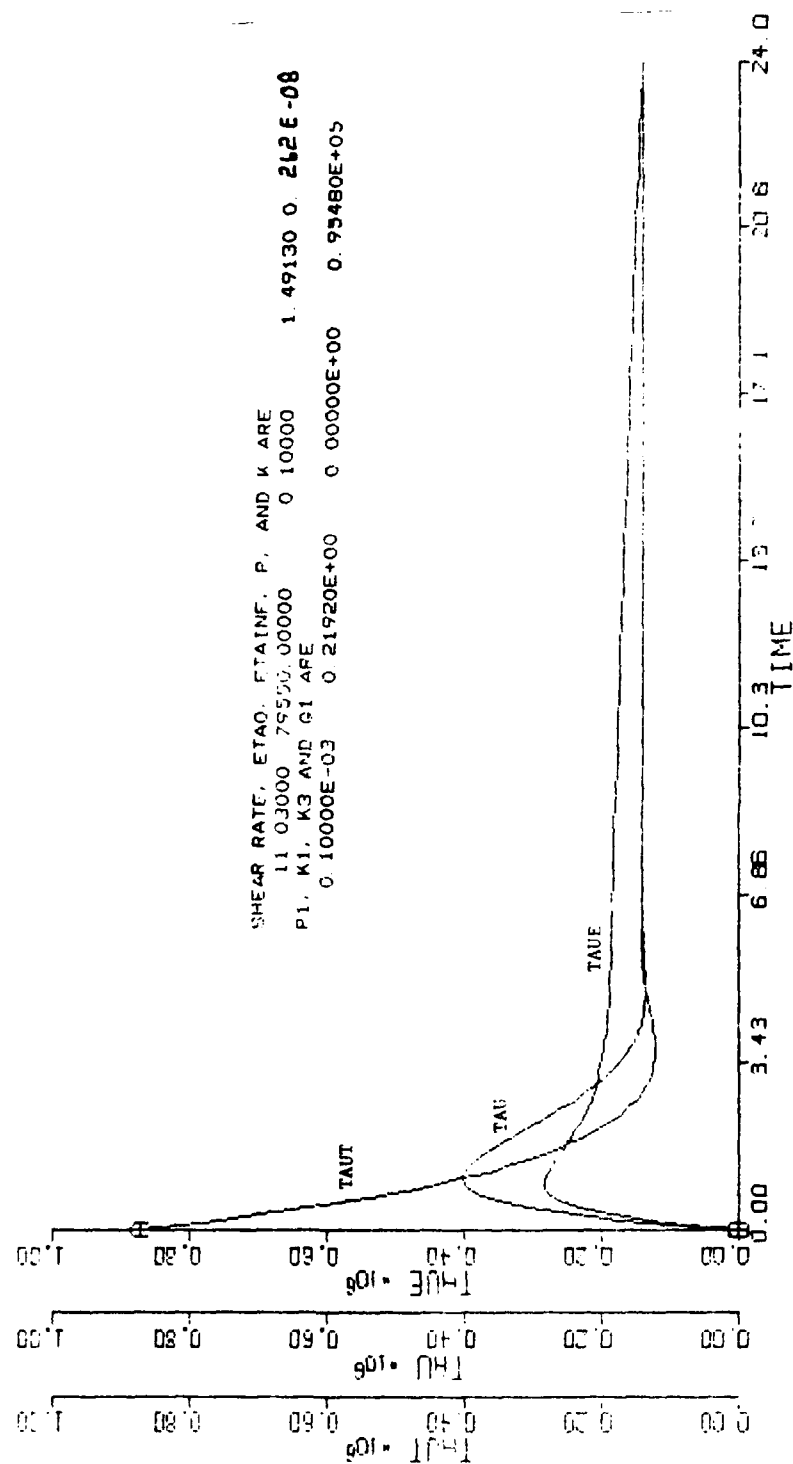
Figure 14. Experimentally measured stress (TAUE), calculated Thixotropic Stress
(TAUT), and Stress (TAU). Using first guess values.

39
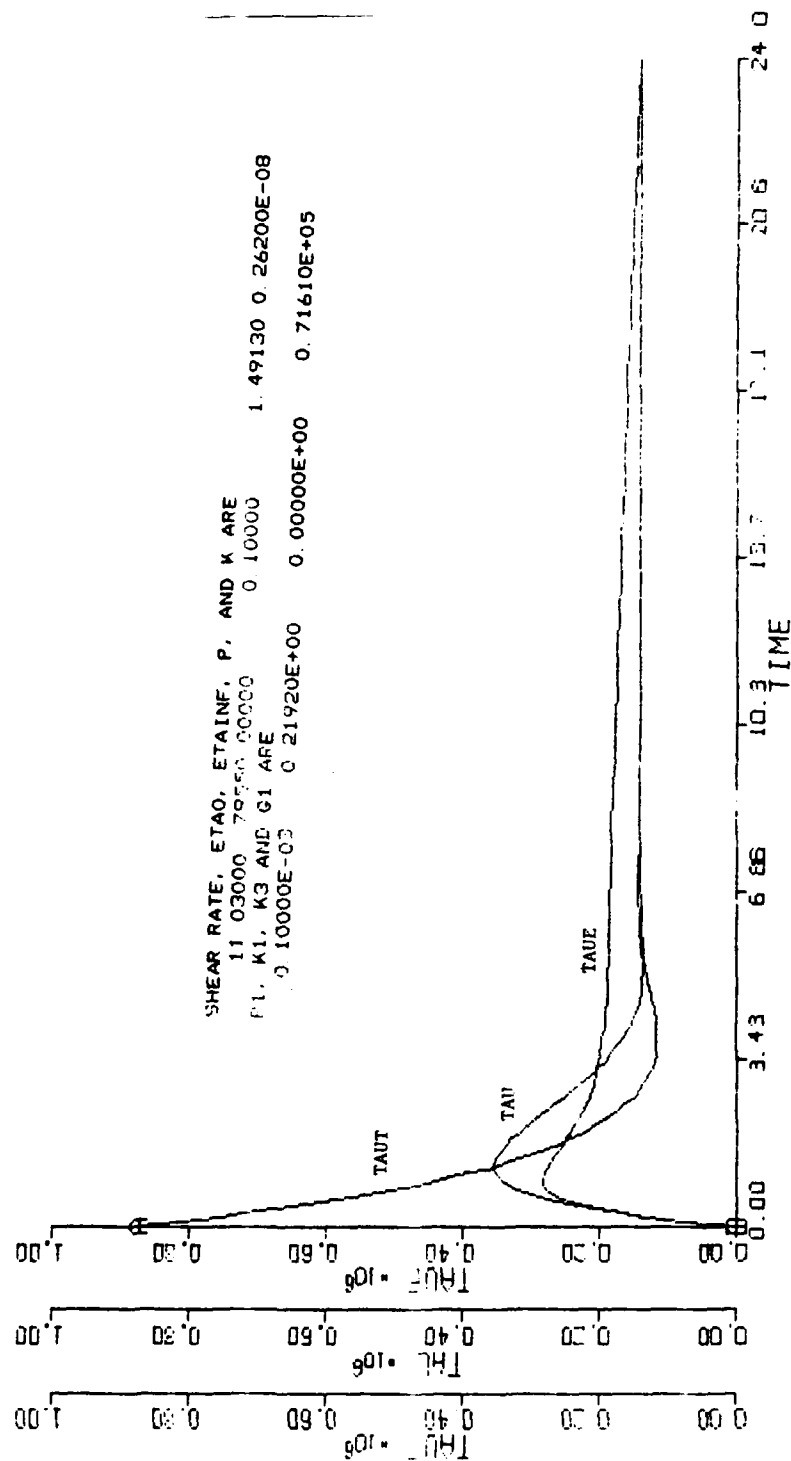
Figure 15. Experimentally measured stress (TAUE), calculated Thixotropic Stress (TAUT), and Stress (TAU). Using adjusted G_1 value.

40

Figure ... ...imentally measure stress (TAUE), calculated Thixotropic Stress ... ... and Stress (TAU). Using adjusted G_1 and k_1 values.
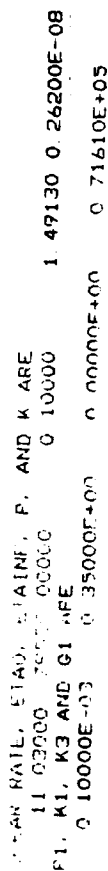
41
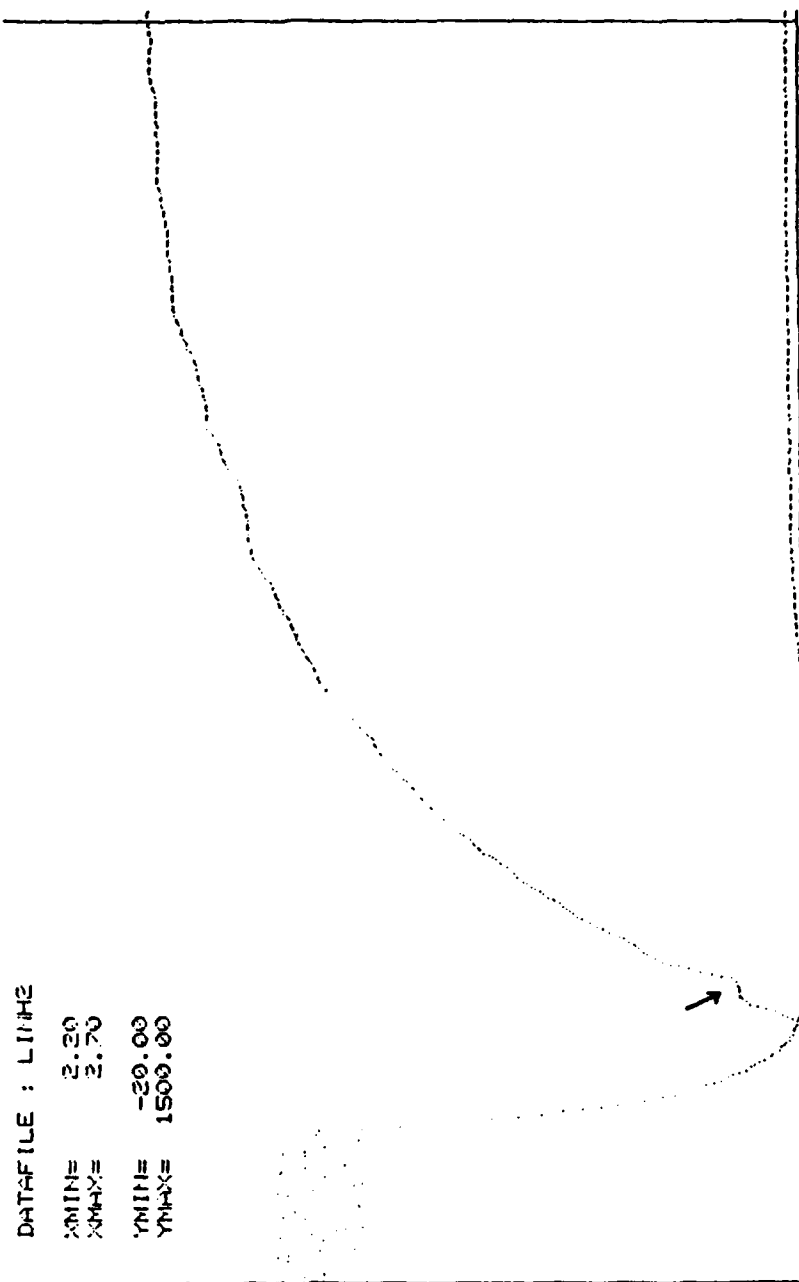
Figure 17. Data with gear movement problem.

DATAFILE : LINK2

XMIN=   2.20
XMAX=   2.70

YMIN=   -20.00
YMAX= 1500.00

When the R-16 is operated in the forward rotation mode, the time transient curves are not smooth as shown in Figures 17 and 18. The cause was traced to worm gear movement and could be completely eliminated by operating in the reverse rotation mode as shown in Figures 19 and 20.

To test the effect of the torsion bar on noise, the 3/8" and 1/4" torsion bars were used. The heavier bar reduced the signal and had no effect on the noise. The ratio of reduction in signal is almost the same as the ratio of the calibration of k_T's of the two torsion bars, as provided by the manufacture. In order to obtain the larger signal, the 1/4" torsion bar was used for further data gathering.

H.2 New Polymer Data

New equilibrium data were taken at various shear rates. The double logarithm plot of viscosity (poise) and shear rate (sec^{-1}) is shown in Figure 21. The behavior of the curve is consistent with that obtained in previous studies. The viscosity at zero shear rate is estimated to be 1.80×10^4 poise.

New sets of time dependent shear stress data for the 38.5% solution of PMMA in DEP were obtained using the Weissenberg R-16 and the VAX 11/780 data gathering systems. The data include shear stress growth and relaxation at constant shear rates over the range of shear rates from 0.11 sec^{-1} to 69.3 sec^{-1}. The shear stress curves for the shear rates of 1.103 and 11.03 sec^{-1} are shown in Figures 22 through 25. The adequacy of these data should be clear. Furthermore, no filtering has been used on any of the data.

I. Detailed Comparisons of Modified Theory and New Polymer Data

In order to present the results in their proper context, we will review the theory as it is now being used. The kinetic-elastic model developed in this laboratory involves two facets. One is the kinetic model for thixotropic change of the viscoelastic material, where the rate of change of a material structure is described by a rate concept. The other is the elastic model and can be described by a modified version of Oldroyd's viscoelastic equation.

The thixotropic kinetic theory can be expressed by the following equation:

$$A \underset{k_2}{\overset{k_1}{\rightleftharpoons}} 2B \tag{6}$$

Utilizing the homogeneous kinetic reaction concept, a simple kinetic equation can be obtained (as shown in Appendix C of the proposal)

$$\frac{d(CF)}{dt} = k_1'(CF)^1 - k_2'[C(1-F)]^2 \tag{7}$$

where F is the fraction of the thixotropic fluid structure unchanged, k_1', k_2' are forward and reverse reaction constants, and C is the concentration of the polymer solution.

43
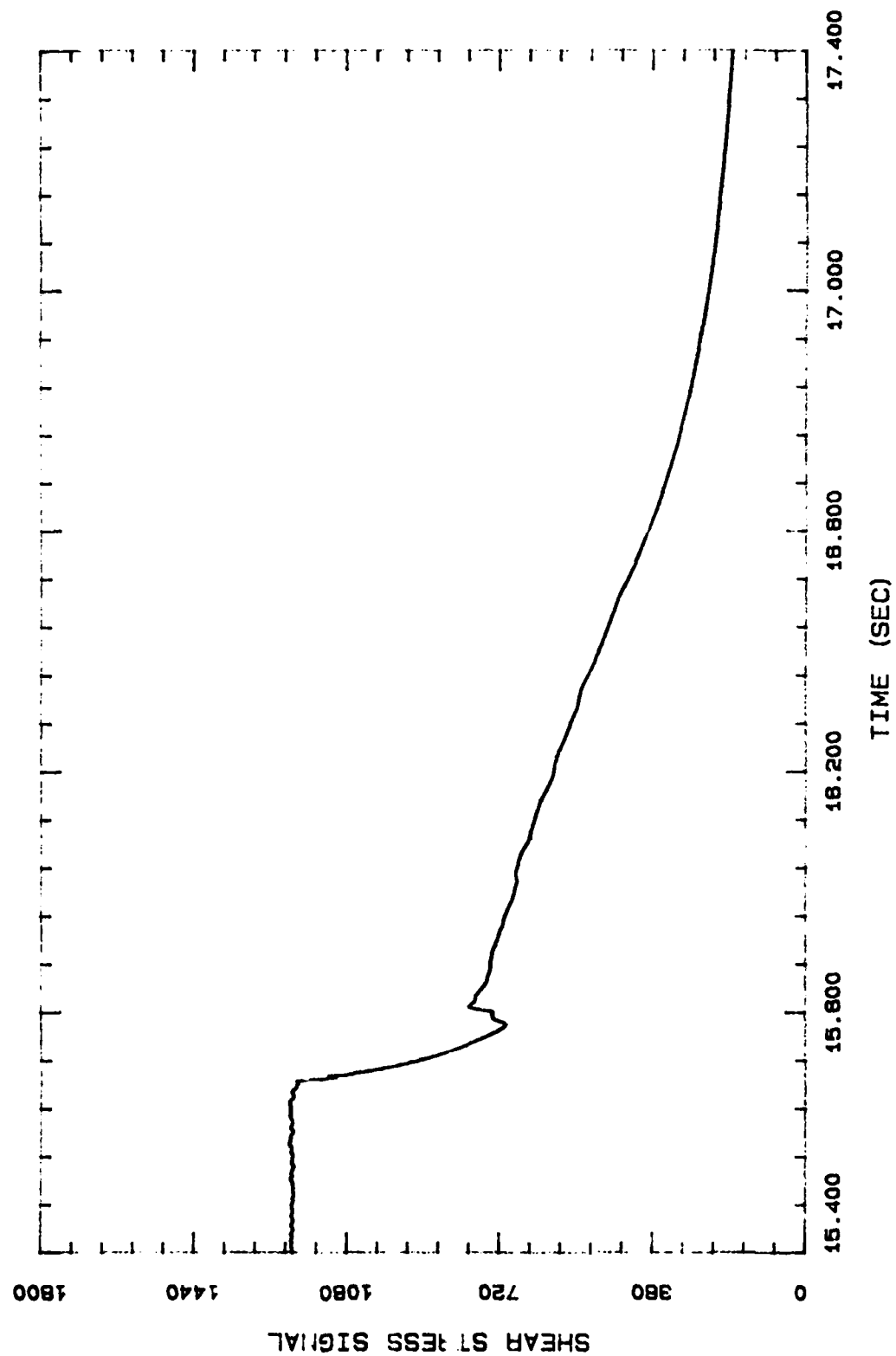
Figure 18. Stress relaxation with dip in relaxation curve (after forward rotation).

44
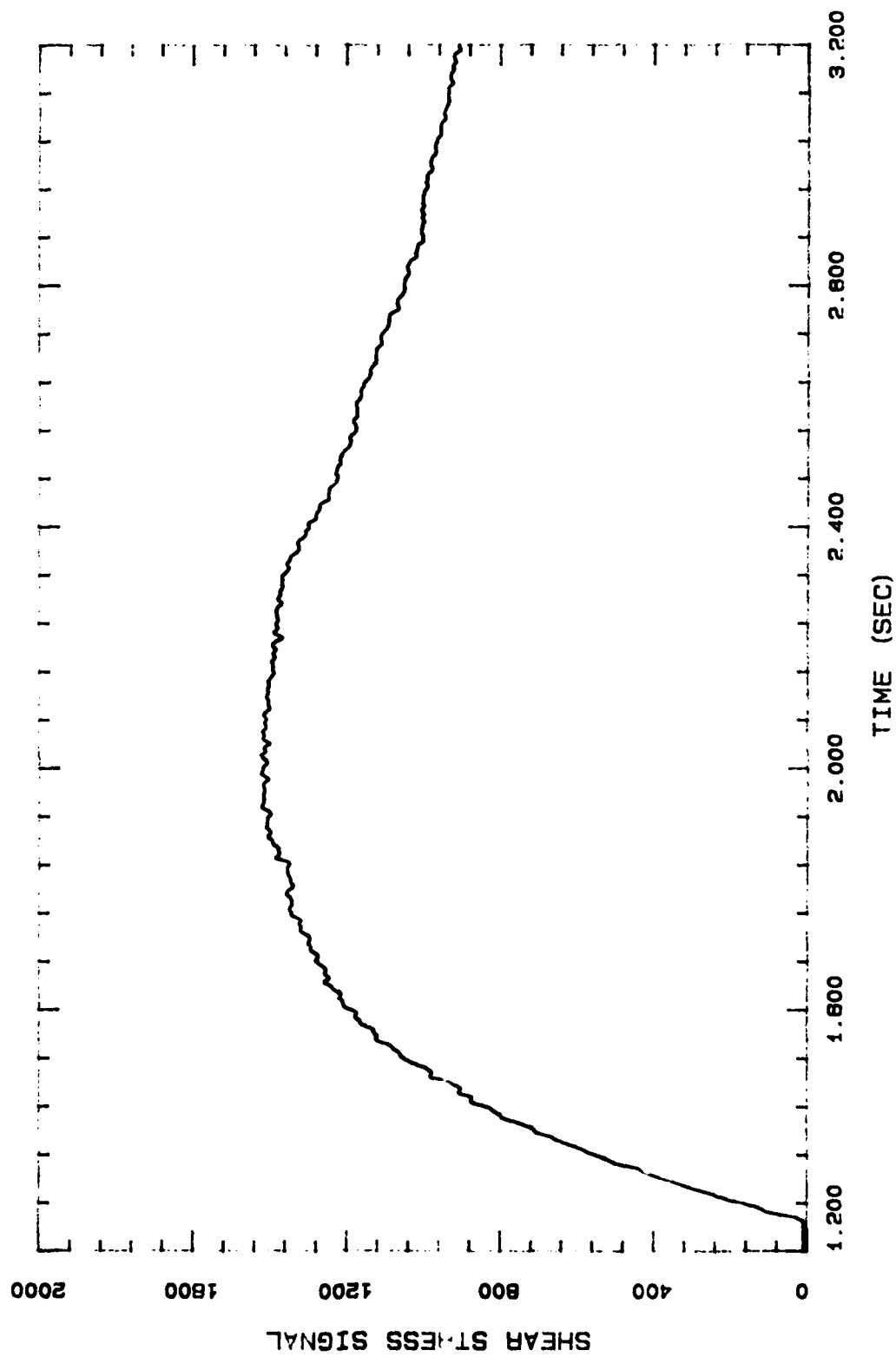
Figure 19. Stress growth using reverse rotation.

45
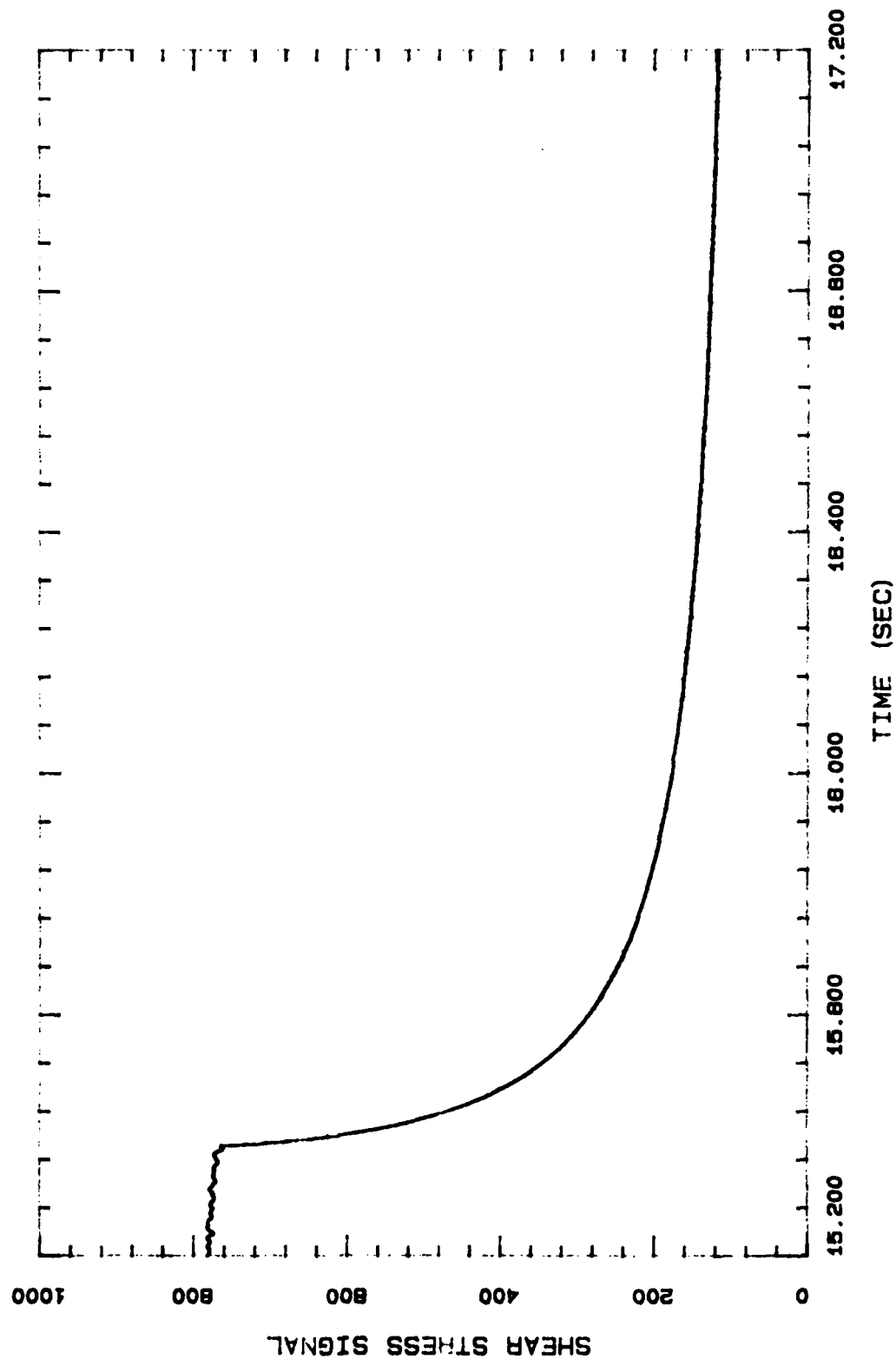
Figure 20. Stress relaxation after reverse rotation using 1/4" torsion bar.

46
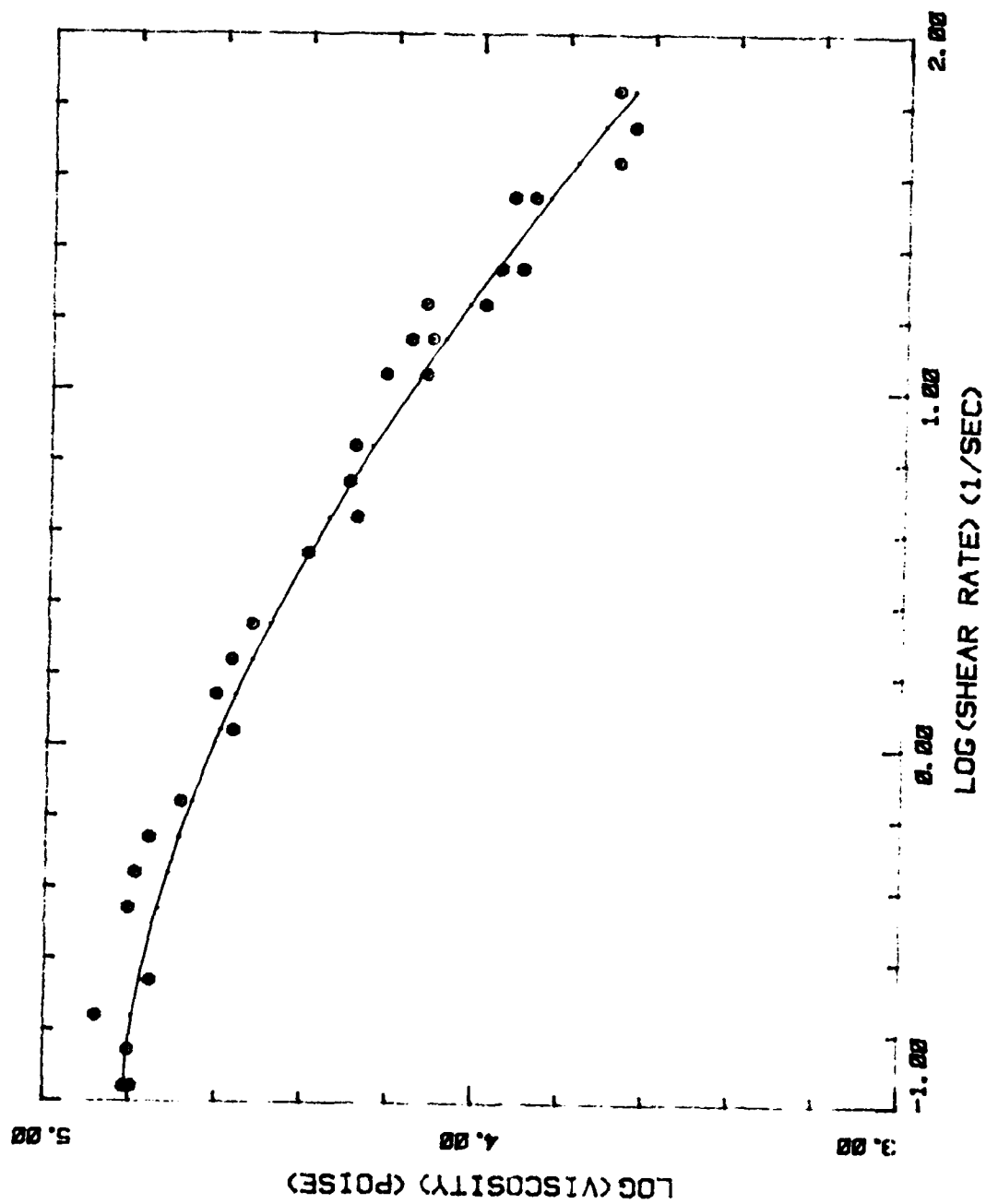
Figure 21. Log of viscosity versus log of shear rate 38% PMMA in DEP.

47

SHEAR RATE: 1.103
TIME RANGE(SEC) =   2.00   12.00
DATA RANGE(VOLT)=   0.00   2.50
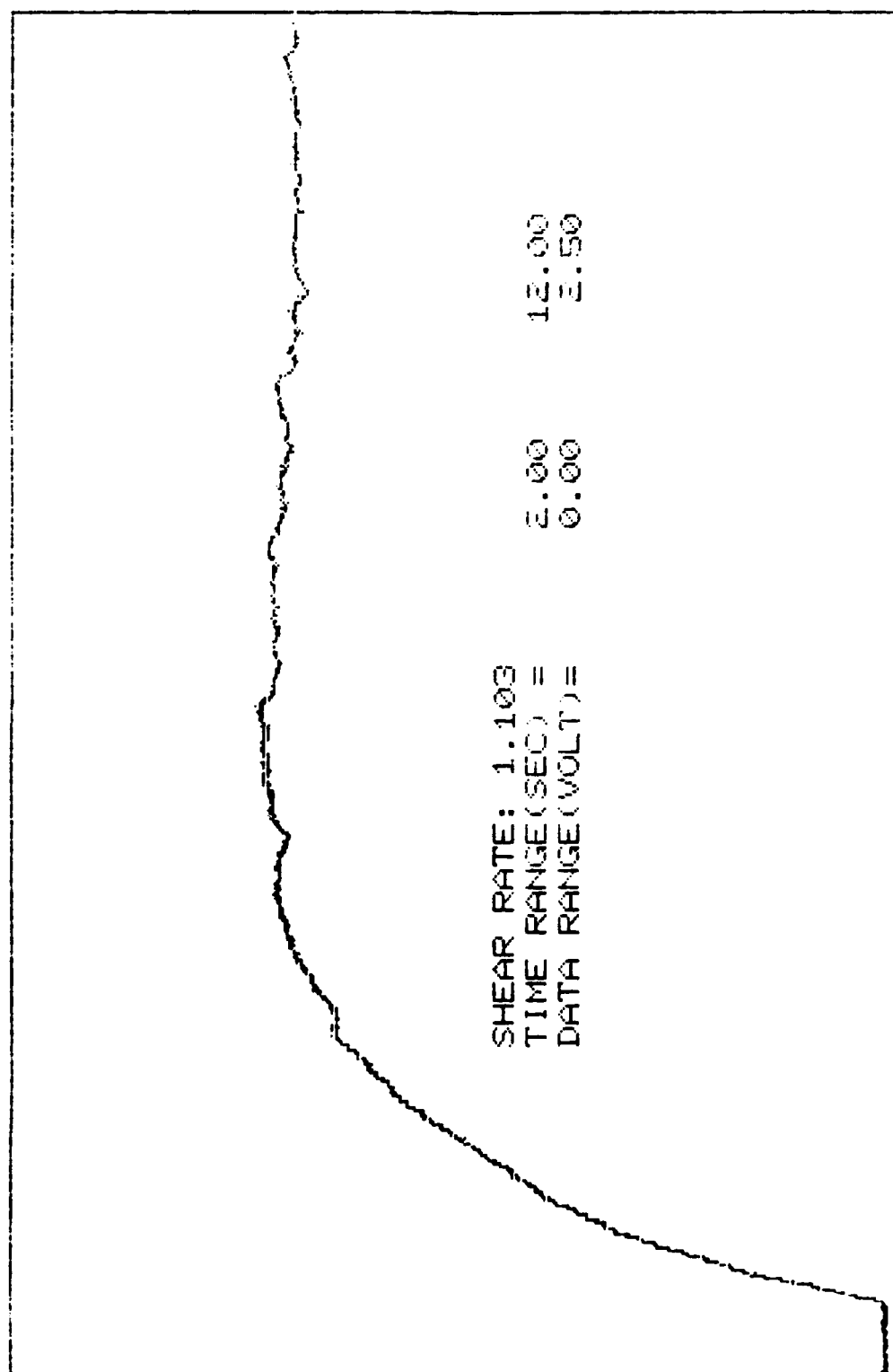
Figure 22. Shear Stress Growth (1.103 sec^{-1}).

SHEAR RATE: 1.103
TIME RANGE(SEC) =   2.00   13.00
DATA RANGE(VOLT) =   -0.10   2.00
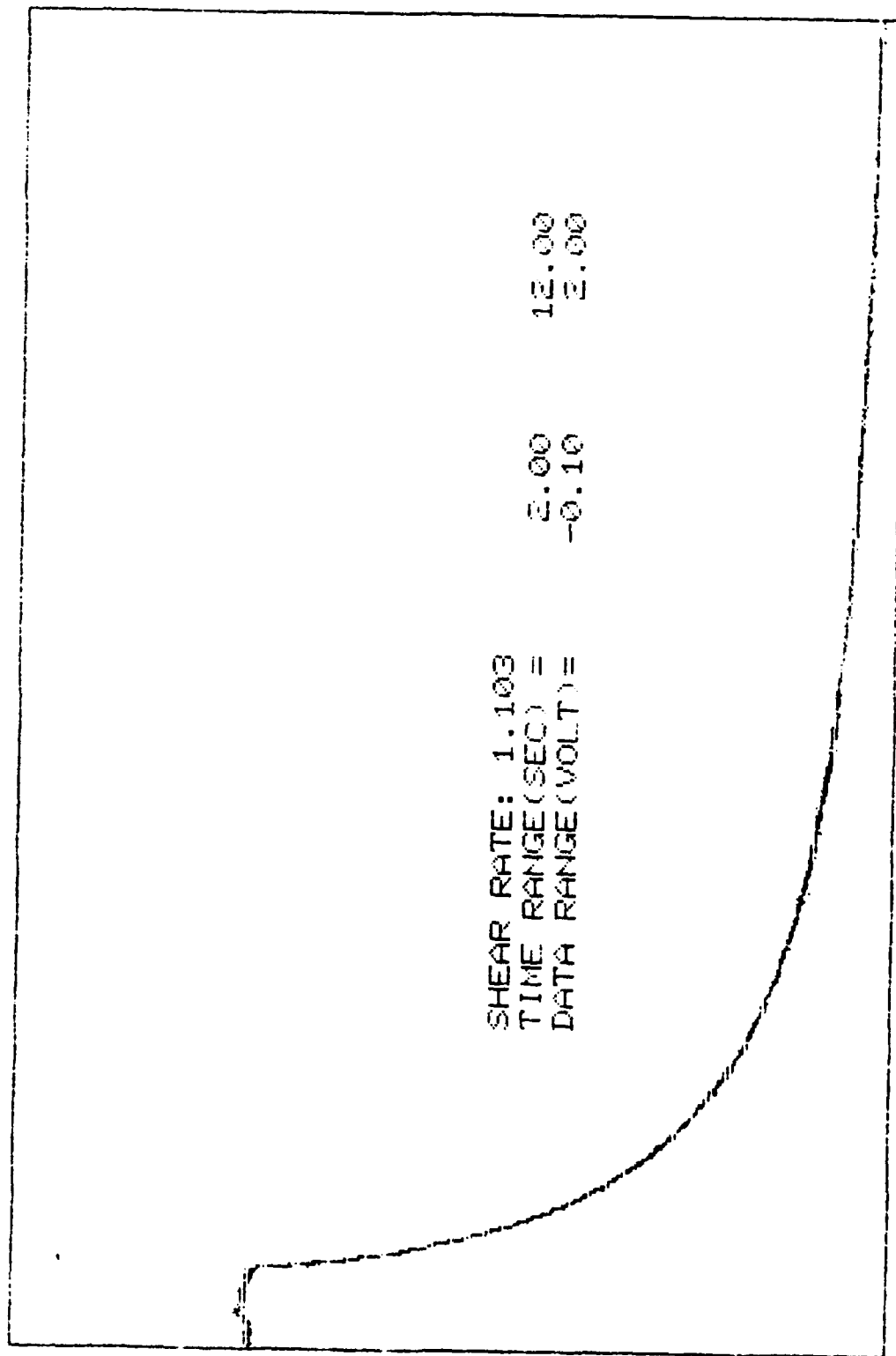
Figure 23.   Shear Stress Relaxation (1.103 sec^{-1}).

49

SHEAR RATE: 11.03
TIME RANGE(SEC) =   5.00   15.00
DATA RANGE(VOLT)=   0.00   5.00
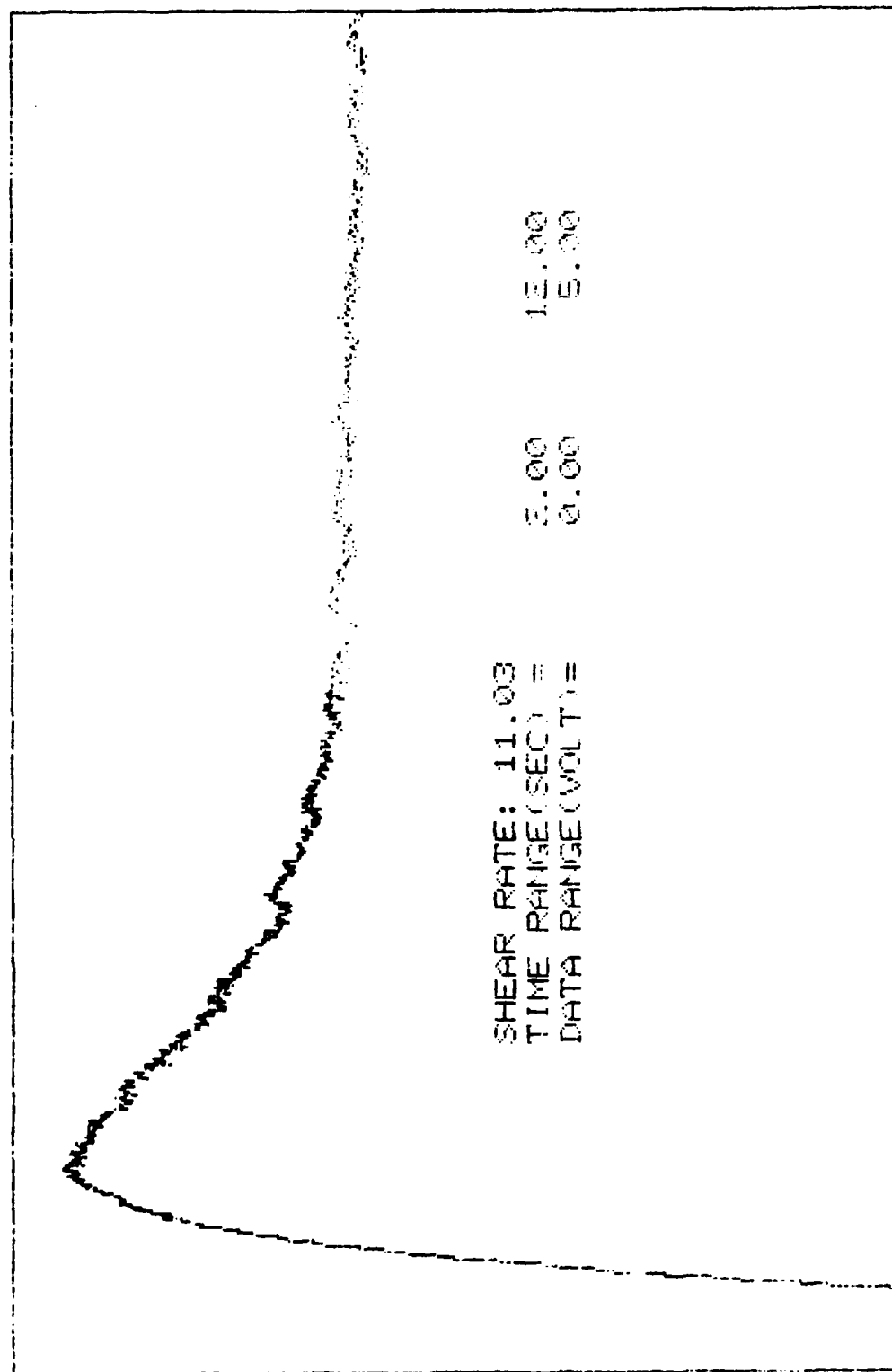
Figure 24. Shear Stress Growth (11.03 sec^{-1}).

SHEAR RATE: 11.03
TIME RANGE(SEC.) =
DATA RANGE(VOLT)=

2.00   12.00
-0.50   3.50
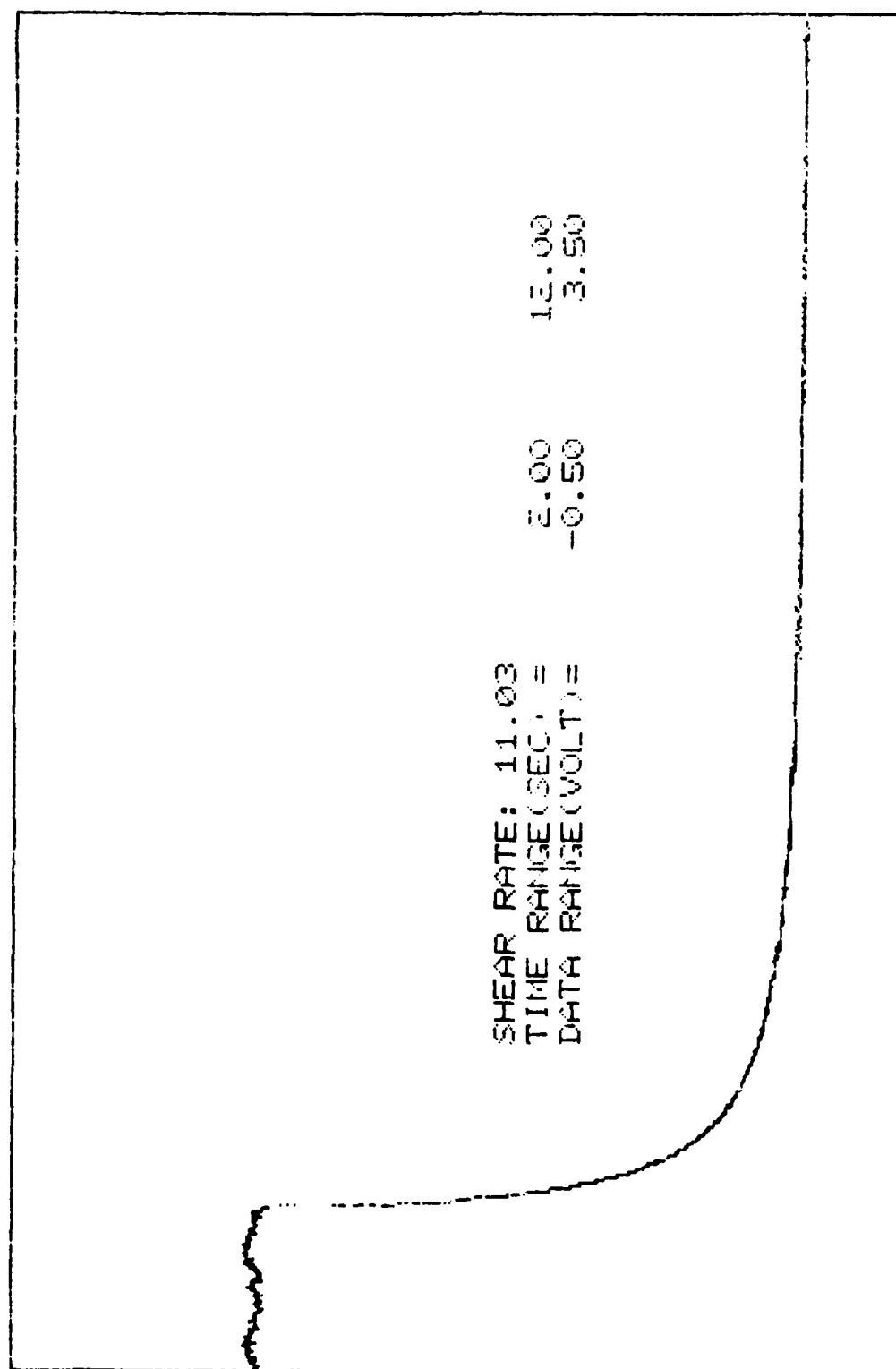
Figure 25. Shear Stress Relaxation (11.03 sec^{-1}).

51

The function of the fraction of the thixotropic fluid, F, is further defined as

$$F = \frac{\eta_t^a - \eta_\infty^a}{\eta_o^a - \eta_\infty^a} \tag{8}$$

the viscosity term; η_t, is the thixotropic structural viscosity. η_o and η_∞ are the viscosities at zero shear rate and infinite shear rate, respectively. η_o and η_∞ were 79,950 poise and 4000 poise, respectively, for this specific polymer solution. The constant a was selected to be (1/3.4) from the evidence (Fox & Allen) that the zero shear rate viscosity, η_o, is proportional to the 3.4 power of the molecular weight.

The rate constants k_1 and k_2 in Equation (7) are functions of shear stress, τ, and temperature. The functional forms can be expressed by Equation (9) and (10) as

$$k_1' = k_1 \tau^{p_1} \tag{9}$$

$$k_2' = k_3 + k_2 \tau^{p_2} \tag{10}$$

For simplification, k_3 in Equation (10) is taken as zero in this model analysis. At equilibrium (or steady state), the forward rate and backward rate are equal, i.e., $d(CF)/dt = 0$ from Equation (7). The equilibrium constant can be expressed in the following form:

$$\frac{C(1 - F_{eq})^2}{F_{eq}} = \frac{k_1'}{k_2'} = \frac{k_1}{k_2} \tau_{eq}^{p_1 - p_2} = K_{eq} \tau_{eq}^P \tag{11}$$

where F_{eq} and τ_{eq} are the F and τ at equilibrium conditions. Based on the equilibrium experimental data, K_{eq} and P were found to be 1.313×10^{-10} and 1.864, respectively. The values of k_1 and p_1 in Equation (9) can be calculated from the initial rate change, i.e., the rate at zero time. p_1 was found to be 6×10^{-3} for all of the experimental data.

The modified Oldroyd viscoelastic equation can be expressed by

$$\tau + (\eta_o/G_1) \dot{\tau} = \eta_t \dot{\gamma}$$

.as was shown earlier in section G 2 and where τ and $\dot{\tau}$ are the shear stress and its first derivative, $\dot{\gamma}$ is the shear rate, and G_1 is the elastic modulus proposed to be a function of τ or F (i.e., time in our experimental) for our kinetic-elastic model.

Figure 26 shows the calculated G_1 values as a function of time from one set of experimental data. It may be that G_1 is a simple function of F, as is η_t [Eq. 8]. Note the similarity of G_1 versus t to such plots as η or G' versus $\dot{\gamma}$. The G_1 function can be expressed mathematically by Equation (13)

$$G_1(t) = G_1(Ast) + G_1(0) \exp [-G_1(TC) (t - t_{cut})] \qquad (13)$$

where $G_1(Ast)$ is the asymptometric value of G_1 function,
$\quad$ $G_1(0)$ is the G_1 value at zero time,
$\quad$ t_{cut} is the time which G_1 starts to decay, and
$\quad$ $G_1(TC)$ is the decay constant started at t_{cut}.

The best fitting kinetic and elastic constants for the kinetic-elastic model at various shear rates are listed in Table V. Examples of the calculated curves and experimental curves for the individual shear rates are shown in Figures 27 through 29. Each curve in this initial fit was optimized individually so that the various constants would be representative and any dependency on shear rate level could be determined.

As can be seen from the examples given, the comparisons are excellent. However, some of the constants tabulated in Table V do vary with the shear rate. Both $G_1(0)$ and $G_1(Ast)$ are functions of (log $\dot{\gamma}$) as expected, with $G_1(0)$ increasing and $G_1(Ast)$ decreasing with an increase in $\dot{\gamma}$. The k_1 value increases linearly with $\dot{\gamma}$. P and P_1 are constant. The other terms [K_{eq}, t_{cut}, $G_1(TC)$] vary, but do not correlate with $\dot{\gamma}$.

J. Implications for Further Work on Polymer Systems

There is an alternate evaluation that should be made. This is to use those terms that did not correlate with shear rate [K_{eq}, t_{cut}, $G_1(TC)$] as constants at their average values and re-evaluate the terms that are a function of shear rate. This should give a clearer and more consistent correlation for $G_1(0)$, $G_1(Ast)$, and k_1.

The second investigation involves a modification of the theory to ascertain whether or not using k_{eq}, t_{cut}, and $G_1(TC)$ as constants will have any effect. The modification is associated with a change in the viscoelastic part of the theory. Currently, although G_1 is computed as a function of time, it has been taken outside of the differential and computed as a difference. This can be illustrated best by observing the equation that was used

$$\tau + (\eta_0/G_1) \dot{\tau} = \eta_t \dot{\gamma} \qquad (12)$$
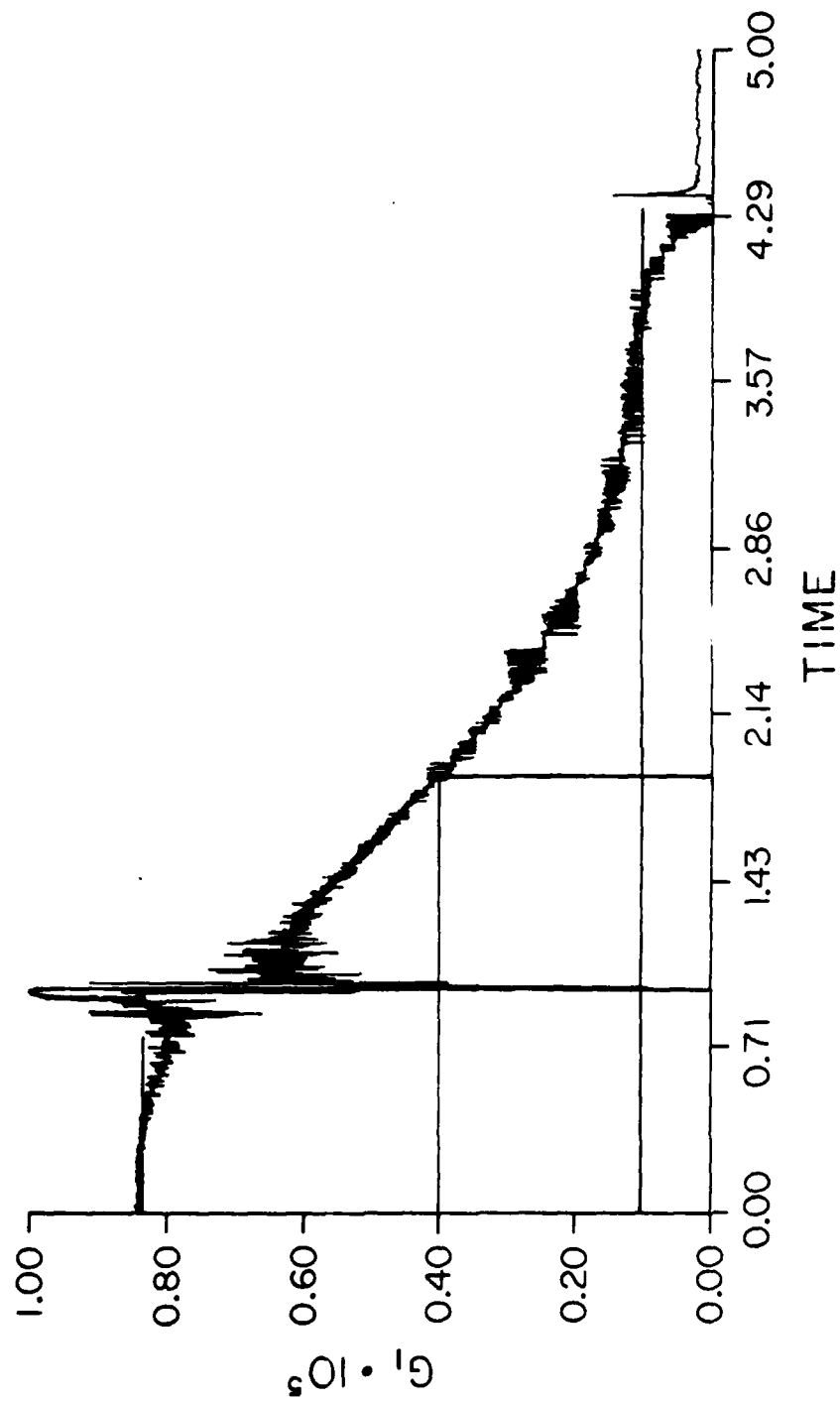
Figure 26. G_1 Function Versus Time

54

Table V $p = 1.864$, $P_1 = 0.006$

Shear Rate (sec^{-1})	$\tau_{eq}(\frac{dyne}{cm^2})$	K_{eq}	$G_1(0)$	$\dot{k}_1$	t_{cut}	$G_1(TC)$	$G_1(AST)$
0.3475	2.222×10^4	5.5×10^{-11}	3.2×10^4	independent	20.0	---	---
0.5513	3.162×10^4	4.5×10^{-11}	4.15×10^4	independent	20.0	---	---
1.103	4.072×10^4	2.07×10^{-10}	3.75×10^4	0.15	3.0	0.5	10000.0
1.388	5.622×10^4	9.6×10^{-11}	5.0×10^4	0.135	2.0	0.5	4600.0
1.743	6.508×10^4	7.7×10^{-11}	4.95×10^4	0.145	3.0	0.5	10000.0
2.19	7.339×10^4	5.5×10^{-11}	4.59×10^4	0.162	20.0	---	---
4.383	8.405×10^4	2.25×10^{-10}	5.72×10^4	0.59	2.0	0.5	3000.0
6.95	1.35×10^5	2.55×10^{-10}	5.415×10^4	0.632	2.0	0.65	3800.0
11.03	1.539×10^5	1.90×10^{-10}	8.25×10^4	0.650	1.0	1.0	1900.0
17.43	2.3316×10^5	7.02×10^{-11}	9.4×10^4	0.80	0.6	0.6	1500.0
21.9	1.90×10^5	2.20×10^{-11}	8.37×10^4	1.32	1.0	0.7	2000.0
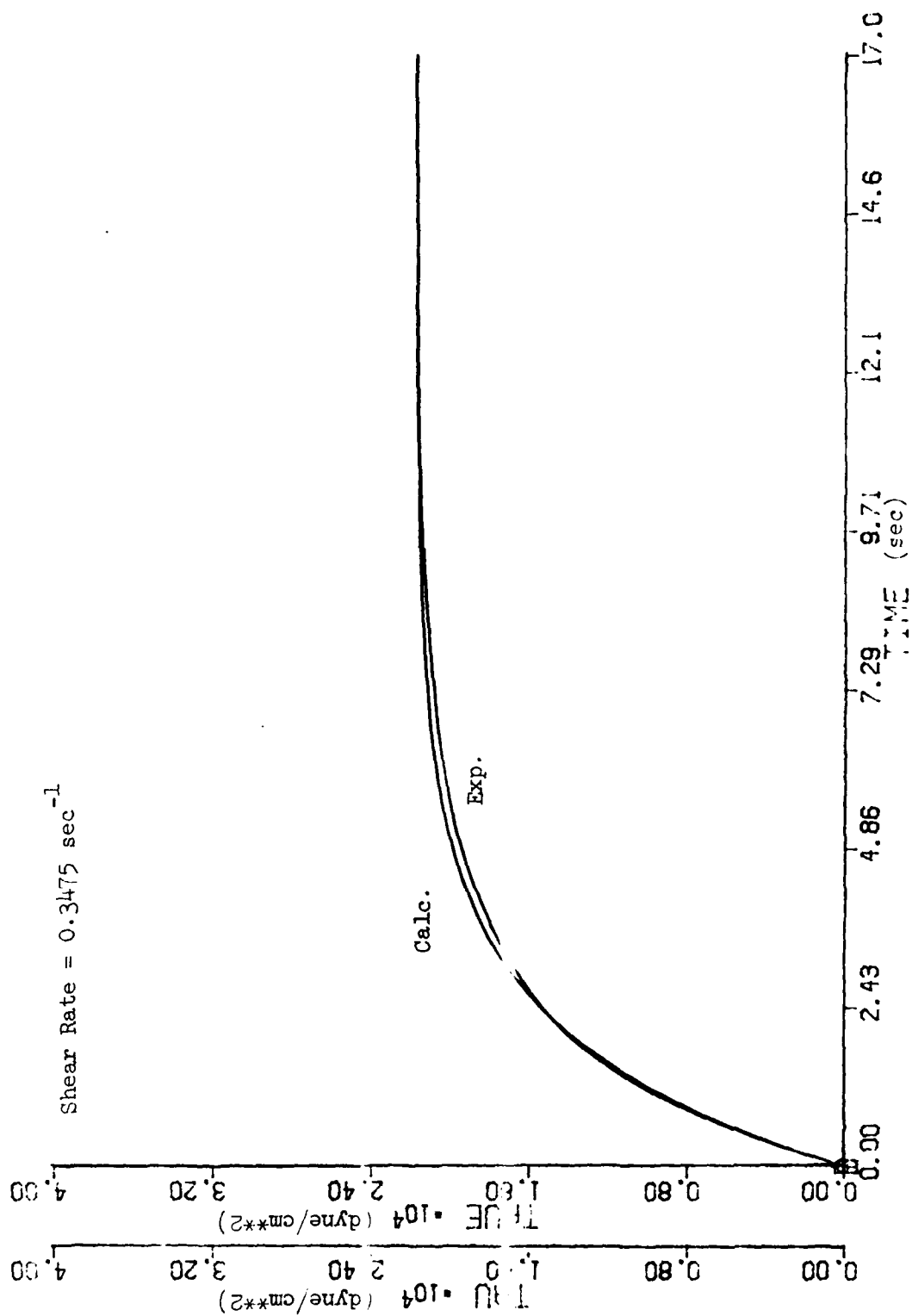
Figure 27. Stress Development Versus Time

Shear Rate = 0.3475 sec^{-1}

Calc.

Exp.

TIME (sec)

TRUE ·10^4 (dyne/cm**2)

T$_{1}$U ·10^4 (dyne/cm**2)

Figure 28. Stess Development Versus Time

57
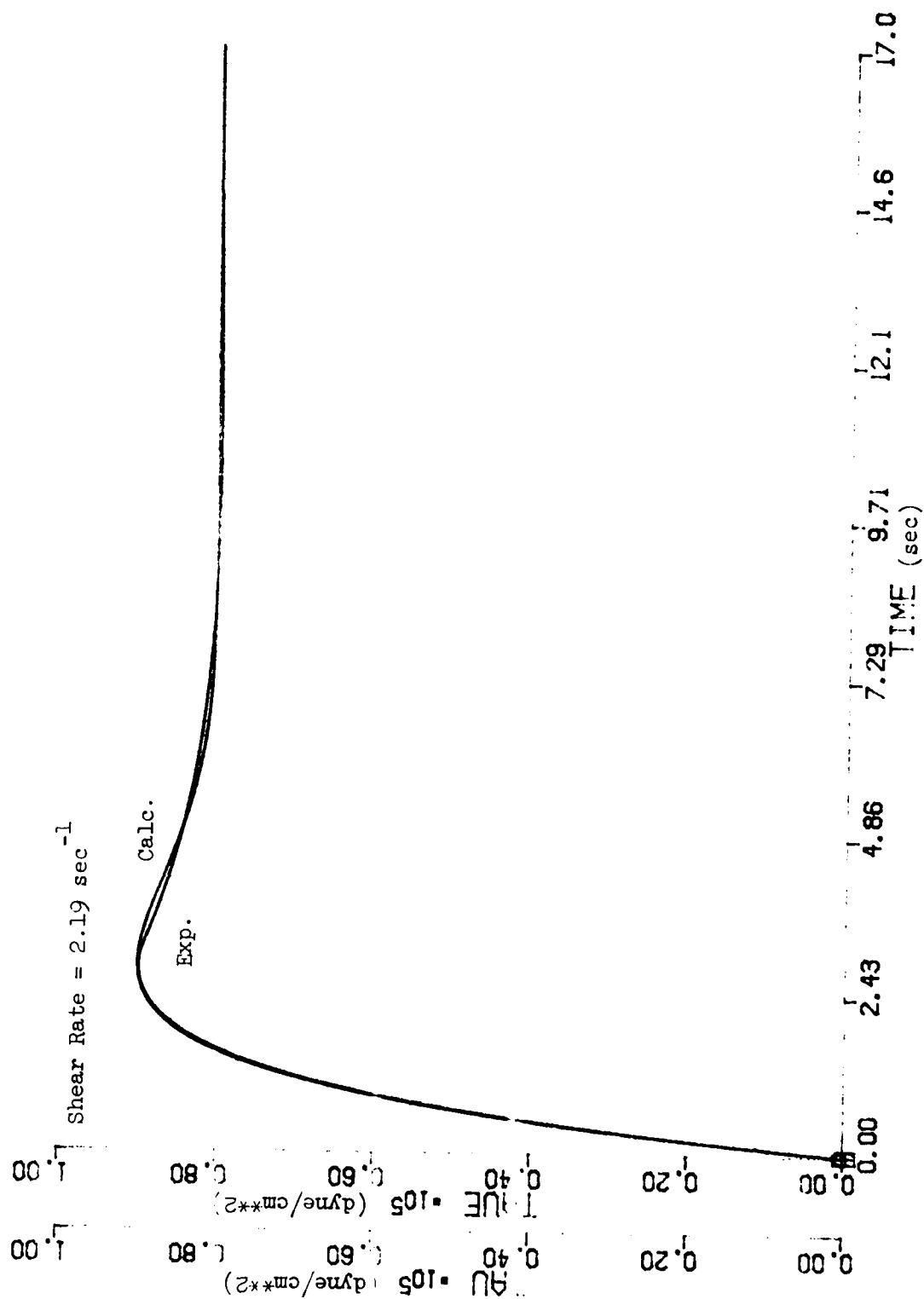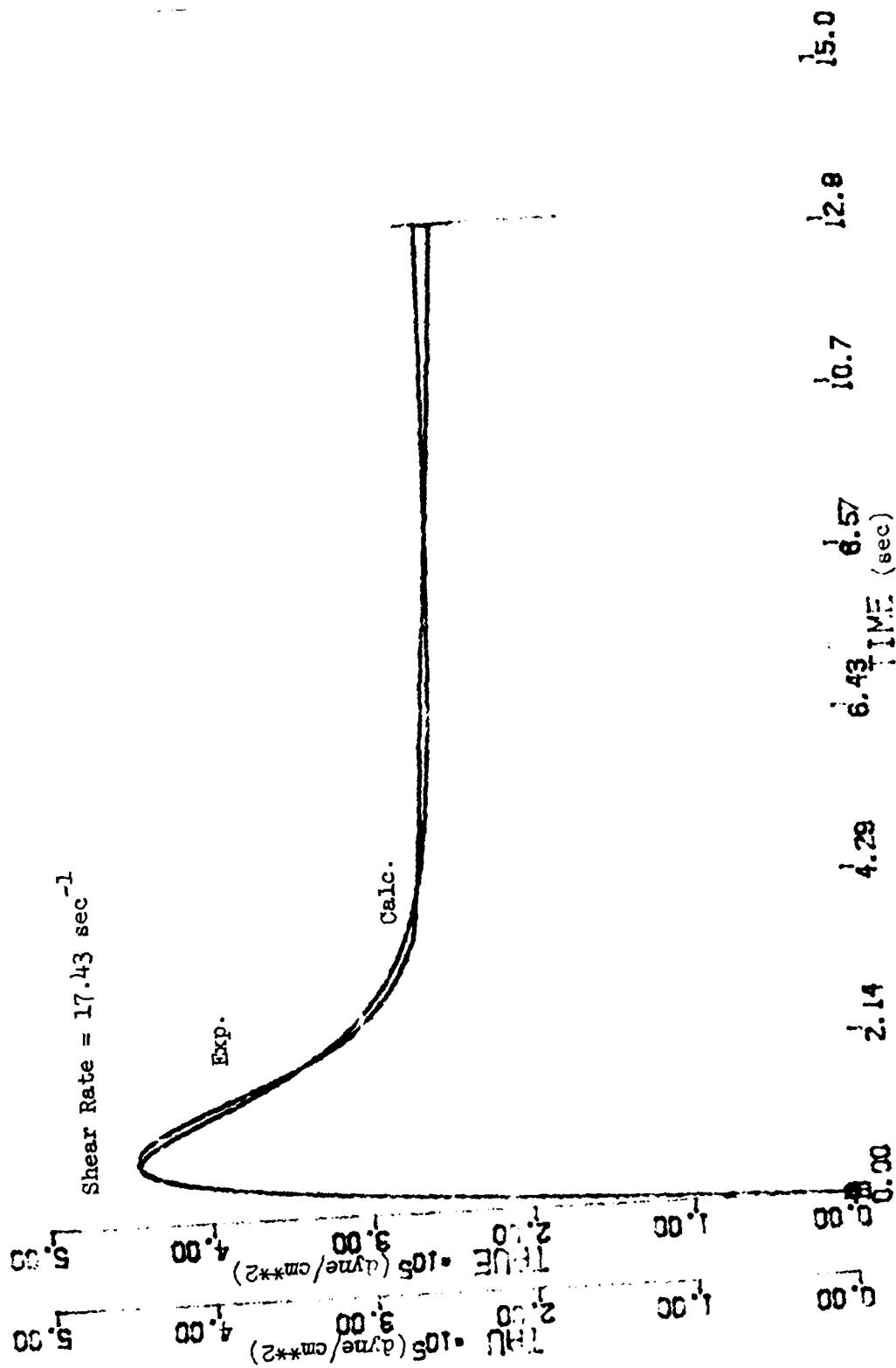
Figure 29. Stress Development Versus Time

and the following equation, which would be more accurate

$$\tau + \eta_o(\tau'/G_1) = \eta_t \dot{\gamma} \qquad (14)$$

that is, G_1 is now varying with time and should be inside the differential:

$$(\tau'/G_1) = d(\tau/G_1)/dt \qquad (15)$$

At this stage it may well be that the older formulation which seems logically more correct could be utilized, i.e.,

$$\tau + \eta_t(\tau'/G_1) = \eta_t \dot{\gamma} \qquad (16)$$

where η_t is used in place of η_o. This substitution could give more reasonable variations of k_1 and G_1. In addition, it could aid in fitting stress relaxation data.

These equations [(14) and (16)] can be tested by our simulation with minor changes, although the use of eq. (16) will introduce a trial and error iteration for the G_1 time function.

These formulations might improve the logical nature of the variation of the elastic constants in the forward reaction rate; however, they will not improve the already excellent fit that has been obtained by allowing G_1 just to be a variable. Consequently, this further work can not only help us zero in on the most logical theory, but could help in improving the fit for stress relaxation. Finally, we would like to extend the best analysis to the treatment of oscillatory data.

59

II.   SLURRY MATERIALS

All of the proposed work on the preliminary slurry formulations
supplied to us by Sun Tech and Exxon (via Wright-Patterson AFB) have been
completed.   In future work we would repeat these tests for the selected
final formulations and extend the measurements to oscillatory
conditions. We also want to further investigate the specific reasons
for the non-Newtonian behavior by using combined visual and rheological
unsteady state measurements. Such results should allow us to improve
the logical formulation of the kinetic-elastic theory for the
description of these materials.

A.   Equipment and Procedures

A.1   Carbon Black Samples

The samples used in this study were suspensions of microsize carbon
black particles dispersed in JP-10 solvent. JP-10 is a pure hydrocarbon
which is used as a jet fuel. It has higher combustion energy than the
current commercial jet fuel, JP-4, but it is more expensive due to its
purity. Carbon black is added to JP-10 to increase its density, and
hence, the amount of energy available per volume.

Four different carbon black suspensions were used in this study:
Exxon 708-61, Sun Tech 809-995, Sun Tech 339-919, and Sun Tech 839-988.
The basic physical and chemical properties of JP-10 and the carbon black
slurries are shown in Table VI. As can be seen, the carbon black
loading is about 50 weight %, or 0.33 volume fraction based on 1.86 and
0.93 specific gravities for carbon black and JP-10 respectively. The
particle size is approximately 0.1 m. The small particle size and high
loading level generally result in a yield stress. Since we were
interested in materials with a yield stress, more emphasis was put on
the yield materials: Sun Tech 839-988 and Exxon 708-61.

Due to the high vapor pressure of the solvent, evaporation occurs
causing the slurry to skin over at the edge of the plate and cone. The
change in solvent content not only changed the measured viscosity, see
Figure 30, but also made the measurement difficult. A Mooney type
system, which combines a cylinder with a cone and plate, was used to try

61

Table VI
Physical and Chemical Properties of JP-10

Property	JP-10
Formula	$C_{10}H_{16}$
Molecular Weight	136
Heat of Combustion (BTU/gallon)	142,115
Flash Point, F	130
Freezing Point, F	-130
Boiling Point, F	360
Autoignition Temp., F	474

Physical and Chemical Properties of Slurries

Sample Number	708-61	839-988
Composition		
Carbon Black type	United SL90	SAF
Carbon Black size, nm	103	70-80
Carbon, Wt. %	51	50.4
Dispersant Type	W	ST-107
Dispersant, Wt. %	2	2.0
JP-10, Wt. %	47	47.6
Heat of Combustion, Calc (BTU/gallon)	168,300	173,700
Density gm/ml @20 C	1.24	1.234
Particle Size, μ by FOG		
Average	<6	-
Largest	13	10
Yield Stress of 25 C	-	220.0

Sun Tech 839-919
Files: SUN901, SUN905, SUN906, SUN907

⊟
▲] Different Runs
⊙
+

VISCOSITY (poise)

SHEAR RATE (sec^{-1})
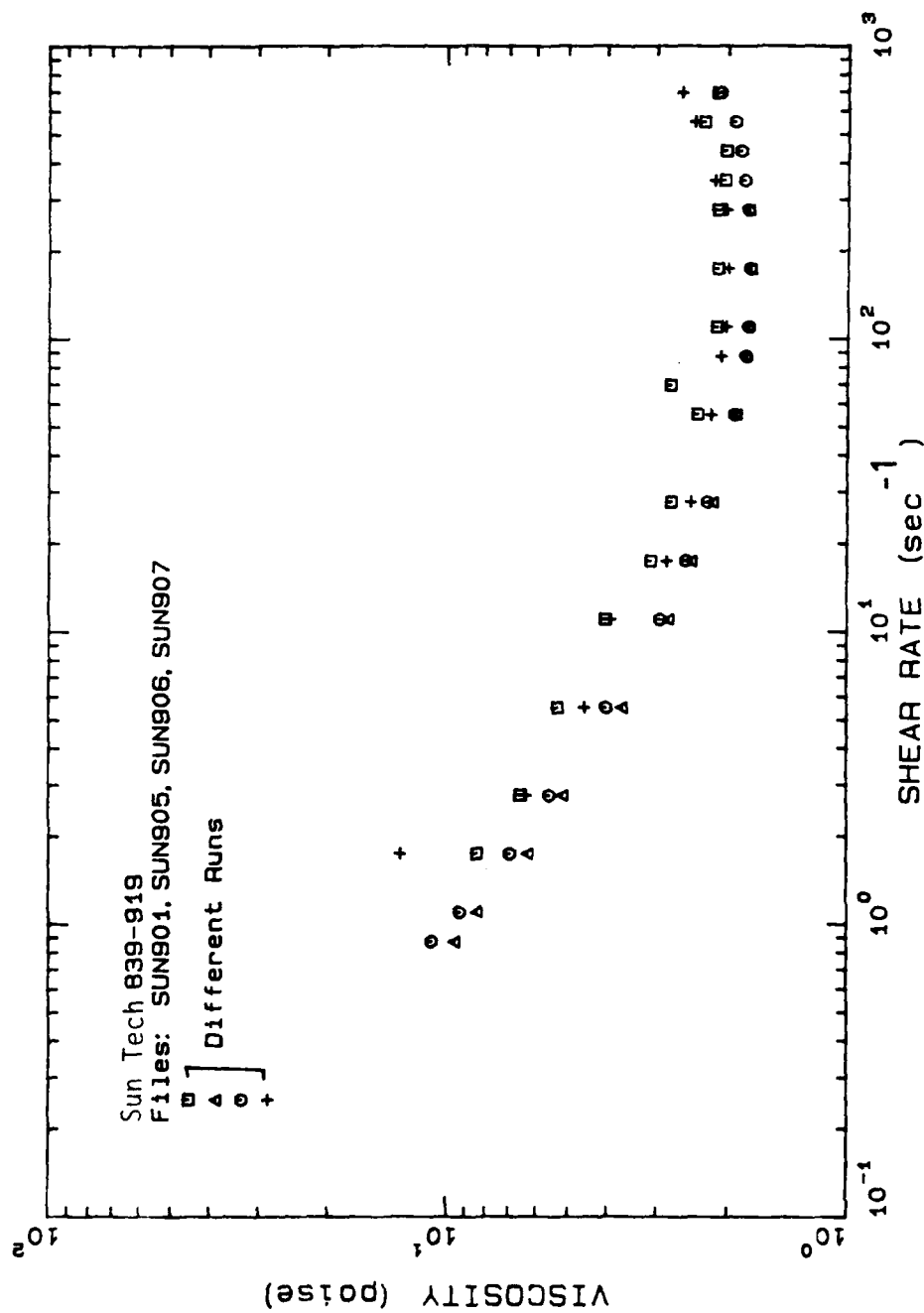
Figure 30. Viscosity Change Due to Skinning During Measurement.

63

to solve the skinning problem. A guard ring was placed on the top of the cylinder to minimize the surface area that is exposed to air. Thus, it should have minimized the vaporization of solvent from the slurry. Unfortunately, the setup did not stop the solvent, JP-10, from evaporating. There was a small space between the guard ring and the outer cylinder, so that the skinning occurred in this space. This not only caused difficulty in the outer cylinder's rotation, but also affected the motion of the torsion head. This approach was abandoned and new methods were investigated. Evaporation could be avoided by keeping the sample in a saturated vapor pressure environment. Since this procedure would be difficult to use with the R-16, another approach was tried. Attempts were made to cover the sample with non-miscible solvents to prevent the JP-10 from evaporating. Water was tried first, but due to gravity, the water mixed with the slurry. Next, pure JP-10 was used for the same purpose.

The slurry sample was poured until the cylinder was filled to the free surface at the edge of the plate. Then, JP-10 was carefully put on the top of the sample. In this way, evaporation was confined to the JP-10, which was not under shear. The excess slurry sample and JP-10 had negligible effect on the measured torque which was tested by using the above setup with Newtonian fluids of 3.5 Poise and 9.85 Poise as the primary samples. The error introduced was less than 4%, which is within the experimental error. Thus, in all runs JP-10 was carefully placed on top of the slurry as a coating to prevent the skinning problem. The mixing between JP-10 and the sample took place by molecular diffusion only. Mass transfer by diffusion was negligible during the measurement. This was checked by measuring the equilibrium viscosity for samples resting between 0.5 to 6 hours. As shown in Table VII, the equilibrium viscosity at a shear rate of 27.6 sec^{-1} was independent of the resting time with the JP-10 coating on the sample.

At low temperatures, condensation of water on the sample was a more serious problem than skinning. Especially when the temperature is lower than the freezing point of water, 0 C, it is important to isolate the sample from moisture. During the resting period, a plastic cover was used to cover the sample, which prevented both condensation of water and vaporization of the sample. Inert nitrogen gas was slowly bled into the chamber to keep the plate and cone in an inert environment. This worked quite satisfactorily, except at the top of the chamber which was open to the atomsphere. However, this condensation did not interfere with the measurements.

64

Table VII Equilibrium Shear Stress at $\dot{\gamma}$ =27.6 sec^{-1}

rest time (hr)	shear stress(dyne/cm**2)
0.5	49.23
1.0	48.13
2.0	48.53
4.0	50.21
5.0	48.12
6.0	49.40

A.2   Rheometer   Auxiliaries

In this stu.., all the data were obtained on a Weissenberg Rheogoniometer, R-16, and its supporting electronic devices. The measuring system can be divided into three subsystems: the rheometer itself, signal conditioning equipment, and data processing facilities, as shown in Figure 31.

A.2.1   Weissenberg Rheogoniometer

The Weissenberg Rheogoniometer, R-16, is a plate and cone rheometer which provides a constant shear rate in the gap. The R-16 has been modified and updated. The current version has the capability of measuring the shear viscosity, normal stresses, dynamic viscosity, and the more complex situation of superposition of rotation and oscillation. In this section, a brief description of the R-16 is given, with an emphasis on the newer facilites. More detailed descriptions of the R-16 have been provided by Denny(81), Lee(82), and Song(11) and the operation manual(83). The rheometer has three major parts: the drive unit, the plate and cone section, and the torsion head.

The drive units consist of two motors and two speed controls. A three phase synchronous motor and a gear box are used to control the rotational speed of the bottom plate at 50 selected output speeds. A DC motor, fixed gear box reducer, and SCR control are used to set the frequency of oscillation. The instrument allows torsional testing in oscillation as well as in steady rotation, and is capable of measuring not only viscosity but also elasticity, dilatancy, thixotropy, etc. In addition, by using a magnetic clutch to start or stop rotation, measurements as a function of time (transient response) can be obtained. The response time of the instrument is small, less than 0.01 sec(75).

The plate and cone are the heart of the measurement, and the sample is placed between them. The bottom plate can be moved by the drive units in steady rotation and/or in a sine-wave oscillation. The moment is transferred from the bottom plate to the cone through the sample is measured by the torsion head, which can be used to determine the shear stress, and thus viscosity. The Weissenberg Rheogoniometer can cover rates of shear between 7×10^{-4} sec^{-1} to 9×10^{3} sec^{-1} by changing the rotational speeds and angles of the cones. In this study a 7.5 cm plate and a 58 minute 46 second (nominal 1°) cone were used.

Figure 31. R-16 Rheometer and auxiliaries
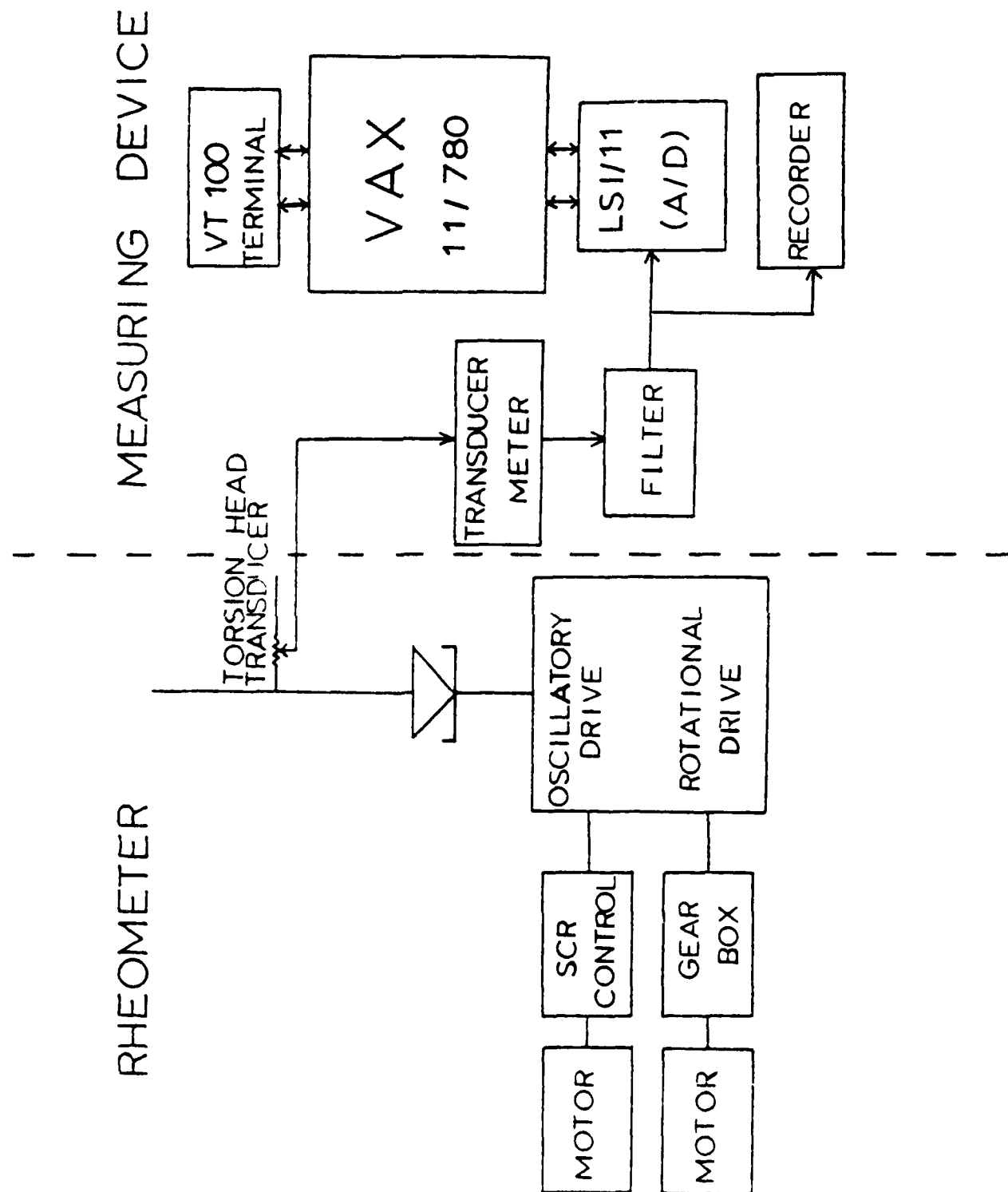
The shear rate range varied from 3.54×10^{-3} to 10^3 sec^{-1}.

The torsion head includes an air bearing, torsion bar, and transducer. The air bearing is used to provide frictionless rotation for torque measurement. The torsion bar and transducer are used to determine the torque and thus the shear stress. Torsion bars with diameters of 1/16" and 1/8" were used depending on the magnitude of torque.

Because of the improved stiffness of the system, the piezoelectric crystal load cell has proven to be a better force sensor than the LVDT (linear variable differential transformer), as shown by Brodkey et al.(6), and by Crawley and Graessley(84). However, the torque generated by the slurries was too small to be detected by crystals. Instead, a LVDT, type F51TM made by Boulton Paul Aircraft Ltd., was used to measure the torque. It can produce an electrical output proportional to the displacement of a separate movable core. This transducer has a high sensitivity for the measurement of small displacements up to 0.1×10^{-3} inch with reasonable accuracy.

A.2.2   Signal Conditioning Equipment

The signal conditioning subsystem consists of a transducer conditioning meter (type EP597, B.P.A. Electronics) and an analog filter. The output signal from the transducer is fed to the conditioning meter. The proper range of the meter is selected to amplify and transform the signal so as to have an output voltage within $\pm10V$ to meet the requirements of the A/D converter for data acquisition. The output voltage from the meter then passes through a filter to remove the carrier frequency. A simple RC filter with a cutoff frequency of 2000Hz is used.

68

A.2.3   Data Processing Facilities

The data processing system includes a microprocessor (Digital Equipment Co., LSI 11/02 with an RTP-A/D converter), a VT100 graphics terminal(Digital Engineering), chart recorder(Offner Electronics Inc.), and minicomputer (Digital Equipment Co. VAX 11/780) with all of its supporting devices. The new data acquisition system was a major change from previous equipment (6,75), and has greatly improved the data acquisition and data processing. With the on-line minicomputer, data can be taken fast and accurately. Data analysis also becomes easier because of the ready access to a fast computer with a high level of interactive graphics. The present system replaces the PDP-15 dual processor installed about 10 years ago.

The microprocessor has 32 K memory, of which 24 K was used for data storage, and 8 K was used for the data acquisition program. The microprocessor contains a 12-bit analog-to-digital (A/D) converter which accepts signals between -10 and +10 V and converts them to decimal values between -2000 and 2000 counts (or -2047 to 2047). The A/D converter is a zero order hold and is able to digitize eight signals simultaneously. A crystal oscillator generates the pulse which subsequently samples and acquires data. The LSI 11/02 can sample signals up to 300K Hz. The sampling frequency is determined interactively by a table which can have at most 20 elements. These elements are the sequence,rate,and amount of data to be acquired. In general, the LSI is a dummy device without an operating system. It has to be initialized by the VAX 11/780 minicomputer first by downloading an absolute loader and the data acquisition program (object code of LSIPGM program). It can only start to acquire data after the downloading is completed. The microcomputer takes the data at a rate based on the frequencies set by the operator, stores the data in its own memory, and later transfers the data to the VAX, which stores it on disk.

The VAX 11/780 is a minicomputer with a semiconductor memory of 1.5 megabytes and a virtual memory of 200 megabytes. All computations were done with the aid of this unit. Programs were stored on the VAX disk and were then used for computation or downloading to the LSI for data acquisition through a VT100 terminal. The VT100 graphics terminal was used to communicate with the minicomputer, preview data, and evaluate the results.

A Dynograph recorder was used to simultaneously record the signal as it was being digitized. The recorder contains type 461 preamplifiers and a type 462 dual channel amplifier. It was used to monitor the tranducer output to help decide if the data was satisfactory for transfering to the VAX. A digital voltmeter (Fluke 8020A Multimeter, John Fluke MFG. Co., Inc.) was also used to monitor the magnitude of signal to ensure that the signal was in the range of $\pm 10V$.

A.2.4 Thermostat

A cryogenic unit, Ultra Kryostat UK-60-SD(made in Germany), was used to control the temperature. Freon R-13-B1 which could cool to -60 C in an hour, was used in this unit. Methanol was used as the cooling medium for the rheogoniometer and was circulated through the chamber which surrounds the plate and cone. The temperature and the flow rate of methanol could be set at the cryogenic unit. Water-free, pure nitrogen was slowly blown into the chamber to enhance the convective heat exchange and prevent moisture condensation. The temperature was measured on the cone by means of a digital thermister thermometer (Keithley 870 Digital Thermometer). In a typical experiment, the temperature remained constant to within ± 0.5 C.

A.3 Calibration

Although the Weissenberg Rheogoniometer is widely used to study the viscoelastic properties of materials, Davis(87) recommended that the user calibrate the instrument with Newtonian fluids of known viscosity. He found a 30% difference between the experimental and manufacturer's values of the torsion bar constants. He also found that the constant used to convert the ratio of transducer meter output voltages to amplitude ratio was 15% smaller than quoted in the manual.

In order to obtain reliable data from our Weissenberg R-16, each piece of equipment was checked and calibrated carefully. The major components included the transducers, transducer meters, recorder, and computers.

70

A.3.1 Drive Unit

The rotational speed of the bottom plate is set by the gear box setting. A stroboscope was used to try to measure the rotational speed of the plate. Because the rotational speed of the plate was too small to be detected by the stroboscope, a stopwatch and optical observations were used. Two speeds were selected for comparison with the values given in the manual. The results are shown in Table VIII.

A.3.2 Transducers and Transducer Meters

There are three Type EP597 transducer meters(TM). Each transducer meter was checked with the same transducer (B.P.A. Electronics, Type F13B, series N 440) which is the type used for gap setting. The amplification ratio of the first meter was 1.31 times larger than that of the second. For the 100 range,

$$V = 22.3 \text{ d for TM } \#1$$

$$V = 17.4 \text{ d for TM } \#2$$

where V is voltage output and d is the transducer displacement.

Since it was more convenient when setting the gap to use the meter reading as a displacement measurement, the calibration was done through the meter reading. Most gap sizes (depending on the cone angles) fall in the meter ranges of 2.5 and 10, i.e., between 2.5 and 10.0 milliinches. Therefore, the range 10 was tested first to establish the relationship between meter reading and actual displacement. The meters were zero set first. Then, on range 10, the gain of the gap setting transducer (type F13, Series No. 435) was adjusted so that the meter would have a full-scale deflection when the input displacement was 0.01 inch. Unfortunately, no matter what the gain, the second meter did not have full-scale deflection on range 10 when the input displacement was 0.01 inch. There was a linear relationship between deflection and displacement. Thus, the second meter was selected for the torque measurement while the first meter was used for the gap setting.

71

Table VIII   Rotational Speed of Plate

gear setting	no. of rotation	time	time/rev
2.0, 0.0	1	13.2	13.2
(13.3)	1	13.4	13.4
	1	13.4	13.4
	1	13.3	13.3
	2	26.6	13.3
	2	26.6	13.3
1.5, 0.0	1	4.2	4.2
(4.2)	1	4.2	4.2
	2	8.3	4.15
	2	8.35	4.17
	3	12.6	4.2

All the transducers were calibrated using a micrometer to establish the constant k, where $V = k \times d$. V is the voltage output from the transducer meter, and d is the displacement of the transducer in milliinches. The gap setting transducer was calibrated by mounting the transducer in a micrometer calibration unit. The transducer meter was zero set first. Next, the displacement of the micrometer (in both directions) and the meter reading or voltage output were recorded simultaneously. The calibration curve of meter at range 10 is shown in Figure 32 and the data are shown in Table IX. The torsion head transducer differs from the gap setting transducer in that its stator and armature are not connected mechanically and thus do not contribute any friction during measurement. Since this tranducer cannot be calibrated in the micrometer unit, the micrometer was mounted directly on the rheometer to measure the displacement. Both 1/8" and 1/16" torsion bars were used to calibrate for different meter ranges (1.0-25). It was found that the correlation constants are independent of the torsion bar as expected(see Figure 33 and Table X). The percent error of calibration is 3% or less.

For data acquisition, the LSI 11/02 microprocessor was used to record the data rather than the transducer meter. One calibration (on TM #1, range 2.5) was done by using the transducer meter and the computer, simultaneously. The results checked well as shown in Table XI. The A/D converter provided 200 counts/volt. Tests on the second meter showed the same results. In Table XI, D is the reading taken from the micrometer, V is output voltage , and C is computer output.

The entire system, plate and cone, transducer, and transducer meter, was calibrated by standard Newtonian Brookfield solutions of 9.85P and 118.4 P. Several torsion bars (1/16", 1/8", and 1/4") were used to measure the viscosities, as shown in Figure 34. A 118.4 P Brookfield solution and a 9.85P Brookfield solution were tested using a 1/16" torsion bar as shown in Figure 35. The others are similiar. The results are summarized in Table XII. The average error was less than 5%, which means that the torsion bar constants provided are reasonably accurate.

In contradiction to the Davis(87) observation, the torsion bar constants of our rheometer agreed to within 5% of the values stated by the supplier. The same results were found by Enthoven and Jalink(86).

73
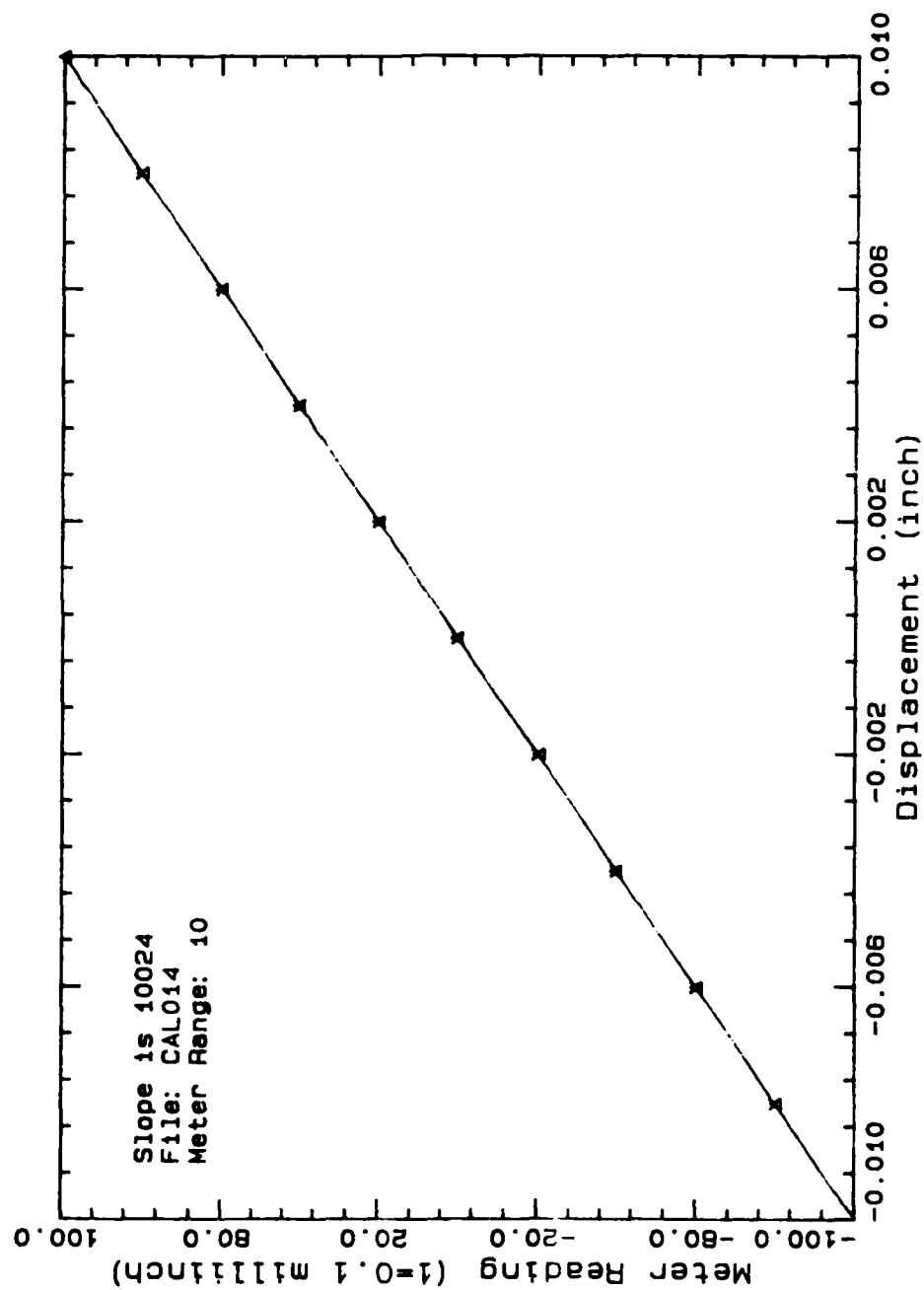
Figure 32. Typical Displacement Meter Calibration.

Slope is 10024
File: CAL014
Meter Range: 10

74

Table IX Calibration of Transducer Meter
at Range 10

displacement *10**3 inch	meter reading (full scale 100)
10	100.0
8	79.8
6	60.0
4	40.2
2	20.0
0	0.1
-2	-20.4
-4	-40.0
-6	-60.2
-8	-80.4
-10	-100.0

Table X Calibration Constants k from V=k*d

	Calibration constants k		
RANGE	1/8"	1/16"	AVE k
1.0	1.5663	1.6241	1.5952
2.5	0.6531	0.6570	0.6551
10.0	0.1617	0.1642	0.1630
25.0	0.06562	0.06654	0.0661
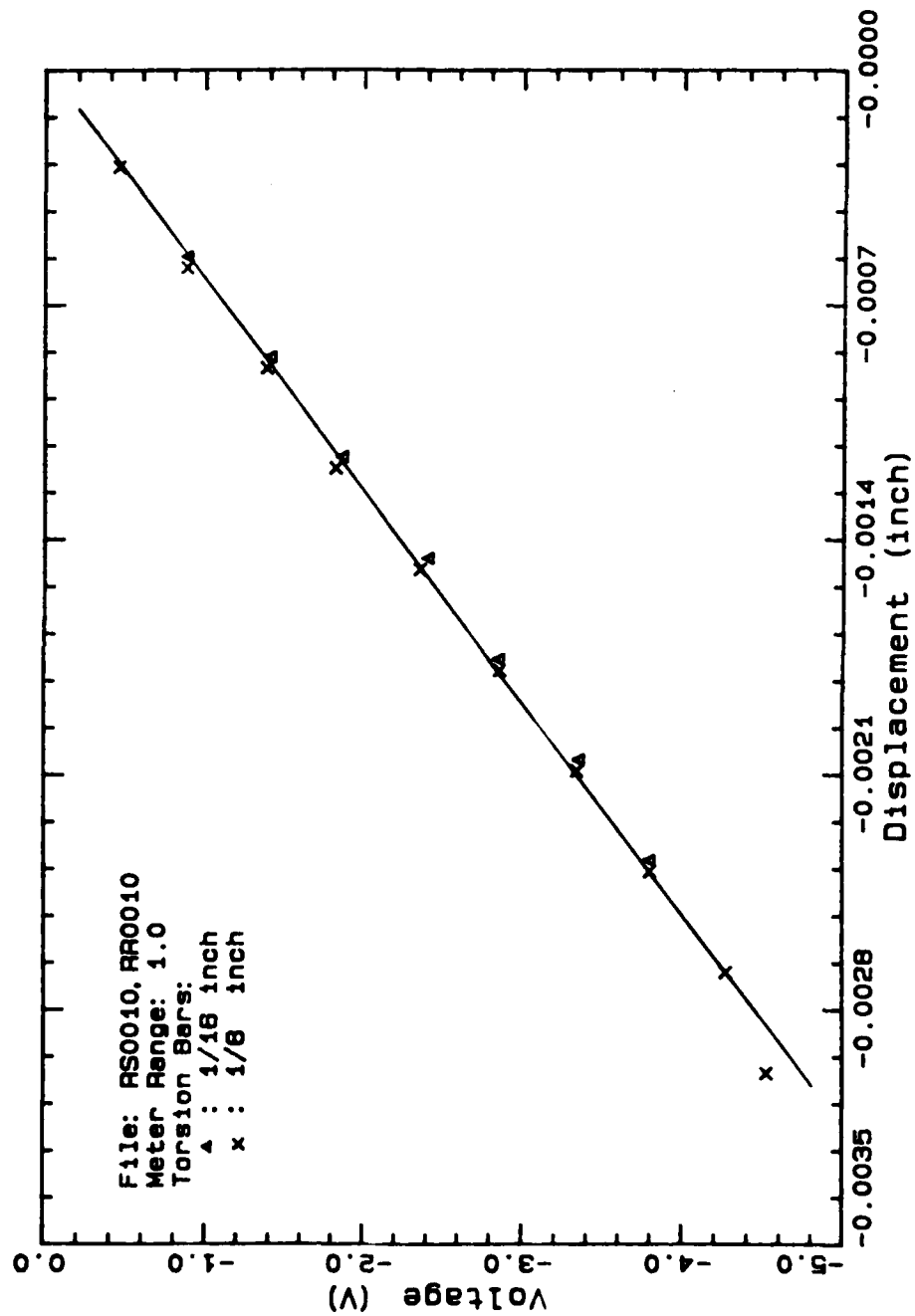
Figure 33. Calibration for Two Torsion Bars.

File: RS0010, RR0010
Meter Range: 1.0
Torsion Bars:
▲ : 1/16 inch
x : 1/8 inch

Table XI   Calibration Values at Range 2.5
                    TM   1

D	V	C	Ratio(C/V)
0.502	1.74	346.5	199.1
0.5015	1.306	260.1	199.2
0.501	0.868	172.3	198.5
0.50005	0.425	84.1	197.9
0.5	−0.013	−3.71	(285.4)
0.4995	−0.438	−88.4	201.8
0.499	−0.883	−177.1	200.6
0.4985	−1.323	−265.2	200.5
0.498	−1.756	−351.6	200.2
0.4975	−2.19	−437.7	199.9

Table XII.   Calibration by Newtonian Fluids

| Brookfield | Measured Viscosities | | | Haake |
Solution	1/16"	1/8"	1/4"	Measurement
9.85P	9.34	8.71	–	10.02
118.4 P	112.5	111.9	118.8	124.83

77

Brookfield Solution 118.4 Poise
Files: ANEW4, ANEW3, ANEW6
Torsion Bars:
◘ : 1/16 inch
▲ : 1/8 inch
✕ : 1/4 inch

Shear Sress (dyne/cm^2)

0   8000   12000   18000   24000   30000

SHEAR RATE (sec^{-1})

0.000   60.000   120.000   180.000   240.000   300.000

Figure 34.   Three Torsion Bars Used to Measure Standard
Solution Viscosity of 118.4 Poise.
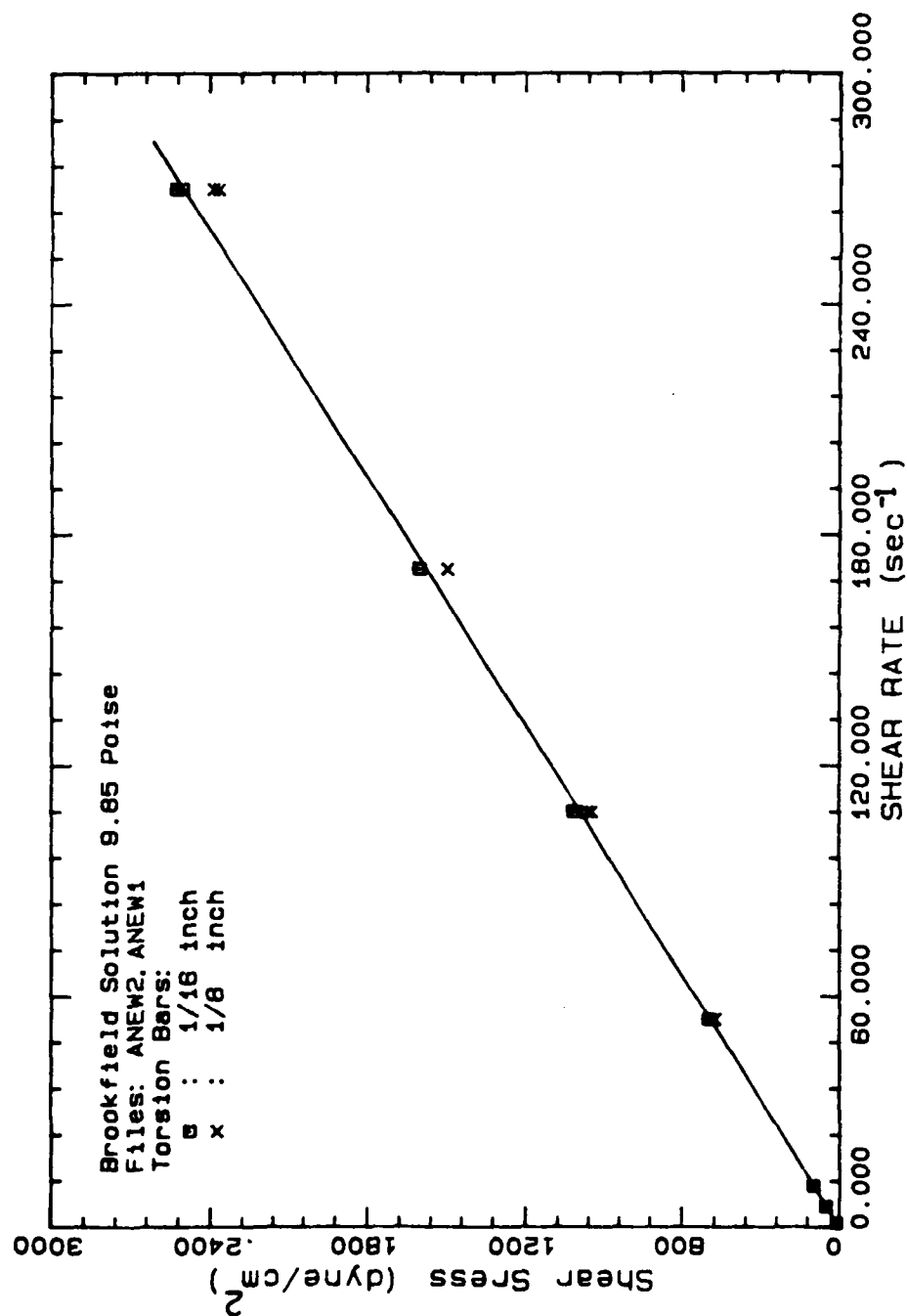
Figure 35. Measurement of Low Viscosity Standard Solution.

Brookfield Solution 9.85 Poise
Files: ANEW2, ANEW1
Torsion Bars:
◼ : : 1/16 inch
x : : 1/8 inch

Shear Sress (dyne/cm^2)

SHEAR RATE (sec^{-1})

79

During a low temperature measurement, the armature of the torsion head transducer was accidentally broken. The armature was repaired and the transducer recalibrated. The 2.5 and 10.0 ranges, with the 1/8" torsion bar, were checked. The results were close to the previous values (Table XIII), so the original calibration constants were used.

On April 20,1982, TM#2 started to show nonlinearity in its output; it was replaced by TM#3. The gap setting transducer was used first to compare TM#1 and TM#3, and it was found that the gains of the two transducer meters were almost the same. The constants are shown in Table XIV.

TM#3 was then used for gap setting and TM#1 was used for the torsion head measurements. TM#1 was again calibrated with the torsion head transducer. The calibration constants are shown in Table XIV.

A quick test was made to measure the viscosity of water at 25 C. The viscosity of water was 0.9671 cp which is close to the literature value of 0.95 cp. The measurement of the water is in the most critical range for the instrument since high shear rates and the most sensitive meter range must be used. The result was better than expected.
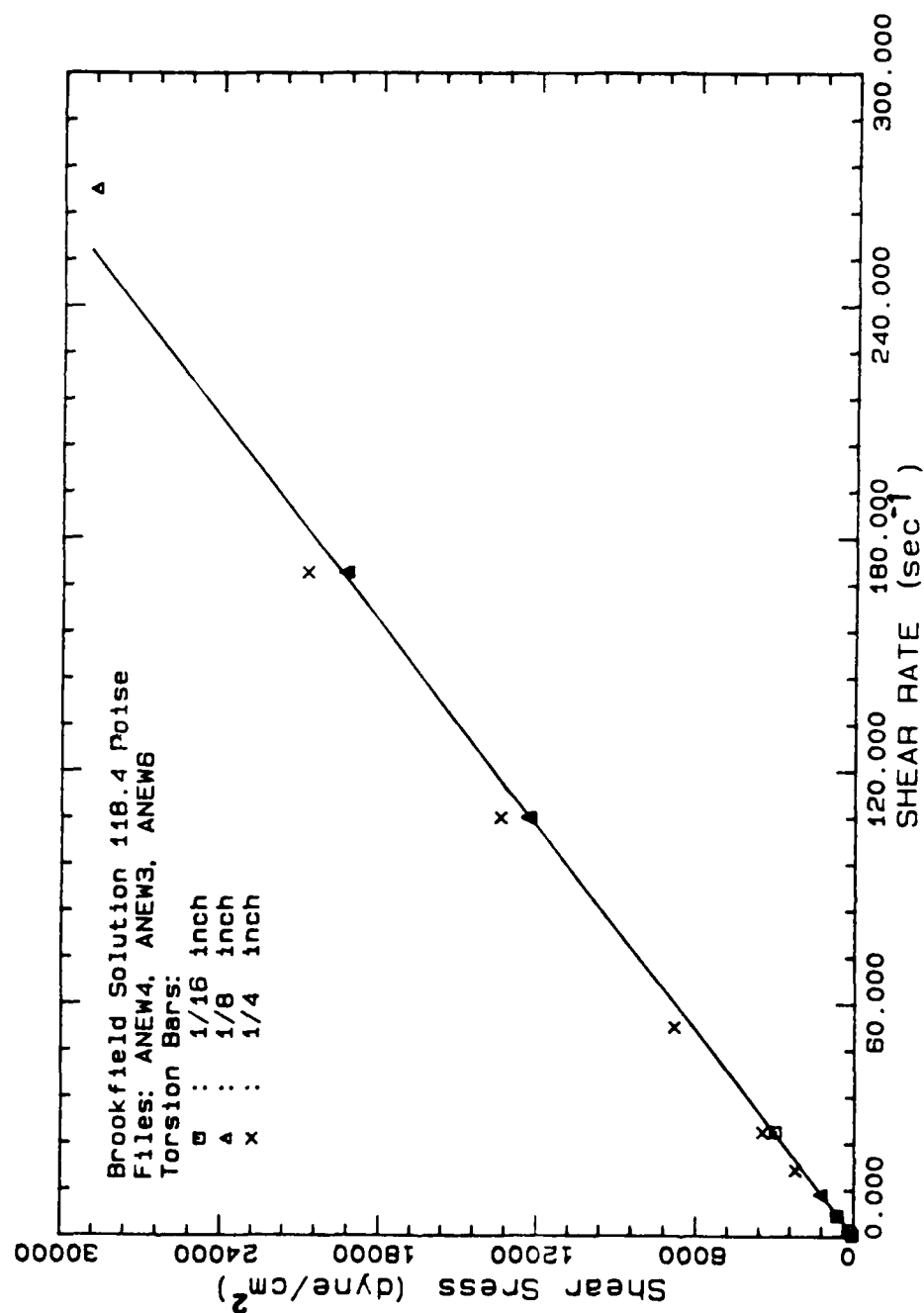
The transducer meters are quite old (20 plus years) and cannot stand working too long. The transducer meter #1 failed during a low temperature measurement and it was found that some transistors wer out of range in both TM#1 and TM#2. They have been repaired and recalibrated, but should be replaced when funds become available. The new calibration constants are given in Table XV.

A.4   Noise Analysis and Filter Technique

The noise of the system was analyzed and the sources of the noise were identified. The output of the transducer meter was found to contain an appreciable amount of carrier frequency "noise". The output of the transducer meter is d.c., but there is a high frequency carrier ripple in the output which is significant on the more sensitive ranges. The amplitude of the noise depends on the d.c. signal. The other predominant noise is from mechanical sources and is due mainly to the natural frequency of the torsion bars. The natural frequencies of the bars are low (around 10Hz for 1/16" and 60 Hz for 1/8") which prevent using analog filters to remove the noise. Filtering of the noise was

80

Table XIII Conversion Constants

Range	Original Constants	New Constants
2.5	0.6551	0.6424
10	0.1630	0.1597

Table XIV Torsion Head and TM#1

Range	K	K
0.25	8.7464	8.7083
1.0	2.1687	2.1414
2.5	0.8758	0.8590
10.0	0.2169	0.2152
25.0	0.0868	0.0870
100.0	0.0220	0.0216

Table XV. Calibration Constants

Range	k
0.25	7.8547
1.0	1.9396
2.5	0.78066
10.0	0.19443
25.0	0.07821
100.0	0.01963

done by using a digital filter technique (fast Fourier transform).

The carrier noise from the transducer meters was measured and filtered. The carrier noise as estimated by using an oscilloscope was 2000 Hz. Since the maximum sampling frequency used during data acquisition was 1000 Hz, a low-pass RC filter with a cut-off frequency of 2000Hz was used at the output of the transducer meter to eliminate the carrier frequency. At zero output, the output with and without the filter is shown in Figure 36. The filter reduced the signal by only 4.5%.

Further tests were conducted to identify other sources of noise. First, noise was measured with the motor and air bearing air supply shut off. Noise of 28 Hz and 36 Hz was present, which must have come from the transducer meter (see Figure 37). Next, an amplifier was connected to the output of the meter to see if it would contribute noise. The result showed that no additional noise was coming from the amplifier. Then the air was turned on and the torsion bar could freely vibrate at its natural frequency. The noise from the torsion bar's natural frequency was the major source of noise, as shown in Figure 38. Finally, different sampling frequencies, 100 Hz, 500Hz, 1000 Hz, were used to see if there was any difference in the frequency domain analysis. The results showed no difference in the noise frequency analysis, but the faster the sampling period, the more accurate was the frequency analysis.

A filtering technique which couples curve fitting and fast Fourier transform (FFT) was used to analyze and to filter the noise. First, a curve fitting technique was applied to the raw data. The deviatory data, the difference between the raw data and fitted value, was then analyzed. The deviatory data was transformed from the time domain to the frequency domain by a fast Fourier transform (FFT). The frequencies were then analyzed to determine which frequencies were noise.

The noise was filtered out by a suitable filter: low-pass, high-pass, band-pass, or band-reject filter. Next, the filtered deviatory data was readded to the fitted curve to reconstruct the filtered data. In this case, the filtered data retained the original trend and minimized the "leakage" during FFT.
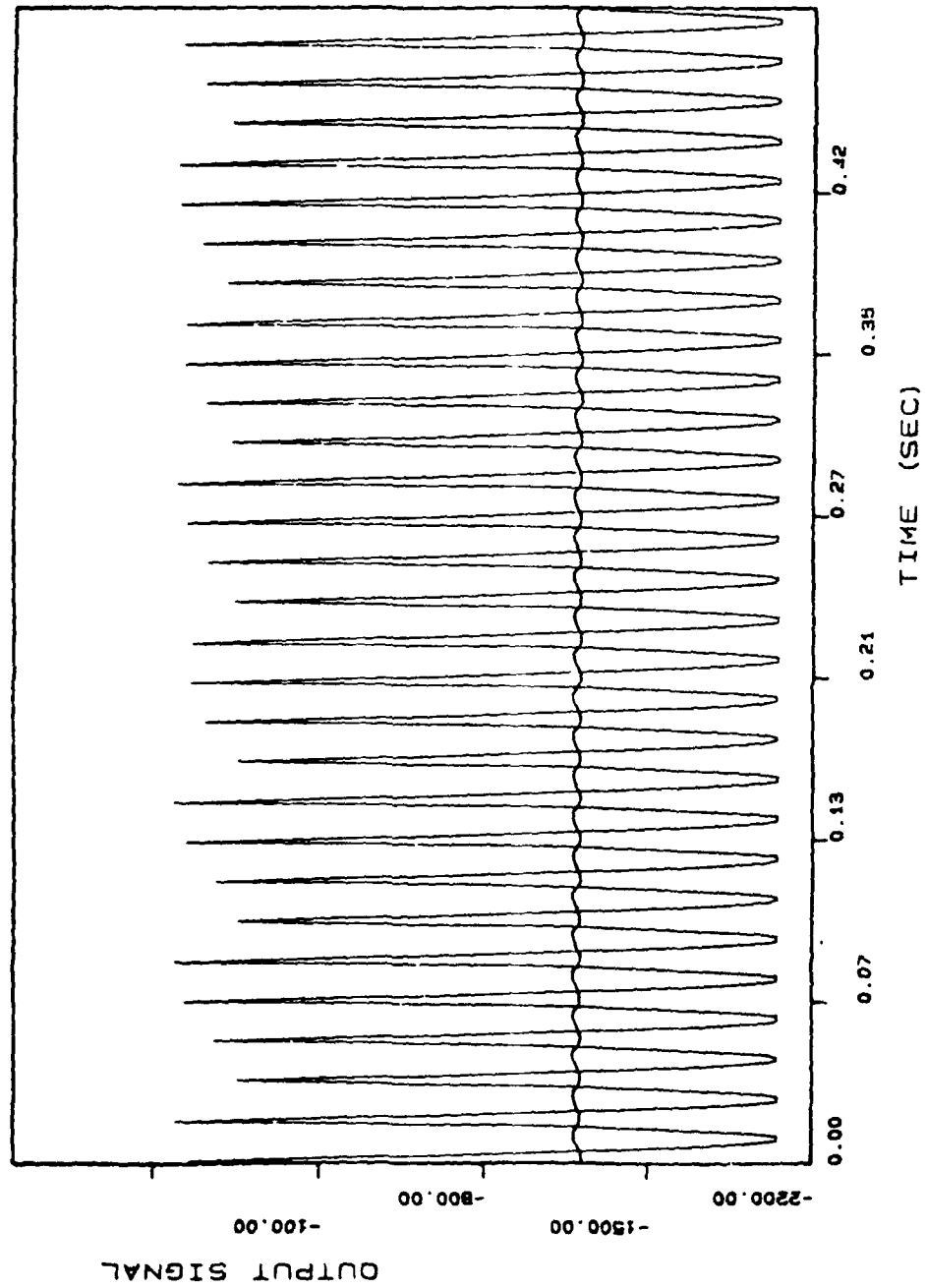
82

Figure 36. Transducer Meter Output Showing Carrier Frequency and with Carrier Frequency Filtered Out.

83

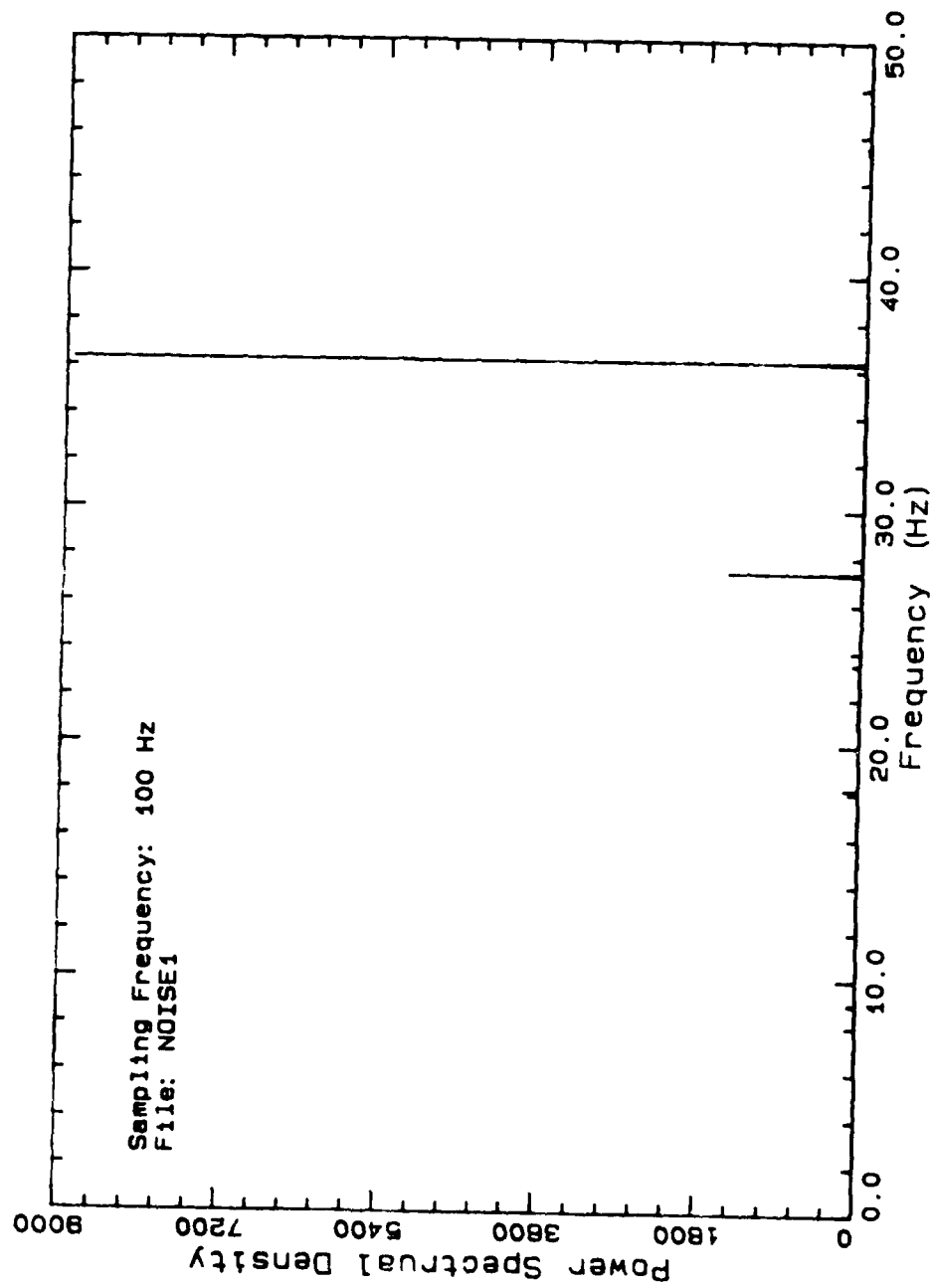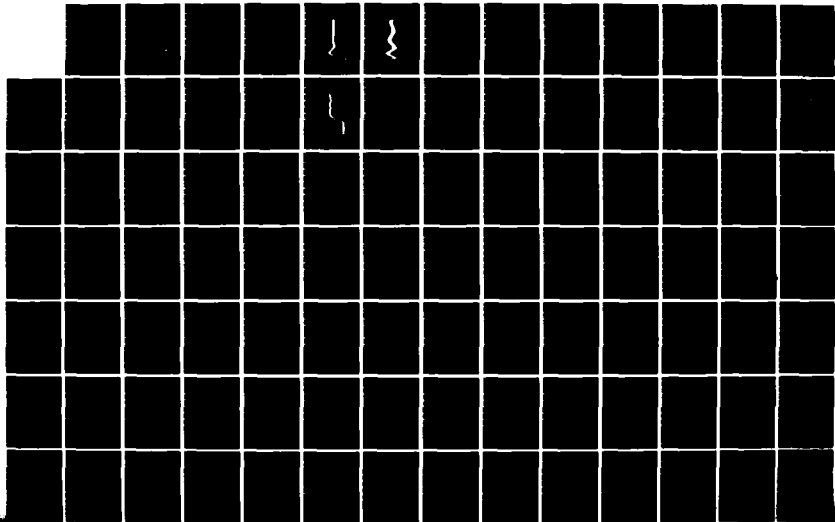Figure 37. FFT of Noise with Motor, Air Bearing, and Amplifier Off.

84
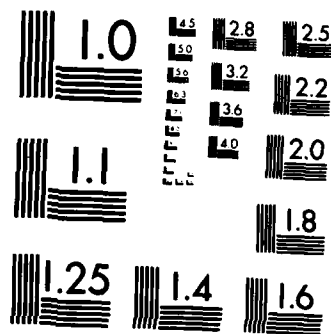
MICROCOPY RESOLUTION TEST CHART
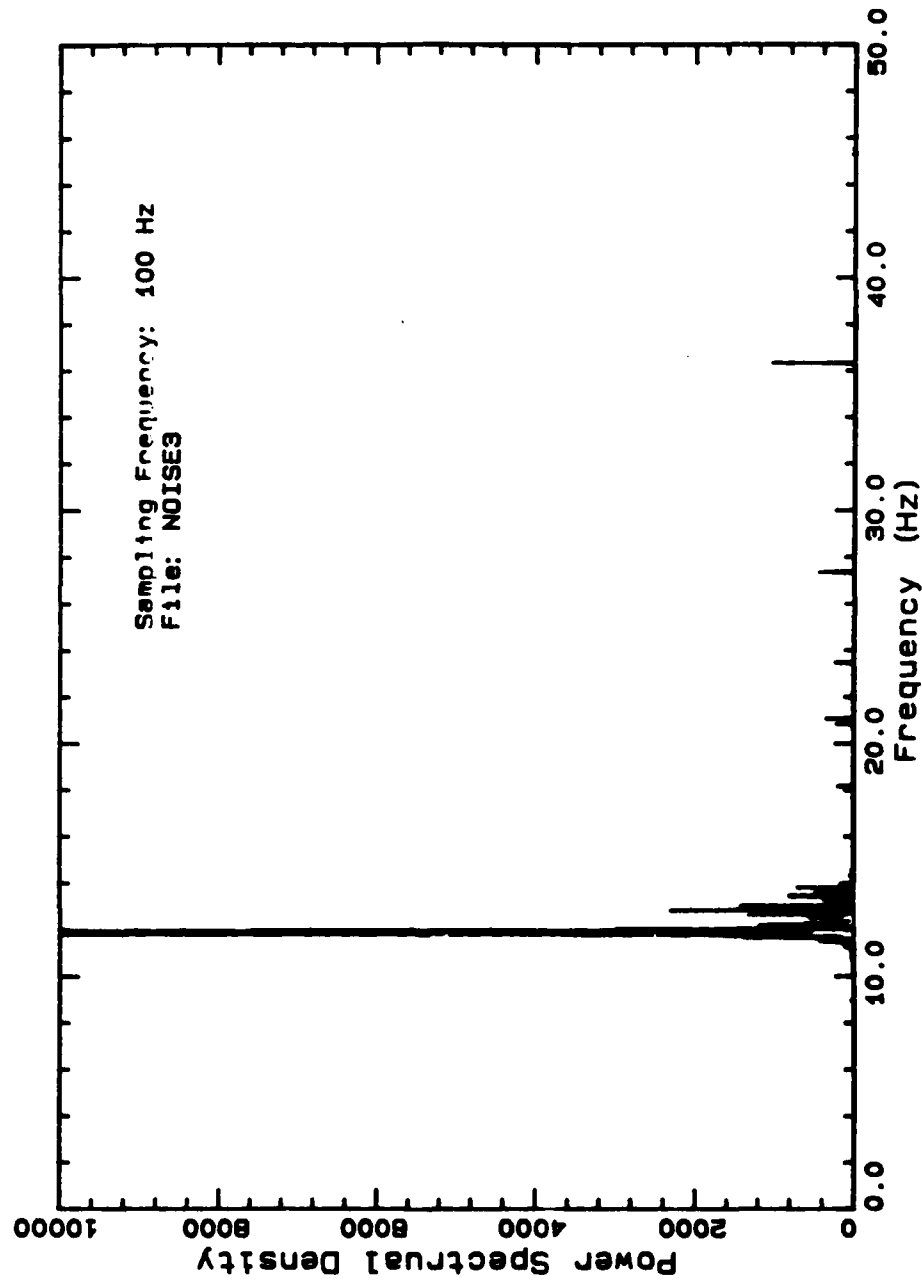NATIONAL BUREAU OF STANDARDS-1963-A

Figure 38. FFT of Noise with Air on, Major Source of Noise is Natural Frequency of Torsion Bar at 100 Hz Sampling Frequency.

85

The filtering technique can be better explained by using an example, a second-order response. A second-order response ,shown in Figure 39, with a time constant of 1 sec and = 0.4 was generated. A sampling frequency of 100 HZ was used and then 20 Hz and 30 Hz noises were superimposed. The data was fitted with a 5th-order polynomial as shown in Figure 40. The deviatory data (Figure 41), which is the difference between the raw data and the fitted data, was transformed to the frequency domain by the FFT. In the frequency domain, the spectral density was evaluated and analyzed. Figure 42 shows that there are 3 major frequencies, one is at 30 Hz, another is at 20 Hz, and the last one is the low frequency contribution. The low frequency includes the natural frequency of the system and the frequency generated by the curve fitting. A band-reject filter with rejected frequencies of 20 Hz and 30 Hz was then used to filter out the noise. The filtered deviatory data in the time domain is shown in Figure 43. There are some undesirable vibrations at both ends of the filtered data. This is due to errors in spectral computation introduced by truncation and is known as "leakage". The filtered deviatory data is then readded to the polynomial fit to construct the final curve. It was found that the filtered data and the original data essentially coincided except at the very ends (Figure 44). The deviation at both ends is due to the leakage of discrete FFT as mentioned earlier.

Since the initial response of the curve is important to us, further studies were done to eliminate the leakage. Unfortunately leakage is a natural consequence of using a FFT and cannot be avoided even if a Hanning window is applied. The only possible way to avoid the leakage in the initial response was to move the initial response away from the starting point, i.e., sampling at t<0.

The same set of second-order response data was used again; but this time was shifted to the right by starting the response at t=1.0 min. The same technique was used with the same curve fitting and filter. Clearly, we can reconstruct the original second-order response without the leakage problem by pushing the origin away from the desired point (Figure 45). This technique was very helpful in analyzing the initial response in our data.

Curve fitting techniques were further studied to find the best way of obtaining the deviatory data. Step changes and polynomials of different degrees were used to fit the data. A set of transient data on the Exxon 708-61 at a shear rate of 0.55 sec^{-1} was used for the

Second Order Response
XI=0.4, TAU=0.5
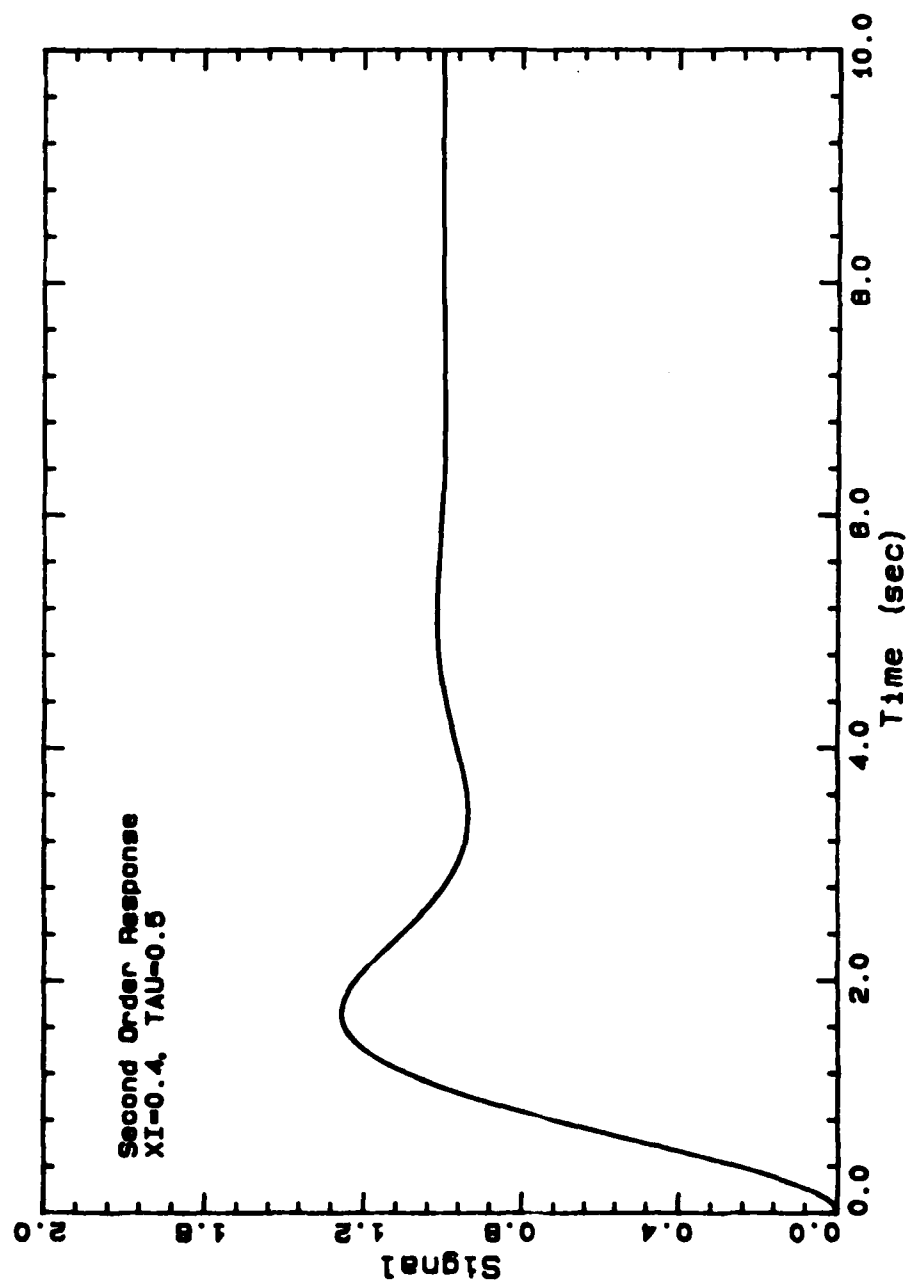
Figure 39. A Generated Second Order Response Curve.
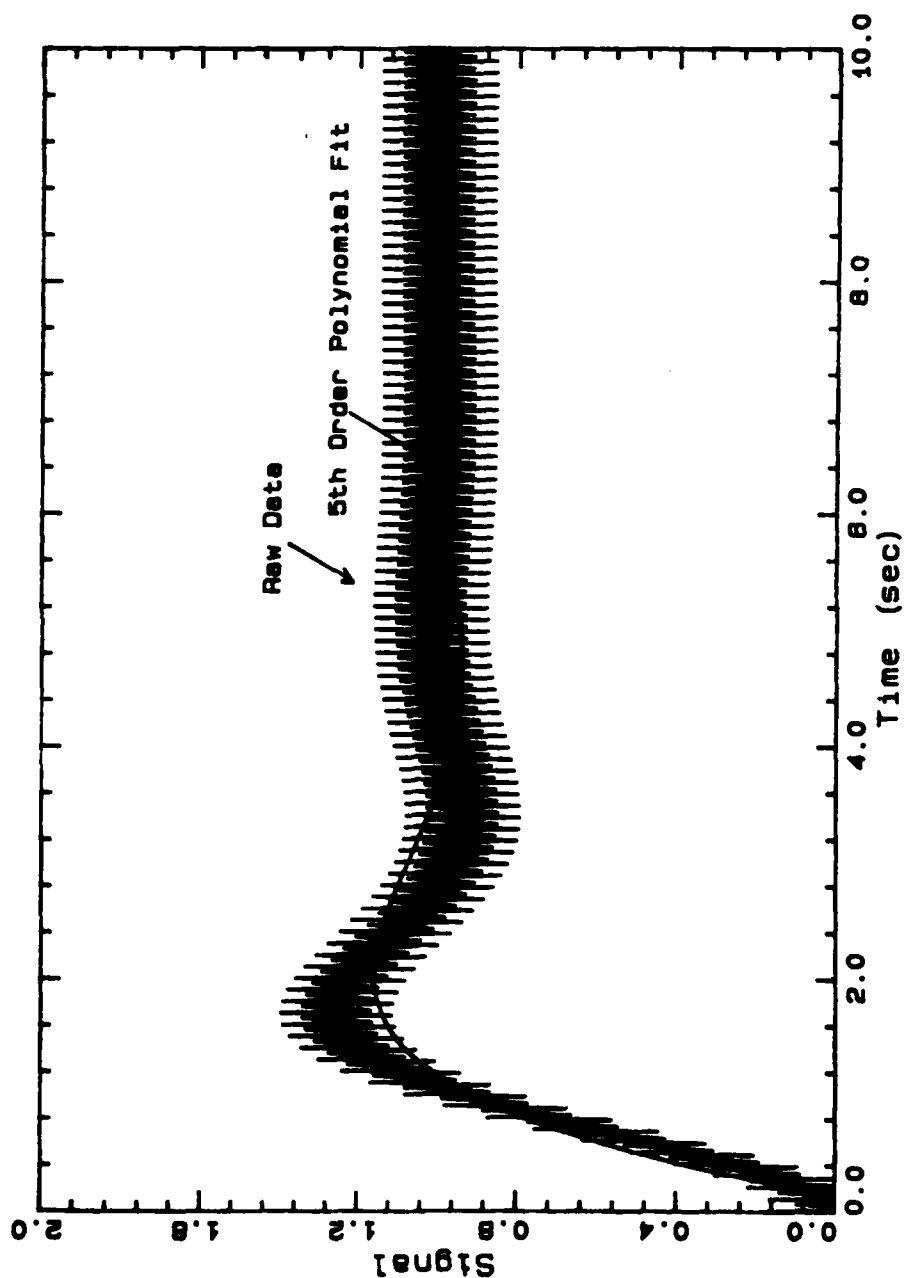
Figure 40. Second-order Response Curve Plus Added
Noise Frequencies and 5th-order Fit.

88
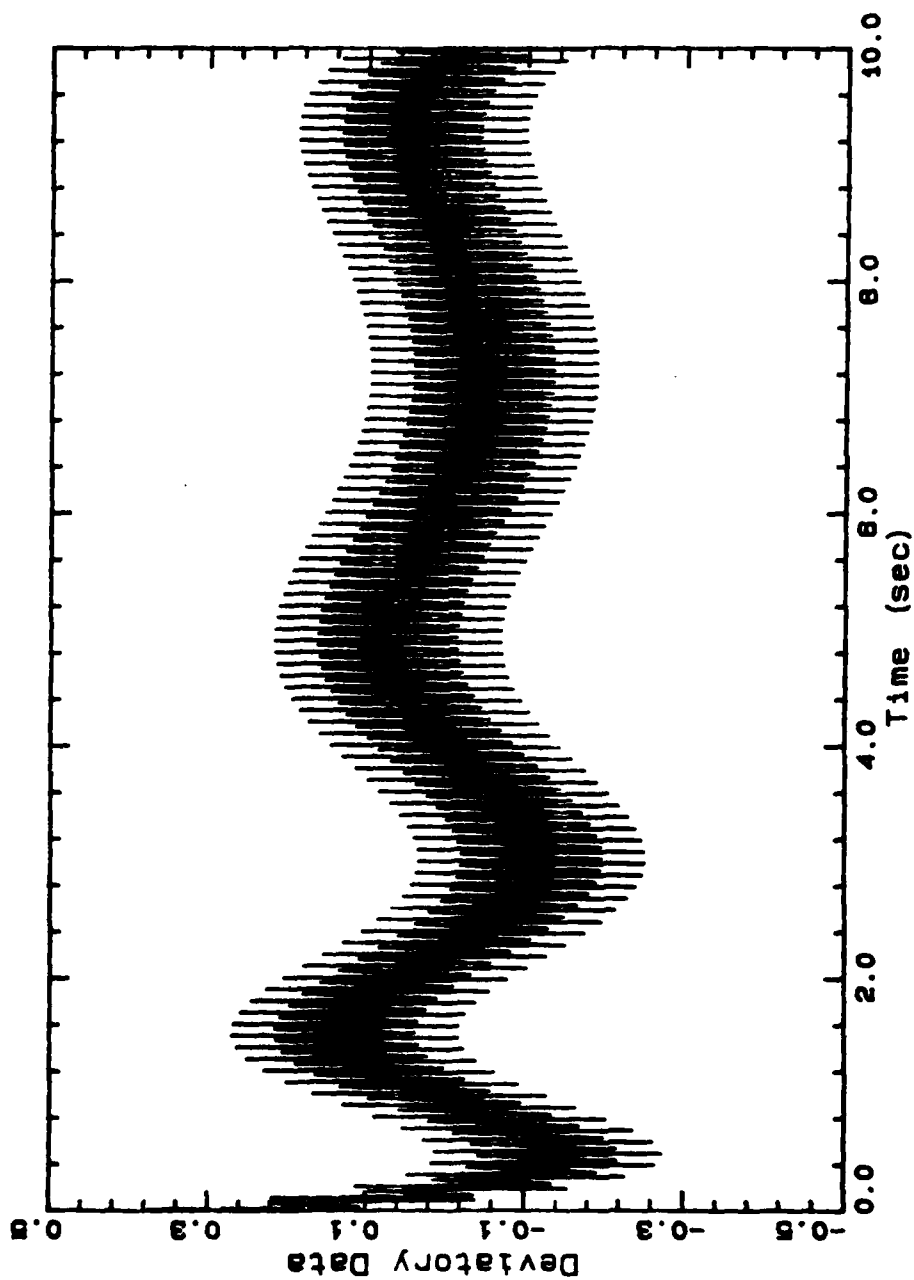
Figure 41. Deviatory Data Between 2nd-order Curve and 5th-order Fit.

89
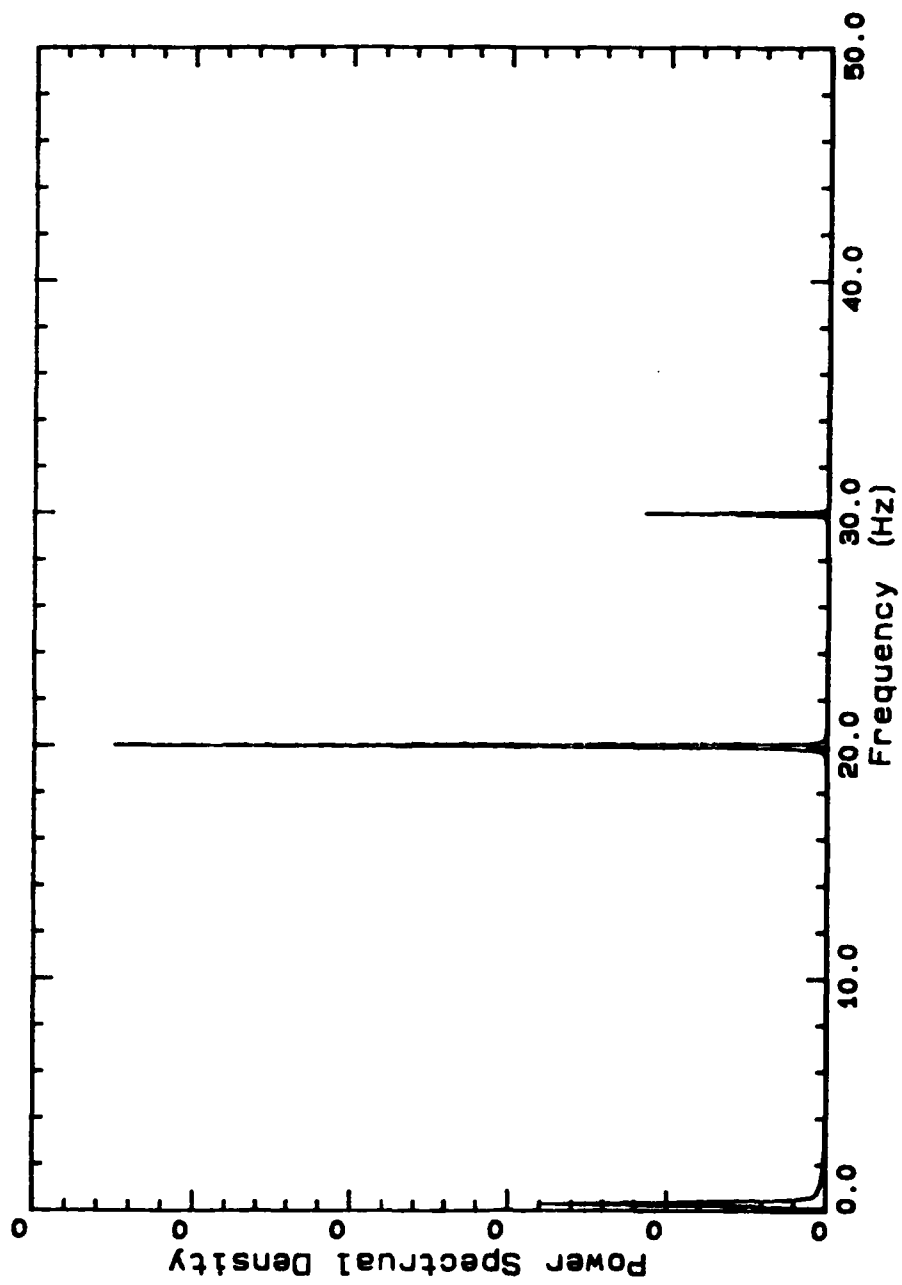
Figure 42.   FFT of Deviatory Data.

90
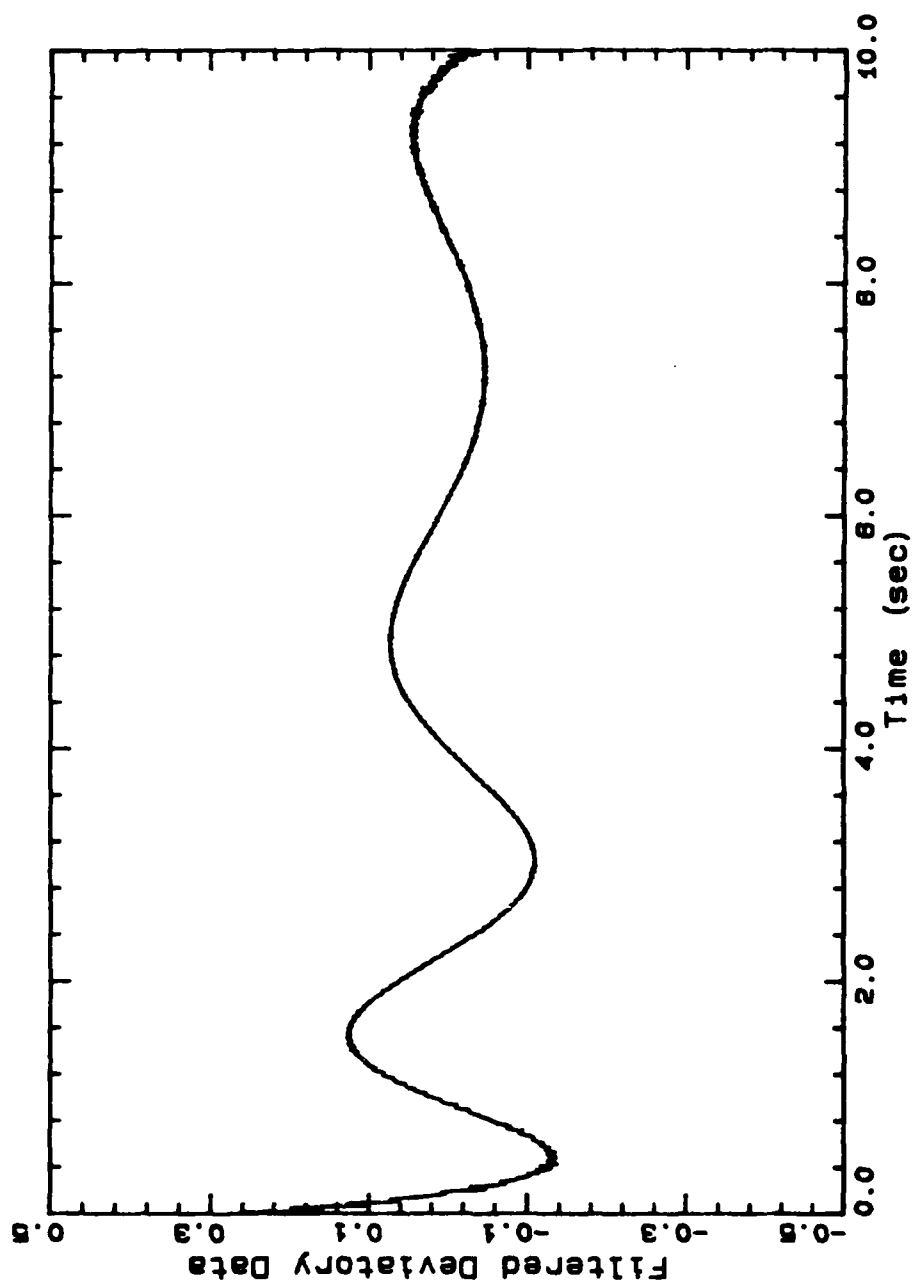
Figure 43. Deviatory Data of Second-order Curve
With Band-reject at 20 and 30 Hz.
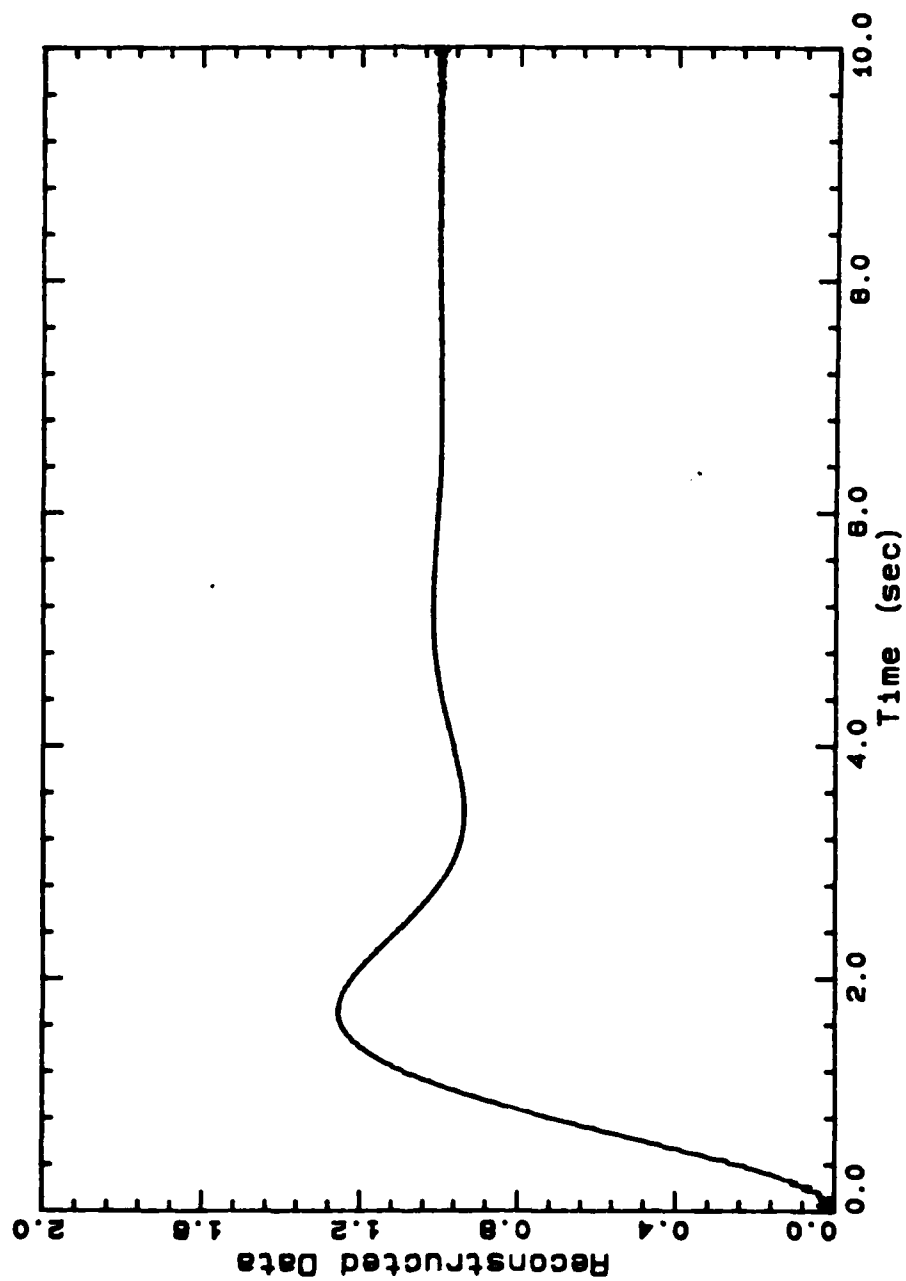
Figure 44. Reconstructed Second-order Response Curve.

92
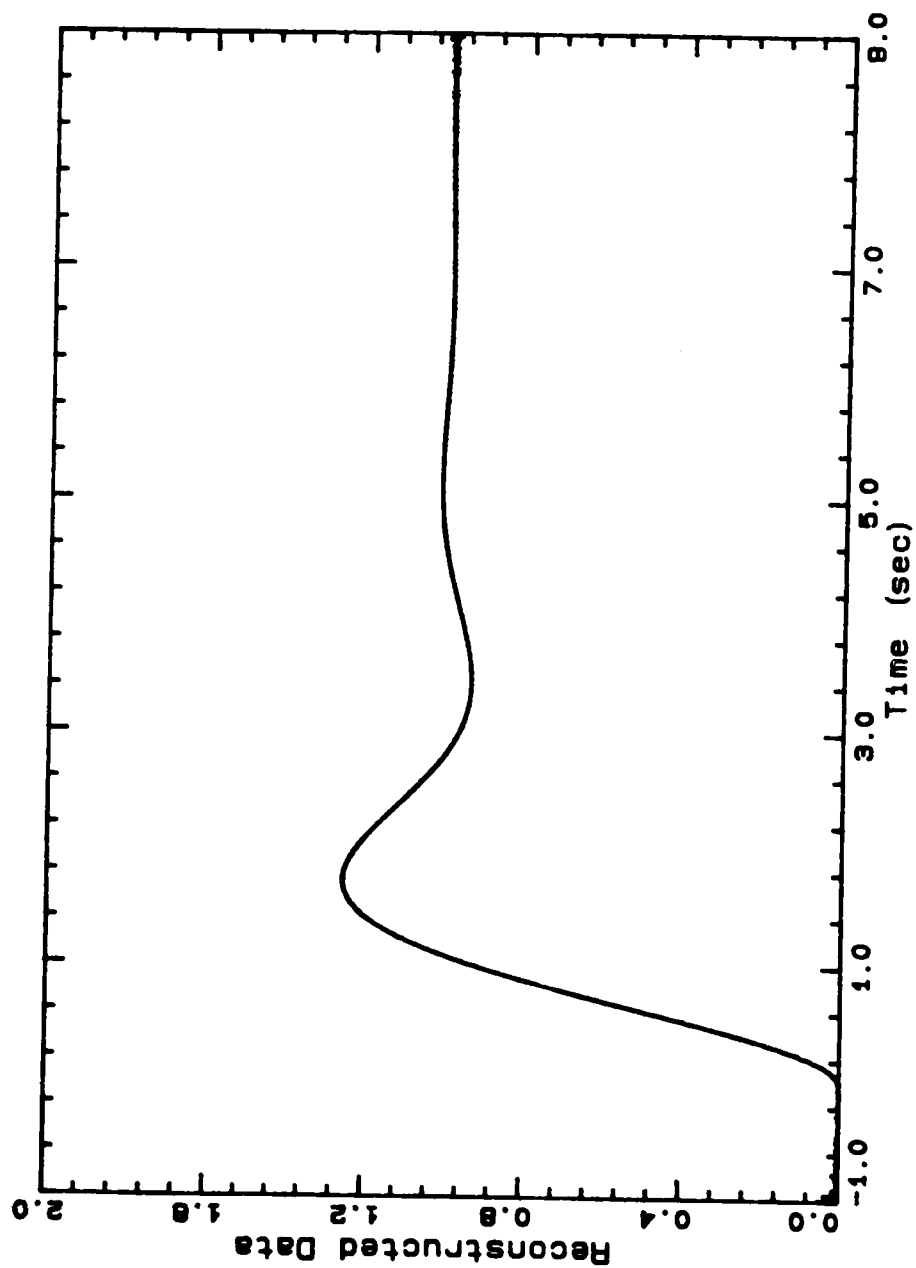
Figure 45. Reconstructed Second-order Curve with Origin Shifted.

93

comparsion. Polynomials with degrees of 5, 10, and 15 were used. It was found that they give different deviatory results and different spectral density functions. As expected, they have the same noise frequencies: 30 Hz and 48 Hz (Figures 46 to 48). The major difference between them is the low frequency response: the frequency that is generated by the curve fitting. Therefore, it is desirable to fit the data with polynomials of the lowest possible degree. The only limitation to using the low order polynomial is in minimizing the leakage during Fourier Transform. For example, for the same set of data, the "leakage" was more serious on both ends when no curve fitting was done on the data, as shown in Figure 49. With the low-pass filter with a 10 Hz cut-off frequency, the filtered data using different fitting polynomials are shown in Figures 50 to 52. There is little difference between them. For a better comparison, a set of raw data, fitted data, and filtered data are plotted in Figure 53.

A.5   Experimental Procedures

All measurements were conducted as follows: precool the apparatus to the desired temperature, set the zero gap, load the sample, then wait at least 3 hours at the set temperature before data acquisition.

A.5.1   Temperature Setting

In this program, a wide range of temperatures was studied, -25 C to 25 C. Measurements at room temperature, 25 C, were controlled by air-conditioned room temperature. Measurements other than room temperature were controlled by the cooling medium circulating in the chamber which surrounds the plate and cone.

For the low temperature measurements the following procedures were followed. The cryogenic unit was turned on an hour in advance by setting the main switch to "<-0 C". It stabilized at about -60 C in an hour with the external circulation valve closed. The circulation valve was then opened to allow the cooling medium to circulate around the plate and cone. At the beginning, a large temperature difference was used to force the system to cool faster. When the temperature of the plate and cone approached the desired temperature, the temperature of the refrigerator was reset to allow the heat transfer in the chamber to just balance the heat loss. The temperature difference at this stage

4
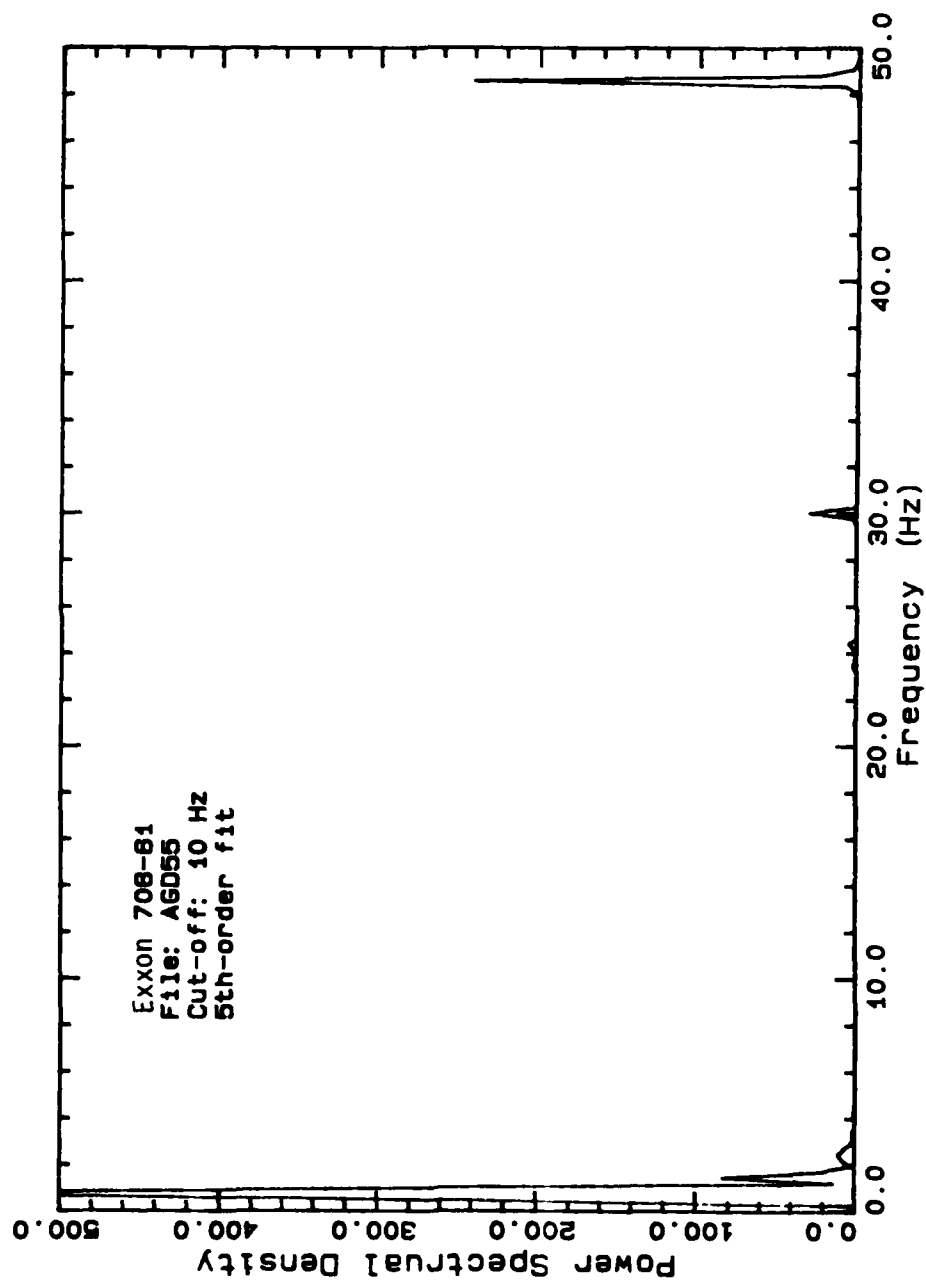
Figure 46. FFT of Deviatory Data from 5th-order Fit.

The plot shows:
- Y-axis: Power Spectrual Density, ranging from 0.0 to 500.0 (marked at 0.0, 100.0, 200.0, 300.0, 400.0, 500.0)
- X-axis: Frequency (Hz), ranging from 0.0 to 50.0 (marked at 0.0, 10.0, 20.0, 30.0, 40.0, 50.0)

Text box in plot:
Exxon 708-81
File: AGD55
Cut-off: 10 Hz
5th-order fit
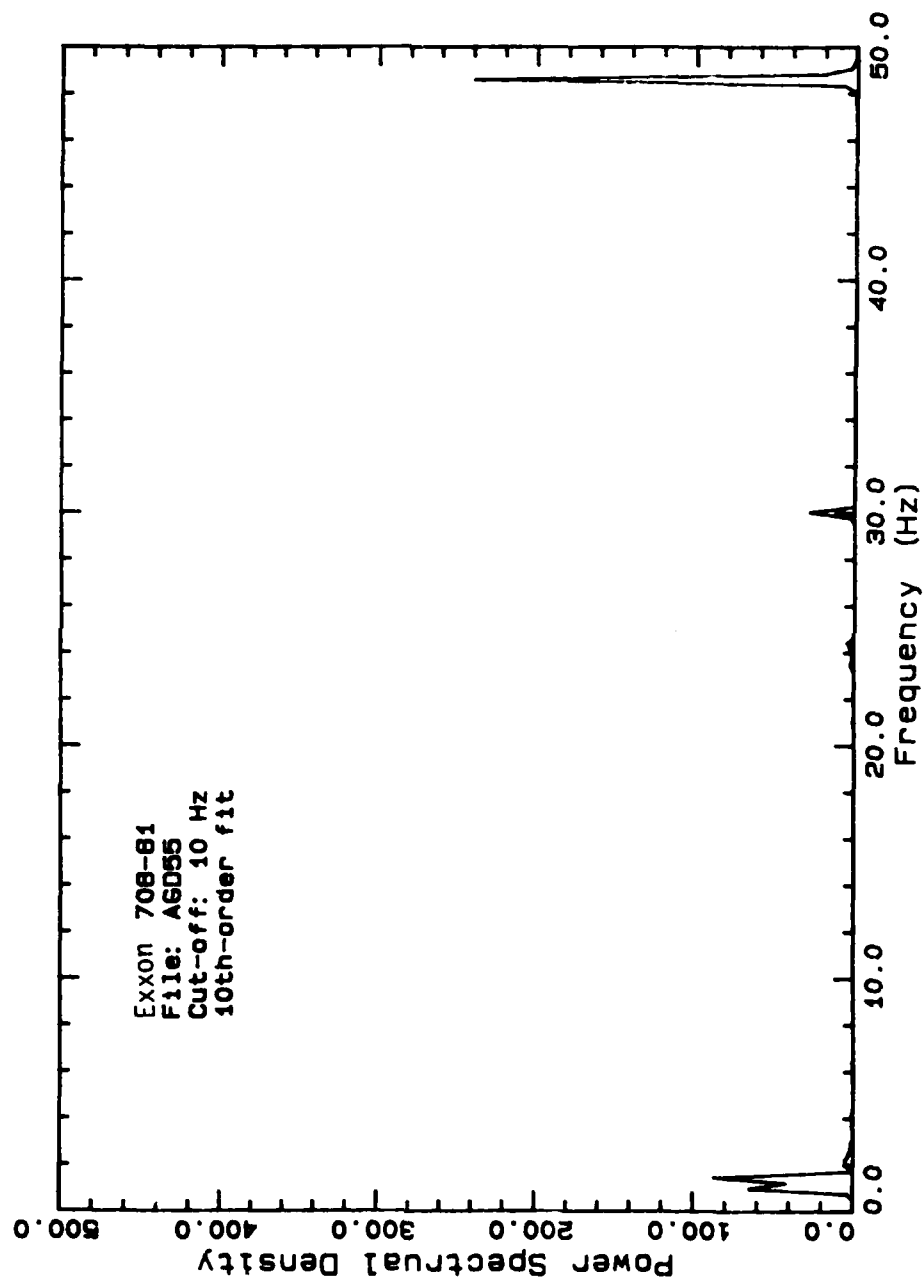
Figure 47. FFT of Deviatory Data from 10th-order Fit.

The plot shows:
- Y-axis: Power Spectrual Density, ranging from 0.0 to 500.0
- X-axis: Frequency (Hz), ranging from 0.0 to 50.0

Annotations on plot:
Exxon 708-81
File: A6D55
Cut-off: 10 Hz
10th-order fit
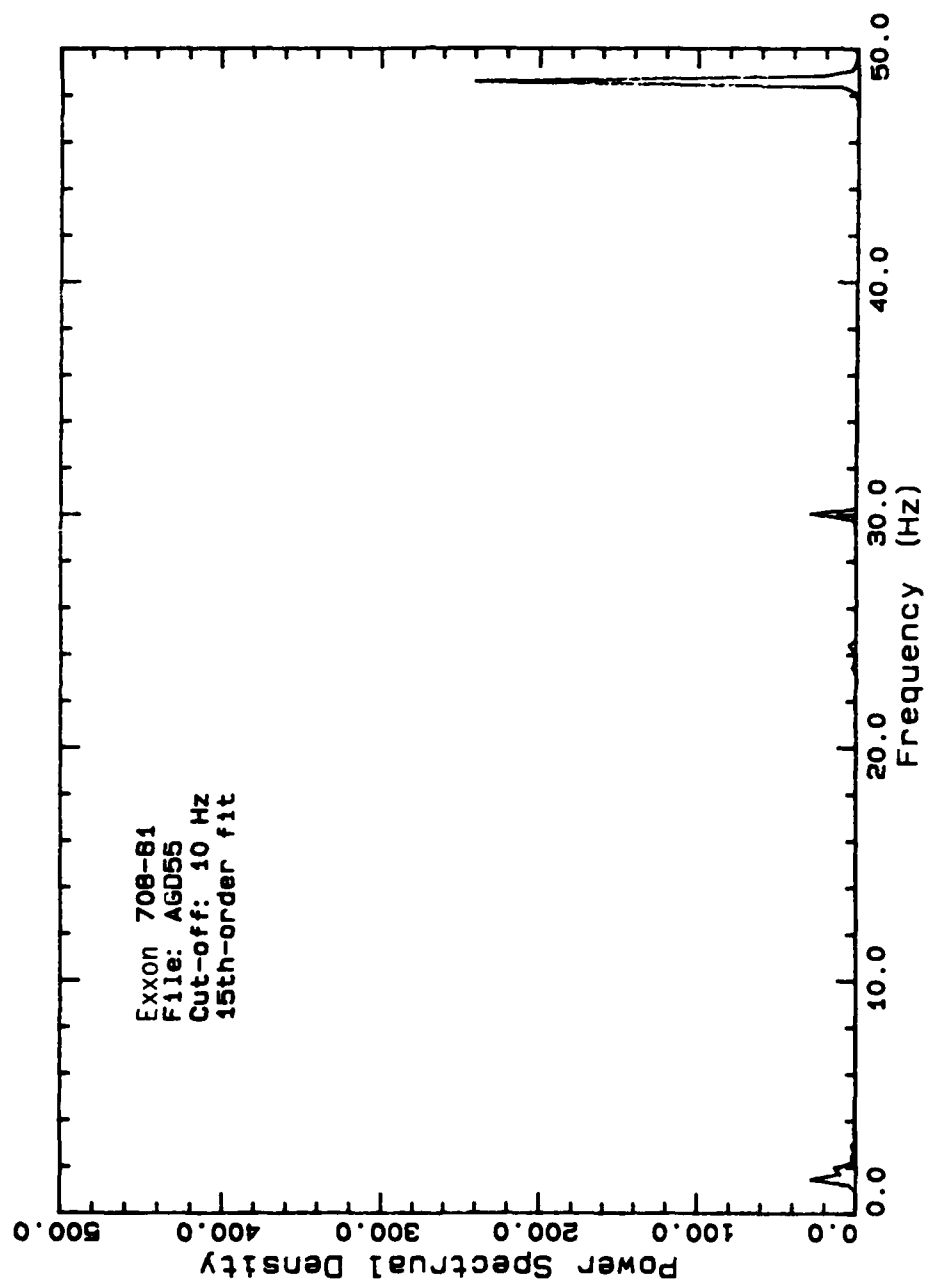
Figure 48. FFT of Deviatory Data from 15th-order Fit.

97
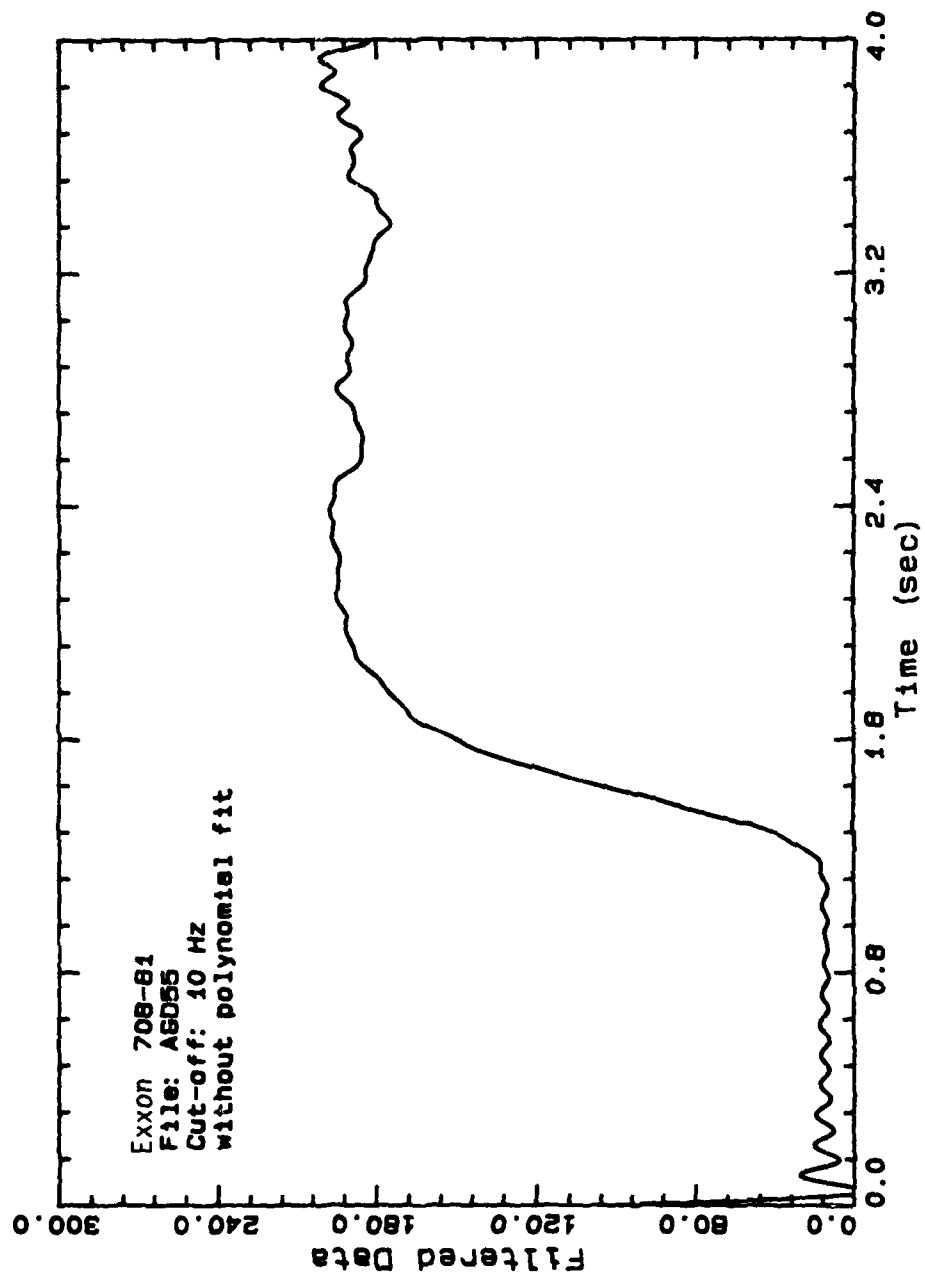
Figure 49. Filtered Data without Use of Polynominal Fit.

The figure shows a plot with axes labeled "Time (sec)" (horizontal) and "Filtered Data" (vertical). The horizontal axis ranges from 0.0 to 4.0 with marks at 0.0, 0.8, 1.8, 2.4, 3.2, 4.0. The vertical axis ranges from 0.0 to 300.0 with marks at 0.0, 80.0, 120.0, 180.0, 240.0, 300.0.

Exxon 70B-81
File: A6D55
Cut-off: 10 Hz
without polynomial fit

98
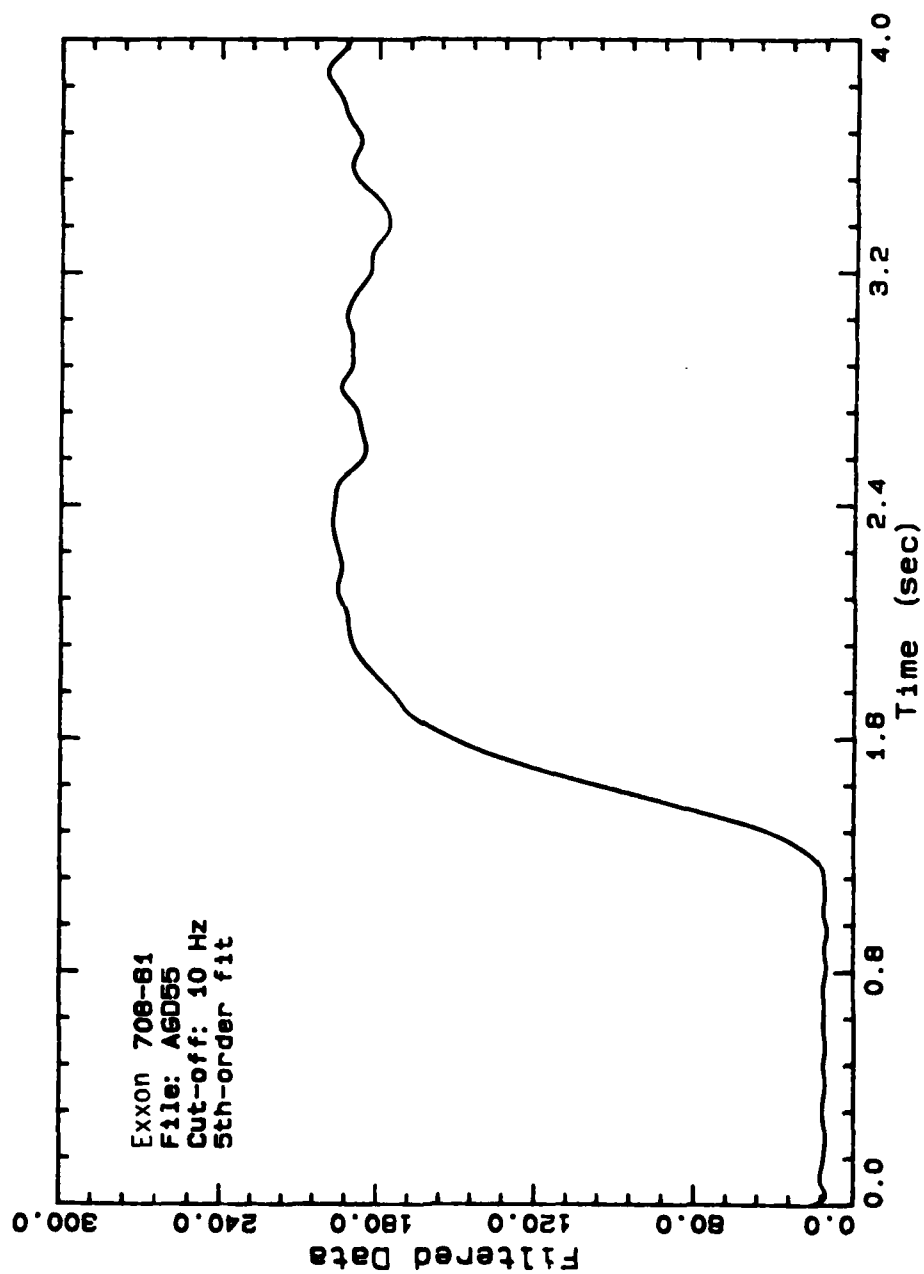
Figure 50. Filtered Data Using 5th-order Fit.

Exxon 708-81
File: AGD55
Cut-off: 10 Hz
5th-order fit

Time (sec)

Filtered Data

99
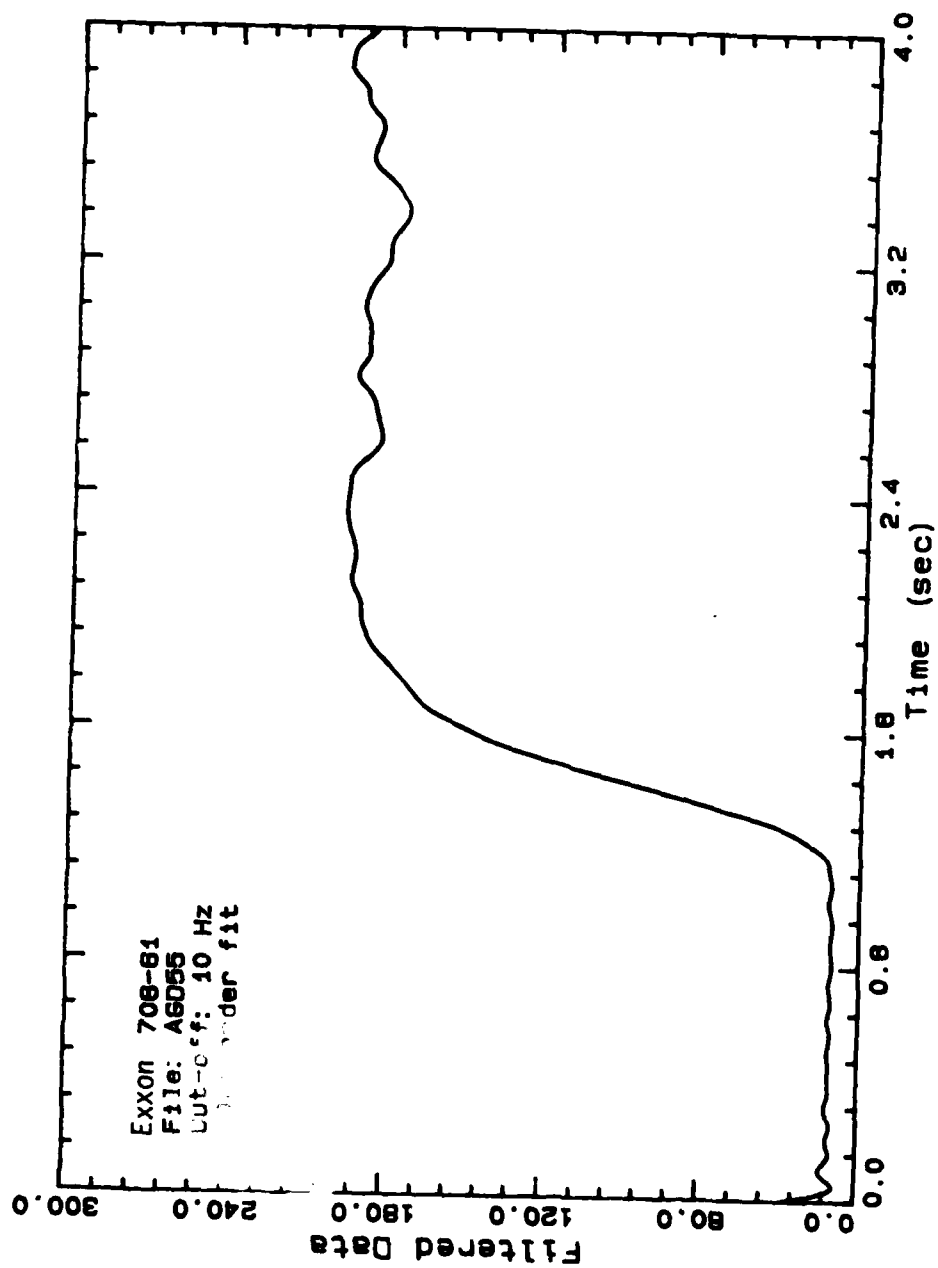
Figure 51. Filtered Data Using 10th-order Fit.

Exxon 708-61
File: A6D55
Cut-off: 10 Hz
...der fit

100

Figure 52. Filt.. 15th-order fit

Exxon 708-81
File: AG055
Cut-off: 10 Hz
15th-order fit

Filtered Data

Time (sec)

101
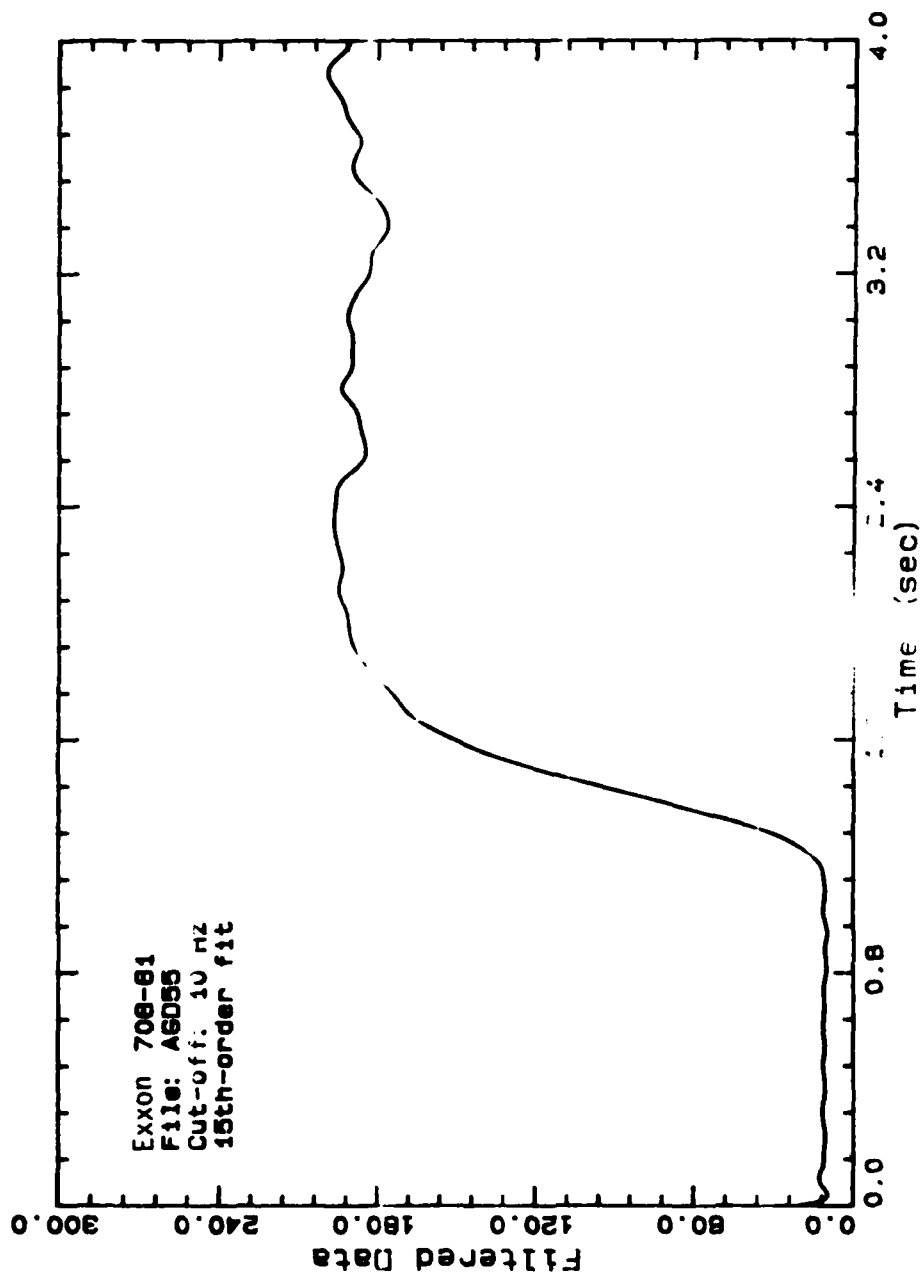
Figure 53. Comparison of Raw Data, 5th-order Fit, and Filtered Data.

was 10 to 20 C depending on the experimental temperature. The nitrogen valve was also opened to let the gas flow at a rate of around 0.5 SCFM. Minor adjustment could be made by changing the flow rate of the cooling agent and the flow rate of the nitrogen gas in the chamber to keep the temperature of the sample constant. The nitrogen helped circulation and prevented the condensation of water on the plate and cone.

To further reduce the interaction between the chamber and room, a plastic wrap was used to cover the chamber to minimize the air entering from the bottom.

A.5.2 Loading Sample

After the plate and cone reached the desired temperature, the gap setting reference measurement was determined as described in the manual(83).

Gap setting was much more difficult at the low temperatures than at room temperature. Studies were undertaken to correlate the change in the zero gap with temperature. Repeat runs were measured by decreasing then increasing the temperature. The results were not reproducible at a fixed temperature. There was always a jump at zero temperature. By disregarding the zero temperature jump and bracketing the gap size change into two regions, it was found that the change of gap size with temperature was 0.05×10^{-3} inch per degree centrigrade. For better reliability, the zero gap was determined individually at each temperature.

The sample was loaded as quickly as possible and allowed to rest at least 3 hours. The sample had to sit a sufficient amount of time to recover to its ground state. Different rest hours were tested at a shear rate of 27.6 sec^{-1} and it was found that at least 3 hours was needed to obtain a reproducible result (within the noise limits as caused by the natural frequency of the measuring torsion bar) in transient response as shown in Figure 54.

103
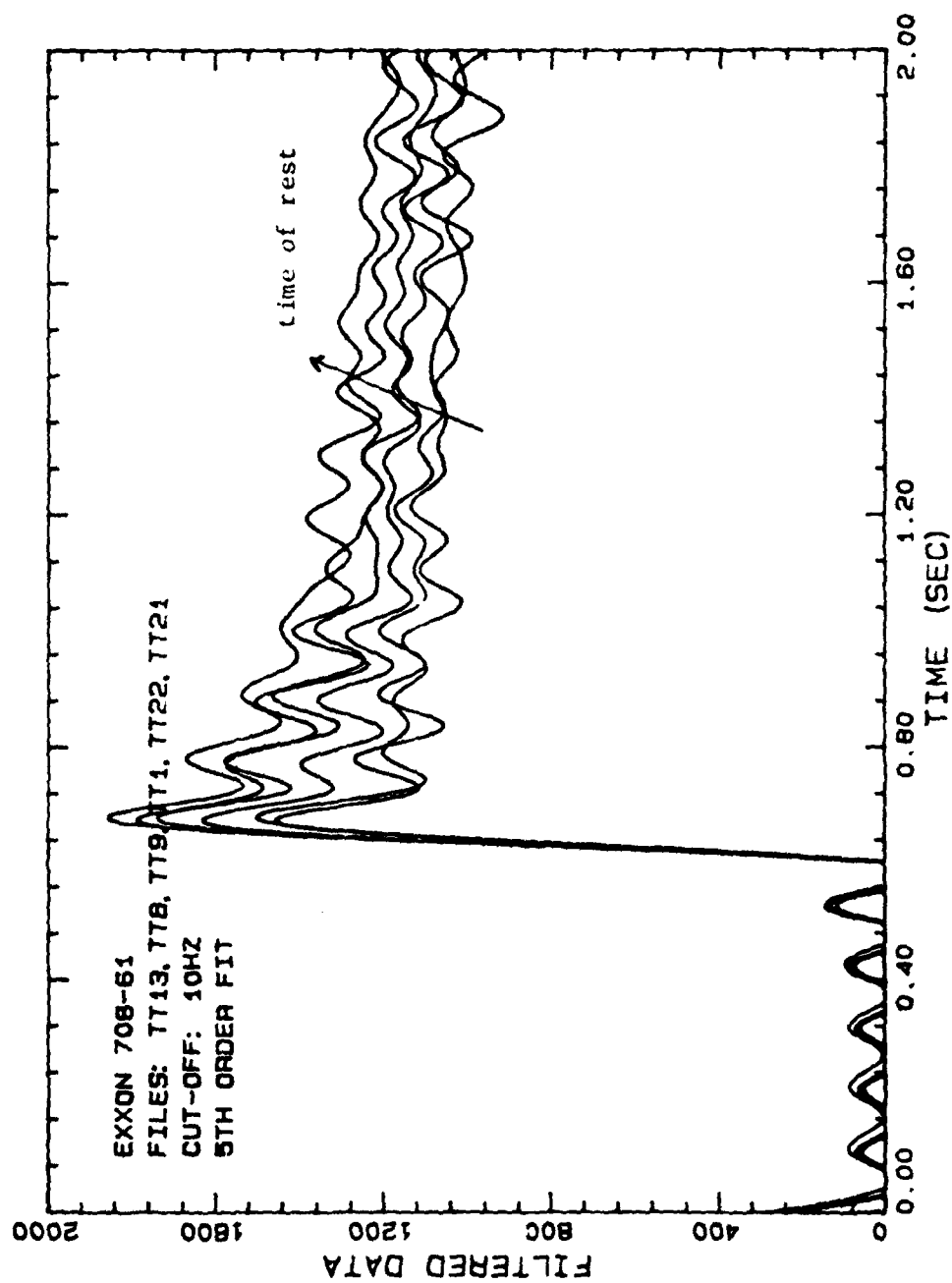
Figure 54. Transient Response of Exxon 708-61 at
$\dot{\gamma} = 27.6 \, sec^{-1}$ as a Function of Rest Time.

EXXON 708-61
FILES: TT13, TT8, TT9, TT1, TT22, TT21
CUT-OFF: 10HZ
5TH ORDER FIT

time of rest

FILTERED DATA

TIME (SEC)

104

A.5.3 Data Acquisition

A software package written by Kibler and Mohler was used to acquire data. The programs were written in an interactive mode which made the data sampling flexible. The flow chart of the operation is shown in Figure 55.

After the sample reached and rested at the desired temperature, the following steps were used to sample the data.

(1) Run "PASSTHRU" to initiate the LSI 11/02.
(2) Load the "absolute loader" and "LSIPGM.OBJ" to the LSI 11/02.
(3) Set up a frequency table on the LSI 11/02, to ready the LSI to acquire data.
(4) Select the required shear rate by the gear box setting.
(5) Turn on the motor and set the electromagnetic clutch to "brake" position.
(6) Switch clutch from "brake" to "drive" position, simultaneously turning on the data acquisition switch of the LSI. The data are taken by LSI automatically based on the table setup, and terminatation occurs either at the end of selected time or when the switch is turned off.
(7) Transfer the data from the LSI to the VAX.
(8) Repeat (3) to (7) until finished collecting data.

For most measurements, 1000 Hz was used to sample the first part of stress growth or stress relaxation, and 100 Hz was used for steady state measurement.

105

```
VT100          RUN PASSTHRU
Terminal    -------------------------    VAX 11/780
                                               ||
                   ABSOLUTE LOADER             ||   TRANSFER
                          LSIPCM               ||     DATA
                                               ||
                                               ||
                                               ||
                                               ||
                                               ||
                   SAMPLING DATA               ||
R-1 )       -------------------------    LSI 11/02
```
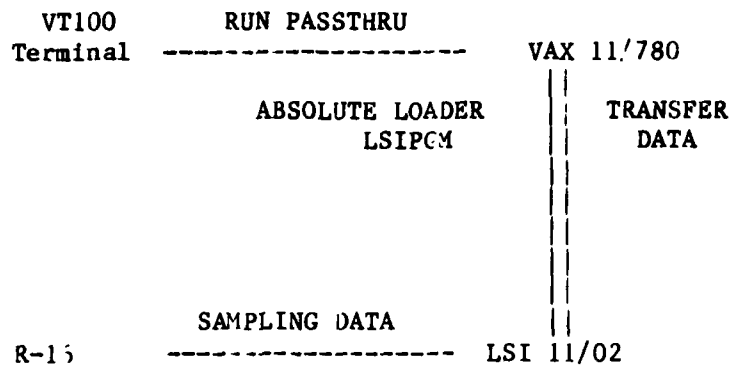
```
PROGRAMS NEEDED
==== :=========
ALDR GM.LSI
.SIG M.OBJ
PASS HRU.EXE
```

Figure 55.   Flow Chart of Data Acquisition

B.   Results

B.1   Structural Viscosity

A simple test was conducted on each material to see if there was a
structural viscosity. Each sample was rested for 2 hours before
testing. Then, the sample was sheared under a constant shear rate, an
increasing shear rate and then a decreasing shear rate. The shear rate
was changed fast enough so that the material did not have time to relax
to its ground state. It was found that there were hysteresis loops for
Sun Tech809-995, Sun Tech 839-988, and Exxon 708-61 materials, which show
that these materials do have structural viscosities. Clearly, the
materials take time to recover their original states; i.e., the
relaxation time of materials is not negligible. Suntech 839-919 had no
hysteresis loop. The viscosity of Sun Tech 839-919 decreased with shear
rate but was independent of the shearing history. The results are shown
in Figure 56.

An easy and general technique (88) was used to demonstrate the
structural viscosity and thixotropy of Sun Tech839-938. Shear rates
were increased stepwise from 0.11 to 348 sec^{-1}, and the sample was
sheared at each shear rate for about 15 seconds. The shear stress was
recorded by the LSI 11 microprocessor at a rate of 10 Hz. The material
showed time-dependency over the entire shear rate range. At high shear
rates, thixotropic behavior was observed; i.e., the viscosity decreased
with time. At low shear rates, upon sudden start up, the viscosity
increased to a maximum then decreased to an asymptotic value. After
cessation of shear, the viscosity did not return to zero because of the
yield stress of the material. The response curves at different shear
rates are shown in Figure 57.

After the sample was sheared at the highest rate of 348 sec^{-1}, the speed
was reduced, step by step. The sample was then rested for a short time,
about 5 minutes, and the shearing was repeated ascending from the lowest
shear rate. As seen in Figure 58, after each abrupt decrease in shear
rate, a small increase in stress was observed. The initial peak in the
repeat shearing was not as high as in the original test. Figure 58 also
shows that the longer the rest time, the higher the initial peak. This
type of study provided a preliminary picture of Sun Tech 839-988: it is
a material with structural viscosity and a yield stress. The magnitude
of yield stress can be determined from the basic shear diagram.
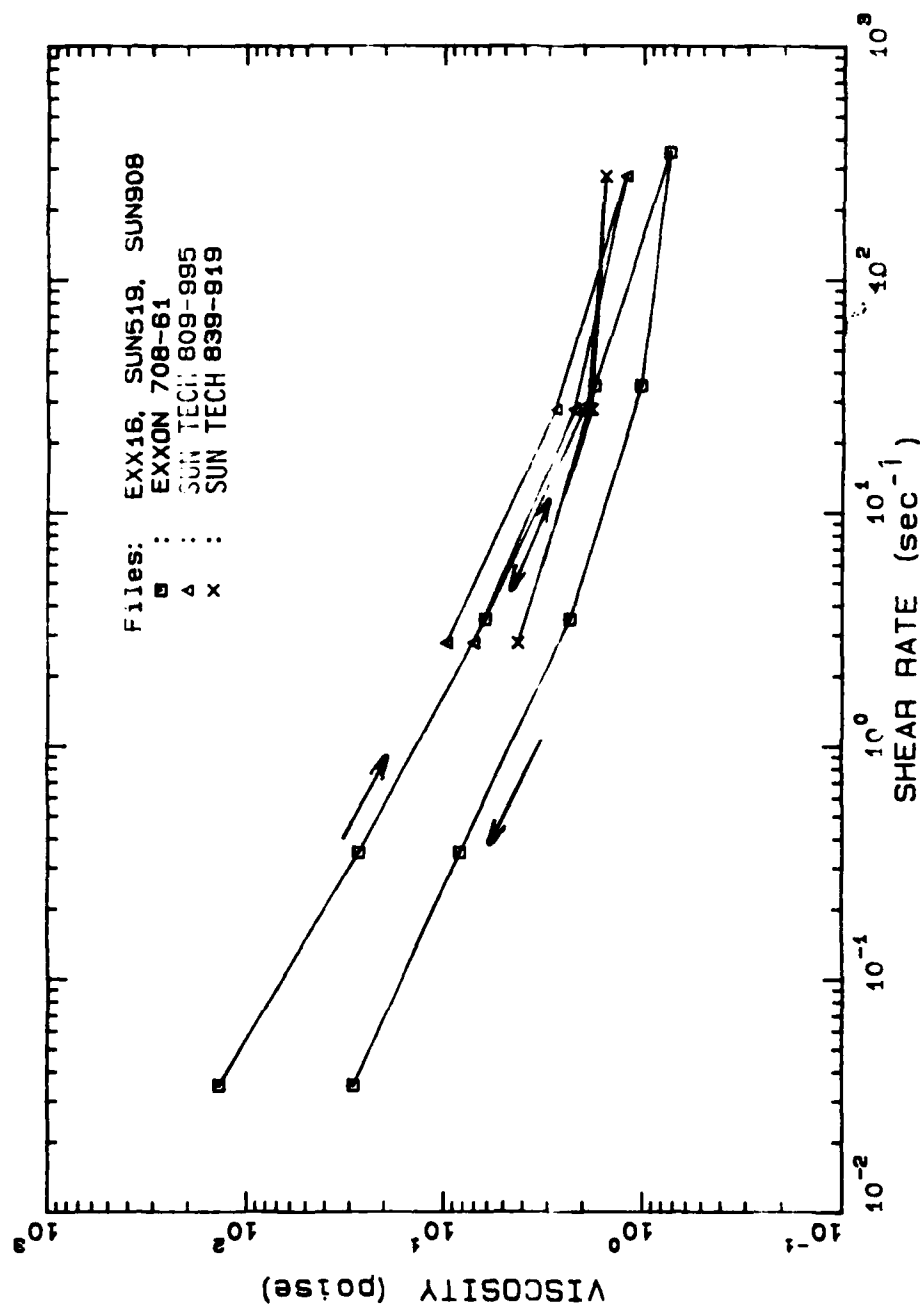
107

Figure 56. Hysteresis loop test for Structural Viscosity.
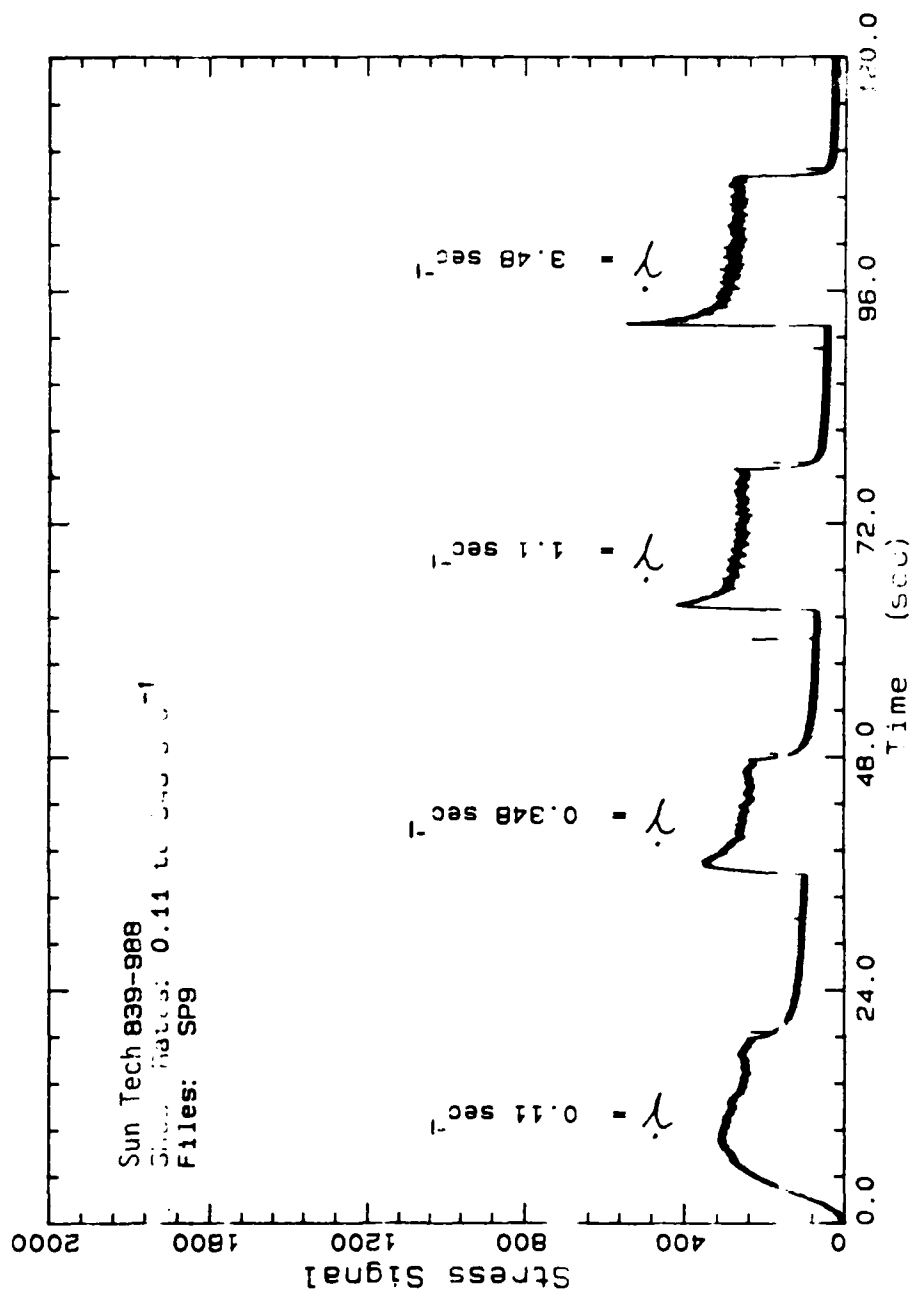
108

Figure 57 (Part 1). Stepwise Increase of Shear Rate to Show Structural Viscosity and Thixotropy.
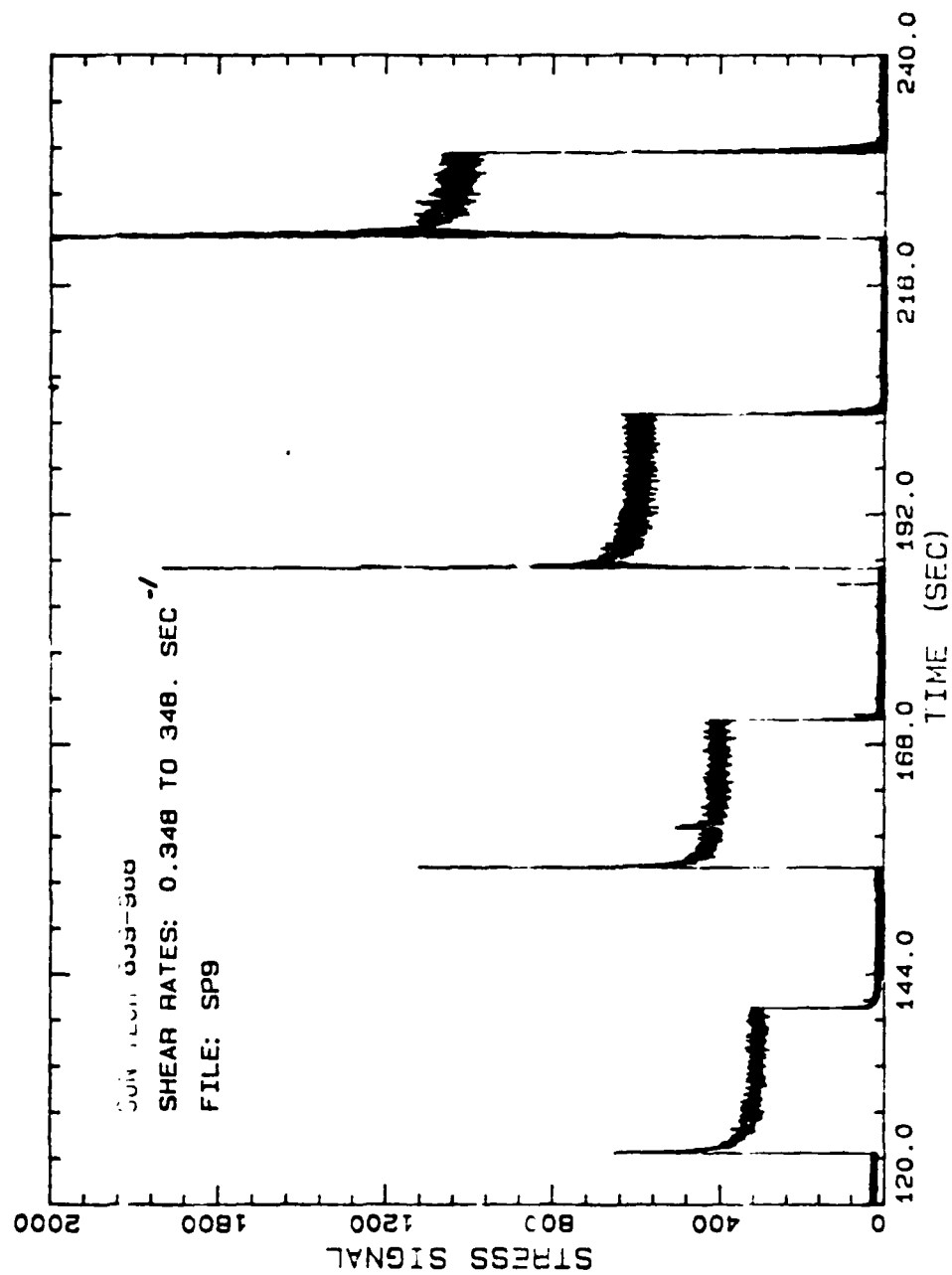
109

Figure 5? (Part 2). Stepwise Increase of Shear Rate to Show Structural Viscosity and Thixotropy.

110
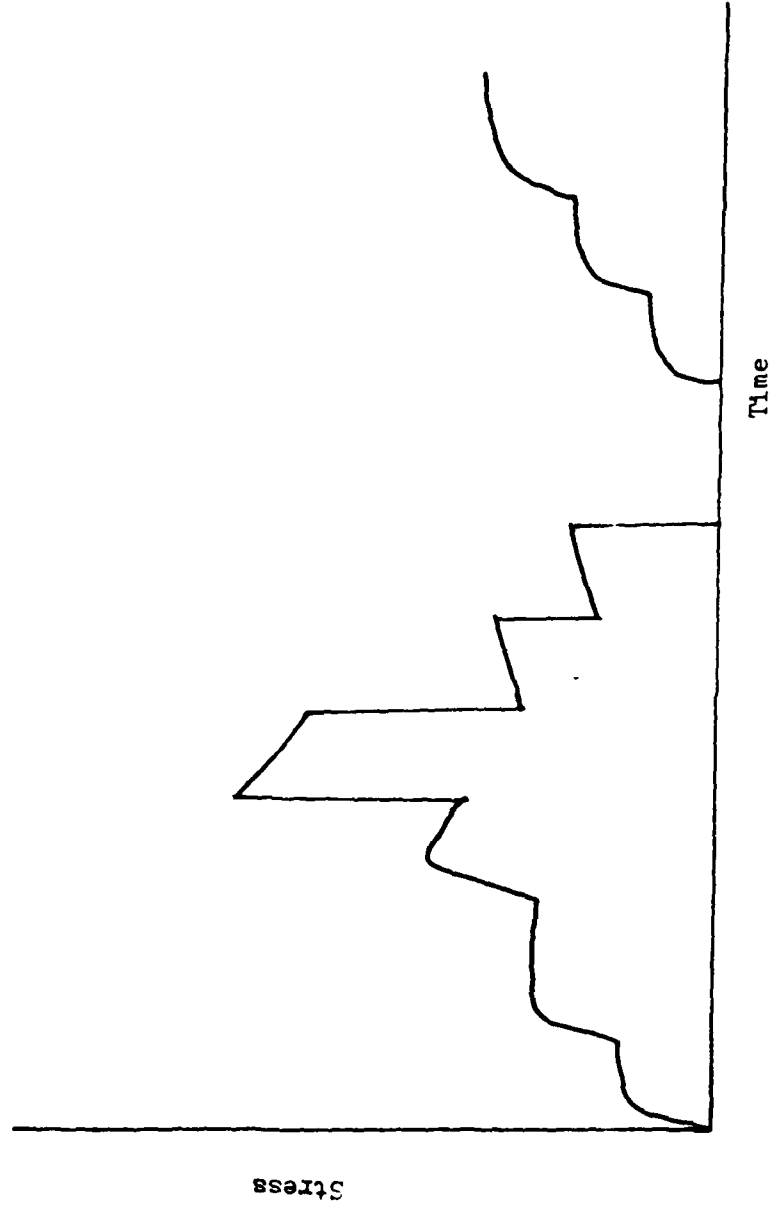
Figure 58. Preliminary Test to Demonstrate Structure Recovery.

111

B.2   Basic Shear Diagram

All of the measurements were taken based on the new technique
previously mentioned; i.e., the sample was covered with JP-10 while
resting to avoid the skinning effect. At high shear rates, the excess
JP-10 was removed to minimize any edge effects. Equilibrium stresses
were obtained by shearing the material until reaching steady state,
beginning with the lowest shear rate. The procedure was repeated at
high shear rates until the highest shear rate was obtained. All of the
equilibrium stresses were digitalized at a rate of 100 Hz. Repeated
runs were conducted on each material to obtain reliable data. The
results were quite reproducible and were used to construct the basic
shear diagrams (BSD).

B.2.1   Room Temperature Results

The BSDs of slurry materials (Sun Tech809-995, Sun Tech839-919,
Sun Tech839-988, and Exxon 708-61) at room temperature are shown in
Figures 59 to 62. The equilibrium stresses are given in Table XVI. The
plots of the apparent viscosity as a function of the shear rate for the
four slurries are shown in Figure 63.

Over the range of shear rates studied, the four slurries are
non-Newtonian with shear-thinning behavior. Except for Sun Tech839-919,
the slurries are yield materials. Though Sun Tech839-919 showed a
tendency to increase viscosity at high shear rates, it is difficult to
say if the increase was due to dilantancy or instability.

B.2.2   Low Temperature Results

Since part of the temperature effect on the viscosity of slurries
comes from the solvent, the viscosity of JP-10 was studied from 25 C to
-20 C, as shown in Figure 64 and Table XVII. The viscosity of JP-10 did
not change much with temperature. The viscosity increased from 2.76 cp
to 9.25 cp as the temperature dropped from 25 C to -20 C. The change of
viscosity of JP-10 with temperature can be described by an Arrhenius
type equation:

$$\eta = 0.0023545 * [\exp(2098.348/T)]$$
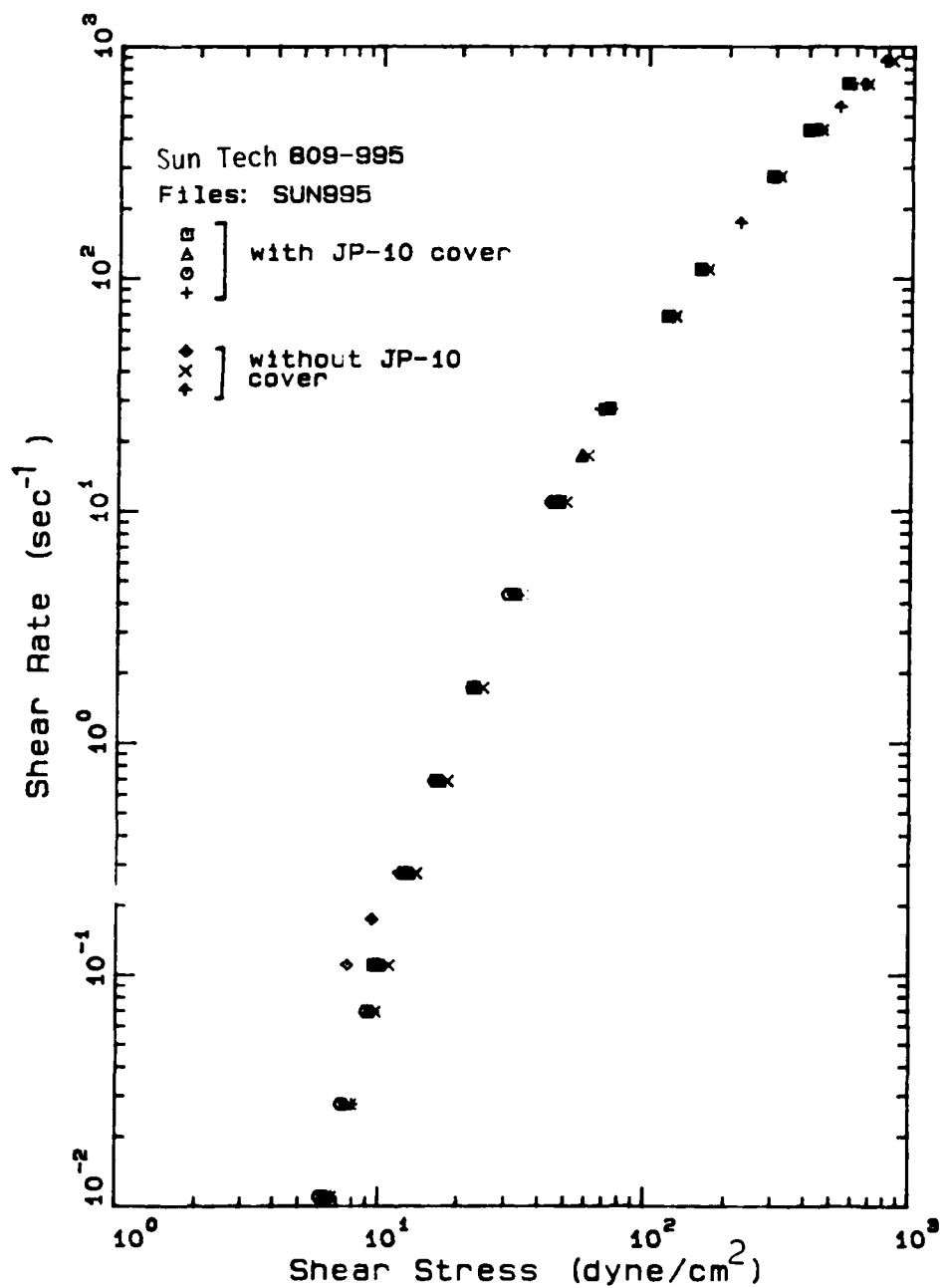
Figure 59.   Basic Shear Diagram of
            Sun Tech 809-995 at
            Room Temperature.

113
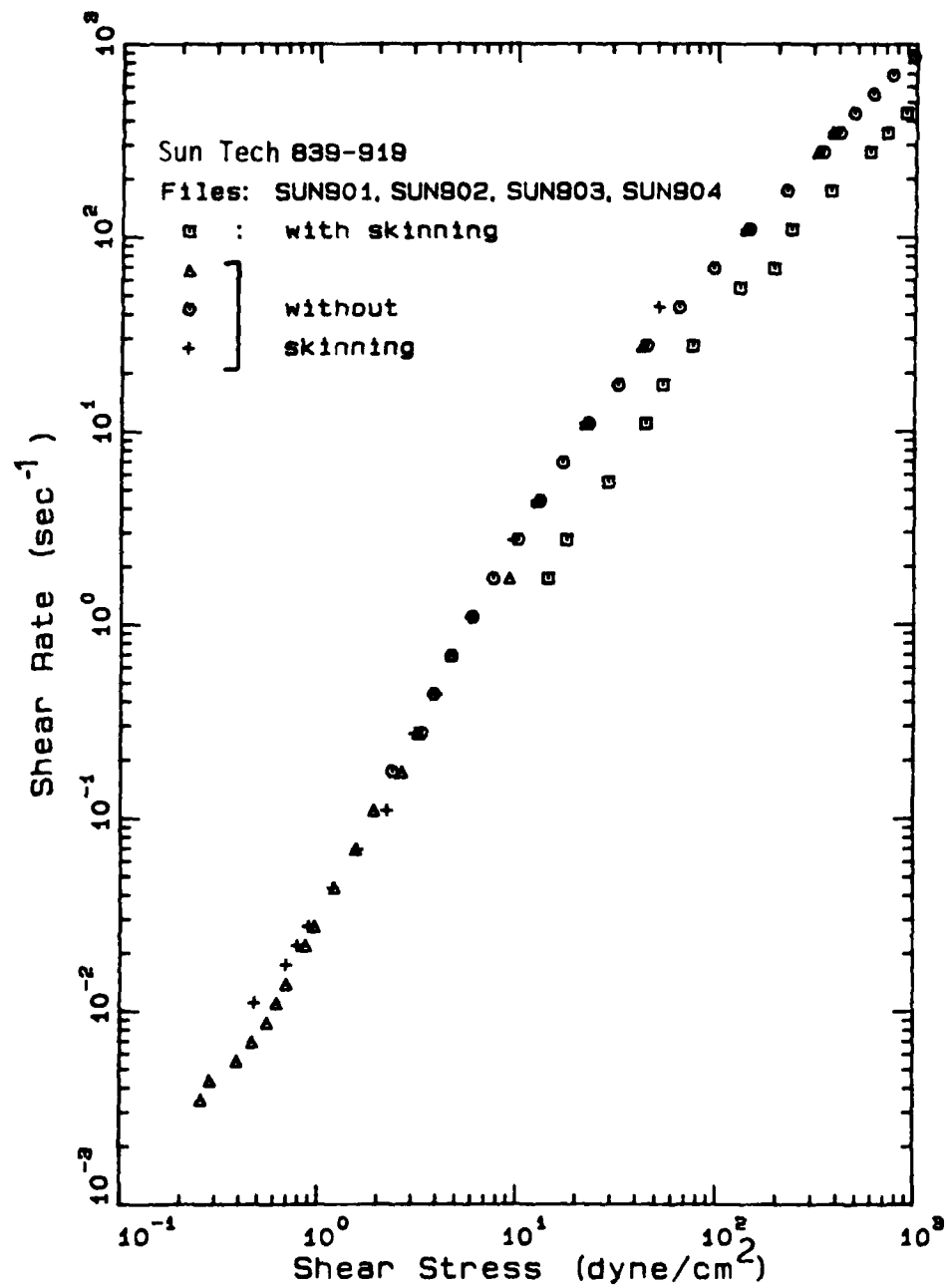
Figure 60. Basic Shear Diagram of
Sun Tech839-919 at
Room Temperature.

114
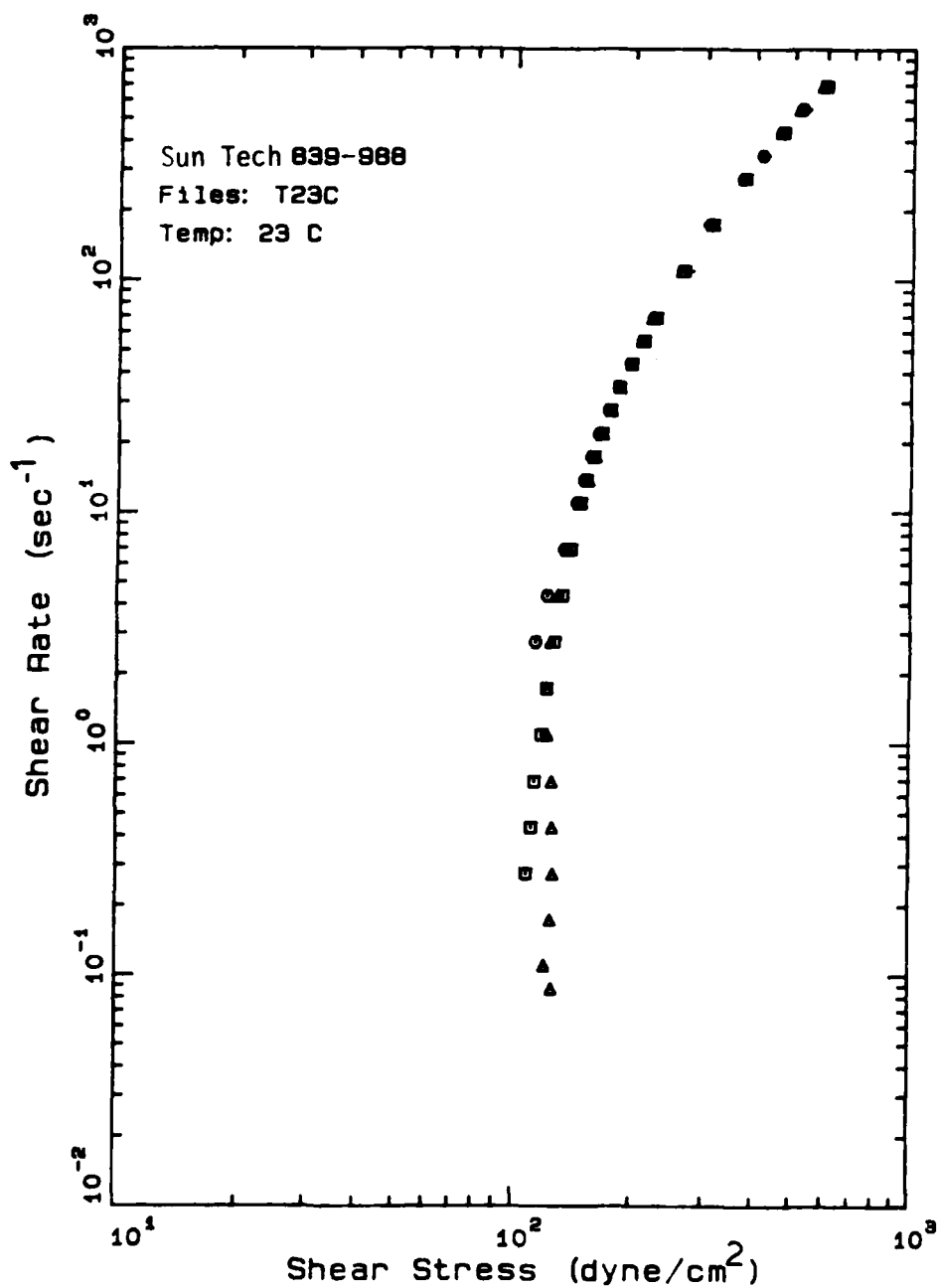
Figure 61. Basic Shear Diagram of
Sun Tech839-988 at
Room Temperature

115
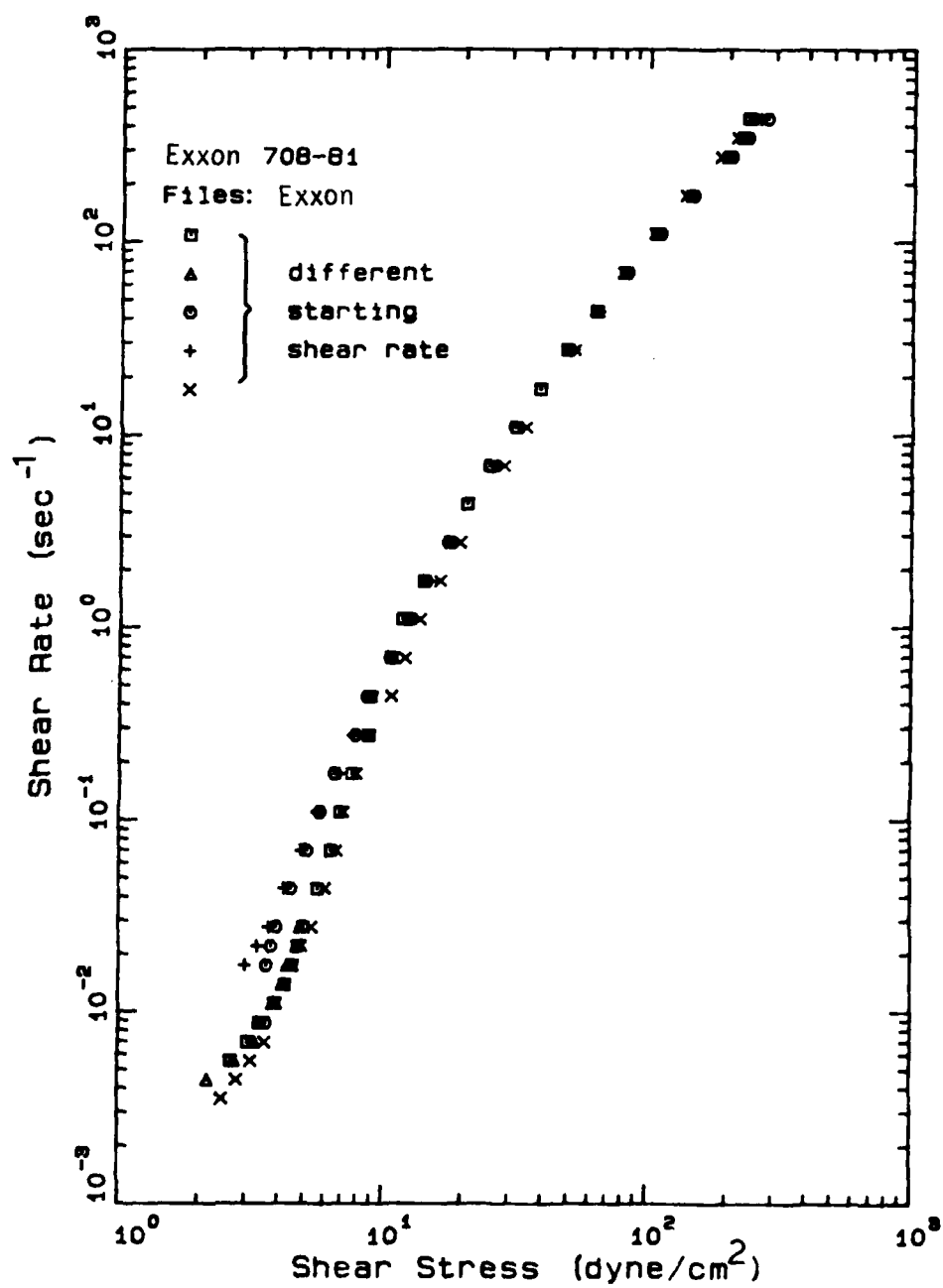
Figure 62. Basic Shear Diagram of Exxon 708-61
at Room Temperature.

Table XVI. Equilibrium Stresses of Slurries

rate	stress			
	919	995	988	708-61
0.00348	0.27	-	-	2.33
0.00438	0.32	-	-	2.61
0.0055	0.37	-	-	2.90
0.00692	0.42	-	-	3.20
0.0087	0.49	-	-	3.51
0.011	0.57	6.47	-	3.83
0.0138	0.65	-	-	4.14
0.0174	0.75	-	-	4.46
0.0276	0.97	7.44	-	5.10
0.0438	1.25	-	-	5.76
0.0692	1.60	8.96	-	6.45
0.11	2.02	9.98	116.3	7.19
0.174	2.53	11.21	116.6	8.01
0.276	3.16	12.71	116.8	8.96
0.438	3.94	-	117.2	10.08
0.692	4.92	16.71	117.9	11.43
1.1	6.19	-	118.8	13.11
1.74	7.83	22.73	120.9	15.22
2.76	10.02	-	124.4	17.91
4.38	13.03	32.07	129.6	21.40
6.92	17.17	-	136.7	25.90
11.0	23.13	47.17	146.3	31.90
17.4	31.69	58.24	158.8	39.76
27.6	44.44	73.04	175.3	50.29
34.8	53.09	-	185.4	-
43.8	63.68	-	196.8	64.39
69.2	92.98	120.52	224.6	83.07
110.0	138.6	159.69	261.8	108.4
174.0	209.52	215.67	310.6	141.8
276.0	321.61	299.04	376.8	186.1
348.0	400.22	-	418.7	213.3
438.0	497.82	426.22	467.4	244.1
550.0	618.14	513.15	524.1	-
692.0	768.6	623.26	591.8	-
870.0	953.6	763.56	-	-
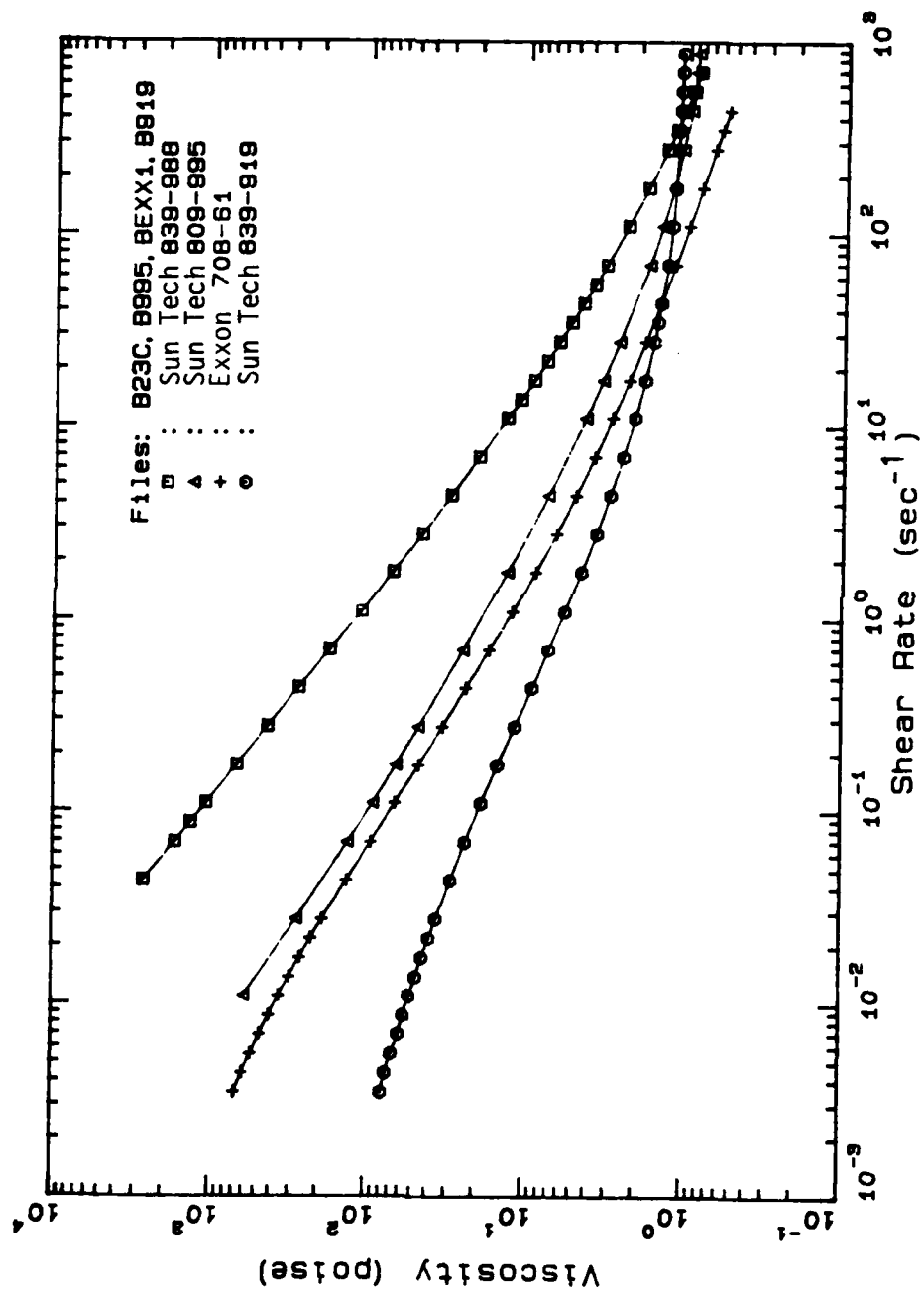
Figure 63. Apparent Viscosity of Slurry Fuel Samples.
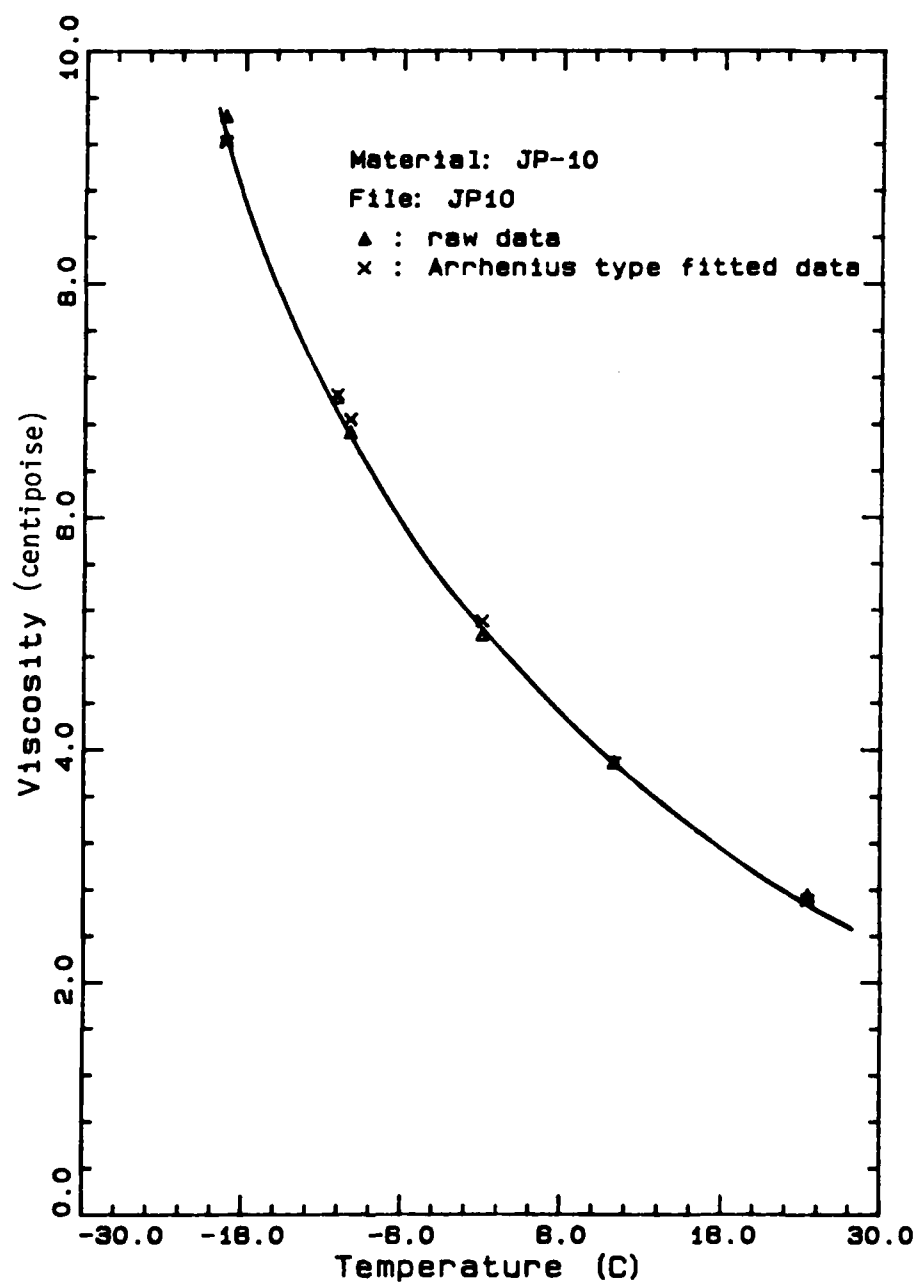
Figure 64. Viscosity of Solvent JP-10
at Different Temperatures.

Table XVII. Viscosity of JP-10 at Different Temperatures

Temp(#C)	Viscosity(cp) Measured	Viscosity(cp) Calculated
24.5	2.7564	2.7135
10.0	3.8954	3.8932
0.0	4.9886	5.1067
-10.0	6.7256	6.8379
-11.0	7.0249	7.0490
-19.5	9.4395	9.2177
-19.5	9.2486	9.2177

Standard Deviation = $1.82 * 10^{-2}$

These results check well with the results recently provided by Wright-Patterson AFB.

Only selected slurries were studied at low temperatures. Sun Tech 809-995 was studied because of its ease of handling. Sun Tech839-988 and Exxon 708-61 were measured at low temperatures due to their prominent yield stresses.

The BSDs of Sun Tech809-995 at temperatures of 25 C, 0 C, -5 C -10 C, and -20 C are shown in Figure 65. Flow curves at different temperatures have the same shape and shift to the right as temperature decreases; that is, the lower the temperature, the higher the viscosity. Exxon 708-61 was also studied at 1 C and -14 C as seen in Figure 66. As expected, the viscosity increased with a decrease in temperature and the BSD shifted to the right as the temperature decreased. A strange phenomenon was observed; the viscosity did not change much with temperature at low shear rates. This will be discussed later.

More interesting results were obtained for Sun Tech839-988 at low temperatures. The BSDs of Sun Tech839-988 at temperatures of 23, 9, 0, -10, -20, and -25 C are shown in Figure 67. One interesting result was that the viscosity increased or decreased as the temperature decreased depending upon the shear rate. At low shear rates, the viscosity decreased as temperature decreased, while at high shear rates, the viscosity increased as temperature decreased. The shear rate of 15 sec^{-1} was the break point for all temperatures. This will be discussed in the next section.

B.2.3   Yield Stress

BSDs in Figures 59 to 62 show that Sun Tech809-995, Sun Tech 839-988, and Exxon 708-61 are yield materials. The existence of a yield stress complicated the measurement at low shear rates. In turn, the yield stress was difficult to measure because very low shear rates were not attainable and because the instrument lacked enough sensitivity to measure the shear stress at low shear rates.

The yield stress can be determined from the vertical section in the log-log plot of the BSD or by extrapolation of the BSD to zero shear rate. The extrapolation is accomplished by fitting the data at low shear rates with a polynomial with a minimum deviation, then

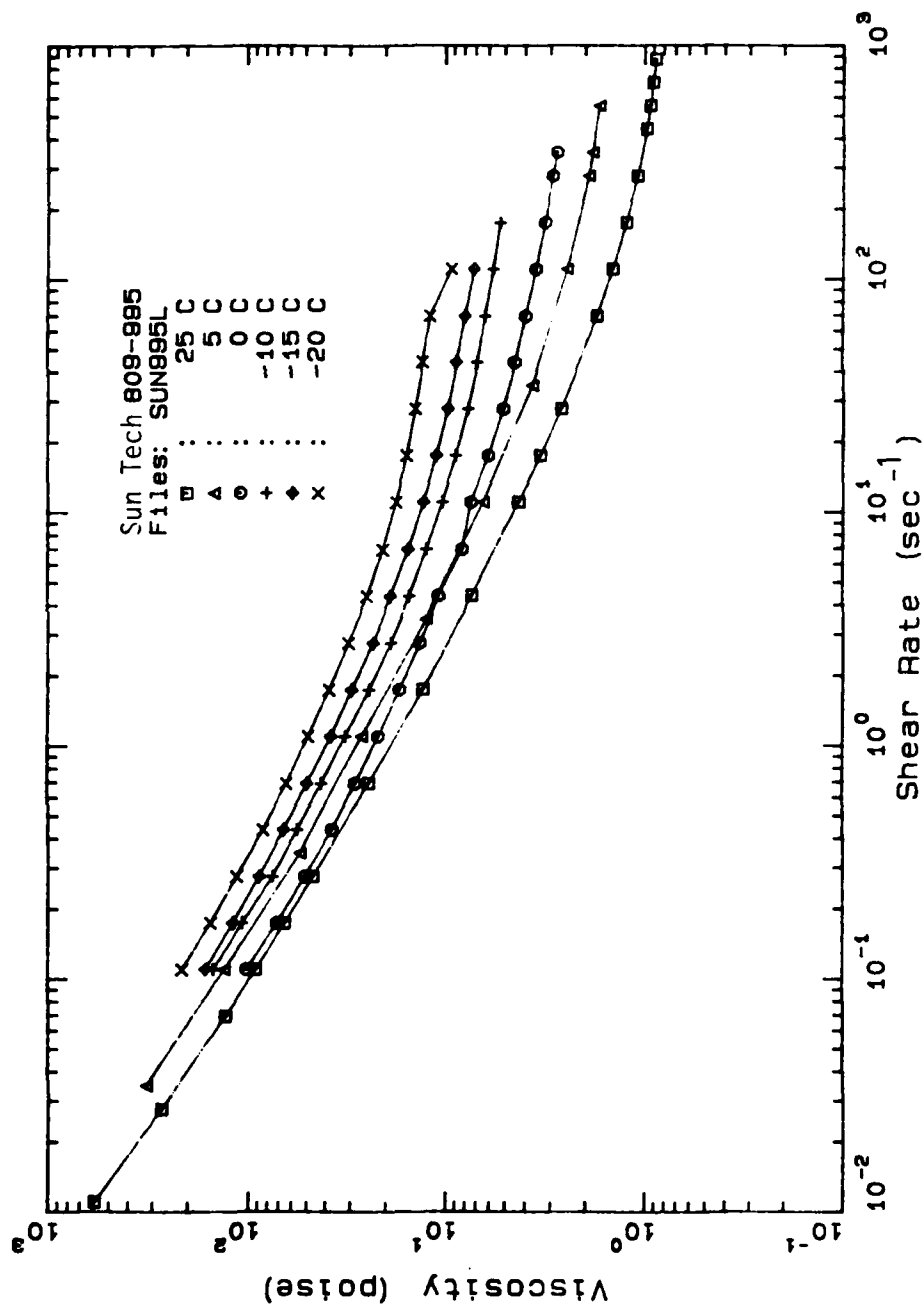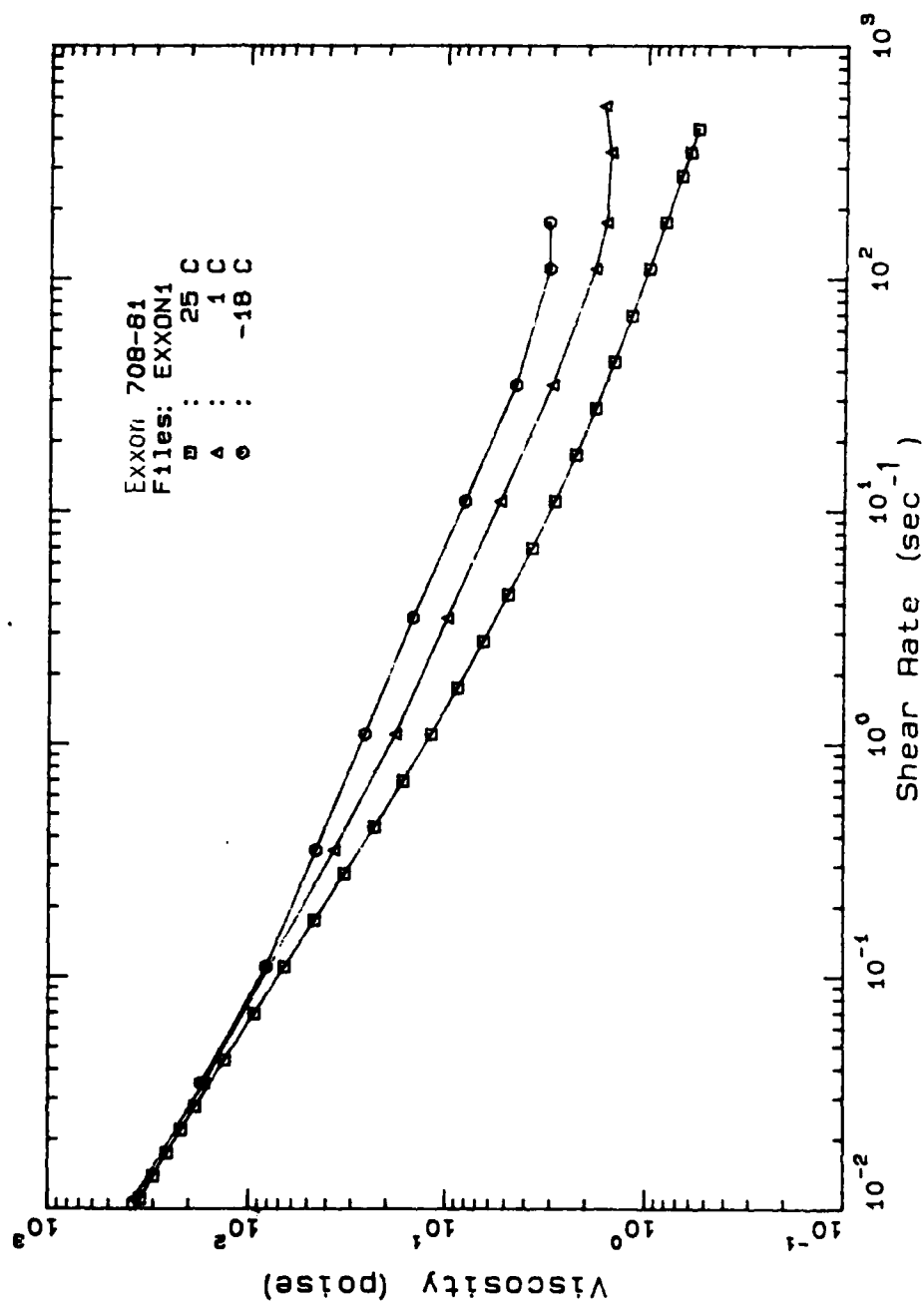Figure 65. Apparent Viscosity of Sun Tech809-995 Over a Range of Temperatures.

122

Figure 66. Apparent Viscosity of Exxon 708-61 over a Range of Temperatures.

123
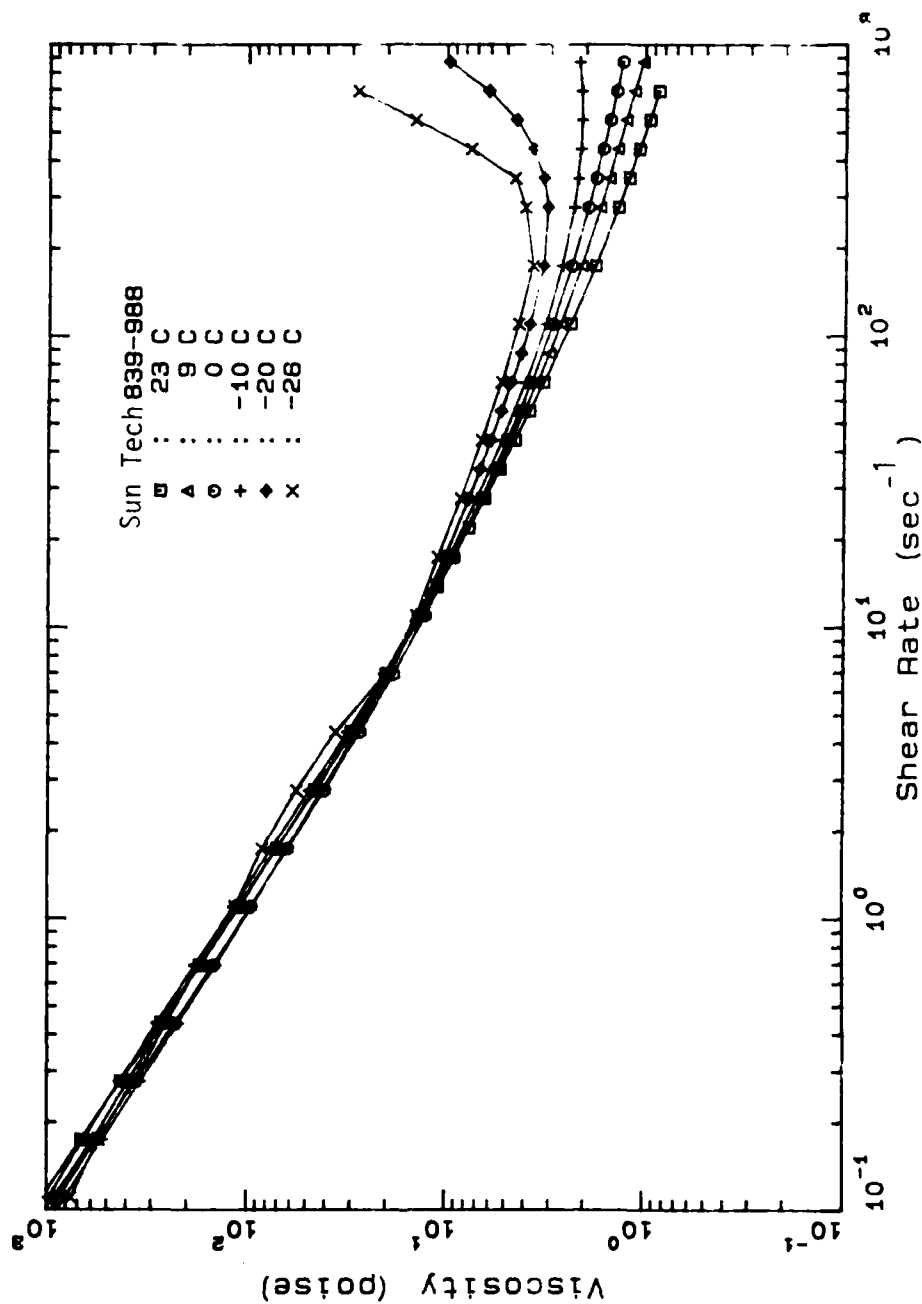
Figure 67. Apparent Viscosity of Sun Tech 839-999 Over a Range of Temperatures.

124

extrapolating the polynomial to zero shear rate. Yield stresses
obtained by both methods are listed in Table XVIII. Sun Tech 809-995 and
Exxon 708-61 both had a small yield stress, on the order of 5 dyne/cm^2.
The yield stress of Sun Tech 839-988 was appreciable, around 110
dyne/cm^2. The yield stresses of Sun Tech 839-988 at different
temperatures are given in Table XIX.

B 2.4 η_0 and η_∞

η_0 and η_∞ are lower and upper Newtonian viscosities. For
materials without a yield stress, such as Sun Tech 839-919, η_0 and η_∞
were determined from the apparent viscosity at low and high shear rates,
respectively. For yield materials, η_0 is infinite and $\eta_\infty \to \eta_p$ as
$\dot{\gamma} \to \infty$, where η_p is the plastic viscosity or Bingham viscosity.
Therefore, η_∞ was taken as the plastic viscosity which was determined
from the slope of the linear portion of the BSD plots at high shear
rates. Table XX gives η_0 and η_∞ of different materials at room
temperature. The change of η_∞ with the temperature of Sun Tech 839-988
is given in Table XXI.

B.3 Transient Response

Before model constants were evaluated, transient data were all
pretreated in the following sequence: filtered to remove noise,
adjusted for top plate movement, and normalized on the equilibrium
value.

First, a Newtonian fluid was studied. As expected, the transient
response of the viscosity was a step change after a step change was
imposed in the shear rate (see Figure 68). This response was
independent of shear rate. The study of the Newtonian fluid also
confirmed that the response time of the instrument is fast enough to
study the transient response of slurry materials.

The transient response of Sun Tech 839-919 and Sun Tech 809-995 were
similiar to Newtonian fluids. They showed little time dependency except
at high shear rates. Typical transient behavior of these two materials
is shown in Figures 69 and 70. Since these materials showed fast
response, they were not studied further by this technique.

125

Table XVIII. Yield Stresses of Slurries

| material | Yield Stress (dyne/cm**2) | |
	log-log plot	Curve fitting
Sun Tech909-995	8.0	5.0
Sun Tech839-988	110.0	110.0
Exxon 708-61	6.0	2.0

Table XIX. Yield Stresses of Sun Tech839-988
at Different Temperatures

Temperature(C)	Yield Stress(dyne/cm**2)
23.0	110.
9.0	100.
0.0	87.0
-10.0	88.0
-20.0	92.0
-26.0	101.0

Table XX. η_o and η_∞ of Slurries

Material	η_o	η_∞
Sun Tech809-995	∞	0.6
Sun Tech839-919	100.0	1.0
Sun Tech839-988	∞	0.3
Exxon 708-61	∞	0.3

Table XXI. η_∞ of Sun Tech839-988 at Different Temperatures

Temperature (C)	(Poise)
23.0	0.3
9.0	0.5
0.0	0.8
-10.0	1.4
-20.0	2.12
-26.0	3.0
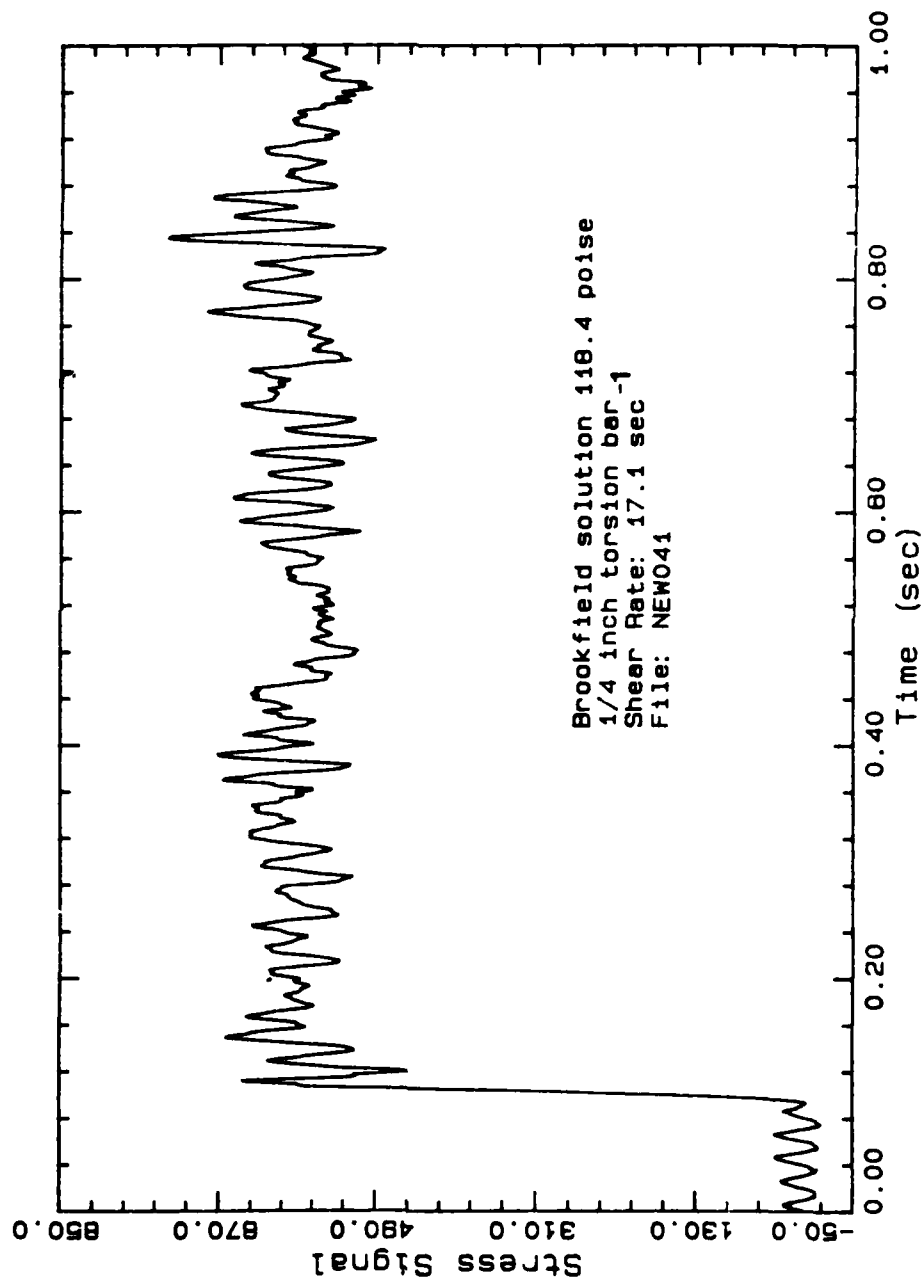
Figure 68. Transient Response of a Brookfield Standard Newtonian Solution.

Brookfield solution 118.4 poise
1/4 inch torsion bar
Shear Rate: 17.1 sec^{-1}
File: NEW041

128
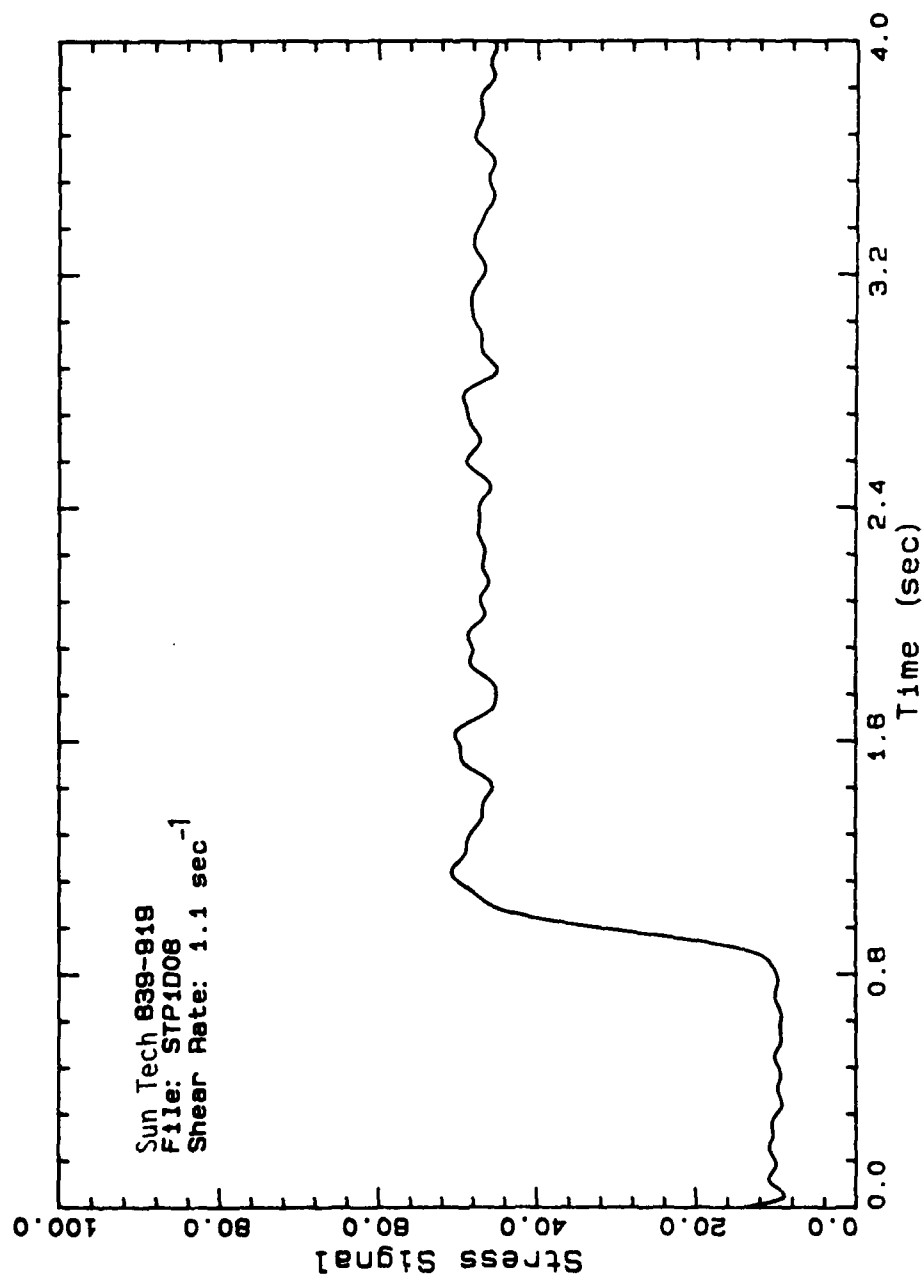
Figure 69. Transient Response for Sun Tech 839-919 at Low Shear.
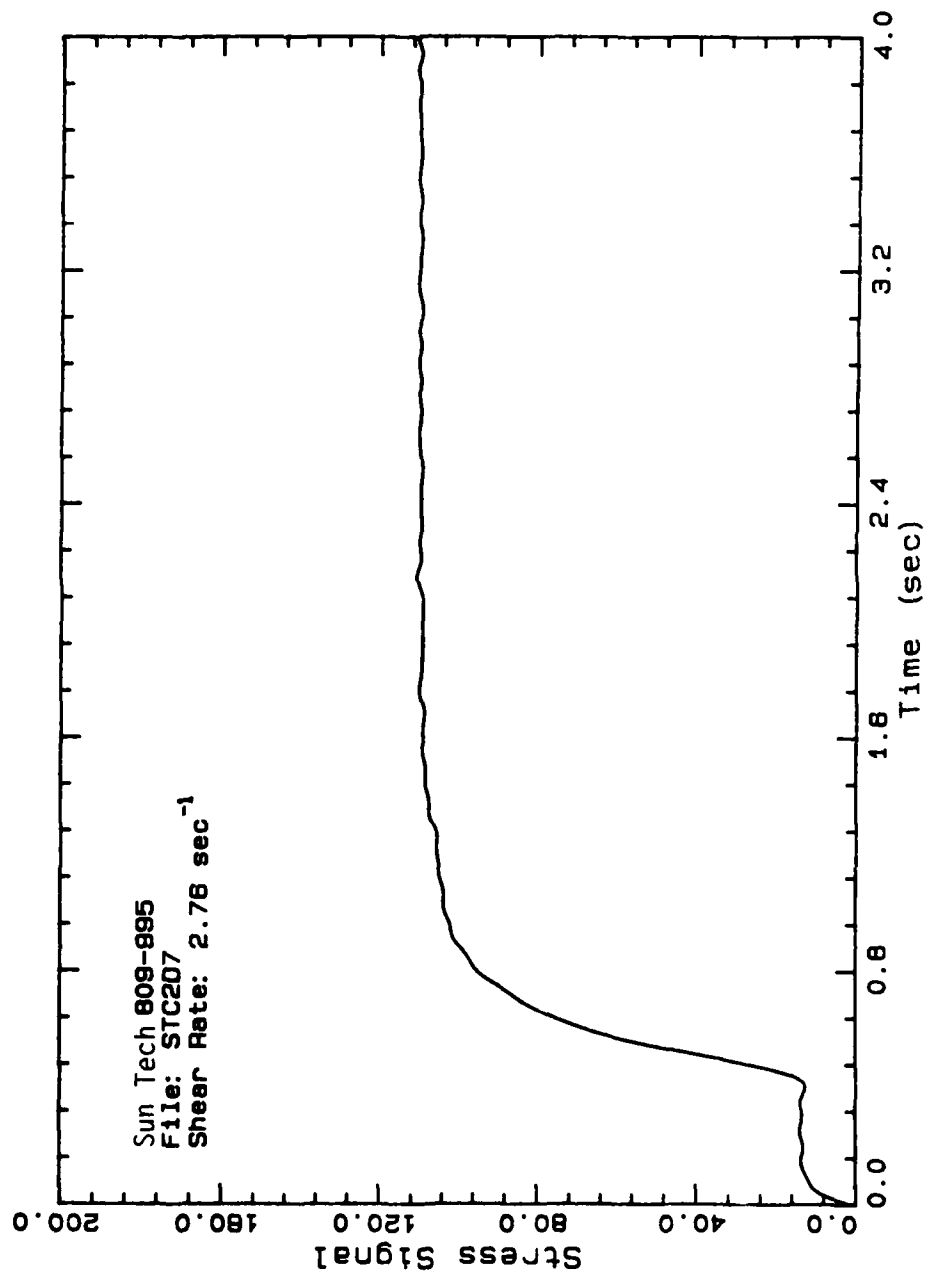
129

Figure 70. Transient Response for Sun Tech 809-995 at Low Shear.

130

The transient response of Exxon 708-61 is shown in Figure 71. The material showed a small peak at low shear rates and behaved as a thixotropic material.

The transient response curves for Sun Tech 839-988 at shear rates from 0.055 to 2.76 sec-1 are shown in Figure 72. The curves show solid property characteristics and structural viscosity at low shear rates. Even at low shear rates, overshoot was observed.

The original and corrected data for top plate movement at two different shear rates are shown in Figure 73 and 74. The correction was minor and did not adversely affect the initial slope. The peak values were slightly shifted.

B.4   Kinetic-Elastic Model

The kinetic-elastic model was modified to describe the flow behavior of slurry materials for both steady state and transient conditions. The yield stress, τ_y , was incorporated into the equation. Different approaches were tried and the best result was obtained by replacing values of the τ in the equation by $\tau_y - \tau$, which is equivalent to a shift in the axis by τ_y, as shown in Figure 75. For convenience, τ' is used to represent $\tau - \tau_y$ in the following section. Actually, this is a generalized definition of the kinetic model. For a material with no yield, $\tau_y = 0$, the equation reduces to the original form. The modified equation can be applied to any system with or without yield stress.

B.4.1   Definition of Structural Parameters

The structural parameter, F, is a function of viscosity. Different functions have been tested to define F. Though different definitions of F can be used with the kinetic theory to correlate the steady state data, some of them fail to describe the solid behavior at the low shear rates in the transient response. The inverse level rule and the Richardson-Zaki equation were used depending on the nature of the slurry.

131
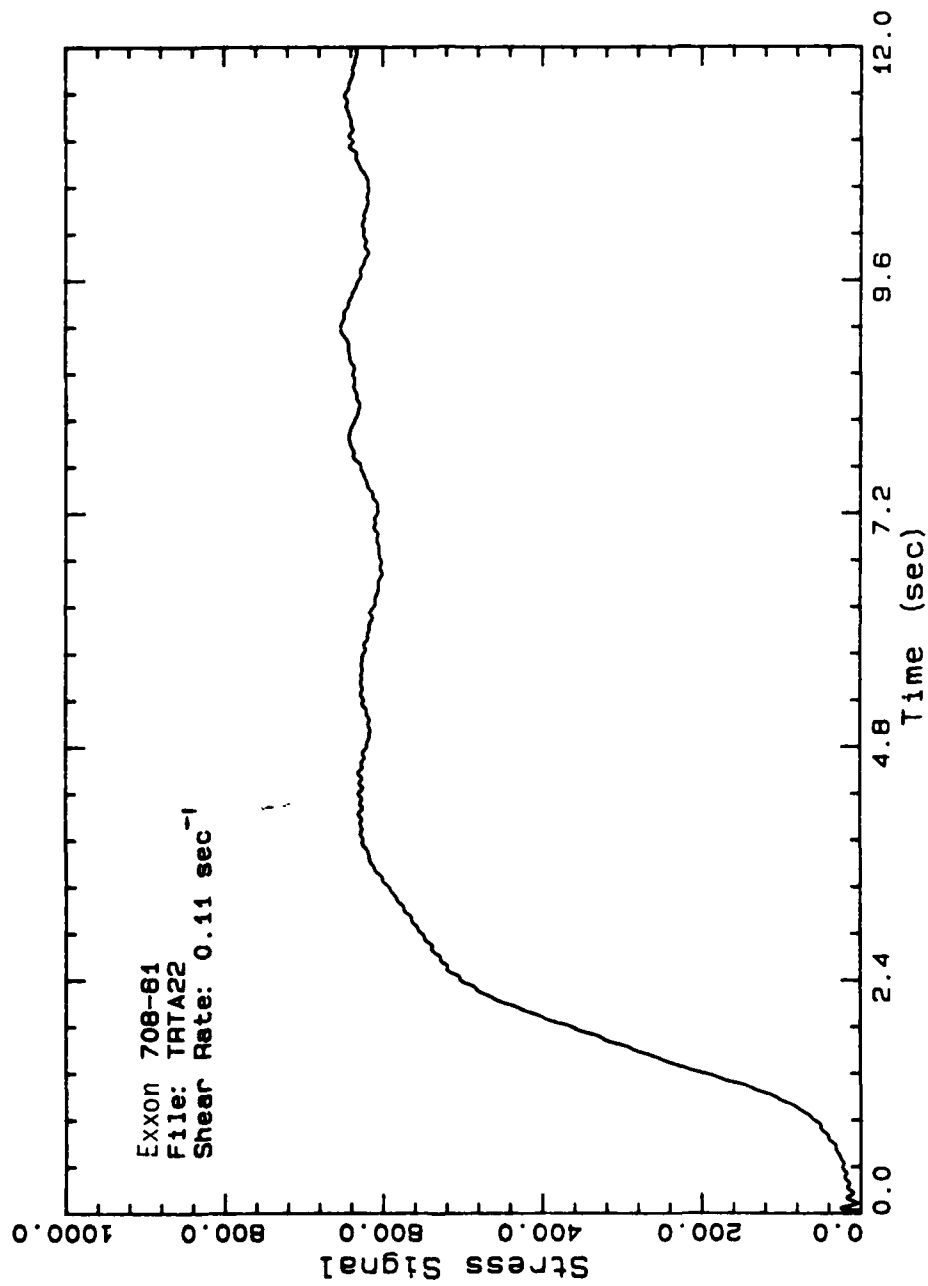
Figure 71. Transient Response for Exxon 708-61 at Low Shear.

Exxon 708-61
File: TRTA22
Shear Rate: 0.11 sec^{-1}

132
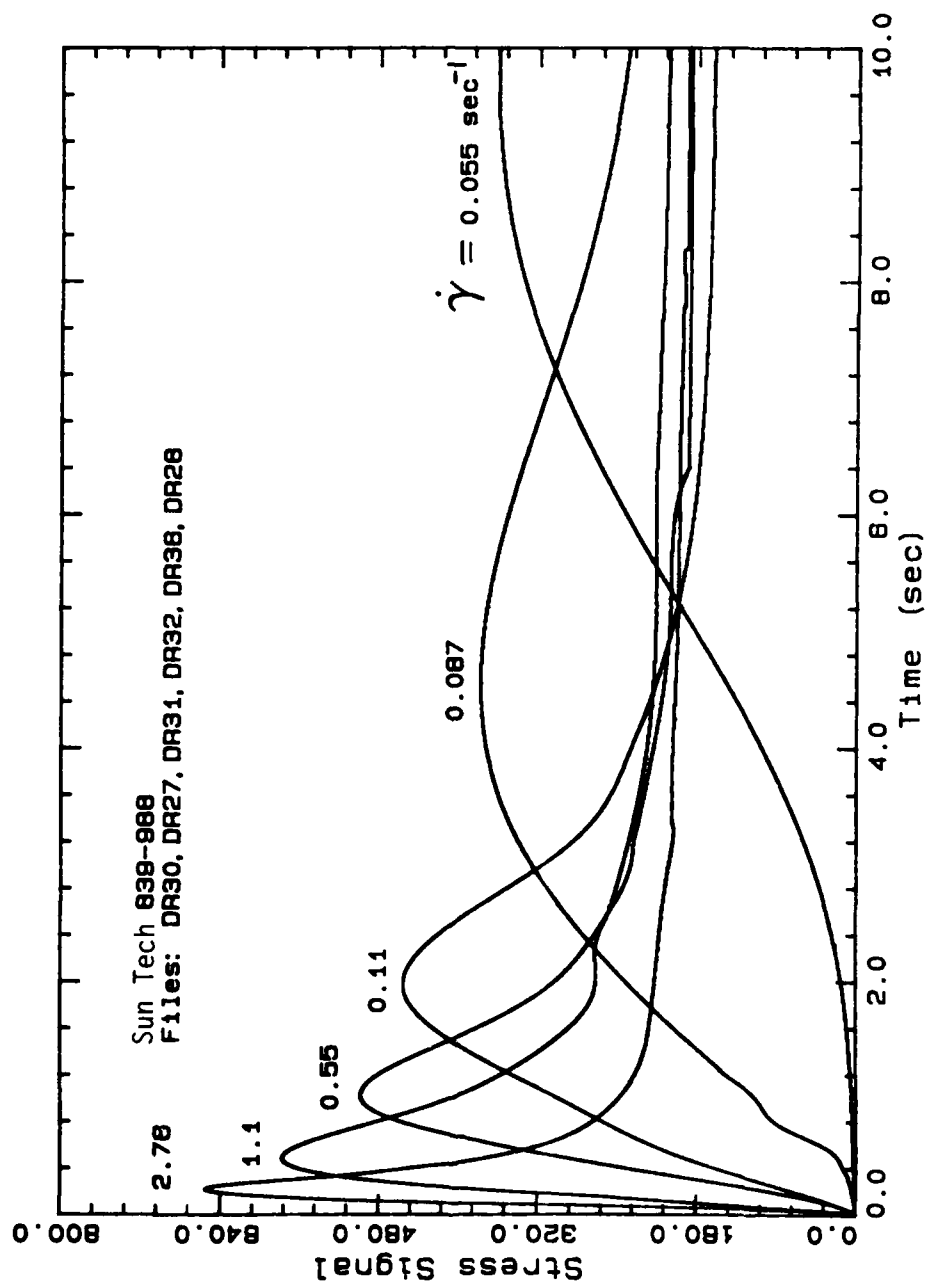
Figure 72. Transient Response Curves for Sun Tech 839-988 at Low Shear Rates.

133
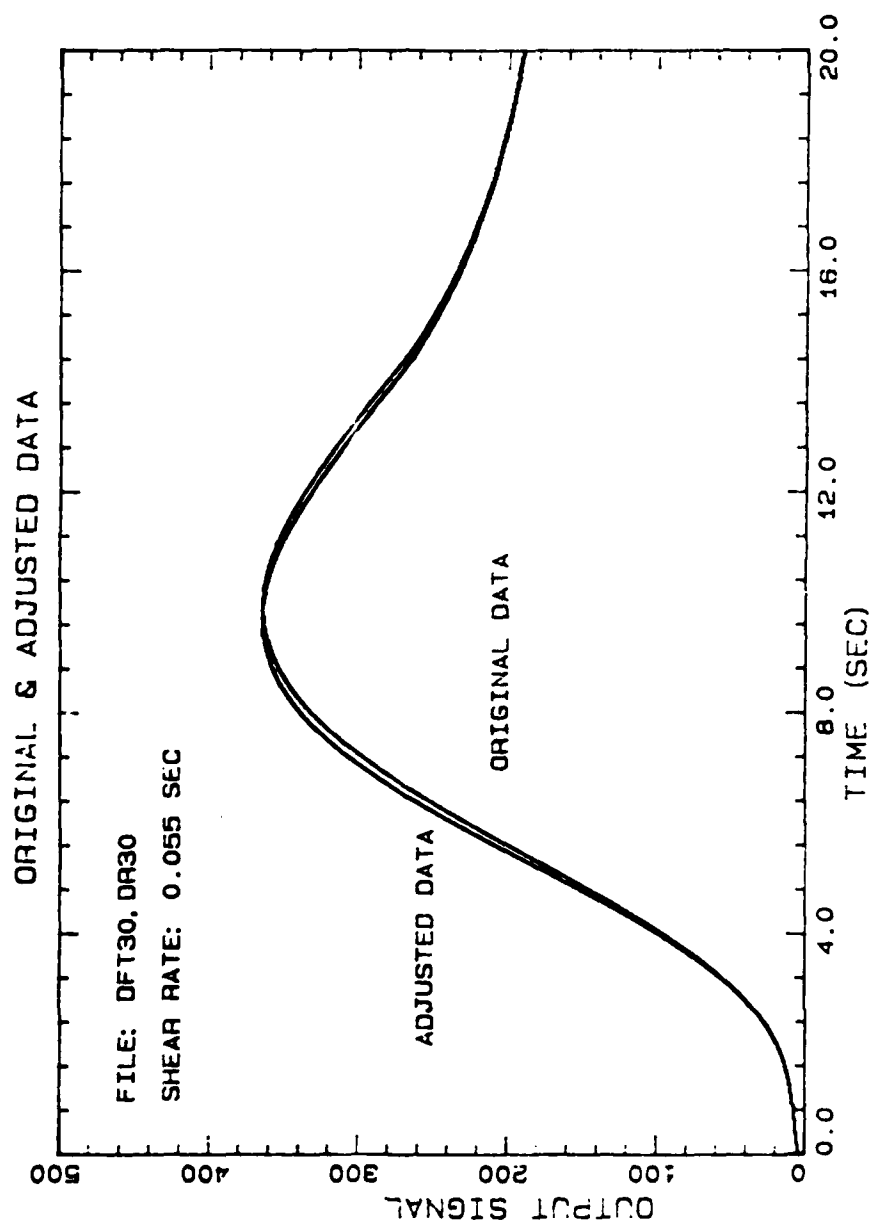
Figure 73. Data Correction for Top Cone Movement.

134
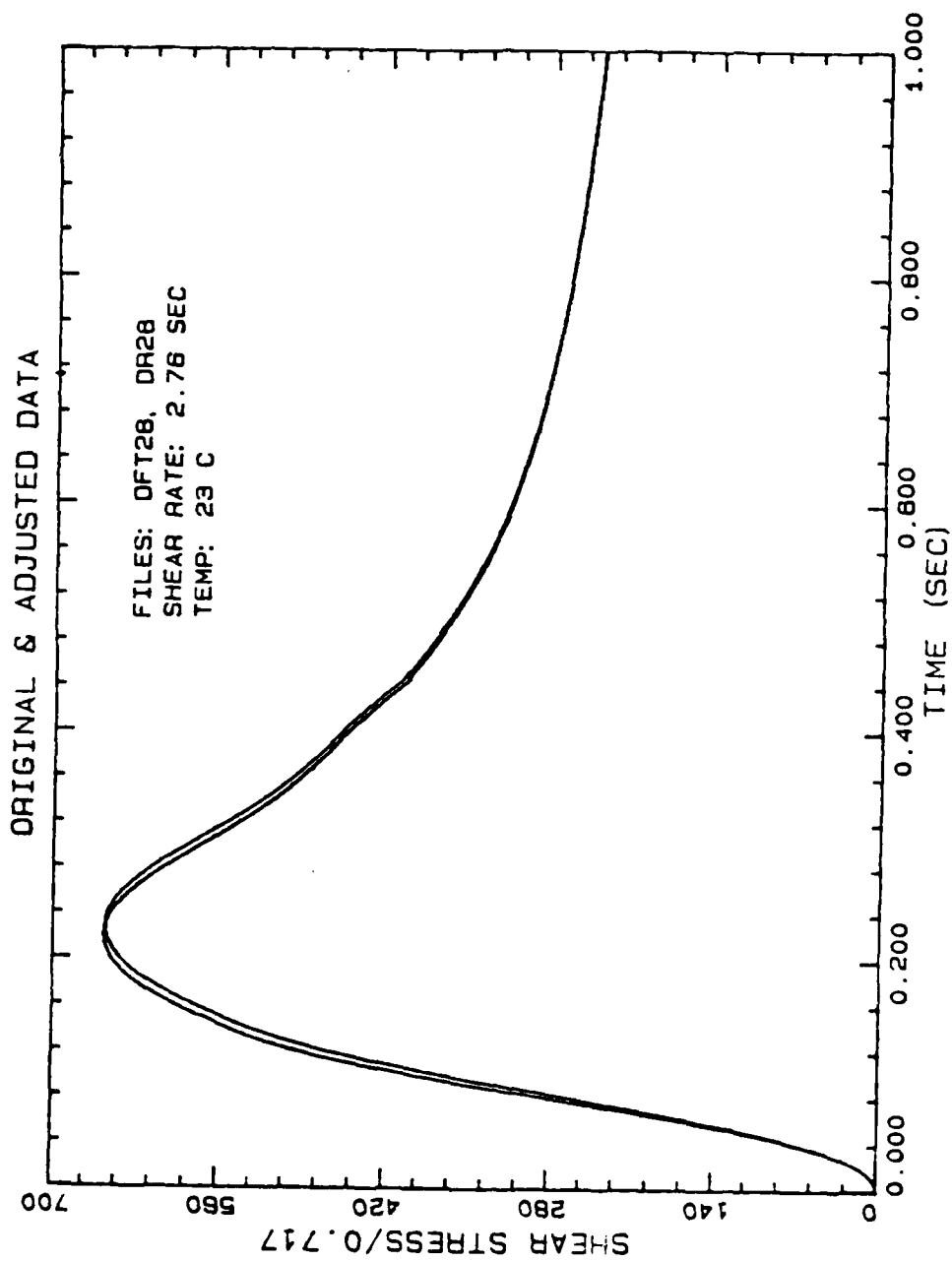
Figure 74. Data Correction for Top Cone Movement.

135
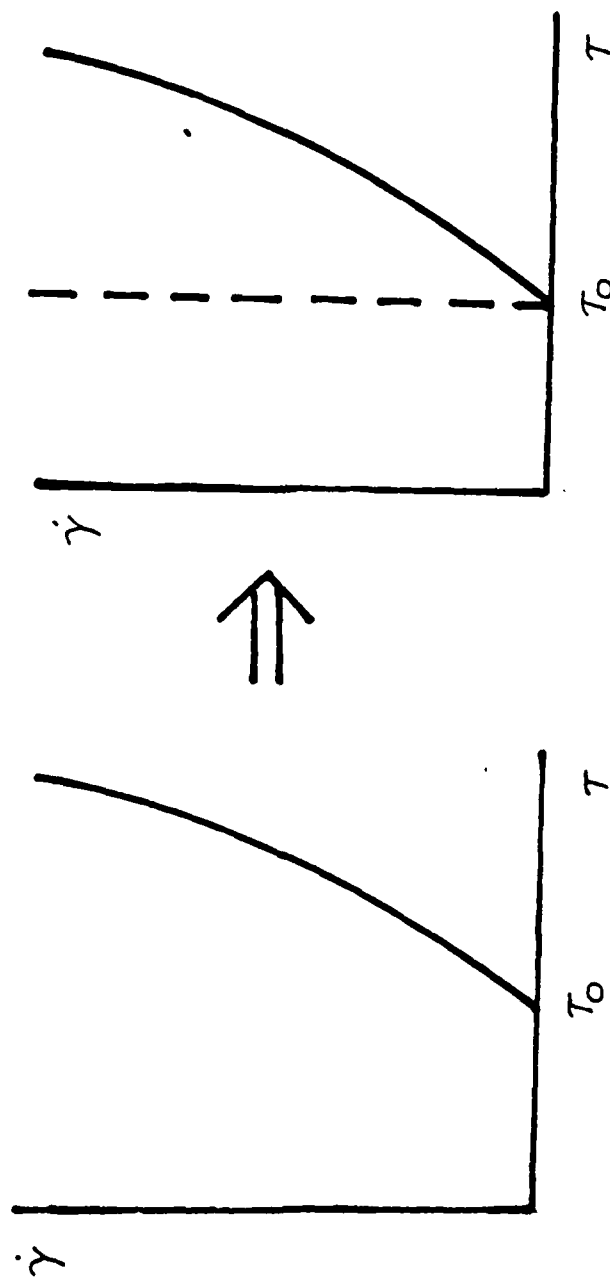
Figure 75. Data shifted by yield stress

136

For a slurry without a yield stress and having η_o and η_∞, the inverse level rule is used to define F. F is defined as

$$F = \frac{\eta^a - \eta_\infty^a}{\eta_o^a - \eta_\infty^a} \qquad (17)$$

where a=1.

The Richardson-Zaki equation is used to define F for the yield materials: Sun Tech 839-988, 839-995, and Exxon 708-61. In this case, F is defined as

$$F = 1 - (\eta_\infty/\eta)^{1/2.65} \qquad (18)$$

B.4.2 Steady State

The kinetic equation alone is used to correlate the steady state viscosity. At steady state, the kinetic equation can be rearranged to

$$K\tau^P = \frac{k_1}{k_2} \tau^{P_1 - P_2} = \frac{(1 - F)^n}{F^m} C^{n-m} \qquad (19)$$

where C is the concentration and m=1, n=2 are used. K and P were found by a least squares fit of $\log [(1-F)^2/F]$ versus $\log \tau$. The optimized equilibrium constants (P's and K's) for different slurries are tabulated in Table XXII. The experimental data and the predicted values are shown in Figures 76 to 79. The K's and P's of Suntech 839-988 at different temperatures are summarized in Table XXIII.

137

Table XXII. K and P of Slurries by Richardson-Zaki

Material	K	P
Suntech 809-995	0.010670	0.9991
Suntech 839-919	0.110107	0.89086
Suntech 839-988	0.014745	0.78287
Exxon 708-61	0.003988	0.9935

Table XXIII. K and P of Suntech 839-988 at
Different Temperatures

Temp (C)	K	p
23.0	0.014745	0.78287
9.0	0.02270	0.7184
0.0	0.03633	0.6719
-10.0	0.047614	0.73443
-20.0	0.10424	0.66912
-26.0	0.01899	1.1031
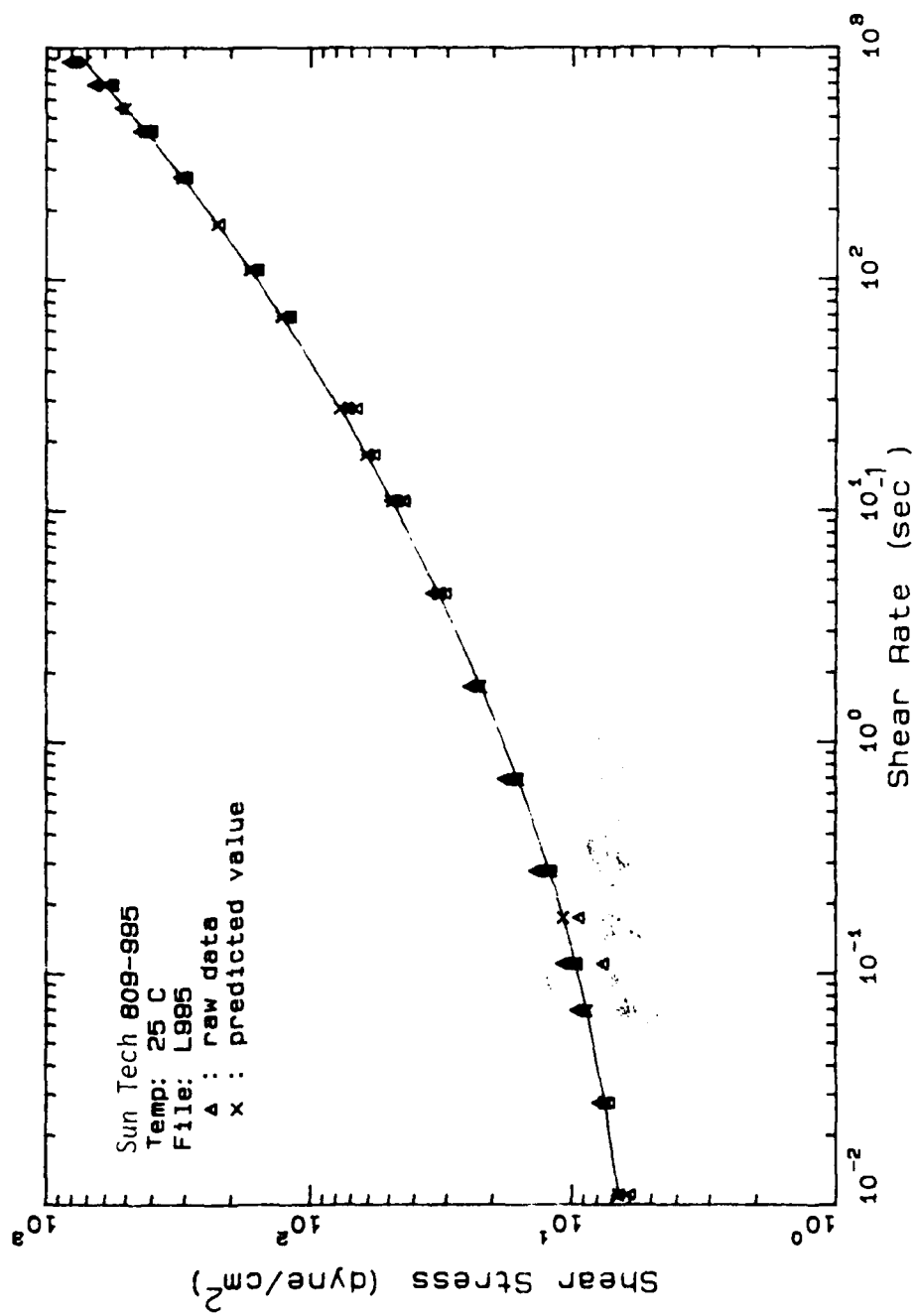
Figure 76. Kinetic Theory Fit for Sun Tech809-995 Equilibrium Data.

139
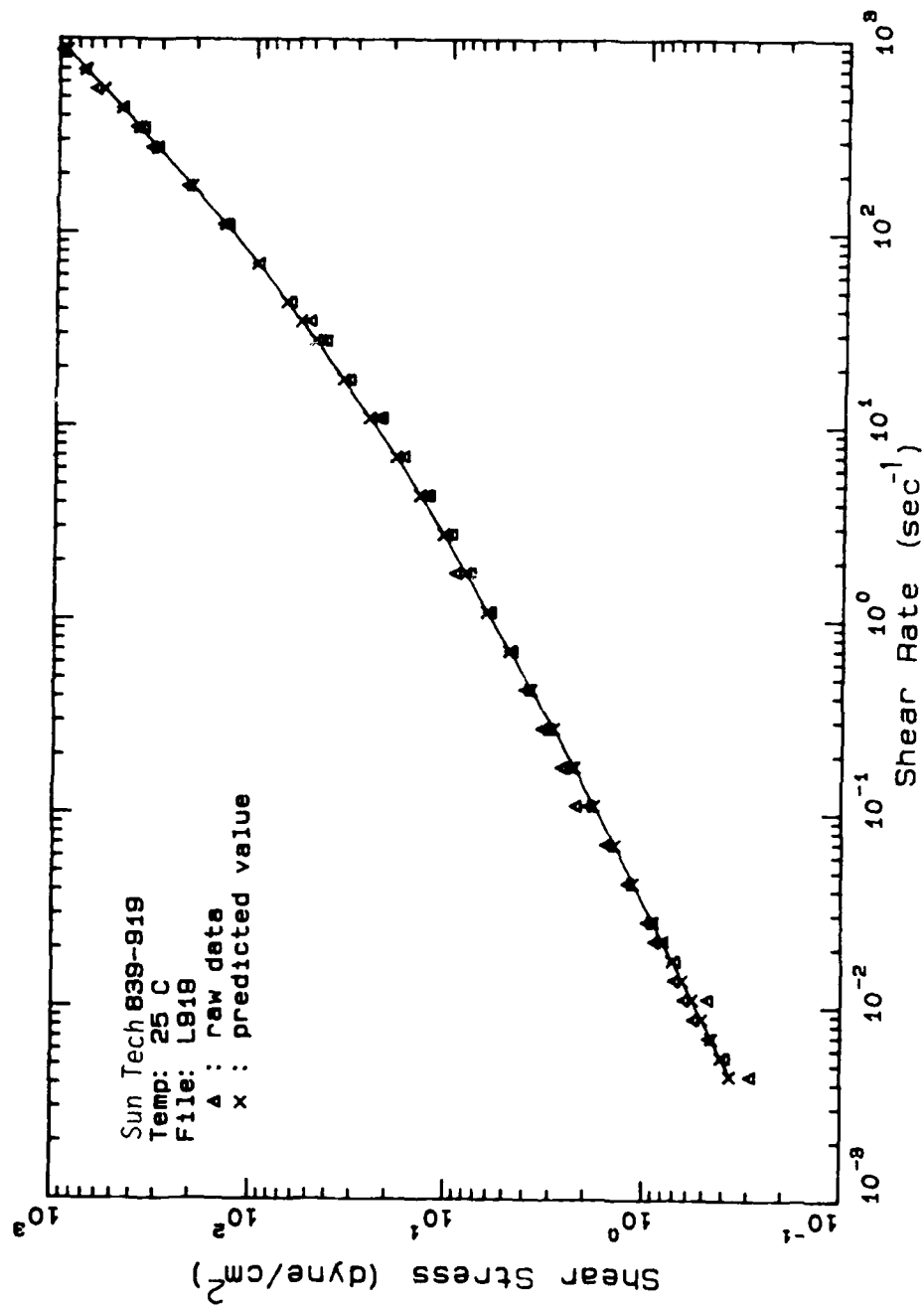
Figure 77. Kinetic Theory Fit for Sun Tech 839-919 Equilibrium Data.
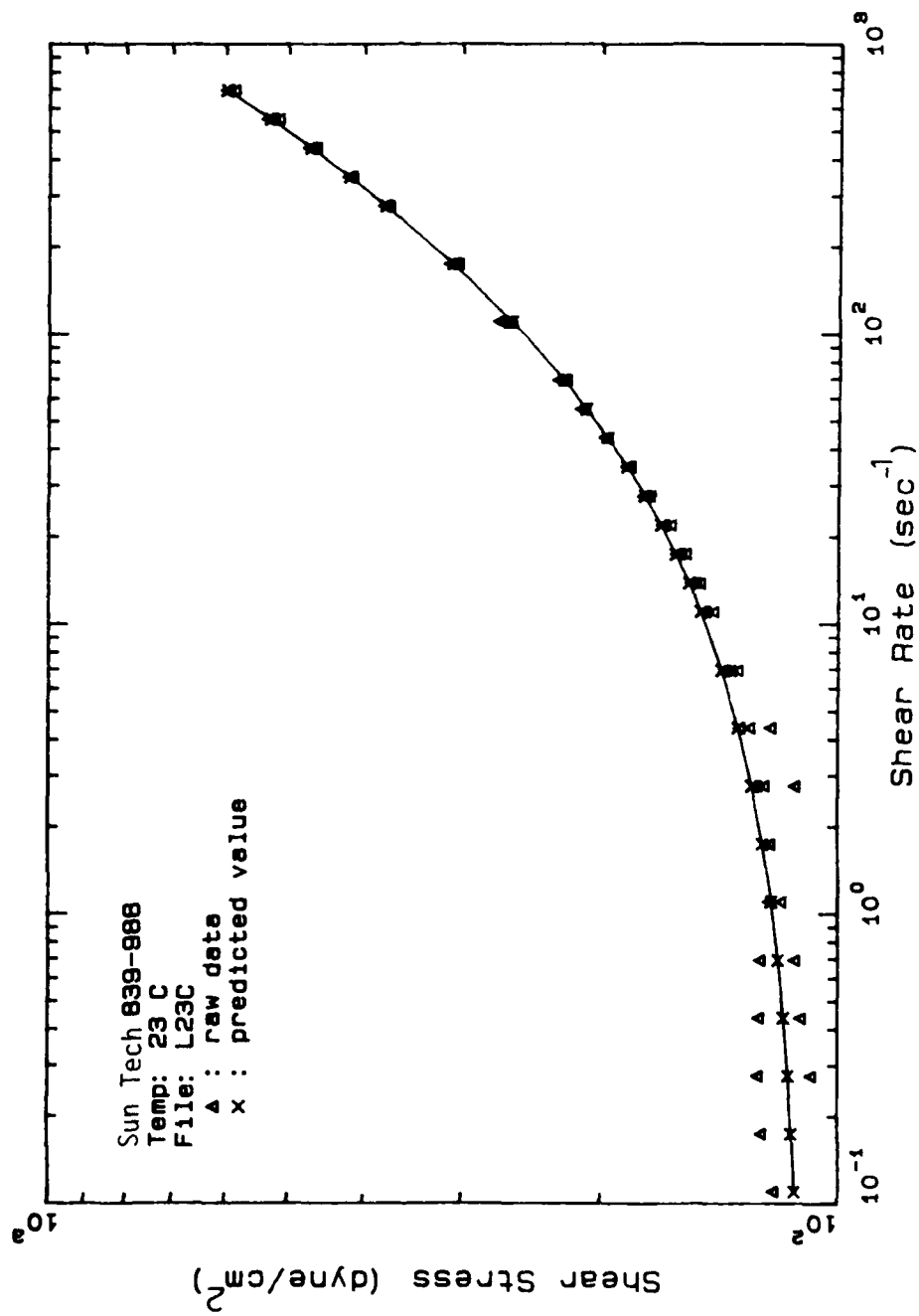
Figure 78. Kinetic Theory Fit for Sun Tech 839-988 Equilibrium Data.
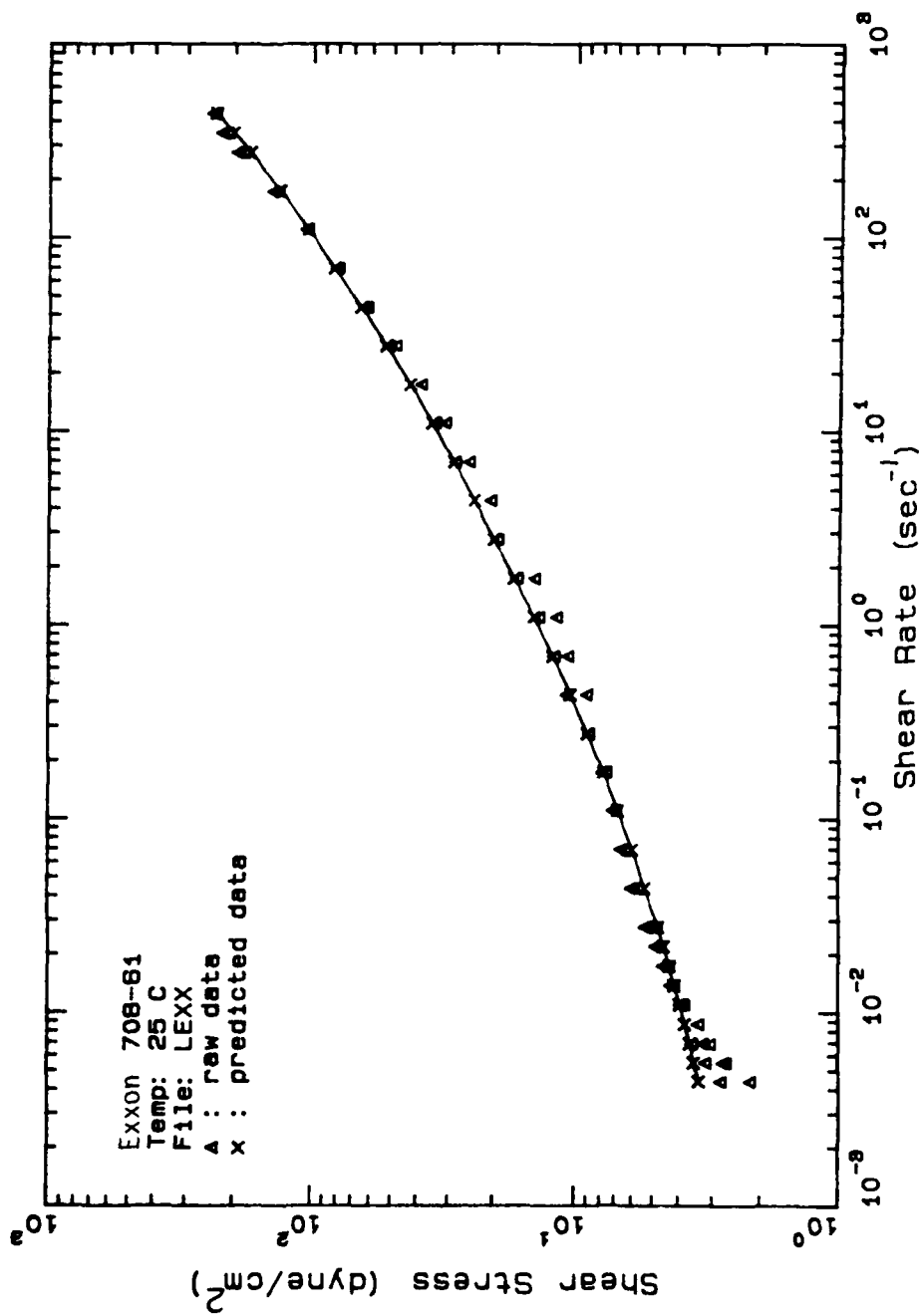
Figure 79. Kinetic Theory Fit for Exxon 708-61, Equilibrium Data.

142

B.4.3 Transient Response

Transient response is a combinative result of thixotropy and elasticity. The thixotropic constants, k_1, p_1, k_2, p_2 and elastic modulus G_1 were evaluated from transient data. Sun Tech 839-988 was used for this study.

For convenience, the kinetic and elastic equations with structural parameter F are listed again.

$$-dF/dt = k_1\tau^{p_1}F - k_2\tau^{p_2}(1 - F)^2$$

$$(\eta_t/G_1)\dot{\tau} + \tau = \eta_t\dot{\gamma} \tag{20}$$

The parameter G_1 can be evaluated from equation (21)

$$G_1 = \frac{\eta_t\dot{\tau}}{\eta_t\dot{\gamma} - \tau} \tag{21}$$

at the initial time, $\dot{\gamma}\,\eta_t \gg \tau$ so

$$G_1 \sim \frac{\dot{\tau}}{\dot{\gamma}} \tag{22}$$

The values of G_1 at different shear rates are tabulated in the Table XXIV. The values of k_1 and p_1 were calculated from the initial stress change, i.e., the stress growth near zero time. Once k_1 and p_1 are determined , k_2 and p_2 can be obtained from the equilibrium constants K and P, i.e., $k_2 = k_1/K$, and $p_2 = p_2-P$. A set of these constants obtained for Sun Tech 839-988 at a shear rate of 2.76 sec^{-1} are summarized in Table XXV. All the constants were obtained by the best fit of the data using an Advanced Continuous Simulation Language (ACSL) simulation package.

The single G_1 obtained from the initial response cannot describe the whole transient response, as shown in Figure 80. G_1 is thus defined as a function of time as already proposed for polymers. With a variable G_1, the experimental data and the predicted transient response are compared in Figure 81.

143

Table XXIV. G_1 as a Function of Shear Rate

Rate (1/sec)	G_1
0.055	887.
0.087	960.
0.55	960.
1.10	1270.
2.76	1500.

Table XXV. Constants of Transient Response at Shear Rate of 2.76 sec^{-1}

Constant	Value
G	1500.
k_1	0.00053
P_1	1.10
K	0.009
P	1.0355

144

Figure 80. Kinetic-Elastic Theory Fit Using a Single
Value of G1 at a Shear Rate of 2.78 sec⁻¹.

145
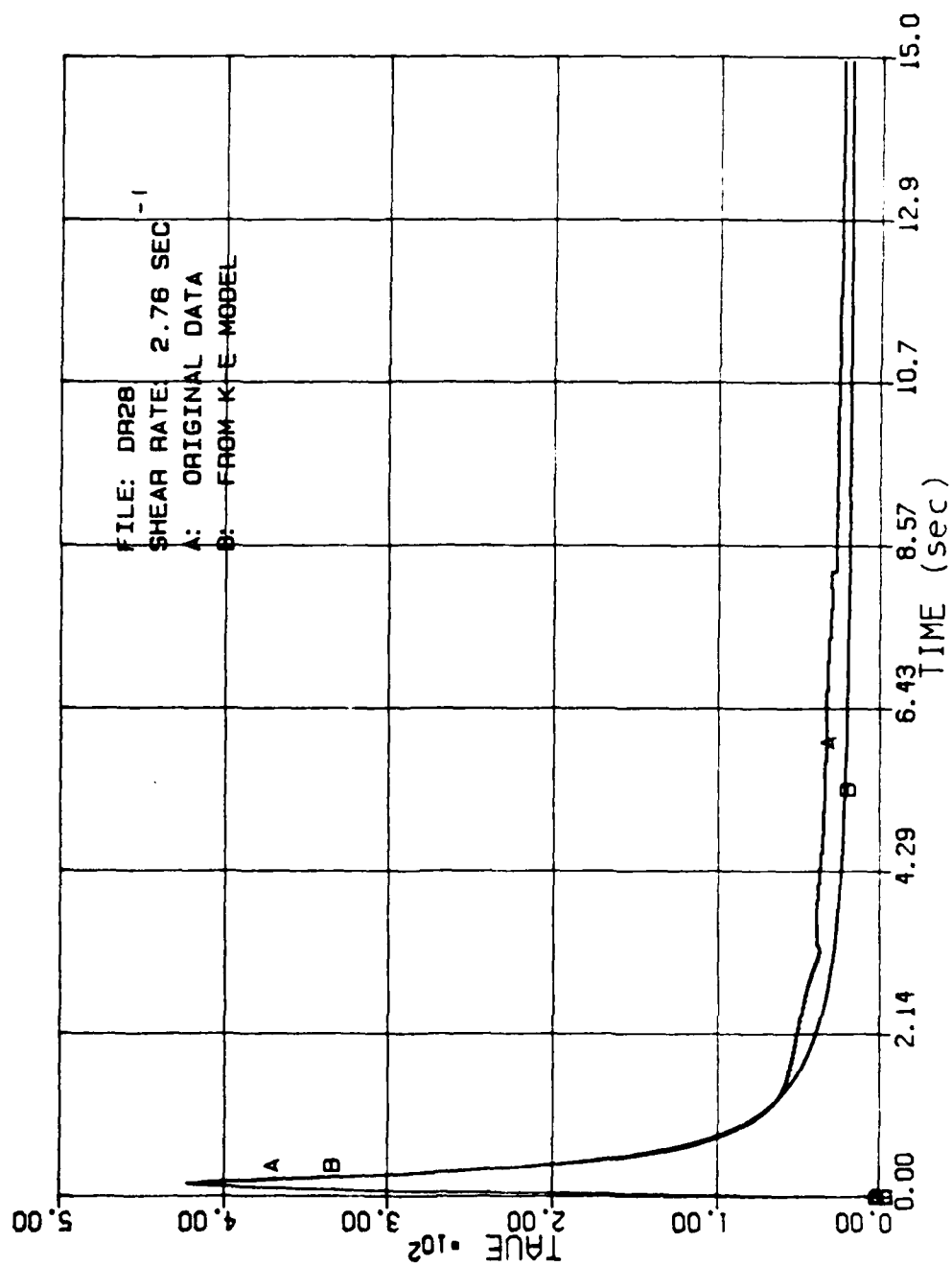
Figure 81. Kinetic-Elastic Theory Fit Using Variable G1 with Model (II) at a Shear Rate of 2.76 sec^{-1}.

C.   Discussion

The main purpose of this study was to obtain a better understanding of the rheological properties of carbon black slurries and to extend the kinetic-elastic model to predict their flow behavior. The discussion focuses on these two aspects.

C.1   Shear Dependence of Carbon Black Structure
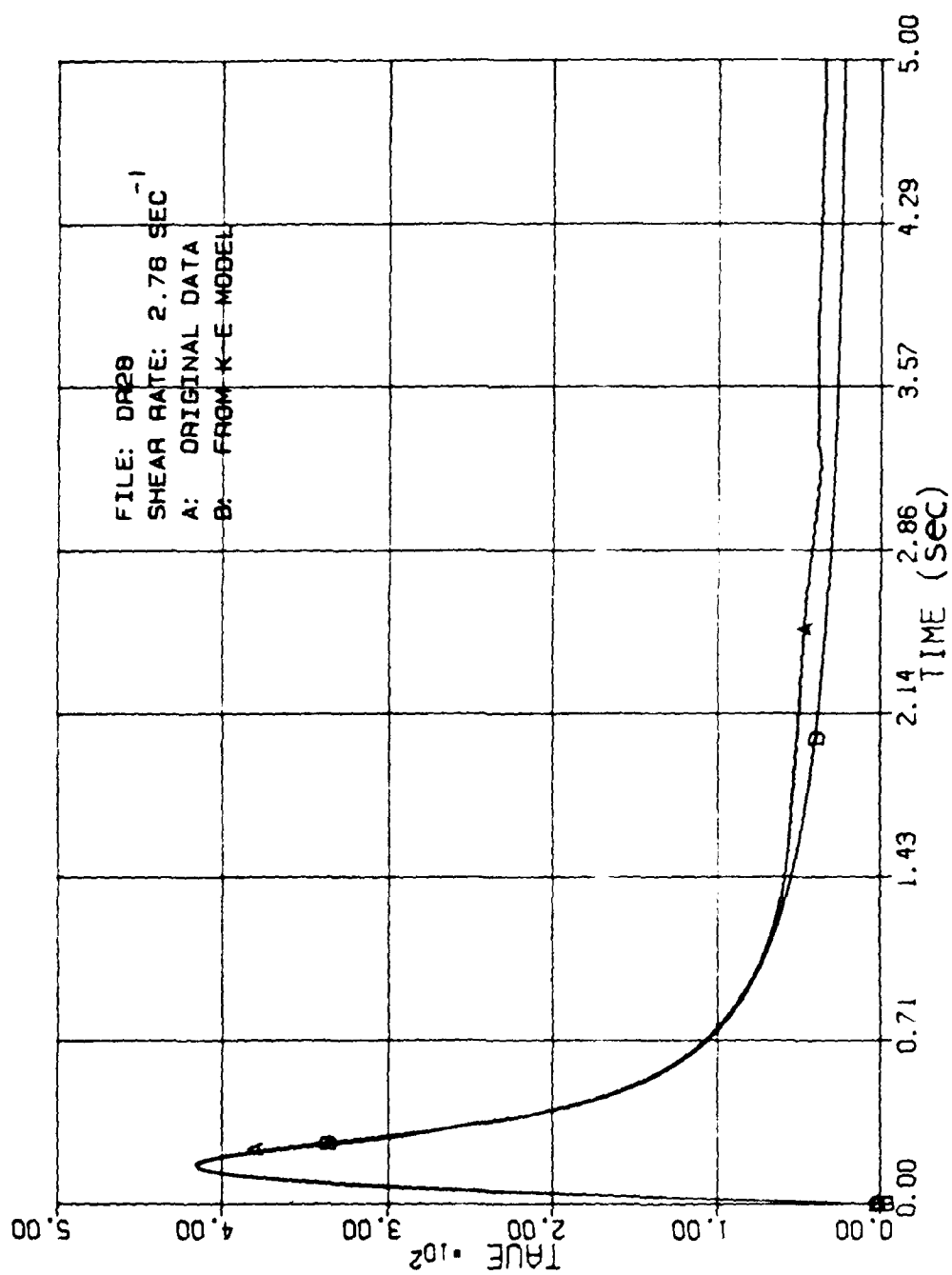
The results showed that all of the carbon black slurries tested are shear-thinning materials. This suggests that, as in other suspension systems, at reasonably high concentrations carbon black has a structure which can be broken down under shear. The structure could be aggregate or a network which is groups of particles held together by attractive forces. The formation of structure results in a larger effective volume fraction than the actual volume fraction of particles. The higher effective volume fraction and the interaction between particles increase the resistance to flow, and this causes the much larger viscosity of the suspension than of the solvent.

In a shear field, the structure is broken down by the shear forces. The degree to which the structure is broken down depends on the magnitude of shear force and the strength of the bonds between the particles. As the shear force increases, more of the structure will be broken down. At each level of shear rate, an equilibrium structure can exist corresponding to an equilibrium viscosity. The effective volume fraction decreases with an increase in shear rate as does the viscosity. This accounts for the shear-thinning behavior of these slurries.

Moreover, at high enough shear rates, the structures can be broken into non-interactive units (not necessarily individual particles but any basic flow unit) and the fluid behaves as a Newtonian fluid. This is commonly called the upper Newtonian region. In this study, even at the highest shear rate, nearly 1000 sec^{-1}, the upper Newtonian region was barely achieved.

Hysteresis loops(Figure 56) and thixotropic behavior in the time domain confirmed the existence of a shear rate dependent structure. In the hysteresis loop study, with an increasing shear rate(upcurve), structure is broken down. As the shear rate decreases(downcurve) the structure builds up. The structure that exists at each shear rate(in

147

the downcurve) is close to that at the highest shear rate, unless the structure build-up is very fast. Therefore, different structures can exist at the same shear rate as a result of different history. This has been shown by Jones and Brodkey(4). They constructed flow curves of a thixotropic material at different structural levels. The structural curve would be identical to the downcurve if the time scale of measurement is fast enough. They found there was an equilibrium structure associated with each shear rate and that different structures could exist at the same shear rate depending on the shear history. As a result different viscosities are measured, which results in the hysteresis loop. During transient response at constant shear rate, the viscosity decreases with time as caused by the breaking of the structure. The structure can recover its ground state at rest. The rebuilding of the structure can be demonstrated by repeating the transient experiment. After a sample is sheared to its steady state structure, stop the shearing, pause for a few minutes, and repeat the test. The time dependent behavior is still present, except that the initial peak in the stress is smaller, as illustrated in Figure 82.

The hysteresis loop shown in Figure 56 is often used as a measurement of thixotropy and is sometimes called the "thixotropic loop". The degree of thixotropy is often related to the area between the upward and downward curves. Although this measurement can describe a few systems, it is usually regarded suspiciously because of possible errors arising from the method of measurement. The area in the thixotropic loop is dependent on the procedure used for the measurements. If different paths are used to change the shear rates, different areas will be obtained. Even if the same shear rate path is used, different shearing times will result in different areas within the loop. The instrument can also contribute errors in thixotropic loop measurement, for example, heating effect, change of apparent rate due to the movement of the torque spring, and inertia of the moving parts. The area within the loop is not a satisfactory measurement of the degree of thixotropy shown by a material. Therefore, the thixotropic loop studies made here were only used as an indication of thixotropy or structural viscosity. The best way to describe thixotropy should be based on a) the equilibrium curve and b) the rate of approach to equilibrium after a change of shear rate.
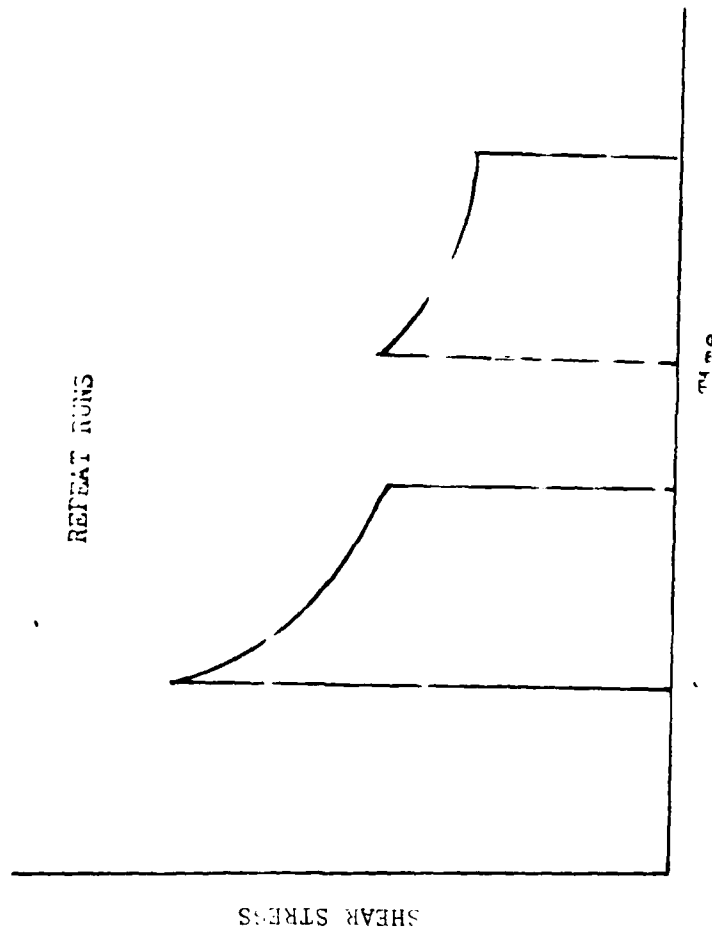
Figure 82. Sketch of Repeating Transient Experiment with Time.

C.2   Flow Curves

Umega(89) suggested that the rheological behavior of suspensions could be described by an extended Ostwald flow curve(Figure 83) if a sufficiently wide range of shear rates was studied. The flow behavior of materials progressively passes from a lower Newtonian region(A-B) to a pseudoplastic flow region(B-C), followed by an upper Newtonian region(C-D), a dilatant region(D-E), and then another Newtonian region(E-F). In this study, the shear rate range covered was not high enough to include the whole flow curve; only the lower part of the curve was observed.

C.2.1   Measurements and Characteristics of BSDs

Some interesting results were observed at both low and high shear rates. They will be discussed individually.

Sun Tech309-995 is the only material that showed little skinning. The BSD of Sun Tech809-995 was studied with and without JP-10. There was little difference between the two cases, except at high shear rates (see Figure 59). The sample with JP-10 had a lower viscosity than that without JP-10 at shear rates larger than 276 sec^{-1}. This, no doubt, was due to the dilution of the sample by JP-10 at the higher shear rate. A test was made without JP-10 starting at a shear rate of 69.2 sec and increasing the rate to 692 sec^{-1} and was carried out fast enough to avoid the skinning. The results were the same as those started from a much lower shear rate without JP-10. Therefore, the dilution is more likely to exist at the high shear rate. This problem was avoided by removing the excess JP-10 for the higher shear rate measurements.

The BSD of Sun Tech839-919 was studied with the JP-10 covering over the shear rates range of 0.00348 to 870 sec^{-1} (see Figure 60). One set of earlier data with the skinning problem was also plotted for comparison. Three runs were conducted with different starting shear rates. There was a difference in the low shear rate range which might be due to a weak structure in the material. However, the signal at low shear rates was so small that the difference could be the result of measurement errors. At both low and high shear rates, the slope of the curve was close to 1, which implies that the material was Newtonian at both extremes, i.e., it had high and low Newtonian viscosities.
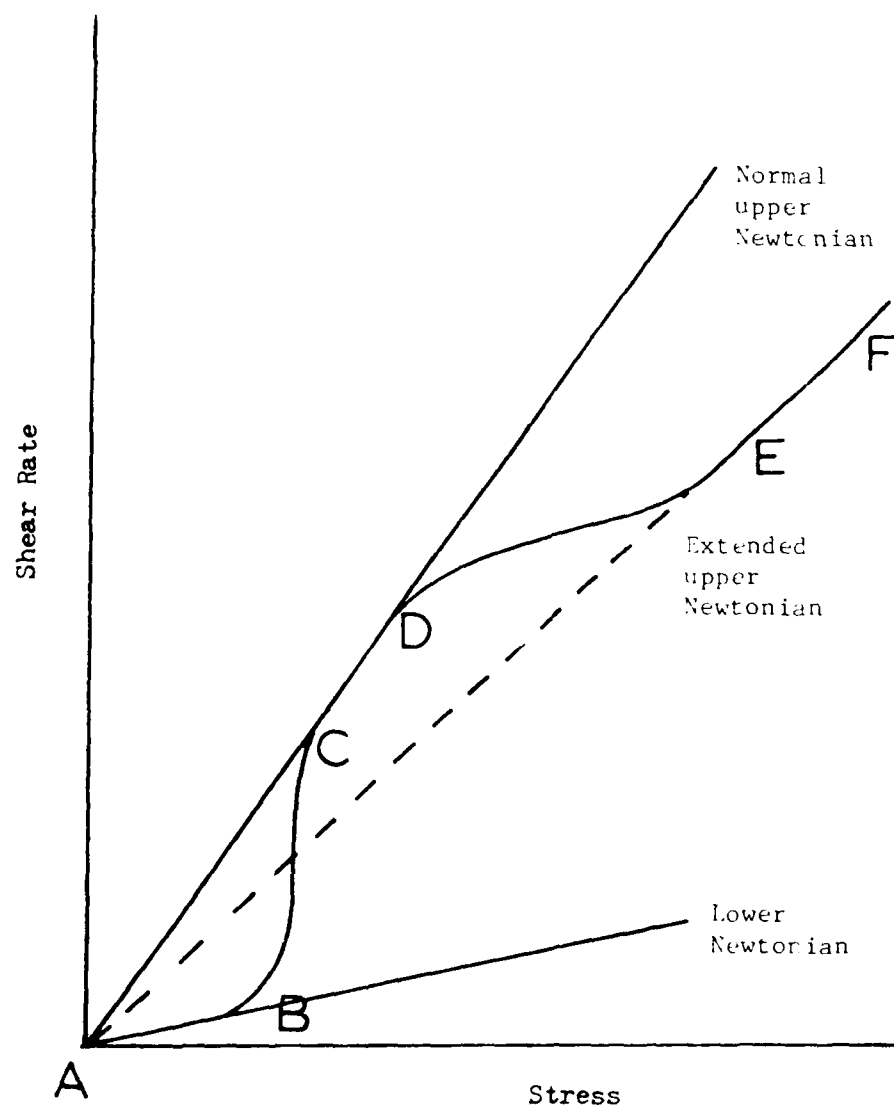
150

Figure 83. Basic Shear Diagram of
Suspension after Umega.

Sun Tech 839-919 was the material which showed no hysteresis between shear rates of 1.1 and 276 sec^{-1} with or without the JP-10 covering. But, at shear rates above 276, it did show hysteresis, as shown in Figure 84. Apparently, something different happened with this material at shear rates higher than 276 sec^{-1}. The explanation is that either the material has some strong structure that is broken down at the higher shear rates or that an instability generated at the higher shear rate changes the nature of the material. There is little possibility that this is due to the mixing of JP-10 with the sample since the hysteresis loop was also observed for the measurement without JP-10 covering.

The BSD of Exxon 708-61 was studied at room temperature from $\dot{\gamma}$ = 0.00348 to 438 sec^{-1}. The data branches out at low shear rates, as seen in Figure 62. It was found that the lower the initial shear rate the higher the viscosity obtained at any specified shear rate. There are two possible reasons: the structural property or rheopetic property of the material. There could be a weak structure which was broken down during the loading of the sample. Such weak structures could build up during resting or under mild shear rate. If the structures build up under a mild shear rate, the material is rheopetic. Otherwise, the structure builds up during the resting period between runs. Studies were made to check if weak structures were broken down during the loading of the sample and if the equilibrium viscosity at the low shear rate depended on the resting time. Several runs were carried out from $\dot{\gamma}$ = 0.0174 sec^{-1} to 174 sec^{-1} by letting the sample rest from 0 to 3 hours. As shown in Figure 65, the viscosity at the low shear rate does depend on the resting time. A large difference was found at the lower shear rates and the curves coincide at $\dot{\gamma}$ > 10 sec^{-1}. This showed that there is a weak structure which was broken easily and took time to rebuild. Moreover, as mentioned in the previous chapter, the viscosity at 27.6 sec^{-1} was independent of the resting time which is consistent with this result. In order to obtain the "true" viscosity at low shear rates, we would have to let the sample sit for a very long period to rebuild its weak structure. From Figure 85, the material would need 3 hours or more to rebuild such a weak structure at the 0.0174 sec^{-1}. Allowing the sample to rest for such a long time induced skinning, thus, we will always have difficulty in obtaining viscosity at low shear rates. In addition, from Figure 85, the shifting of the curves to the right as the rest time increased implies that the material had a yield stress. The yield stress cannot be over 6 $dyne/cm^2$ because any reasonable extrapolation of the 180 min curve would give a value less than this. The transient response of the material was also studied to
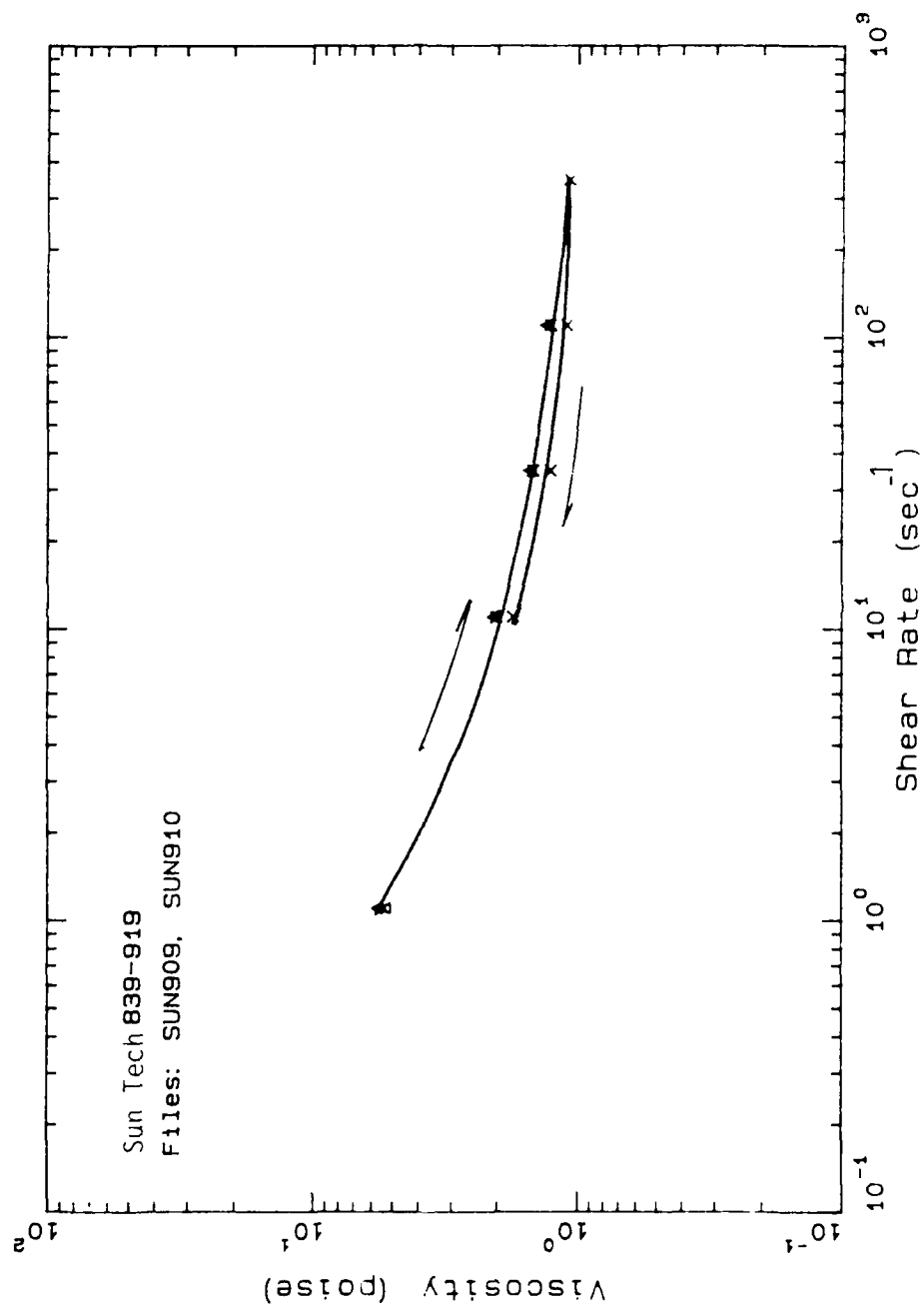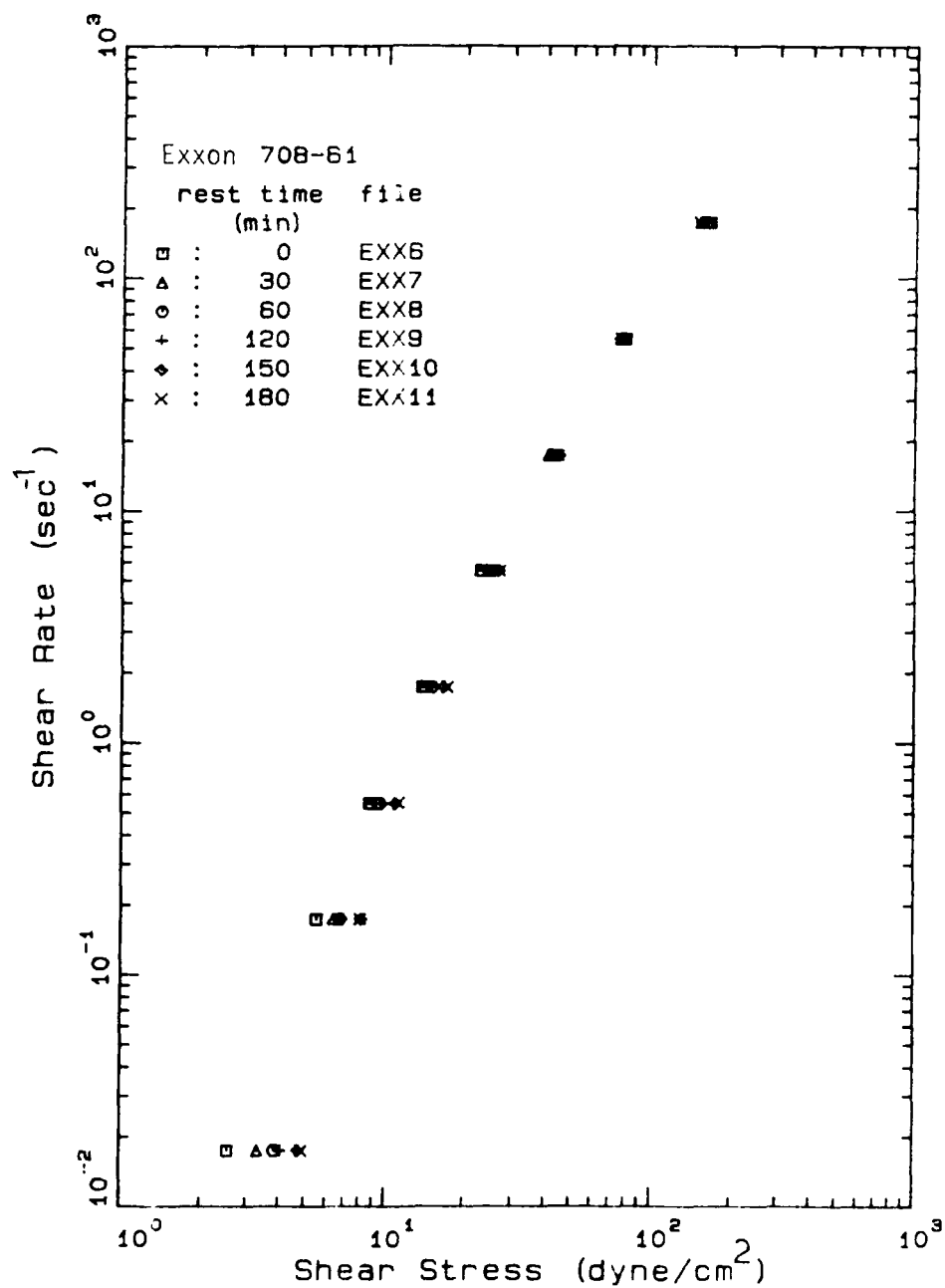
Figure 84. High Shear Hysteresis Loop for Sun Tech839-919.

Sun Tech 839-919

Files: SUN909, SUN910

Shear Rate (sec^{-1})

Viscosity (poise)

153

Figure 85. Dependence of Basic Shear Diagram
of Exxon 708-61 as a Function
of Resting Time.

154

determine the rest time. The transient response at a shear rate of 27.6 sec^{-1} with different resting times ranging from 0.5 hour to 6 hours is shown in Figure 54. Though the equilibrium viscosity at $\dot{\gamma}$ = 27.6 sec^{-1} was independent of the resting time, the transient response did depend on the resting time. Therefore, letting the sample rest to its ground state is important in both transient and steady state studies.

The viscosity of Sun Tech 839-988 was difficult to measure due to the nature of the material. This material was thicker than the other slurry materials, especially at low shear rates, which complicated the measurements. The same technique, covering the sample with JP-10, was used to study the viscosity. It was found that above a critical shear rate (around 1 sec^{-1}) the mixing of JP-10 and the slurry became serious and the viscosity decreased as time proceeded. The mixing was caused by the edge effect. In Figure 86, we can see that the stress was constant over a wide range of shear rates. In this region, there was almost no flow inside the gap because of the yield stress. Above a shear rate of 1 sec^{-1}, the structure of the material was broken and the material started to flow. The curve bends toward lower stresses as the shear rate increases above 1 sec^{-1}.

To check the mixing effect, measurements were made without JP-10 to see if the curve had the same characteristics. As can be seen in Figure 86, they did not. Additional runs with different resting time were carried out to see if the curve inflected above a shear rate of 1 sec^{-1}. No bending was observed and the curves shifted to the right as the resting time increased (Figure 87). We are convinced that the decrease in the shear stress was due to dilution with JP-10.

A systematic experiment was then made to study the resting time effect on Sun Tech 839-988 at different shear rates. The sample was shaken vigorously before loading to insure homogeneity. Then, the shear stress-time data was obtained every hour.

At a shear rate of 0.11 sec^{-1}, it was found that the apparent equilibrium viscosity was a function of time. However, if the initial stress value was used rather than zero as the ground value, the equilibrium viscosity was independent of the resting time as seen in Figure 88. Nevertheless, the transient curves did depend on the resting time. The peak values of the transient response were also plotted as a function of time (Figure 89). They increased initially and then leveled off after 3 hours.
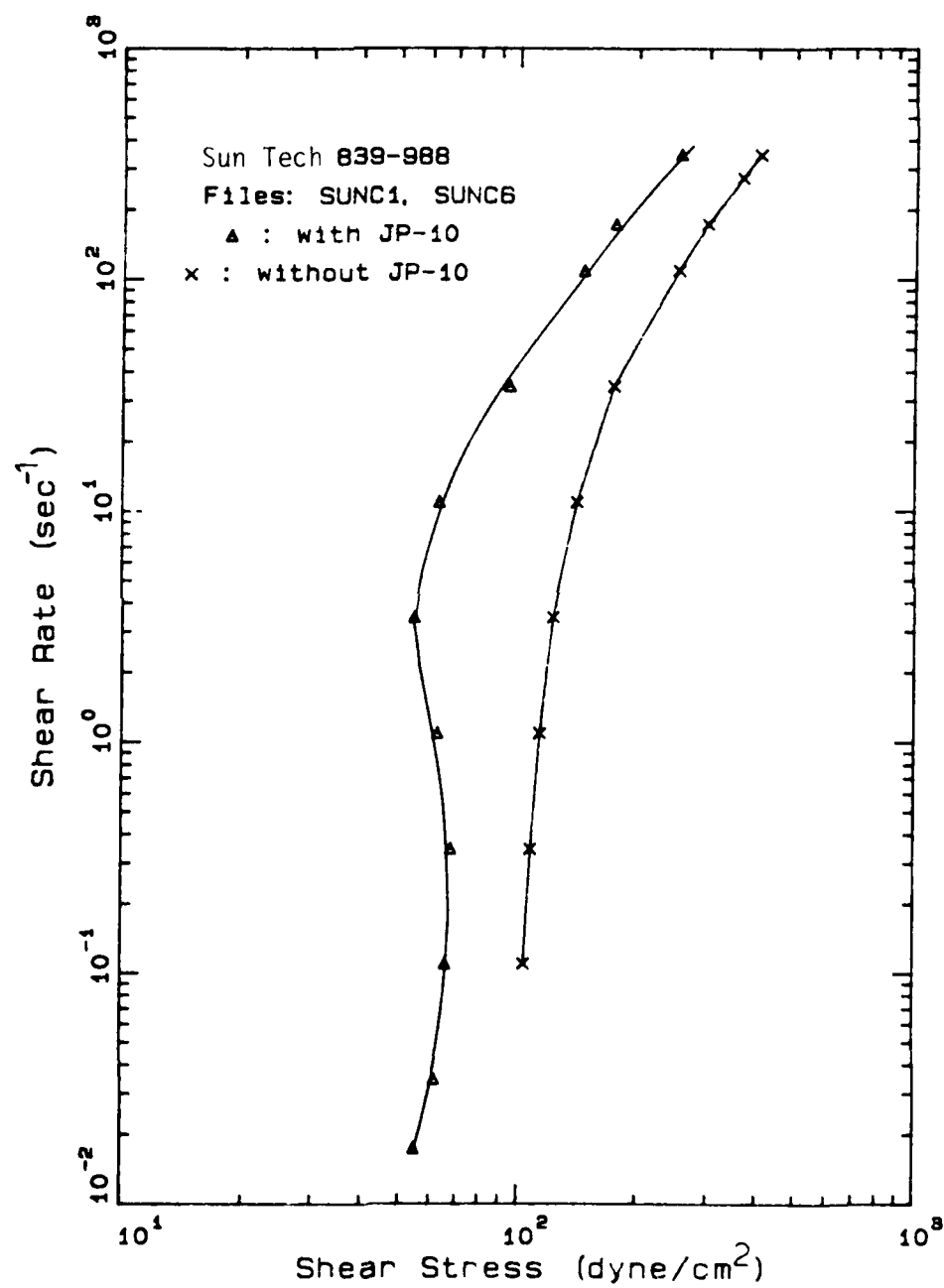
155

Figure 86. Measurement for Sun Tech839-988 Shearing Effect of Mixing of JP-10 into Sample.
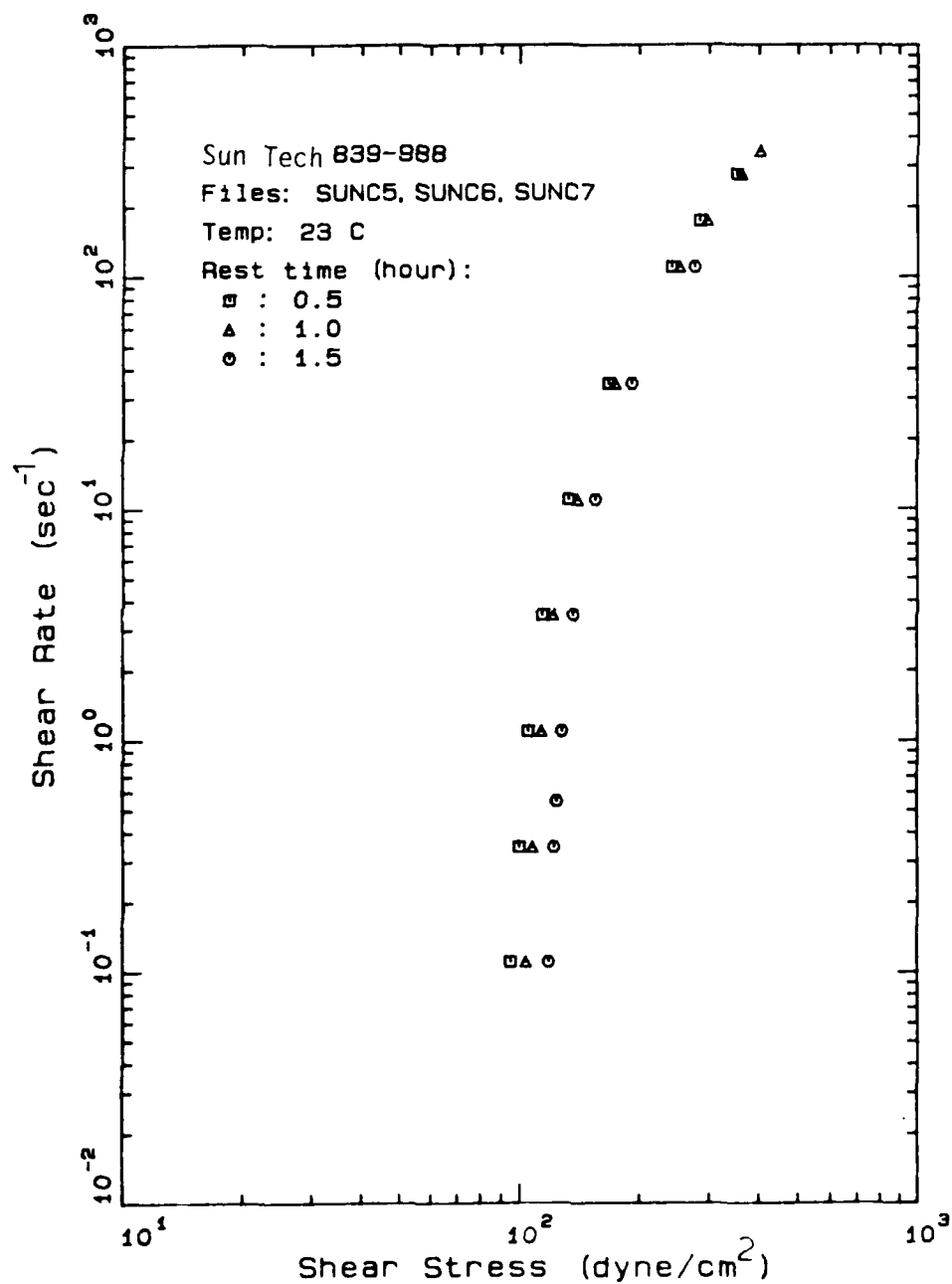
156

Figure 87. Effect of Resting Time on Data
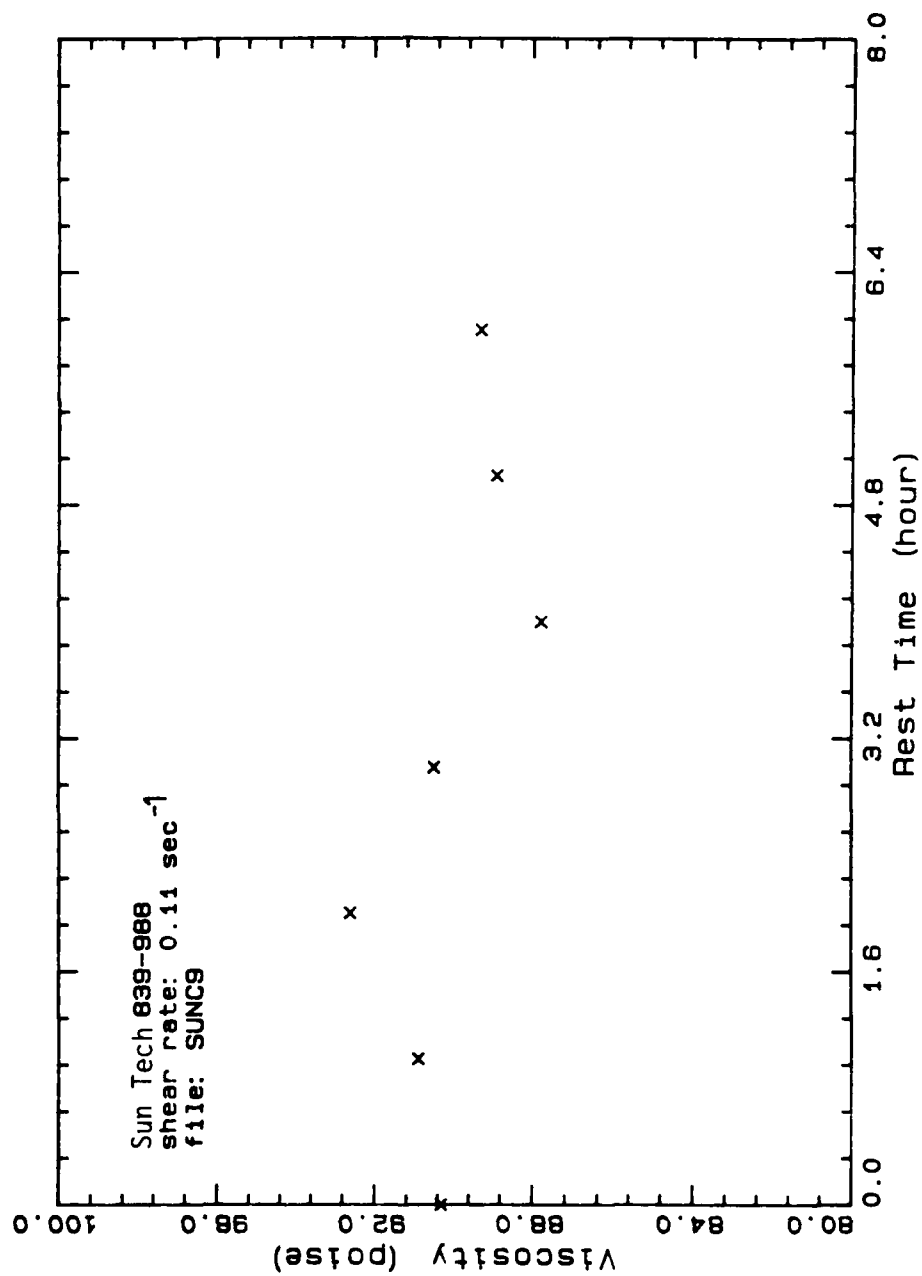Obtained on Sun Tech 839-988.

157

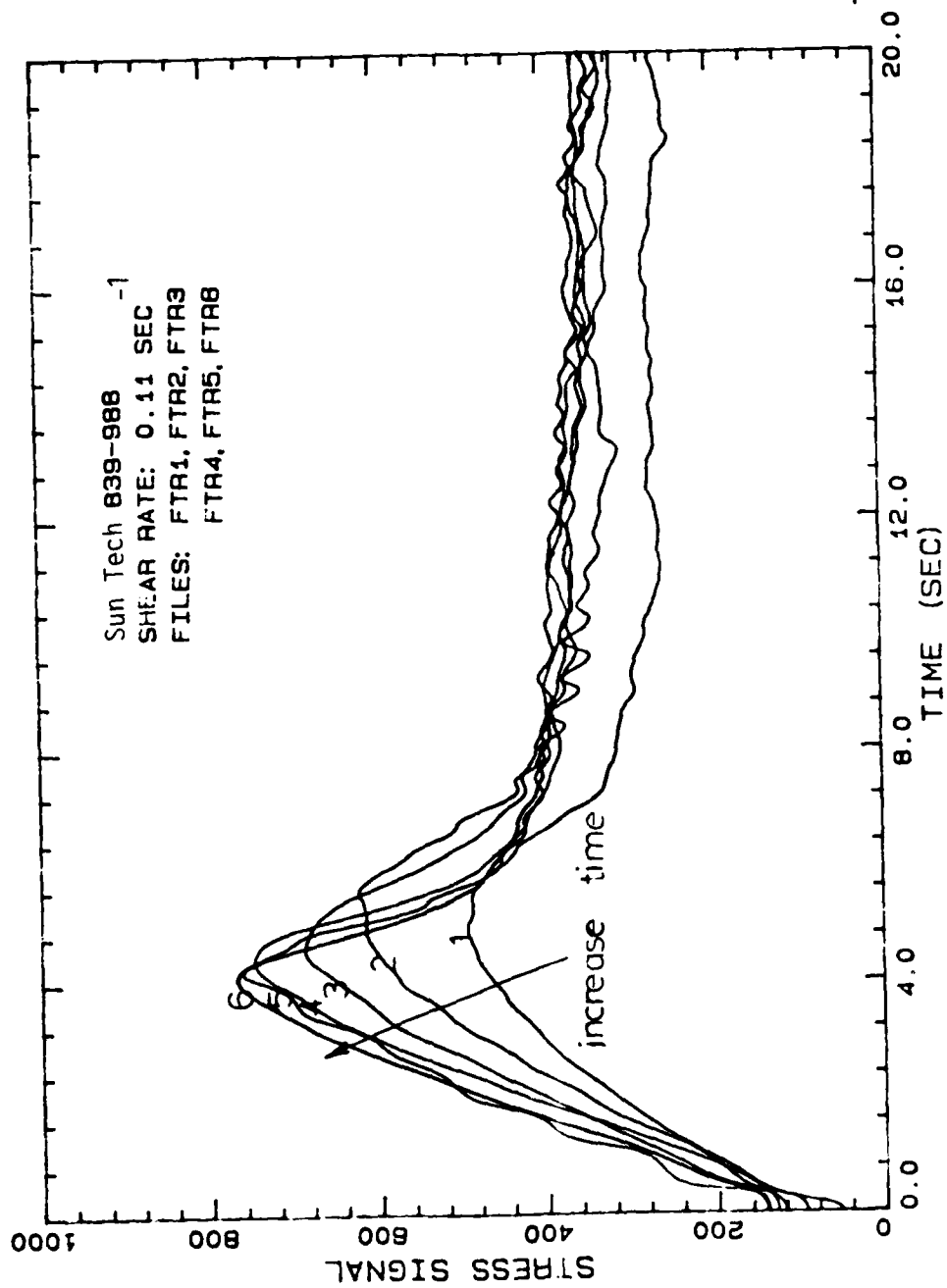Figure 88. Shifted Equilibrium Viscosity (Using Initial Stress as Zero) as a Function of Resting Time.

158

Figure 89. Transient Curves and Shifting of Peak Values as a Function of Resting Time.

159

Shear rates of 2.19, 5.5, and 11) sec^{-1} were studied in the same manner. The equilibrium stress as a function of time is shown in Figure 90. Except for the shear rate of 2.19 sec^{-1}, they all showed the tendency of decreasing viscosity with time. This is further evidence that dilution by JP-10 took place at high shear rates. Though the equilibrium viscosity at $\dot{\gamma}$ =2.19 sec^{-1} approached an asymptote as the time increased, its peak values from the transient responses showed a tendency to decrease with time as seen in Figure 91. This means that the mixing of JP-10 and the slurry took place under this shear rate but not seriously enough to affect the equilibrium value.

Reproducibility was very poor when the data was taken with the sample full to the rim of the plate (Figure 92). Due to the high viscosity of this material, the shear rate difference between the sample in the gap and that in the reservoir caused mixing, which resulted in erroneous measurements. To avoid the edge effect, the viscosity of Sun Tech839-988 was measured without JP-10 covering. Nevertheless, JP-10 was used during the resting period and was removed for the actual measurement. Excess sample was also removed from the reservoir (Figure 92). The results were reproducible as shown in Figure 62. Due to the small signals and low rotational rates, the data scattered at low shear rates. In spite of the scattering, the plot indicates a yield stress of around 110 dyne/cm^2. In addition, by extrapolating the data at high shear rates to zero shear rate, a Bingham yield stress of 220 dyne/cm^2 is obtained. The results are also plotted in Figure 62 and coincide with the measurement using JP-10 at the low shear rate. In order to obtain accurate results for this material, the edge effect must be minimized.

C.2.2   Comparision between Slurries

Though all the slurries contained almost the same loading of carbon black (50 wt%), they possessed different rheological behavior, especially at low shear rates. At high shear rates, the viscosities of the different slurries were not much different and ranged from 50 cp to 100 cp. The difference between them became wider as the shear rate decreased (Figure 63). There is more than 100 times difference between Sun Tech839-988 and the others. This difference was due to the particle size and surfactant used. These two factors affected the formation of structures which were important at low shear rates. Apparently, Sun Tech 839-988 had a smaller particle size, which resulted in a large yield
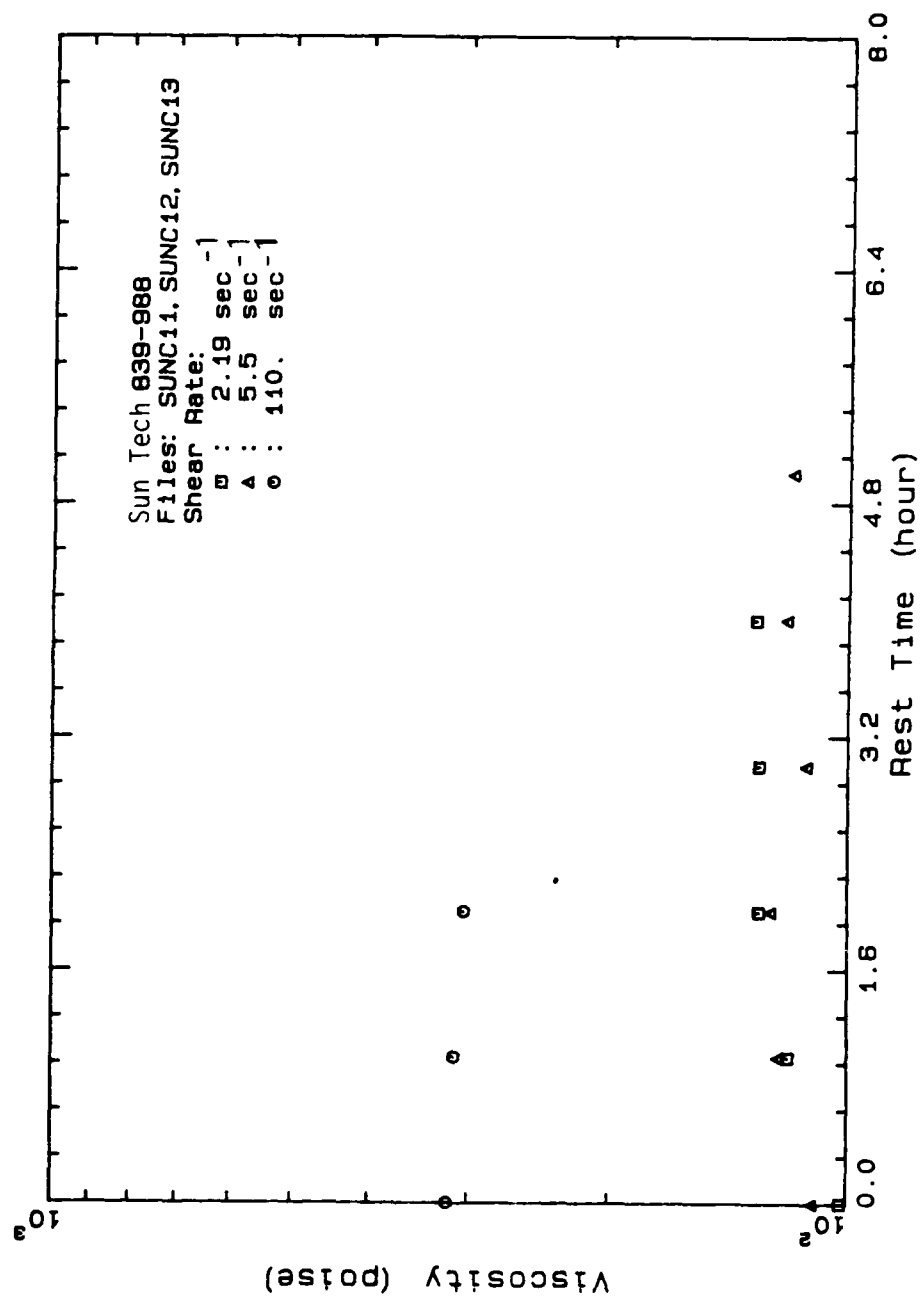
160

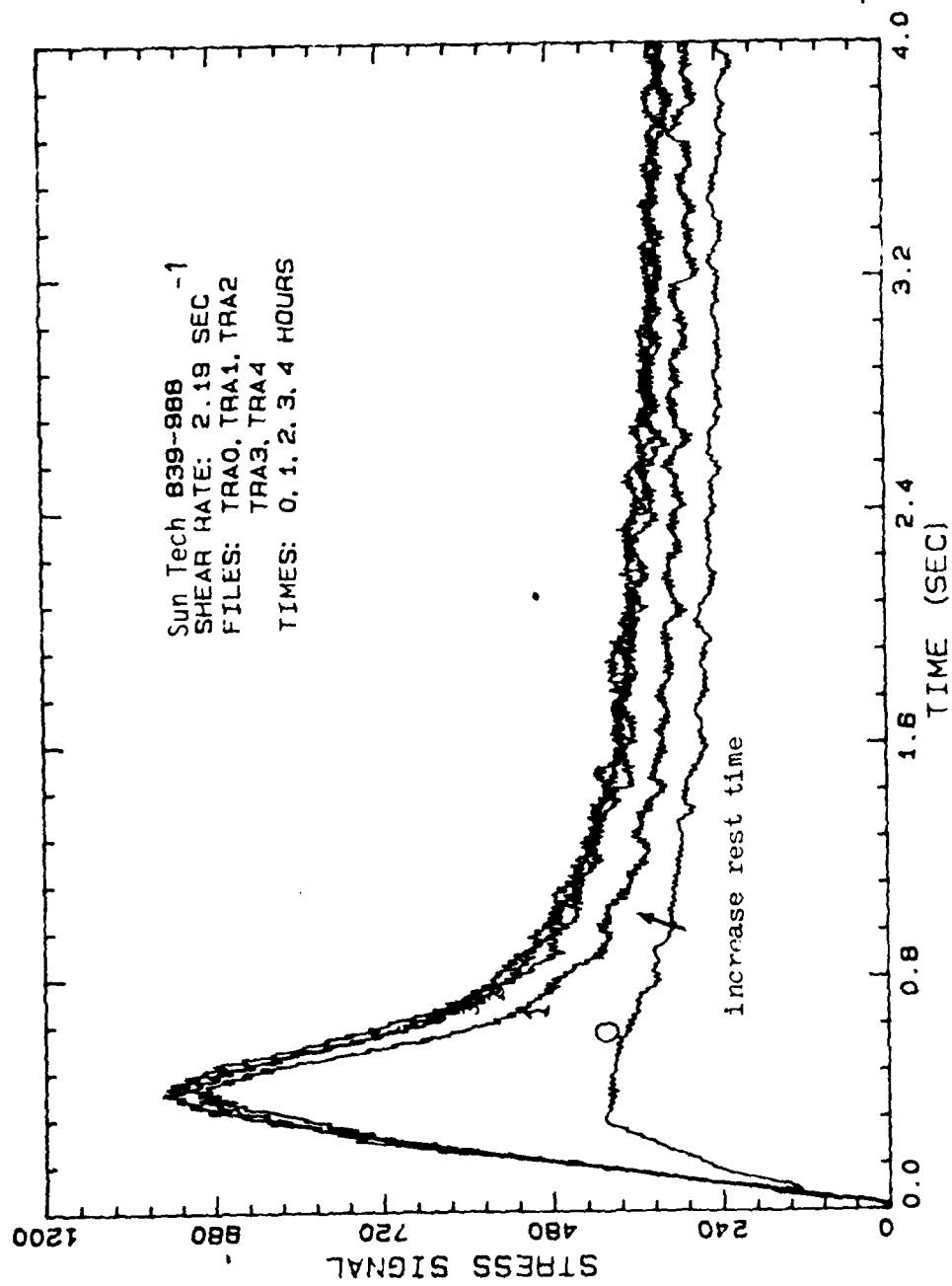Figure 90. Equilibrium Viscosity as a Function of Rest Time at Different Shear Rates.

161

Figure 91. Transient Viscosity at Different Rest Time at a Shear Rate of 2.19 sec^{-1}.

162
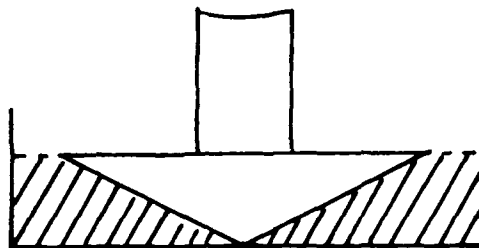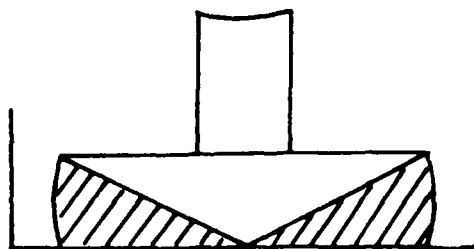
Figure 92. Sketch of Material Configuration
in Open Edge Experiment.

stress at low shear rates. The surfactant was used to stabilize and to increase dispersity. A well dispersed system will favor particle-solvent interaction and prevent strong structure formation . Therefore, a well dispersed system will have weaker structure and lower viscosity.

C.3 Temperature Effects

According to the traditional time-rate-temperature superposition, a decrease in temperature corresponds to a shift to higher effective shear rates for viscosity versus shear rate plots. The data did follow this trend; flow curves shifted to higher shear stress, as temperature dropped (Figures 65 to 67). Results were also consistent with the Ostwald curve; at lower temperatures and higher shear rates, flow curves shifted to the right, falling into the dilatant region.

The phenomenon observed at low shear rates was surprising and had not been noted in the literature. At temperatures below zero, the low shear viscosity showed a systematic decrease as temperature decreased (Figure 67). Though the result was unusual, it can be explained on the basis of structural viscosity. Due to particle interactions, there was a structure which resulted in both a yield stress and thixotropy. The linkage that formed the structure depended on the kinetic energy and the Brownian motion of particles. As the temperature decreased, the linkage became weaker, which was then more easily broken by shear. Though the viscosity of the solvent(JP-10) increased as the temperature decreased, the structure was the dominating factor which determinated the viscosity at low shear rates. When the structure became weaker at low shear rates, the corresponding viscosity became smaller, too.

Structures are not important at high shear rates where most of the structure is broken down under such conditions. Therefore, the viscosity change with temperature followed the traditional trend, i.e., the viscosity increased as the temperature decreased.

The temperature effect on the low shear rate viscosity was a result of the yield stress. The yield stress was almost independent of temperature. η_∞ was highly dependent on temperature. The change of η_∞ with temperature is plotted in Figure 93.

164
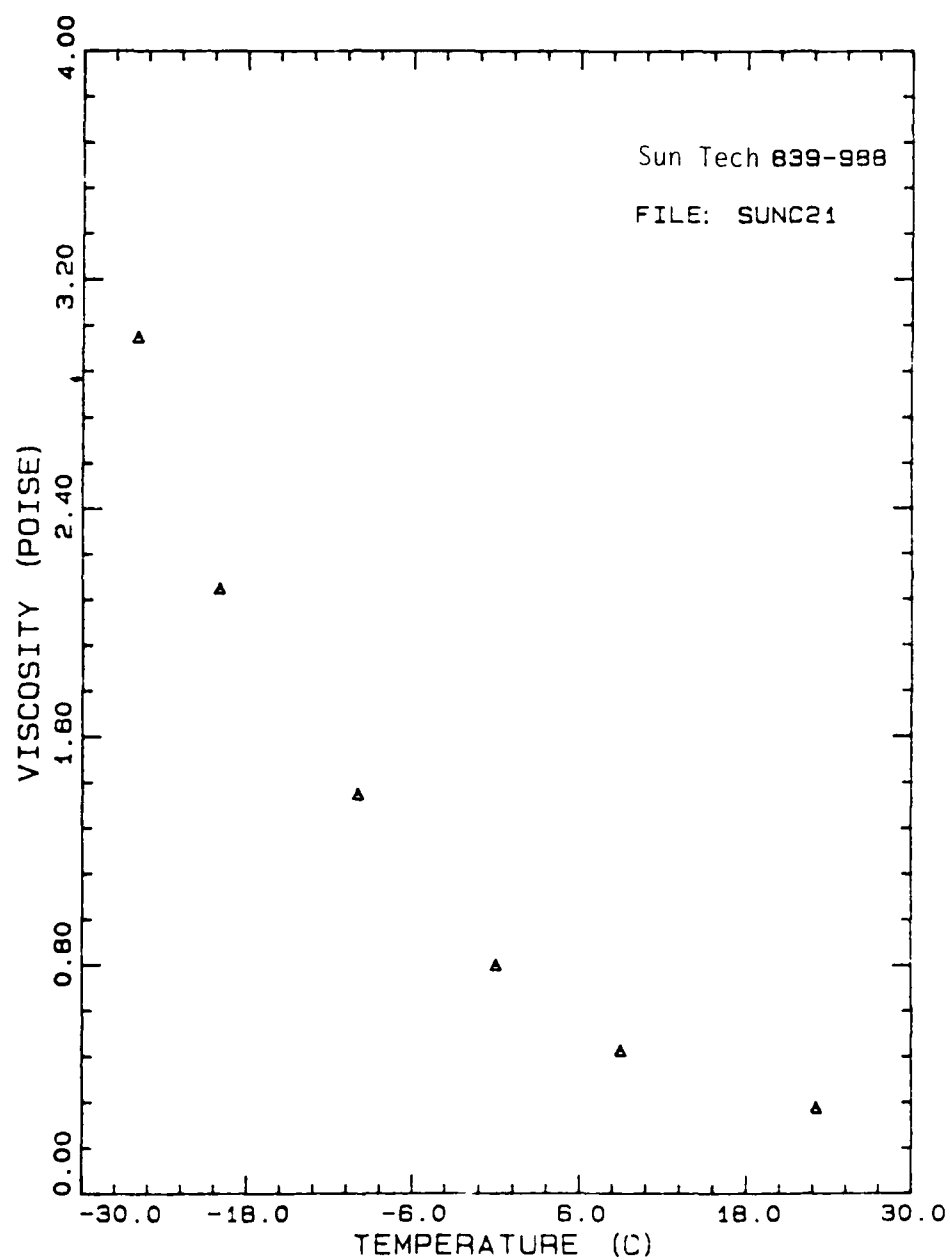
Figure 93.   Change in Upper Newtonian
             Viscosity (η_a) with Temperature.

165

C.4 Transient Behavior

Transient response was used to evaluate the viscoelastic and thixotropic properties of the slurries. At low shear rates, the stress growth after sudden imposition of a step change in shear, showed an overshoot, and approached a steady state value (Figure 72), even at a very low shear rate. The "overshoot" has been reported by many researchers in elastic liquids like polymer solutions. Slurries possess viscoelastic properties at low shears, but the elastic property differs from that of a polymer. The elasticity in slurries comes from particles and their interactions or structure. Since the elasticity in the slurry was due to the structure, an effort was made to find an elastic modulus, G, that could be related to the strength of structure in the slurries. The transient curves were replotted as shear stress against shear strain for various shear rates. The shear strain was obtained by the product of shear rate and time, i.e., $\gamma = \dot{\gamma} \cdot t$. If the material can be described by $\tau = G\gamma$ at low shear strains, it would mean that the material acts as a solid body with a constant elasticity G. Unfortunately, the initial slope for the τ vs γ plot was not constant as shown in Figure 94.

Amari and Watanbe(90) suggested that τ_{max}/γ was a good approximation of elasticity G of the structure. They obtained a constant G of 5.5×10^3 dyne/cm^2 for linseed oil-carbon black suspension. $\tau_{max}/\dot{\gamma}$ for carbon black at different shear rates is plotted in Figure 95. The data are not too far from a constant and can be considered as an elasticity constant, G, related to the strength of the structure.

Stress relaxation after cessation of steady flow was also examined to see if it could be described by a single relaxation time. None could be described by a single constant. The elasticity might change or disappear under steady shear. Other types of study such as creep flow or dynamic study would be needed to measure how the G changes.

Figure 94. Shear Stress Versus Shear Strain for Sun Tech 839-988.

167

Figure 95. τ_{max}/α as a Function of Shear Rate.

168

III. LUBRICANT DATA

The viscosity of lubricant 5P4E measured with Haake rotor MVI was 19.4 poise and with the rotor MVIII was 19.0 poise.

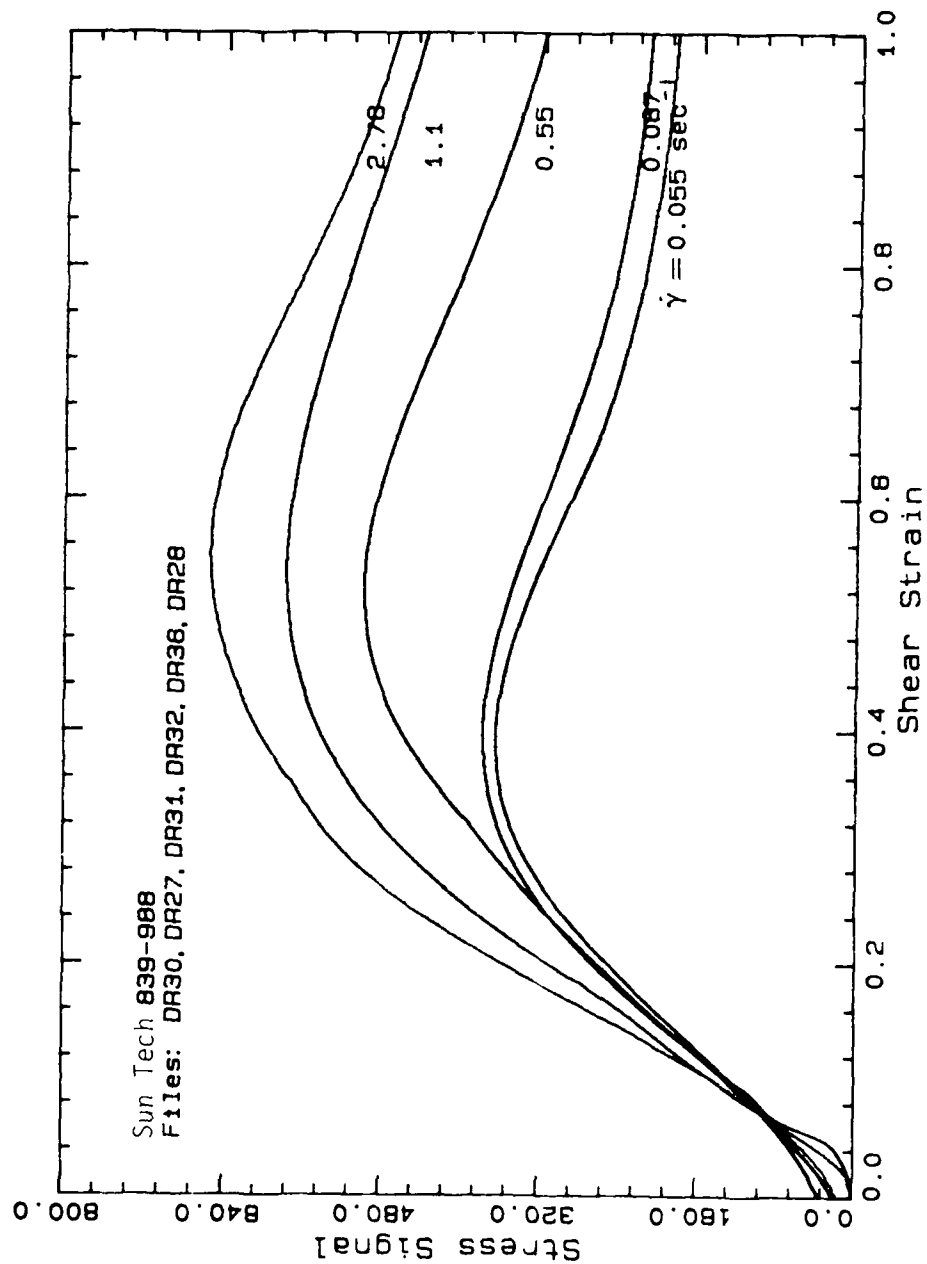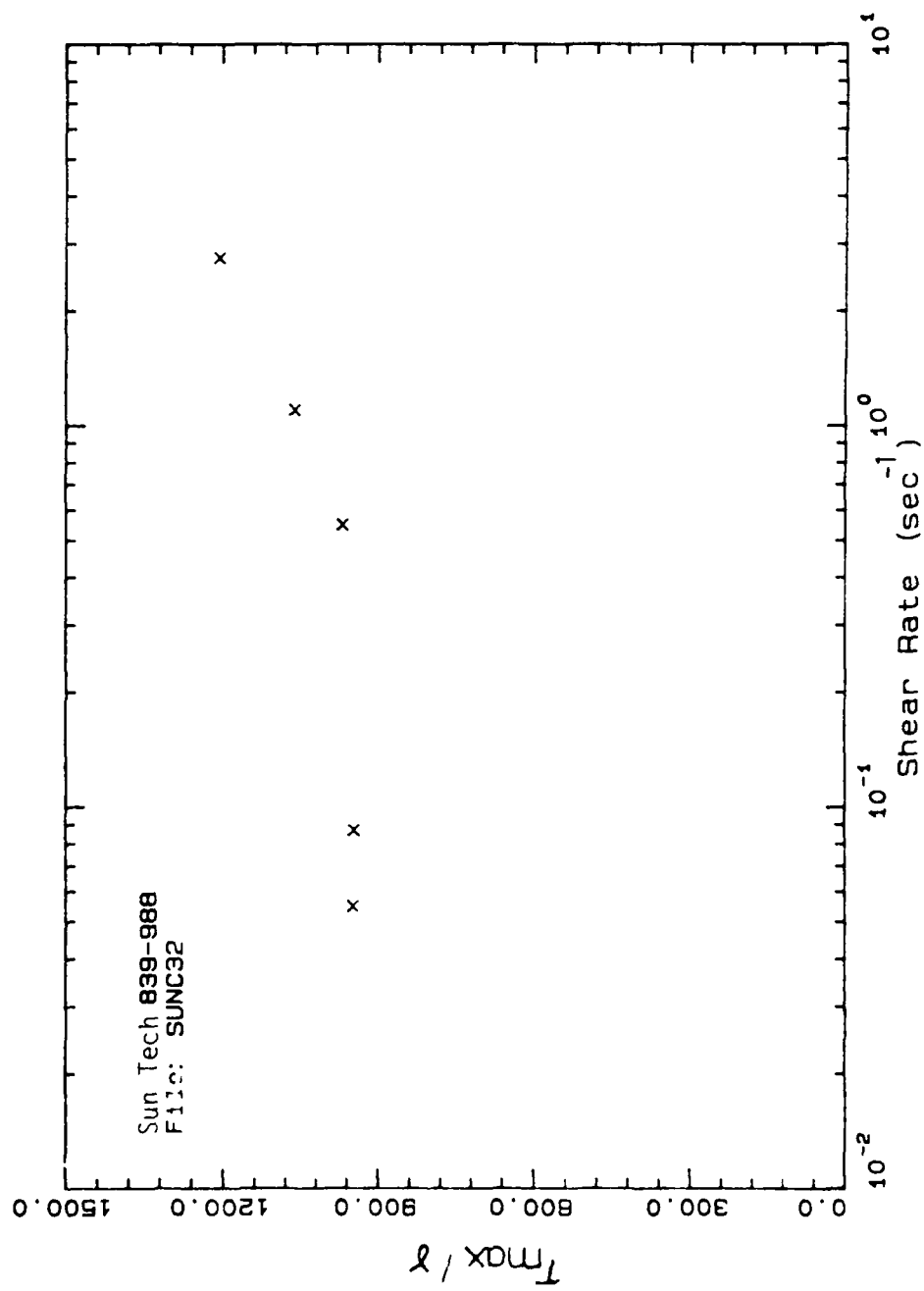Further tests on lubricant 5P4E were done on the Weissenberg R-16 Rheogoniometer. The value of the viscosity, determined in steady state flow, is constant with shear rate varying from 5.4 to 340 sec^{-1} and is 18.6 poise, a value which can be considered in agreement with that obtained from the Haake, i.e., 19.2 poise. Table XXVI summarizes all the lubricant data obtained.

Figure 96 at $10^{\circ}C$ and a high shear rate (348 sec^{-1}) shows overshoot, which is an indication of viscoelasticity. The equilibrium viscosity for this run was 233 poise. Figure 97 is an example of a lower temperature ($2.4^{\circ}C$) run at a low shear rate (11 sec^{-1}). The equilibrium viscosity increased to 5450 poise. No overshoot is observed at this low shear rate. Figure 98 at $-0.7^{\circ}C$ and 34.8 sec^{-1} shows overshoot and an equilibrium viscosity of 9790 poise. Figures 99 and 100 at $4.9^{\circ}C$ and 2.76 sec^{-1} are examples of both the growth and relaxation experiments. The equilibrium viscosity is 229,700 poise. The shear rate was too low to show overshoot. Finally, Figure 101 at $-9^{\circ}C$ and only 2.76 sec^{-1} is a dramatic example of viscoelastic overshoot.

The 2.76 sec^{-1} shear rate of Figure 99 is equivalent to 133 sec/rev. This translates into a movement of 4.72 mm/sec at the transducer. The equilibrium transducer displacement was calculated to be 3.38 mm which, if there were solid body rotation, would be accomplished in 0.72 sec as shown in Figure 99. The instrument response of 0.007 s cannot even be seen on this plot. The material response is noted as being 3.15 sec, which is over 4 times the time of a Newtonian material. Clearly we are dealing with a viscoelastic material. The initial shear rate is not really 2.76 sec^{-1} since the top cone is in motion. The shear rate as determined from the initial slope is only 1.0 sec^{-1} and increases to 2.76 sec^{-1} by 3.15 sec. As a further example, the shear rate had increased to 2.3 sec^{-1} from the measured slope at 2 sec. The difficulty in measuring accurate stress growth curves is clearly illustrated by this example. Actually, for a material of this viscosity, we could have used the piezoelectric crystal measuring system and obtained an accurate transient. We are currently working on the best means of analysis of this type of data so as to extract the viscoelastic characteristics.

One approximate correction, which should be valid at $t = 0$, is to correct the observed stress by the ratio of the desired shear rate to the actual rate. Such a curve is plotted in Figure 99. The initial slope of this curve will be a measure of G_1. Note that the corrected curves show some overshoot, but this may not be real. In any event we do not plan to try to analyze the entire curve; we only want the initial value as a measure of G_1.

We do not want to put much importance on the following values at this time, but from the corrected curve in Figure 99, the value of G_1 is 1.9×10^6 gm cm/sec^2. From the curve as measured and using the G_1 value and $\eta_o = 310,000$ P gives G_2 as -9.1×10^5 gm cm/sec^3. The value of the time derivative of the shear rate was 1.56 sec^{-1}.

TABLE XXVI.   Lubricant 5P4E

Temp (^{0}C)	Shear rate (sec^{-1})	App. Viscosity (poise)	File name
23^{0}C	5.5	18.5	LUB5D4
	11.0	18.5	LUB10D8
	110.3	17.8	LUB108
	174.0	17.9	LUB171
	348.0	17.8	LUB340
	550.7	17.6	LUB540
11.4	11.0	218.1	LB10D8SA
10.6	110.3	254.9	LB108SA
10.3	174.0	268.4	LB171SA
10.2	348.0	233.2	LB340SA
10.4	11.0	316.3	LB10D8SB
-0.2	1.103	24.6×10^3	LB1D8IIIA
-0.8	2.757	28.8×10^3	LB2D7IIIA
-0.7	5.507	26.7×10^3	LB5D4IIIA
-0.0	11.03	18.1×10^3	LB10D8FA
+0.7	11.03	13.1×10^3	LB10D8FB
-0.8	21.93	20.3×10^3	LB21D4FA
-0.4	0.551	12.5×10^3	LBD54FA
-0.9	2.757	14.6×10^3	LB2D7FB
-1.2	11.03	16.8×10^3	LB10D8FC
-1.3	21.93	14.3×10^3	LB21D4FB
-1.1	27.57	12.1×10^3	LN27FA
-0.7	34.8	9.79×10^3	LB34FA

170

TABLE XXVI (cont.)

Temp (^{0}C)	Shear rate (sec^{-1})	App. Viscosity (poise)	File name
-0.2	0.551	8.23 x 10	LUBD54II
+0.6	1.103	9.47 x 10^3	LUB1D7II
1.4	2.757	9.26 x 10^3	LUB27II
2.1	2.757	4.63 x 10^3	LUB27IIB
3.0	5.507	2.99 x 10^3	LUB5D4II
2.4	11.03	5.45 x 10^3	LUB10D8II
-5.0	0.551	288.3 x 10^3	LUBD57
-5.2	1.103	290.5 x 10^3	LUB1D7C
-5.0	1.739	259.9 x 10^3	LUB171
-4.9	2.757	229.7 x 10^3	LUB27A
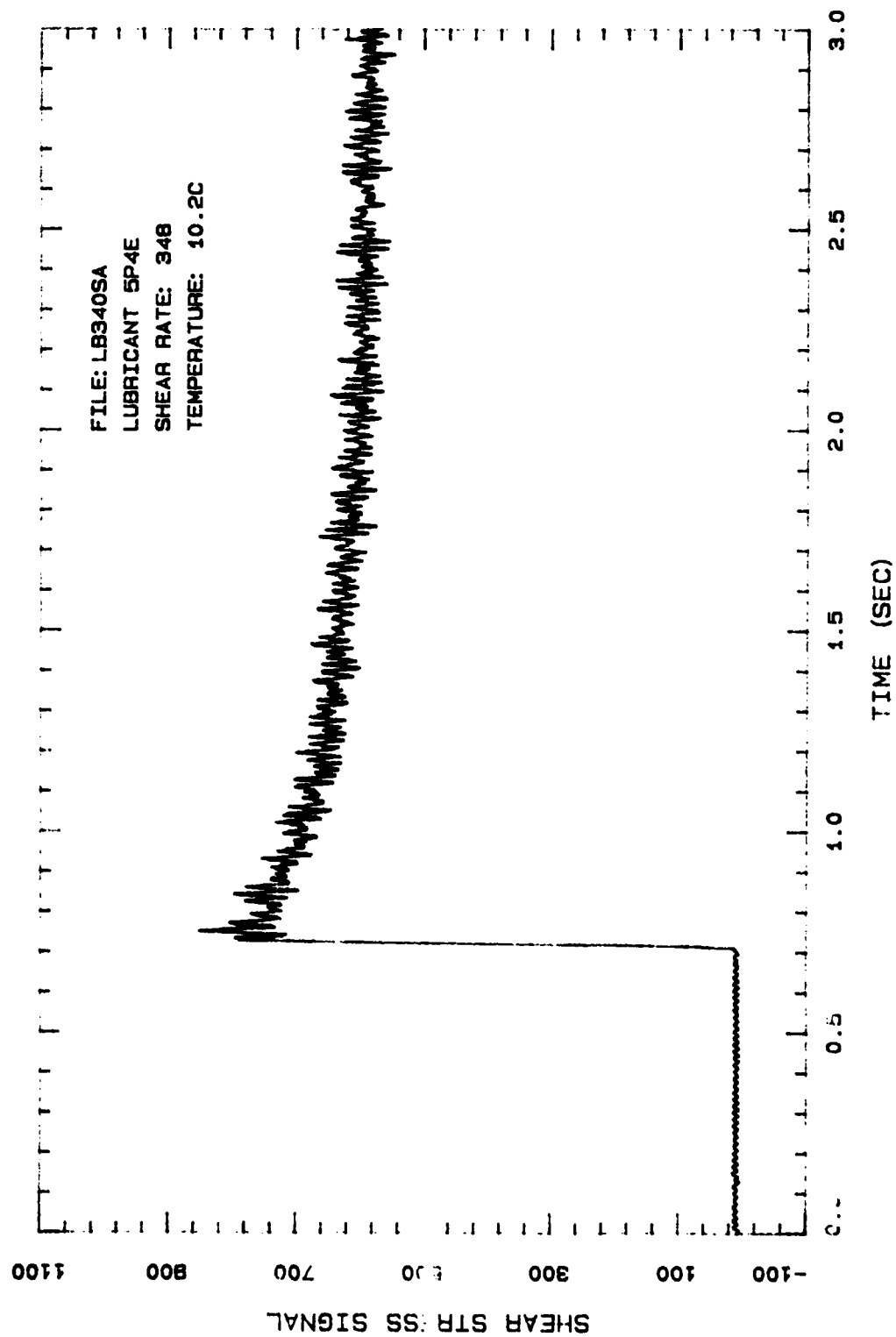
Figure 96. 5P4E lubricant response at high shear rate at 10.2C.

FILE: LB340SA
LUBRICANT 5P4E
SHEAR RATE: 348
TEMPERATURE: 10.2C

TIME (SEC)

SHEAR STR ·SS SIGNAL

172
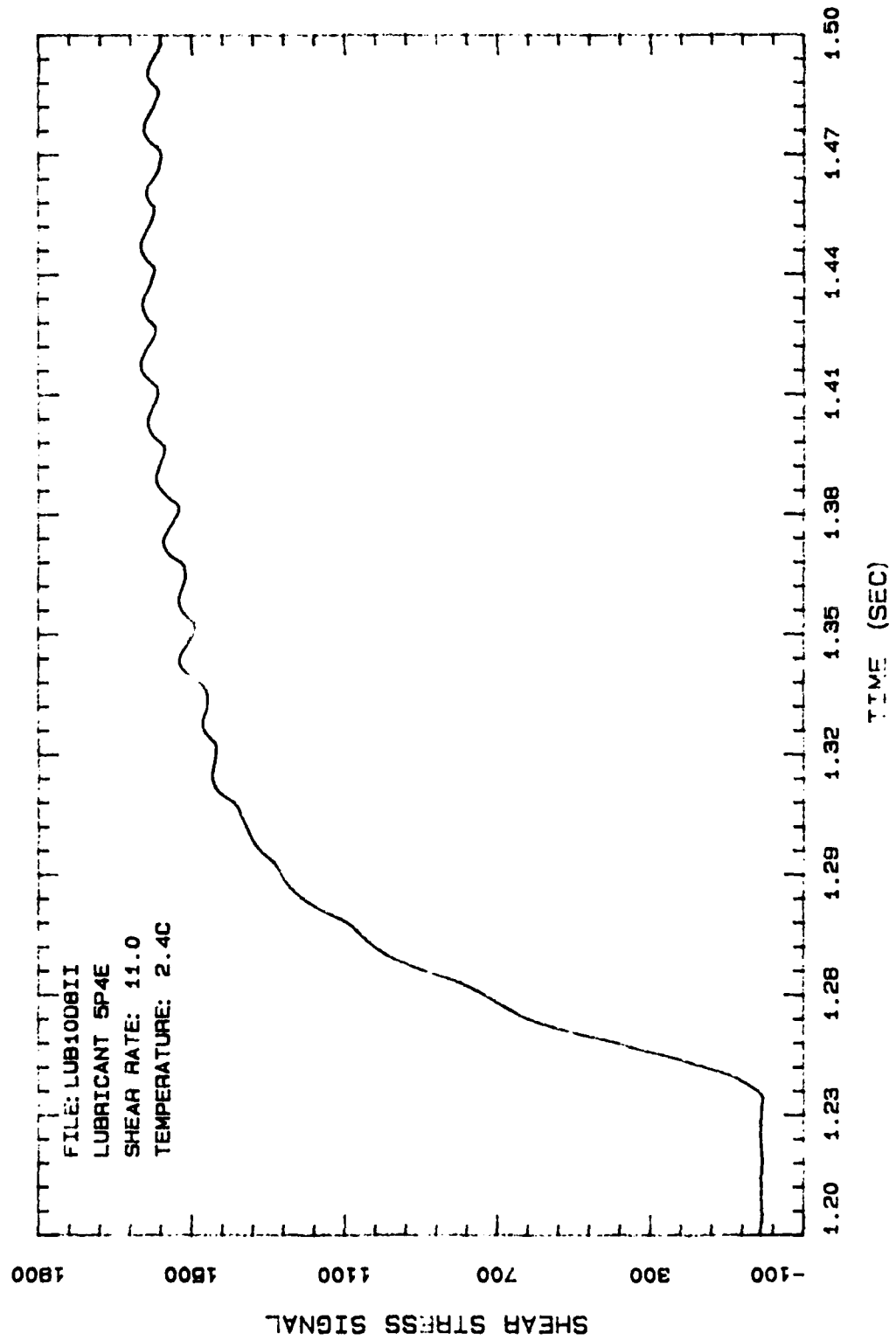
Figure 97. 5P4E response curve at medium shear rate and 2.4C.

FILE: LUB10D8II
LUBRICANT 5P4E
SHEAR RATE: 11.0
TEMPERATURE: 2.4C

173
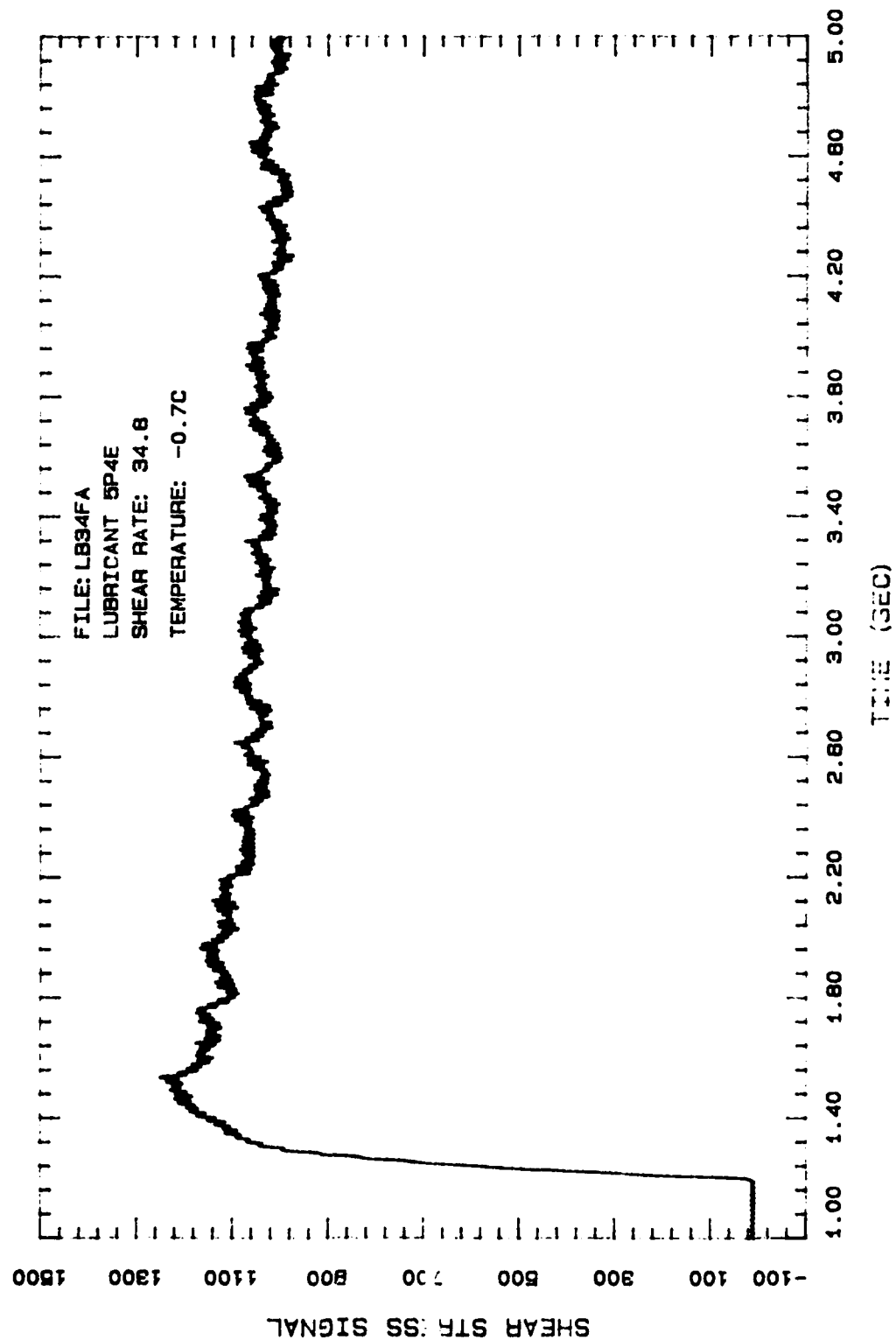
Figure 98. 5P4E lubricant at medium shear rate and -0.7C.

174
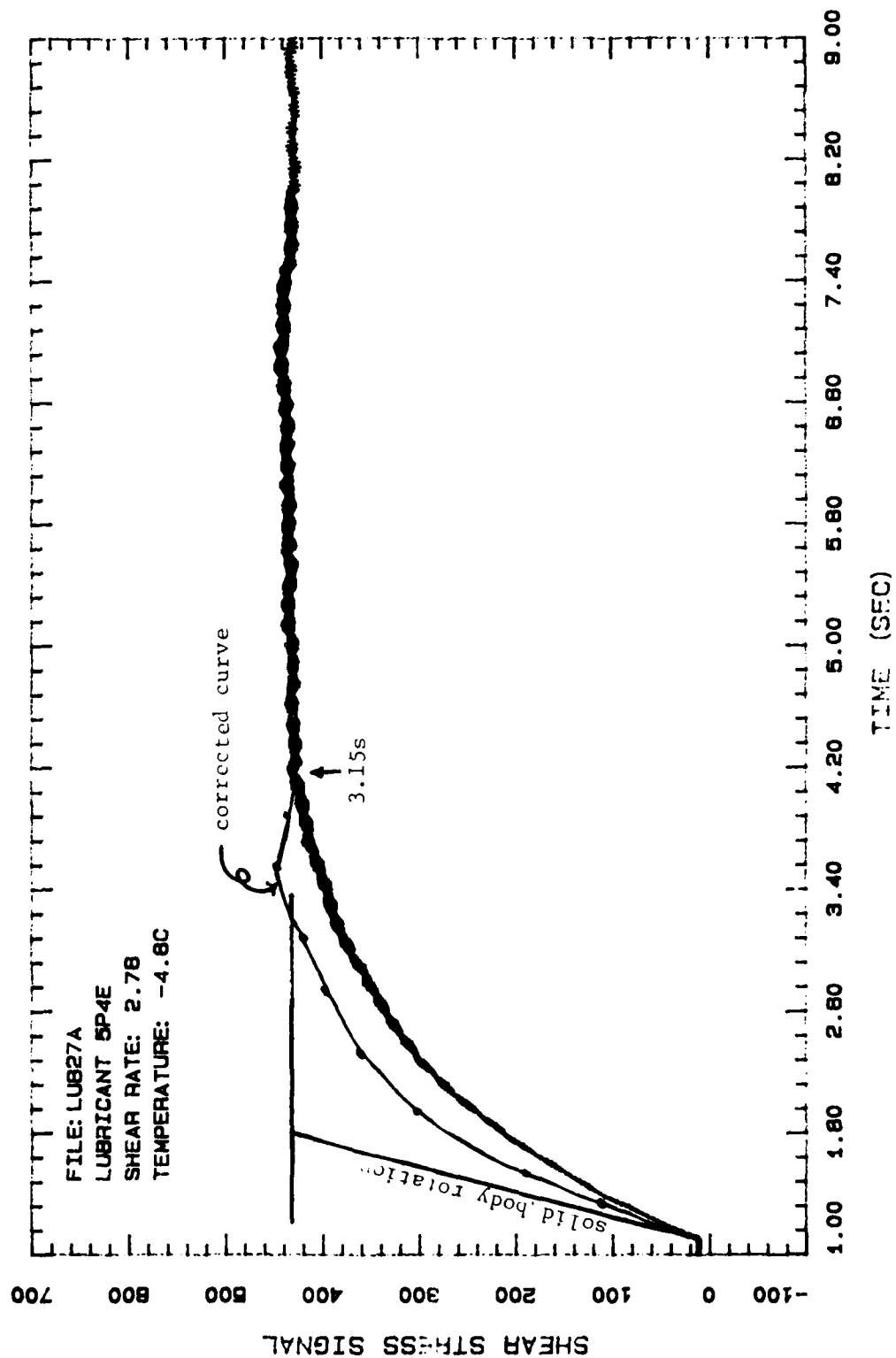
Figure 99. 5P4E lubricant with solid body rotation and corrected whear stress.

175
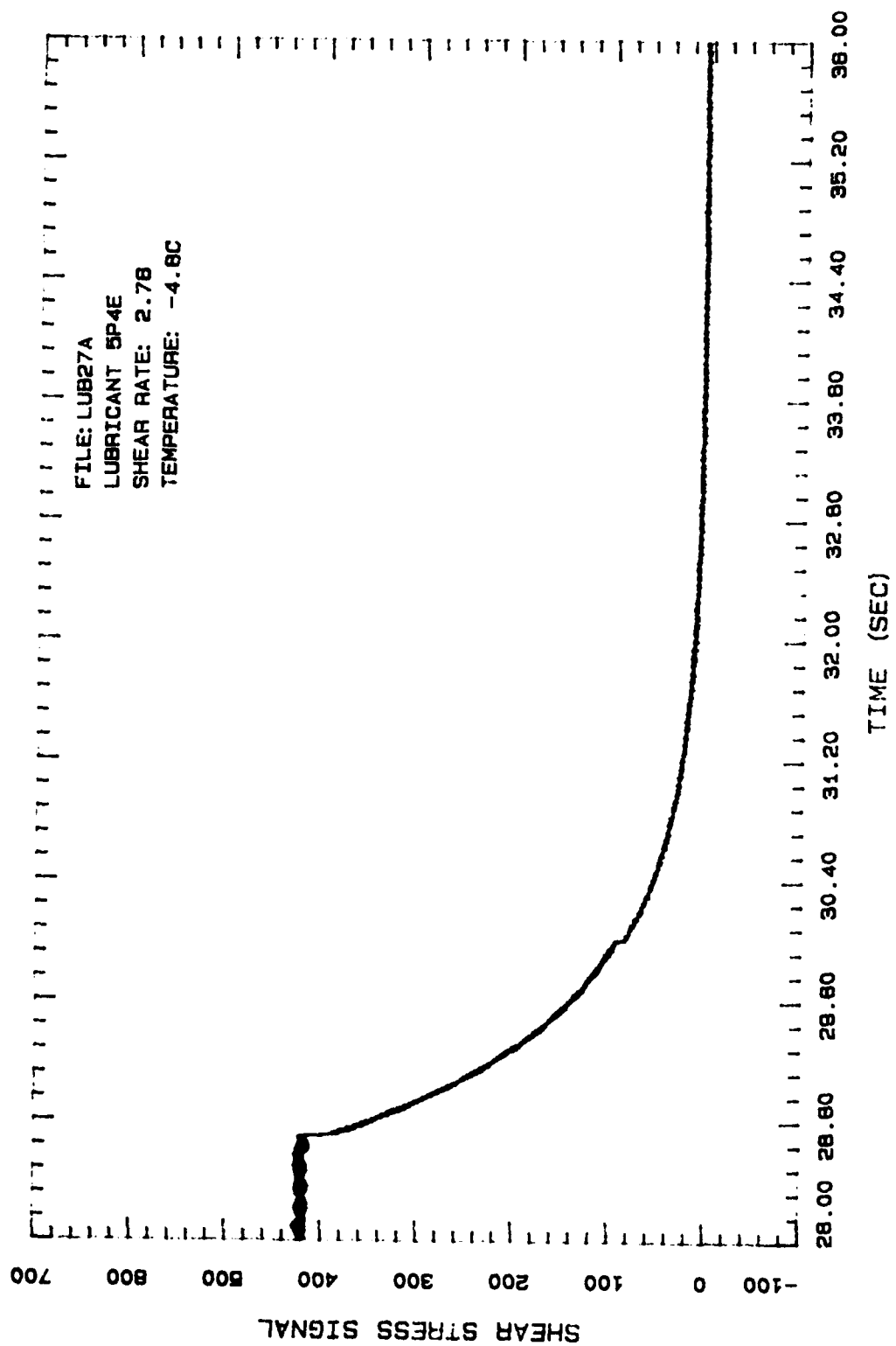
Figure 100. Stress relaxation under same condition as Figure 99.

FILE: LUB27A
LUBRICANT 5P4E
SHEAR RATE: 2.78
TEMPERATURE: -4.8C

TIME (SEC)

SHEAR STRESS SIGNAL

176

FILE: LUB207
LUBRICANT 5P4E
SHEAR RATE: 2.78
TEMPERATURE: -9.2C

TIME (SEC)

SHEAR STRESS SIGNAL
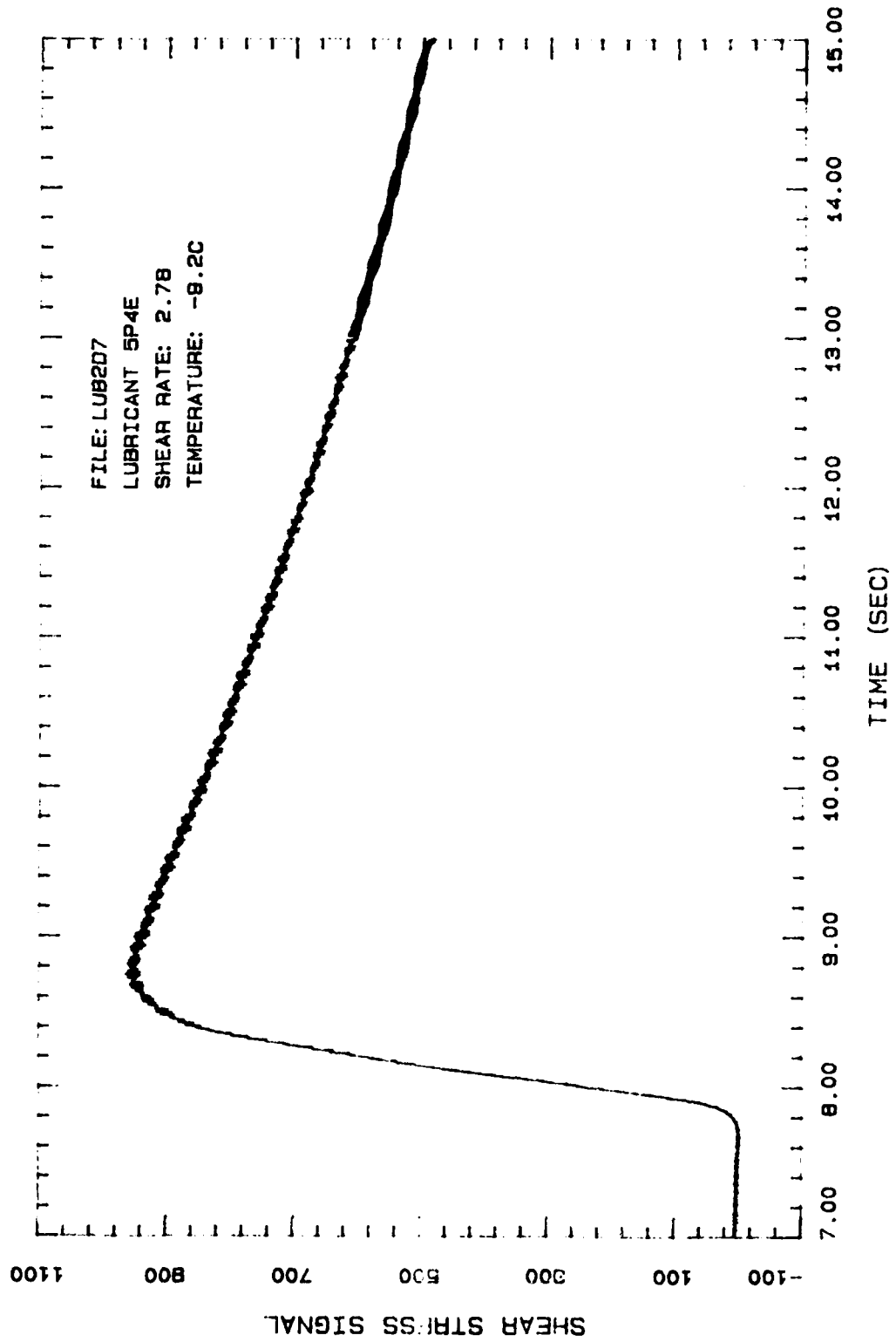
Figure 101. Example of extreme visco-elastic response for lubricant at low temperature.

APPENDIX \

PROPOSAL REFERENCE LIST

1. R.S. Brodkey, The Phenomena of Fluid Motions, Addison-Wesley, Reading Mass. (1967).

2. D. Denny and R.S. Brodkey, J. Appl. Phys. 33, 2269 (1962).

3. H.T. Kim and R.S. Brodkey, AIChE J. 14, 61 (1968).

4. L.G. Jones and R.S. Brodkey, "Thixotropic Behavior of a Collodial Suspension," Trans. 5th Int. Congr. Rheology, Kyoto, Japan 2, 267 (1970).

5. W.E. Levis and R.S. Brodkey, "A Kinetic Interpretation of Time-Dependent Polymer Rheology Data, "Trans. 5th Int. Congr. Rheology, Kyoto, Japan 4, 141 (1970).

6. K.H. Lee, L.G. Jones, K. Pandalai, and R.S. Brodkey, Trans. Soc. Rheol. 1 , 555 (1970).

7. K.H. Lee and R.S. Brodkey, Trans, Soc. Rheol. 15, 62, (1971).

8. P.J. Jachimiak, Y.S. Song, and R.S. Brodkey, Rheol. Acta 13, 745 (1974).

9. P.J. Jachimiak, Ph.D., Thesis, The Ohio State University (1971).

10. Y.S. Song, M.S. Thesis, The Ohio State University (1972).

11. Y.S. Song, Ph.D. Thesis, The Ohio State University (1975).

12. K.R.V. Pandalai, Ph.D. Thesis, The Ohio State University (1975).

13. H.R. Lander, Ph.D. Thesis, The Ohio State University (1977).

14. S. Oka, "Rheology," Vol. 3, F.R. Eirich, ed., Academic Press, New York (1960).

15. W. Ostwald, and R. Auerbach, Kolloid-Z. 38, 261 (1926).

16. F.D. Dexter, J. Appl. Phys. 22, 1124 (1954).

17. R.E. Gee and J.B. Lyon, Ind. Eng. Chem. 49, 956 (1957).

18. A.W. Sisko, Ind. Eng. Chem. 50, 1789 (1958).

19. W. Philipoff, Kolloid-Z. 71, 1 (1935).

20. R.L. Powell and H.J. Eyring, Nature 154, 427 (1944).

179

21. F. Rodriguez, Trans. Soc. Rheol. 10, 169 (1966).

22. S. Middleman, "Principles of High Polymers", Interscience (1968).

23. A.G. Fredrickson, "Principles and Applications of Rheology", Prentice-Hall (1964).

24. H. Eyring, J. Chem. Phys. 4, 283 (1936).

25. H. Eyring and T. Ree, J. Appl. Phys. 26, 793 (1955).

26. S. Hahn, T. Ree, and H. Eyring, Ind. Eng. Chem. 51, 856 (1959).

27. O.F. Goodeve, Trans. Faraday Soc. 35, 342 (1939).

28. I.M. Krieger and T. Dougherty, Trans. Soc. Rheol. 3, 137 (1959).

29. B.T. Storey and E.W. Merrill, J. Polymer Sci. 33, 361 (1958).

30. T. Gillespie, J. Polymer Sci. 46, 383 (1960).

31. C.J. Maxwell, Phil. Trans. Roy. Soc. Al 7, 49 (1867).

32. H. Fromm, ZAMM 25/27, 146 (1947).

33. H. Fromm, ibid., 28, 43 (1948).

34. J.C. Oldroyd, Proc. Roy. Soc. A200, 523 (1950).

35. J.G. Oldroyd, ibid. A245, 278 (1958).

36. K. Walters, Quart. J. Mech. Appl. Math. 13, 944 (1960).

37. K. Walters, ibid. 15, 63 (1962).

38. J.L. White and A.B. Metzner, J. Appl. Poly. Sci. 7, 1867 (1963).

39. R. Roscoe, Br. J. Appl. Phys. 15, 1095 (1964).

40. A.S. Lodge, "Elastic Liquids", Academic Press (1964).

41. T.W. Spriggs, Chem. Eng. Sci. 20, 931 (1965).

42. T.W. Spriggs and R.B. Bird Ind. Eng. Chem. Fund. 4, 182 (1965).

43. R.I. Tanner, ASME Trans. 8, 179 (1965).

44. H. Giesekus, Rheol. Acta, 5, 29 (1966).

45. J.D. Goodard and C. Miller, Rheol. Acta 5, 177 (1966).
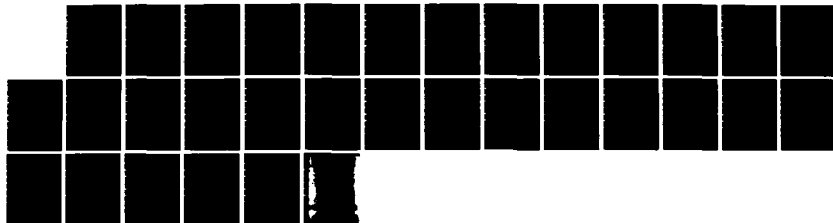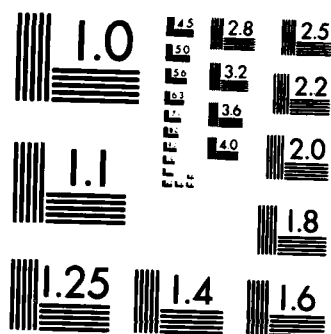
MICROCOPY RESOLUTION TEST CHART
NATIONAL BUREAU OF STANDARDS-1963-A

46. D.C. Bogue, Ind. Eng. Chem. Fund. 5, 253 (1966).

47. T.W. Spriggs, J.D. Huppler and R.B. Bird, Trans. Soc. Rheol. 10, 191 (1966).

48. T.E. Tanner, and J.M. Simons, Chem. Eng. Sci. 22, 1803 (1967).

49. R.B. Bird and P.J. Carreau, Chem. Eng. Sci. 23, 427 (1968).

50. W. Heindl and H. Giesekus, Rheol. Acta 11, 152 (1972).

51. I.J. Chen and D.C. Bogue, Trans. Soc. Rheol. 16, 59 (1972).

52. P.J. Carreau, Trans. Soc. Rheol. 16, 99 (1972).

53. R.B. Bird, O. Hassager and S.I. Abdel, AIChE J. 20, 1041 (1974).

54. E.B. Christiansen and W.R. Leppard, Trans. Soc. Rheol. 18, 65 (1974).

55. W.R. Leppard and E.B. Christiansen, AIChE J. 21, 999 (1975).

56. P.E. Rouse, J. Chem. Phys. 21, 1272 (1953).

57. F. Bueche, J. Chem. Phys. 22, 1570 (1954).

58. A.S. Michaels and J.C. Bolger, Ind. Eng. Chem. Fund., 1, 24, 153 (1962); 3, 14 (1964).

59. A.S. Michaels, Ind. Eng. Chem. 50, 951 (1958).

60. A.S. Michaels and F. Tausch, Ind. Eng. Chem. 52, 857 (1960).

61. S.G. Mason, Paper 2, 4th Intern. Congr. on Rheology, Brown Univ., Providence, R.I. (Aug., 1963).

62. S.G. Mason "Rheology," Vol. 4, F.R. Eirich, ed., Academic Press, New York (in press).

63. G.T. Fox and V.R. Allen, J. Chem. Phys. 41, 344 (1964).

64. H. Jeffreys, "The Earth", 2nd edition, p. 265, Cambridge (1929).

65. G. Pearson and S. Middleman, Trans. Soc. Rheol. 20, 559 (1976).

66. H. Kajiura, M. Sakai, and M. Nagasawa, Trans. Soc. Rheol. 20, 575 (1976).

67. E.A. Kearsley and L.J. Zapas, Trans. Soc. Rheol. 20, 623 (1976).

68. E. Ashare, Trans. Soc. Rheol. 12, 535 (1968).

69. K.L. Johnson and J.L. Tevaarwerk, Proc. Roy. Soc. London, (to be published) (1977).

70. A.W. Crook, _Phil. Trans. Roy. Soc._ A255, 28 (1963).

71. K.L. Jonson and R. Cameron, _Proc. Inst. Mech. Engrs._ 182, pt. 1, 307 (1967).

72. A.J. Barlow, J. Lamb, A.J. Matheson, P.R. Padinini and J. Richter, _Proc. Roy. Soc._ A298, 467 (1967).

73. A. Dyson, _Phil. Trans. Roy. Soc._ A266, 1 (1970).

74. S.T. Moynihan, P.B. Macedo, C.J. Montrose, P.D. Gupta, M.A. DeBolt, J.F. Dill, B.E. Com, P.W. Drake, A.J. Easteal, P.B. Eiterman, R.P. Moeller, H. Sasabe, and J.A. Wilder, _Ann. New York Acad. Sci._ 279, 15 (1976).

75. K. Park, Ph.D. Thesis, The Ohio State University (1981).

76. D.S. Soong, _Rubber Chem. & Tech._ 54, 641 (1981).

77. D.S. Soong and M. Shen, _J. Polym. Sci., Pol. Let._ 17, 595 (1979).

78. D.S. Soong and M. Shen, _J. Rheol._ 25, 259 (1980).

79. D. Acierno, F.P. La Mantia, G. Marrucci, and G. Titomanlio, _J. Non-Newtonian Fluid Mech._ 1, 125 (1976).

80. D. Acierno, F.P. La Mantia, G. Marrucci, G. Rizzo, and G. Titomanlio, _J. Non-Newtonian Fluid Mech._ 1, 147 (1976).

81. D. Denny, Ph.D. Thesis, The Ohio State University (1968).

82. K.H. Lee, Ph.D. Thesis, The Ohio State University (1969).

83. Weissenberg Rheogoniometer Instruction Manual, Sangamo Weston Controls, Ltd., Bognor Regis, Sussex, England.

84. R.L. Crawley and W.W. Graessley, _Trans. Soc. Rheol._ 21(1), 19 (1977).

85. I.M. Krieger and T.F. Niu, _Rheol. Acta_ 12 567 (1973).

86. N.L.M. Enthoven and H.L. Jalink, _Rheol. Acta_ 17 108 (1970).

87. S.S. Davis, _Rheol. Acta_ 11 199 (1972).

88. J.R. Van Wazer, J.W. Lyons, K.Y. Kim an R.E. Colwell, "Viscosity and Flow Measurement -- A Laboratory Handbook of Rheology", Interscience Publishers (1963).

89. K. Umega, _Trans. 5th Int. Congr. Rheolo y_, Kyoto, Japan (1970).

90. T. Amari and K. Watanabe, _Soc. Rheol., Japan_ 8 80 (1980).

182

APPENDIX B

SUMMARY OF EQUATIONS FROM KINETIC ELASTIC THEORY

$$-\frac{d(CF_t)}{dt} = k_1' (CF_t)^m - k_2' [C(1-F_t)]^n \tag{1}$$

$$F_t = \frac{f(\eta_t) - f(\eta_\infty)}{f(\eta_o) - f(\eta_\infty)} \tag{2}$$

$$F_t = \frac{\eta_t{}^a - \eta_\infty{}^a}{\eta_o{}^a - \eta_\infty{}^a} \tag{3}$$

$$k_1' = k_1 \tau^{P_1} \tag{4}$$

$$k_2' = k_3 + k_2 \tau^{P_2} \tag{5}$$

$$\tau = - \eta_t \dot{\gamma} \tag{6}$$

$$\tau + \frac{\eta_t}{G_1} \frac{\delta_\tau}{\delta_t} - \eta_t \quad (\dot{\gamma} + \frac{\eta_t}{G_2} \frac{\delta \dot{\gamma}}{\delta_t})$$

$$\tau + (\eta_t/G_1)\dot{\tau} = -\eta_t \ [\dot{\gamma} + (\eta_t/G_2) \ddot{\gamma}] \tag{7}$$

$$\frac{(1-F_{eq})^n}{F_{eq}^m} = K \ C^{m-n} \ \tau^P \tag{8}$$

$$K = \frac{k_1}{k_2 + (k_3/\tau^{P2})} \tag{9}$$

$$P = P_1 - P_2 \tag{10}$$

183

APPENDIX C

NOMENCLATURE

a	constant in conversion term in kinetic theory
A,B,C	reaction components
C	degree Centigrade, concentration
CSR	constant shear rate
d	displacement
F, F_A, F_B	fraction converted
G, G_1, G_2	elastic constants
$k_1, k_2, k_1', k_2', \ldots$	specific rate constants in kinetic theory
K, K_A, K_B	constant in kinetic theory
K_1, K_2	constants in Eq. (2)
m, m_1, m_2, n, n_1, n_2	order constants in the kinetic theory
M_c	critical molecular weight
N	number
P, P_A, P_B	constant in the kinetic theory
$P_1, P_2, \ldots$	sensitivity to stress constant in kinetic theory
S	parameter in two-step kinetic theory
t	time
t_{cut}	time when G1 starts to decay
TAU	stress
T	temperature
V	voltage

Greek

β	constant for non-constant shear rate experiment
$\dot{\gamma}$	shear rate
η	viscosity
η_0	lower Newtonion viscosity limit
η_∞	upper Newtonion viscosity limit
η_t	thixotropic viscosity
τ	stress

Subscripts

calc	calculated
eq	equilibrium
exp	experimental
n	normalized
0	initial
t	thixotropic

APPENDIX D

SUMMARY OF THE FIELD

CONTENTS

SUMMARY OF THE FIELD AND OUR RESEARCH ENDEAVORS

The various approaches towards the elucidation of the rheological characteristics of materials generally fall into one of five classifications: empirical, phenomenological (mostly rate processes), linear viscoelastic, nonlinear viscoelastic, and microrheological analyses. The empirical methods correlate data by curve-fitting techniques. The rate theories have as their basis the assumption that the nonlinear characteristics can be associated with some structural change of the material whether it involves particle associations and dissociations, link formations and ruptures, or molecular entanglements and disentanglements. The linear viscoelastic models are based upon linear combinations of Hooke's law of elasticity and Newton's law of viscosity. The nonlinear viscoelastic models are based on continuum mechanics and nonlinear combination mechanical models. Finally, microrheological analysis starts with the basic molecular or microscopic variables such as particle sizes, molecular interactions, and chain lengths. A simplified mechanism is proposed, and then it is mathematically represented and solved.

Each approach has made contributions to the field, but with the present state of the art, we cannot completely describe the non-Newtonian behavior even in simple geometries. Steady-state flow behavior has been extensively investigated, and the representations available are adequate. However, little is understood about the unsteady-state flow, such as shear stress and normal stress growth after the onset of a sudden shear rate. The theories in the literature are not able to always predict for example stress growth at a given constant shear rate from data obtained on other experiments.

The kinetic rate theory we are developing can be used to represent

189

transient (unsteady-state), equilibrium, and normal stress difference

information. The theory accounts for elasticity and thixotropy by combining

a kinetic rate approach with a modified form of Oldroyd's model. The basic

approach and preliminary confirmation of the kinetic theory have been

described in the papers by Brodkey, Denny and Kim (2, 3). Kim and Brodkey

(3) provided the test of the steady-state theory by correlating polymer

solution data over a wide concentration range. Lewis and Brodkey (5)

offered further support of the theory by describing the phenomena of

shear stress growth over a range of shear rates. However, thus far the

tests of the theory were still empirical since the necessary constants and

parameters had been obtained from the best fit to the data. Lee and

Brodkey (7) attempted to provide an independent test of the kinetic

approach by using data obtained under constant shear stress conditions

to evaluate the necessary constants and parameters in an idealized manner

as suggested by the theory, and not by simple curve-fitting methods. The

results were then used for predicting time-dependent constant shear rate

measurements as well as the constant stress data. Jachimiak et al. (8)

and Jachimiak (9) extended the approach to allow the prediction of the

first normal stress difference; but, because of the difficulty of obtain-

ing the elastic parameter under constant stress conditions, the prediction

was unsatisfactory. Song (10) did a complete analysis of the theory and

showed that the previous formulations could not be used to predict all the

various possible types of experiments. He was able to formulate one that

could be used which will be presented in the theory section. Song (11)

then obtained a comprehensive set of data on stress growth, stress

relaxation and transient shear rate experiments. He attempted to fit all

of these to the theory with some, but not complete, success. Panlalai (12)

obtained data for very large amplitude oscillation and extended the theory

190

for this. Finally, Landers (13) obtained new and improved oscillatory data on the same system. The most recent is by Park (75) and is summarized in App. C.

The present summary is slanted so far toward our own work, and the background literature has been covered in several of our previous publications. However, it might be well to put our approach into proper perspective with other means of treating rheological data, since the area of research is large and all readers may not be equally familiar with our efforts. First, there are the empirical methods such as the power or Ostwald-deWaele (14, 15), Ellis (16, 17), Sisko (18), Reiner-Philippoff (19), Powell-Eyring (20), and Rodriguez (21) models. Detailed explanation of these can be found in most textbooks (1, 22, 23). The semiempirical or phenomenological models form a second class of which the Eyring work (20, 24-26) is representative. It is in this class that the present effort resides as well as a number of other kinetic approaches (27-30). These latter (27-30) have been less general kinetic approaches that have assumed some specific mechanism and then suggested a rate equation to describe the change; however, since these are specific to a particular suggested mechanism and not general to aid in establishing the mechanism, they will not be discussed further. The basic linear viscoelastic model is due to Clerk Maxwell (31). The equation is a linear combination of Newton's law of viscosity of an ideal liquid and Hook's law for an ideal solid. Even though it is a linear equation, it has been a starting point of almost all the nonlinear rheological models proposed in the last two decades. Most of the models for nonlinear viscoelasticity are a generalization of Maxwell's equation using tensor calculus. Typical equations of this category are discussed in references 32 through 55. Most are formulated in a convected (co-deforming) coordinate system as was first

191

suggested by Oldroyd (34). Some are expressed in a co-rotational coordinate system, which has been reviewed by Bird et al. (53). In spite of all the work, the ability to fit transient data is far from satisfactory as can be seen in Chen and Bogue and Christiansen and Leppard and others (51,54,55, 65 - 67). Figures 1 and 2 show some comparisons from the latter work. Finally, there are the microrheological approaches which assume a mechanism and are directed toward elucidating the basic reason why specific systems are non-Newtonian. In this class are such analyses as Rouse (56), Bueche (57), Michaels et al. (58-60), and Mason (61, 62).

In the empirical models, nothing is learned about the basic mechanism because little specific meaning can be given to the constants. In the phenomenological approaches as little is assumed about the specific mechanism as possible, and one hopes to gain some insight into this by evaluation of the constants and their variation with the parameters of the system (such as molecular weight distribution). The viscoelastic theories have been the recent mainstay of rheological representation and as many believe will eventually be adequate for the task. The micro-rheological analyses depend on a knowl dge of the mechanism and are only valid for systems that fulfill the basic assumption and approximations of the theories. In general, a mechanism is suggested, and then one attempts to confirm the hypothesis by comparison to experimental data. Hopefully, in time the methods will complement each other, then menological approaches providing the necessary insight to allow a more reasonable mechanism to be proposed than has heretofore been possible, and micro correlations allowing estimation and intelligent variation, at the investigation of the characteristic parameters of materials.

Fig. 1
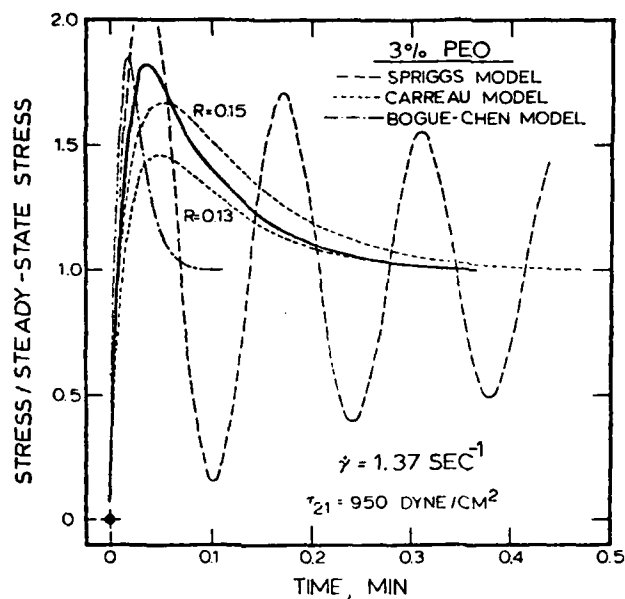
Normalized shear stress growth with the predictions of the
Spriggs, Carreau, and Bogue-Chen models.

Fig. 2
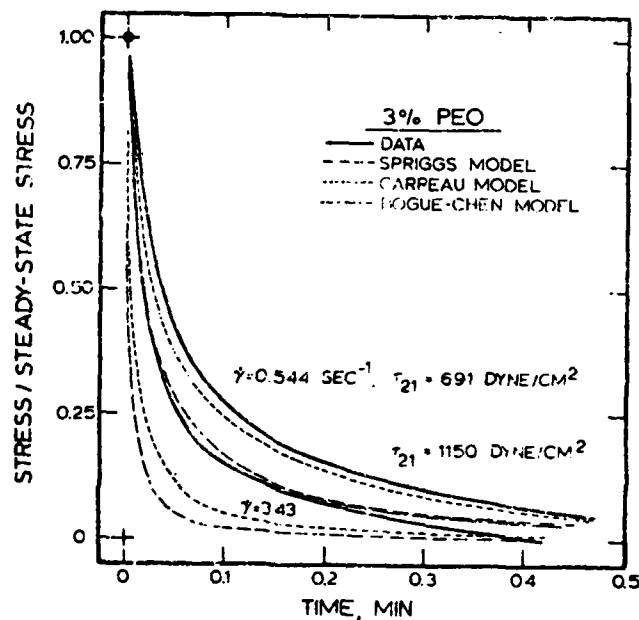
Typical shear stress decay with the predictions of the
Spriggs, Carreau, and Bogue-Chen models.

Both figures reproduced from reference 55

The possible application of our kinetic-elastic model (as well as alternate models) has been mainly to polymer rheology problems where time dependency is recognized but is not as extreme as it might be in elasto-hydrodynamic lubrication ($\sim$ls versus $\sim 10^{-3}$s). Temperature dependency is important in both, but pressure effects are much more extreme in the lubrication application. Johnson and Tevaarwerk (69) have recently reviewed the shear behavior of EHD oil films, but it should be emphasized that the models considered by them can at best only describe a part of the known response characteristics of non-Newtonian materials. Nevertheless, the reasonable success they demonstrated in matching traction curves leads one to hope that a better model, more accurately descriptive of the process, would allow nearly a complete description of the dynamics of the problem.

The model used by Johnson and Tevaarwerk was the simplest form of the sinh law for the non-Newtonian representation (see references 20 and 24-26) and the Maxwell model (31) for the viscoelastic contribution. In both cases, the representation of known response characteristics is limited and does not compare with the kinetic -elastic model to be described. There are of course a number of earlier models that have been used to describe traction curves. Crook (70) suggested a Newtonian fluid and temperature dependence to explain the nonlinear region. Johnson and Cameron (71) showed that non-Newtonian characteristics were indeed important. Barlow et al. (72) showed that lubricants could be viscoelastic. Dyson (73) suggested that viscoelasticity could be important in the linear region under large deformations as well as in the nonlinear region.

The knowledge of the characteristics of lubricants is clearly limited and the best means to describe the fluid during a concentrated contact is

194

still to be determined thus there exists a need for looking into this applied problem in more detail using the rheologically sound kinetic-elastic approach.

The application of the theory to the field of slurry fuels is still another possibility. These materials will usually exhibit a yield stress. Unfortunately, data on the time response of such materials does not appear to have been measured and clearly work is needed here.

THEORY

Polymer rheology is primarily concerned with three fundamental properties of fluids: the time rate of change of viscosity or structure, called here the thixotropic property; the steady-state level obtained, which is a function of the shear rate; and the lag of the stress behind what one would expect from the thixotropic behavior, called here the elastic property. The change in viscosity can be attributed to some reversible internal mechanism such as entanglement, association, or winding of long-chain polymer molecules. The lag of the stress is due to the property of the material which causes it to resist deformation and thereby recover its original shape and size when deforming forces are removed. The nonlinear time-dependent flow behavior for such polymeric materials can best be described by a combination of elasticity and thixotropy. The thixotropic and steady-state behavior is described by the kinetic theory and the elastic property is described by an elastic model.

A KINETIC MODEL FOR THIXOTROPIC CHANGE

In the previous work (1-13), we developed a kinetic model for thixotropic materials which is descriptive of the viscosity change that occurs in polymer solutions. The model is different from previous rate models in that molecular phenomena such as links, particle spheres, dipole moments, or hydrogen bonding are not used directly as a basis of the model. Instead, let us define a new variable, F_t, as the fraction of the thixotropic fluid structure unchanged. This new variable F_t is a lumped parameter which contains the overall effects of molecular phenomena such as disentanglement and entanglement of chains, link rupture and association and others. At zero time and no stress, the fluid thixotropic structure would be

unchanged and $F_t = 1$. As time progresses (unsteady state), the thixo-tropic fluid structure undergoes change and F_t decreases and continues to decrease as the structure changes. Finally, at steady state, an equilibrium is reached between the unchanged and changed thixotropic fluid structure and $F_t = F_{eq}$, the equilibrium value of the variable. The situation being considered reminds one of a simple kinetic reaction of $A \rightleftarrows B$. If we apply the homogeneous kinetic reaction concept, the simplest equation we could get is

$$ - \frac{d(CF_t)}{dt} = k_1' \ (CF_t)^m - k_2' \ [C(1-F_t)]^n \qquad (1) $$

where k_1' and k_2' are forward and reverse reaction constants, m and n are forward and reverse orders of reaction, and C is the concentration of polymer solution. For steady state (equilibrium) conditions, Eq. (1) reduces to

$$ k_1' \ (CF_{eq})^m - k_2' \ [C(1-F_{eq})]^n = 0 \qquad (2) $$

or

$$ \frac{(1-F_{eq})^n}{F_{eq}^m} = \frac{k_1'}{k_2'} \ C^{m-n} \qquad (3) $$

where the subscript eq means that F_t is at the equilibrium state.

What we are eventually interested in is not the thixotropic structure unchanged, but rather the real fluid property viscosity; therefore, we need some functional form of F_t expressed in terms of viscosity. The limiting viscosities (zero shear rate viscosity, η_o, and upper Newtonian viscosity, η_∞) can be utilized to define the thixotropic structure unchanged, F_t, since the apparent viscosity of a polymer solution falls within these two limiting values. The structural variable F_t is defined by an inverse-

197

lever arm principle (1,3):

$$F_t = \frac{f(\eta_t) - f(\eta_\infty)}{f(\eta_o) - f(\eta_\infty)} \tag{4}$$

where η_t can be called the thixotropic structural viscosity. The functional form taken for $f(\eta)$ is $B\eta^a$, which when combined with Eq. (4) gives:

$$F_t = \frac{\eta_t^a - \eta_\infty^a}{\eta_o^a - \eta_\infty^a} \tag{5}$$

where a is constant to be determined. The constant a can be selected to be (1/3.4) from experimental evidence (63) that the zero shear rate viscosity η_o is proportional to the 3.4 power of the molecular weight. But, for specific cases or other materials any value which gives a good fit to the experimental data would be correct. For slurries a value of 1 can be used.

To complete the kinetic model, we need one more basic functional assumption about the reaction constants, k_1' and k_2', in Eq. (1). In general, these reaction constants are considered to be functions of shear stress and temperature. For isothermal condition, the following functional forms are suggested from empiricism and logic (see references 1 to 11)

$$k_1' = k_1 \, \tau^{p_1} \tag{6}$$

$$k_2' = k_3 + k_2 \, \tau^{p_2} \tag{7}$$

where k_1 and k_2, and the p's can be said to be rates and susceptibilities to stress level, respectively. The term k_3 is a constant in this case since it is considered to be a function of temperature only. It accounts for the physical fact that a material recovers its original structure from molecular or Brownian motion without other external help. It might

be considered small and thus negligible compared with other terms, except when shear stress is zero as a result of the material simply standing for long periods of time in order to allow structural recovery. Equation (1) is a scalar equation and the stress in Eqs. (6) and (7) must be scalar. If the structure is only affected by the shear stress then τ in Eqs. (6) and (7) must reflect this. If the structure depends on the total stress in the system then the double dot product of the stress ($\tau:\tau$) might be more appropriate.

We define a thixotropic structual stress, τ_t, as

$$\tau_t = -\eta_t \dot{\gamma} \tag{8}$$

This stress, τ_t, follows the dashed line in Fig. 3. However, the real stress, τ, follows the solid line in the same figure. There is a gap between the real and newly defined thixotropic structural stress. To account for this difference one needs to consider the elastic property of the material.

B ELASTIC MODEL FOR VISCOELASTICITY

The kinetic theory of thixotropy just presented assumed that there was no elasticity in the material; however, most polymeric solutions are viscoelastic and the thixotropic presentation alone is not adequate.

In order to incorporate the elastic property into the theory, a three constant model which is similar to Maxwell's equation:

$$\tau + \frac{\eta}{G} \frac{d\tau}{dt} = - \eta_i \dot{v} \tag{9}$$

and originally proposed by Jeffreys (64) and used by Oldroyd (34,35) is used. The equation is

$$\tau + \lambda_1(d\tau/dt) = -\eta_0 \lceil \dot{\gamma} + \lambda_2(d\dot{\gamma}/dt) \rceil \tag{10}$$

where λ_1 and λ_2 are relaxation times and η_0 is zero shear rate viscosity. In our earlier work (5, 7) an integrated form of Eq. (10) was used. The modified version of Eqs. (9) and (10) currently used is

$$\tau + \frac{\eta_t}{G_1}\frac{\delta_\tau}{\delta t} = -\eta_t (\dot{\gamma} + \frac{\eta_t}{G_2}\frac{\delta\dot{\gamma}}{\delta t})$$

or

$$\tau + (\eta_t/G_1)\dot{\tau} = -\eta_t \lceil \dot{\gamma} + (\eta_t/G_2)\ddot{\gamma} \rceil \tag{11}$$

where G_1 and G_2 are modulus type parameters to be determined. Convected derivatives are used so that normal stresses can be accounted for. This equation will be called the elastic model since it is developed to account for the lagging or elastic part of viscoelasticity. Equation (1) was called the kinetic model since it is formulated with the kinetic concept. Thus, the rate theory is called the kinetic-elastic model.

C LIMITING CONDITIONS FOR THE KINETIC-ELASTIC MODEL

C.1 STEADY-STATE CONDITIONS

Introducing Eqs. (6) and (7) into Eq. (3) gives

$$\frac{(1 - F_{eq})^n}{F_{eq}^m} = K C^{m-n} \tau^p \tag{12}$$

$$K = \frac{k_1}{k_2 + (k_3/\tau^{p2})} \tag{13}$$

$$p = p_1 - p_2 \tag{14}$$

The subscript eq means the equilibrium value.

It has been found that K is essentially constant (3). This would imply that under equilibrium conditions where τ is finite k_3/τ^{p2} is small compared

200

to k_2 and/or that p_2 is very close to zero, so that $K = k_1/(k_2 + k_3)$. Apparently the latter is true since p_2 has been found to be very close to zero (7, 9, 10, 11). In any event K and p can be taken as constants over the entire range of shear rates or stresses. It has been found that m = 1 and n = 2 is satisfactory; thus, if so, Eq. (12) becomes

$$F_{eq} = 1 + (K/2C)\tau^p - \sqrt{(1 + (K/2C)\tau^p)^2 - 1} \qquad (15)$$

If η_∞ is negligible compared with η_0 the non-Newtonian (steady-state) viscosity expression from Eqs. (5) and (15) is

$$\eta = \eta_0 [1 + (K/2C)\tau^p - \sqrt{(1 + (K/2C)\tau^p)^2 - 1}]^{1/a} \qquad (16)$$

C.2 SHEAR STRESS GROWTH AT CONSTANT SHEAR RATE

At constant shear rate and considering only the shear stress, the elastic Eq. (11) can be simplified to

$$d\tau_n/dt = \dot{\tau}_n = (G_1/\eta_t)(\tau_{tn} - \tau_n) \qquad (17)$$

where $\qquad \tau_n = \tau/\tau_{eq}$ and $\tau_{tn} = \tau_t/\tau_{eq}$.

The other equations are:

$$-\frac{d(CF_t)}{dt} = k_1' (CF_t)^m - k_2' [C(1-F_t)]^n \qquad (1)$$

with k_1' and k_2' given by Eqs. (6) and (7)

$$\eta_t = [(F_t(\eta_0^a - \eta_\infty^a) + \eta_\infty^a]^{1/a} \qquad (1?)$$

and

$$\tau_t = -\eta_t \dot{\gamma} \qquad (8)$$

201

The limiting conditions are at time = 0,

$$F_t = 1.0, \quad \tau_n = 0, \quad \eta_t = \eta_o$$

and at time = ∞ or equilibrium

$$F_t = \text{constant} \leq 1, \quad \tau_n = 1.0, \quad \eta_t = \eta_{eq}$$

C.3 SHEAR STRESS RELAXATION AFTER CESSATION OF SHEAR

The elastic Eq. (11) takes the simple form (shear rate equal to zero)

$$d\,\tau_n/dt = -\,(G_1/\eta_t)\,\tau_n \tag{19}$$

Equations (1) and (18) in the previous section apply here. The limiting conditions are at t = 0,

$$F_t = F_{eq} < 1.0, \quad \eta_t = \eta_{eq}$$

and at t = ∞,

$$F_t = 1.0, \quad \eta_t = \eta_o$$

C.4 TRANSIENT SHEAR RATE AT CONSTANT SHEAR STRESS

For this case, a little manipulation of the elastic Eq. (11) at constant stress generates Eq. (20):

$$\frac{d\dot{\gamma}_n}{dt} = \ddot{\gamma}_n = \frac{G_2}{\eta_t} \left[\frac{\eta_{eq}}{\eta_t} - \dot{\gamma}_n \right] \tag{20}$$

where $\dot{\gamma}_n$ is $(-\dot{\gamma})/(-\dot{\gamma}_{eq})$. The other pertinent equations are,

$$-\frac{d(CF_t)}{dt} = k_1'\,(CF_t)^m - k_2'\,[C(1-F_t)]^n$$

and

$$\tag{1}$$

$$\eta_t = [F_t(\eta_o^a - \eta_\infty^a) + \eta_\infty^a]^{1/a} \tag{18}$$

The boundary conditions are at $t = 0$,

$$F_t = 1.0 \text{ and } \dot{\gamma}_n \text{ is guessed by data}$$

and $t = \infty$,

$$F_t = F_{eq} \text{ and } \dot{\gamma}_n = 1$$

The special feature of this case is that Eq. (1) is not coupled with Eq. (20). Thus, Eq. (1) can be numerically integrated, independently. This information is then utilized for the integration of Eq. (20).

C.5 NORMAL STRESS

In a straight forward manner, as shown by Oldroyd (see 1), one can obtain from the model in the form of convective derivatives, the first normal stress difference as

$$\sigma_1 = \tau_{11} - \tau_{22} = -2 \eta_t^2 \left[\frac{1}{G_1} - \frac{1}{G_2} \right] \dot{\gamma}^2$$

$$= -2 \tau_t^2 \left[\frac{1}{G_1} - \frac{1}{G_2} \right] \tag{21}$$

where the latter form is obtained using Eq. (8). In references (8) and (9), σ_1 was not satisfactorily obtained, thus an adequate test of the prediction was not made.

C.6 OSCILLATORY CONDITIONS

The kinetic equation (1) along with the equation to account for the elastic part of the deformation (11) (using a sinusoidal input expression for shear rate) can be solved simultaneously. For the oscillatory shear rate and its derivative one has

$$\dot{\gamma} = \dot{\gamma}_F + \dot{\gamma}_0 \sin(\omega t) \tag{22}$$

$$\ddot{\gamma} = \dot{\gamma}_0 \omega \cos(\omega t) \tag{23}$$

where $\dot{\gamma}_F$ is a fixed shear rate level. Neglecting η_∞ compared to η_o and η_t in Equation (5), we have

$$F_t = \eta_t^a / \eta_o^a \qquad (24)$$

Therefore,

$$dF_t/dt = \frac{1}{\eta_o^a} \, a \, \eta_t^{(a-1)} \, \dot{\eta}_t \qquad (25)$$

Substituting the above equation in Eq. (1), using Eqs. (6) and (7) with $k_3 = 0$ and rearranging gives

$$-\dot{\eta}_t = \frac{\eta_o}{ac(\eta_t/\eta_o)^{a-1}} \left[k_1 \tau^{p_1} \left\{ \left(\frac{\eta_t}{\eta_o}\right)^a \right\}^m c^m \right.$$

$$\left. -k_2 \, \tau^{p_2} \left\{ 1 - \left(\frac{\eta_t}{\eta_o}\right)^a \right\}^n c^n \right] \qquad (26)$$

Rearranging Eq. (11) gives

$$\dot{\tau} = - \frac{G_1}{\eta_t} \left[\eta_t \left(\dot{\gamma} + \frac{\eta_t}{G_2} \ddot{\gamma} \right) \right] \qquad (27)$$

Equations (26) and (27) can be simultaneously solved numerically [using Eqs. (22) and (23)] to get time vs. shear stress and η_t and the results compared to values calculated from experimental data.

D SOME SPECIFIC RESULTS

Figures 4 and 5 show typical predictions obtained from the theory for stress growth and relaxation. Typical constants used for these are:

From equilibrium data, assumed $m = 1$, $n = 2$, $a = 1$ and $\eta_\infty < \eta$

evaluated experimentally $\eta_o = 3.1 \times 10^4$ poise for 35% PMMA (mw = 1.15×10^5) in DEP
evaluated $p = 1.621$ and $\log K = -8.936$

From constant shear rate transient results

$$p_2 = -0.01 \quad k_2 = 20.0$$

$$G_1 = f(\dot{\gamma}) \text{ and is about } 1.0 \times 10^5$$

## From constant shear stress transient results

$$G_2 = f(\tau) \text{ and is about } 0.8 \times 10^5$$

As can be seen from the figures the trend of the predictions are correct. These specific results are not optimized to fit our full range of data and thus any comparison would not be meaningful.

Some limited and specific comparisons can be cited from our previous work (3, 5, 7, 8). Figure 6 is an example of the basic shear diagram compared to the theory for a range of concentrations (3). Figure 7 gives similar results for the polymethylmethacrylate solution (7). Figure 8 (0.44 sec^{-1}) and Figure 9 (8.68 sec^{-1}) show the empirical fit obtained by Lewis (5), while Figure 10 (496 dynes/cm^2) shows the shear rate build-up and the fit obtained by Lee (7). These, as noted, are the earlier empirical fits based on an integrated form of Eq. (10) and are not based on the latest equations given in this proposal. Again, evaluation of the present equations with our data is the subject matter of this proposal.

Pandalai (12) was able to reproduce large amplitude oscillatory data superimposed on a steady shear rate by using the theory as presented in Eqs. (26) and (27) and a set of constants selected to fit the oscillatory data. The set of constants was not necessarily unique since no overall optimization survey was made. Pandalai was not able to reproduce stress growth and relaxation experiments with exactly the same constants but was able to do reasonably well by adjusting only G_1 and k_2.
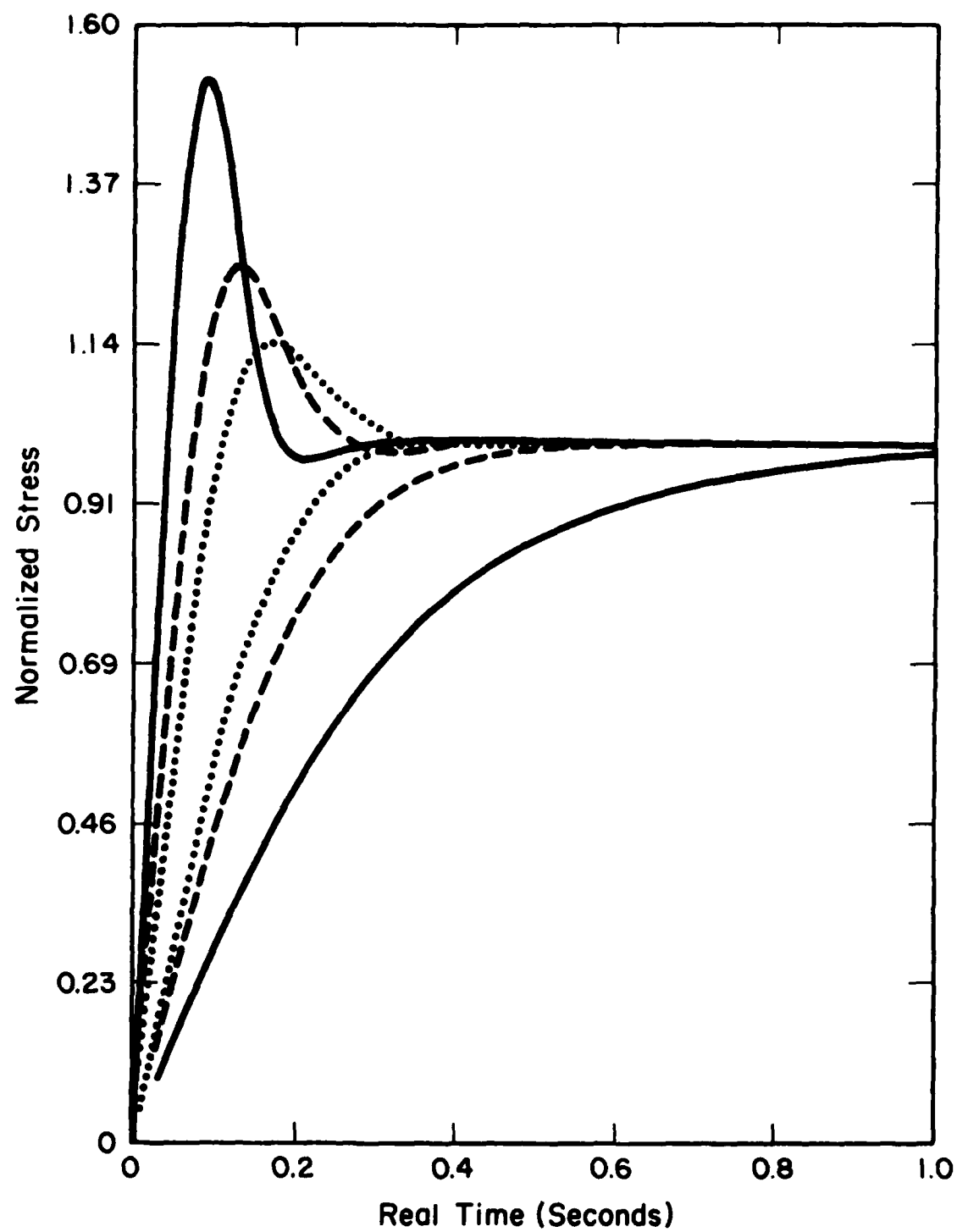
STRESS OVERSHOOT AT VARIOUS SHEAR RATES

Figure 5
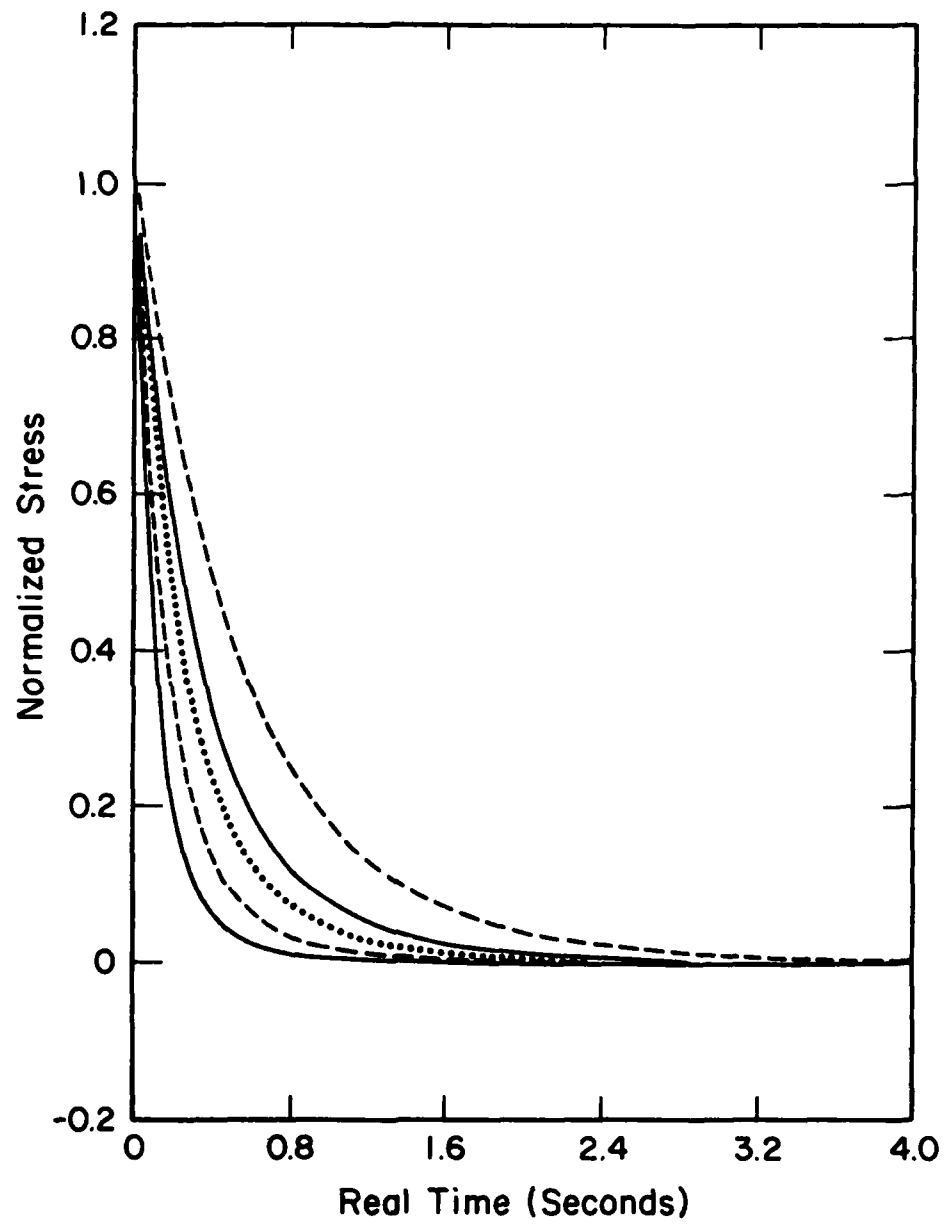
STRESS RELAXATION AT VARIOUS SHEAR RATES

207

Fig. 6

BASIC SHEAR DIAGRAM
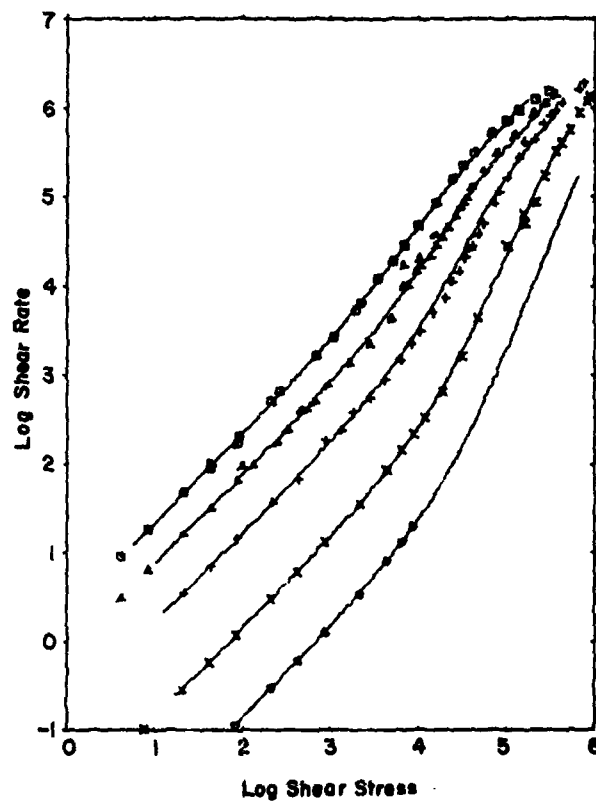FOR POLYACRYLIC ACID

Fig. 7

BASIC SHEAR DIAGRAM
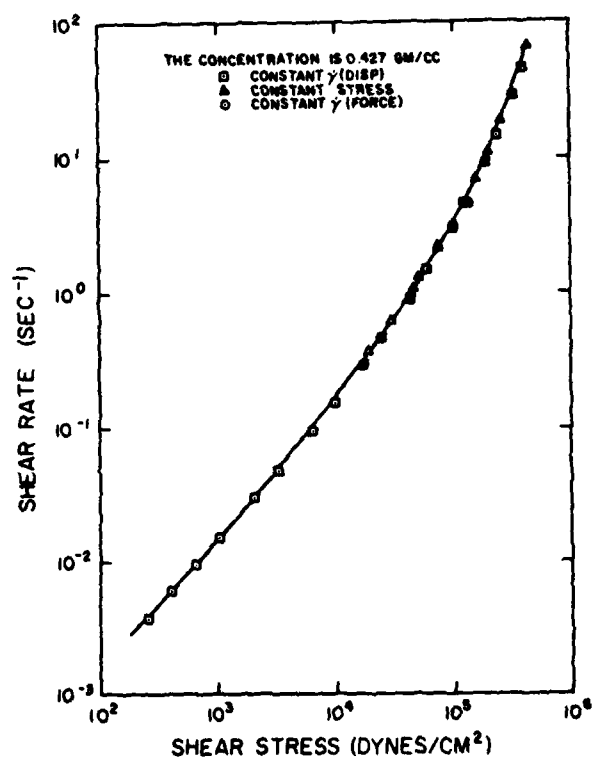FOR POLYMETHYL-
METHACRYLATE IN
DIETHYLPHTALATE

208

Fig. 8

COMPARISON OF
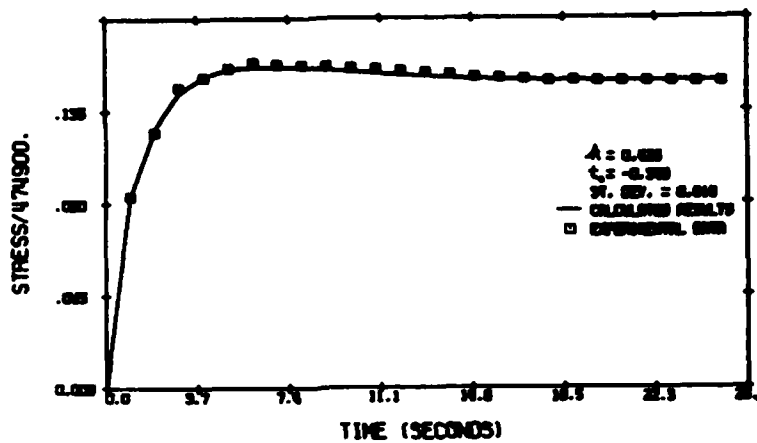DATA AND RESULTS
FOR 0.436 sec^{-1}

Fig. 9

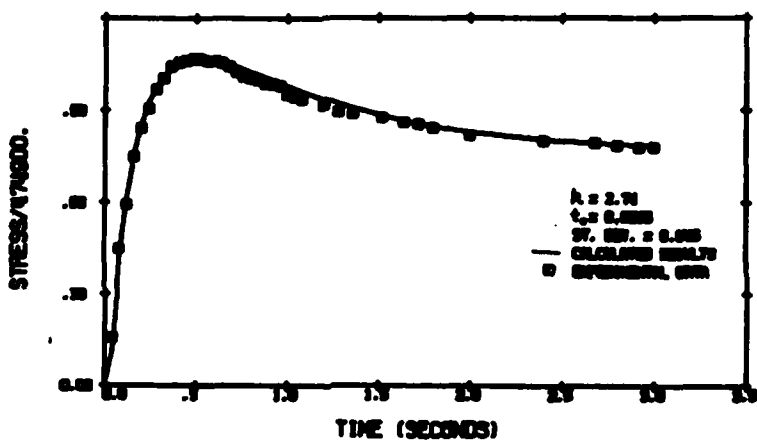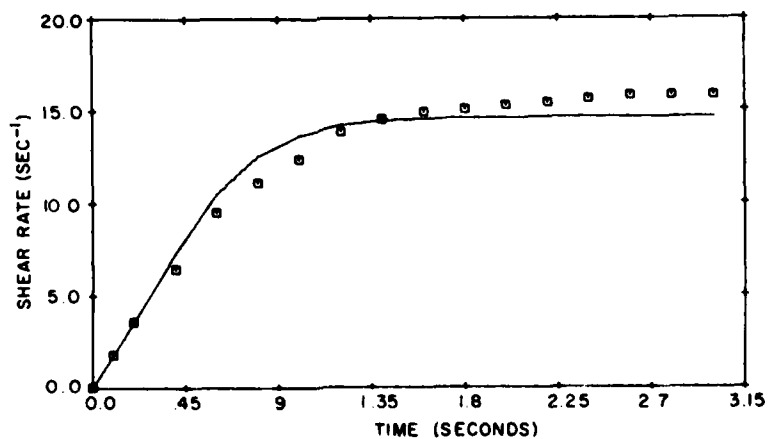COMPARISON OF
DATA AND RESULTS
FOR 8.68 sec^{-1}

Fig. 10

COMPARISON OF
DATA AND RESULTS
FOR CONSTANT
STRESS EXPERIMENT

209

E APPLICATION TO CONCENTRATED CONTACT LUBRICATION

The kinetic-elastic theory is quite general and can be used as a basis for describing lubricating materials. As long as the mechanism of the flow, i.e., the reasons for the nonlinearity of the fluid, does not change the model should be valid. Ideally, one would like to make measurements of the rheological characteristics under isothermal and atmospheric pressure conditions and to be able to use this information under conditions of temperature variation and extreme pressure levels. The degree that the model can be used to describe such changes is unknown and must be determined.

Certainly the time response is realistically described by the kinetic-elastic model. Our past work has demonstrated this for polymers and their solutions and there is no reason to expect lubrication materials to be different.

It should be noted that all alternate means of analysis have been for a Maxwell type model which means the derivative of the shear rate in Eq. (11) has been neglected or effectively G_2 was taken as infinite. Our experiments show that the latter is not true and certainly time rate of changes of shear rate exists in lubrication systems, so that one wonders what is the effect of only using an equation like Eq. (9) rather than (10) or its generalization, Eq. (11).

Temperature changes are introduced naturally through the values for the lower and upper Newtonian viscosities and through the rate constants

210

(k_i) and the equilibrium constant (K) (see reference 1). The rate constants and the limiting viscosities depend on temperature through equations of the form

$$k_i = k_o e^{-E^*/RT} \tag{28}$$

and

$$\eta_o = A'e^{-B/RT}$$

where E^* is an activation energy of the non-Newtonian reaction and k_o, A', B are all constants. A similar equation is used for η_∞ and K obeys a van Hoff type equation of thermodynamics (i.e., from k_1/k_2). The elastic parameters are not expected to depend on temperature, but this will have to be verified by experimentation. We have done some work on the effect of temperature on steady-state results, but have not as yet tried to extend this type of analysis to predict results at one temperature from another.

The effect of polymer concentration and the adequacy of the model to describe steady state conditions was demonstrated with Fig. 6 where data over a wide range of concentrations was represented. It would be interesting to establish if the effect of pressure on the time response problem is simply a change in concentration (i.e., density in gm/cc) in the kinetic equation (1) or does it also involve a coupling through the normal stress given in Eq. (21). Of course, changes in the limiting viscosities with pressure would have to be established by experiments using for example capillary viscometers.

F. APPLICATION TO SLURRY FUELS

We have not been able to locate as yet any existing data that is adquate for the time response analysis of slurry materials with a yield. However, some steady state (equilibrium) data is available and this has been analyized. As far as we can tell, slurry materials with a yield can be treated by the theory by using a minor modification to Eq. (5) for the definition of the fraction converted. This is necessary because n_0 for such materials is infinite (i.e., solid-like). The modifications attempted for the steady-state data that proved promising were: 1) a simple shifting of the stress axis to make the yield point (τ_0) the origin, 2) using a in Eq. (5) as negative (so that the n_0 term would be zero; i.e. $1/n_0{}^a$), and 3) using n defined as the slope of the curve rather than by Newton's law.

END

FILMED